January 2016

Diagenesis And Reservoir Analysis Of The Birdbear Formation, Williston Basin, North Dakota

Sunny Ekwenta

DIAGENESIS AND RESERVOIR ANALYSIS OF THE BIRDBEAR FORMATION, WILLISTON BASIN, NORTH DAKOTA

by

Sunny O. Ekwenta
Bachelor of Science, University of Nigeria, Nsukka, 2005

A Thesis

Submitted to the Graduate Faculty

of the

University of North Dakota

In partial fulfillment of the requirement

for the degree of

Master of Science

Grand Forks, North Dakota
Spring 2016

This thesis, submitted by Sunny O. Ekwenta in partial fulfillment of the requirements for the Degree of Master of Science from the University of North Dakota, has been read by the Faculty Advisory Committee under whom the work has been done and is hereby approved.

Richard D. LeFever, PhD, Chairperson

Stephan H. Nordeng, PhD

Dongmei Wang, PhD

This thesis is being submitted by the appointed advisory committee as having met all of the requirements of the School of Graduate Studies of the University of North Dakota and is hereby approved.

Dean of the School of Graduate Studies

april 29, 2016

Date

PERMISSION

Title	Diagenesis and Reservoir Analysis of the Birdbear Formation, Williston Basin, North Dakota
Department	Harold Hamm School of Geology and Geological Engineering
Degree	Master of Science

In presenting this thesis in partial fulfillment of the requirements for a graduate degree from the University of North Dakota, I agree that the library of this University shall make it freely available for inspection. I further agree that permission for extensive copying for scholarly purposes may be granted by the professor who supervised my thesis work, in his absence, by the Chairperson of the department or the dean of the School of Graduate studies. It is understood that any copying or publication use shall not be allowed without my written permission. It is also understood that due recognition shall be given to me and the University of North Dakota in any scholarly use which may be made of any material in this thesis.

Sunny O. Ekwenta
May, 2016

TABLE OF CONTENT

LIST OF FIGURES

LIST OF TABLES

ACKNOWLEDGEMENTS

I wish to thank the University of North Dakota and the Harold Hamm School of Geology and Geological Engineering for providing me the necessary tools and funding to complete this study. My heartfelt appreciation also goes out to my committee members; Drs. Richard D. LeFever, Stephen Nordeng and Dongmei Wang who gave me the needed insight and guidance at each stage of this study.

Julie LeFever of the North Dakota Geological Survey and other staff of the Wilson M. Laird core library whose inputs and suggestions were handy to piece things together for me and for making the cores and thin sections available. To Francis Nwachukwu who ran this race side by side with me and gave me the moral push to keep going, I say thank you. Kilynn Sanberg for teaching some of those little computer tricks, I'm so grateful. To Cecilia Kalambo who told me I can do it, I appreciate it.

I couldn't have made any progress if not for my understanding and supporting family. My wife Tity, my children Akachukwu and Chizaram, you guys are the best and the reason why I'm here.

Above all to the Almighty God who holds all things together in His hands, I appreciate the privilege.

ABSTRACT

The southwestern part of Birdbear Formation of the Williston basin is part of the three shelf-wide sedimentary cycles in the Devonian transgressive-regressive sequence rock deposit. It is bounded above by the Three Forks and below by Duperow Formation. The formation can be informally divided into an upper A zone and a lower B zone. The common rock types in the Birdbear are dolomites, limestone, and anhydrites as well as combinations of anhydrite limestone, and dolomite limestone that is mostly found in the upper zone usually at the contact between the Three Forks and the Birdbear. Hydrocarbon has been found in the A zone in a stratigraphic trap formed by the anhydrite acting as a seal and in the B zone by the structural trap caused by the dissolution of salt in the Prairie Formation.

The formation has undergone different diagenesis which has altered its primary sediments and giving rise to secondary porosity and permeability. The formation contains mostly wackestone, packstone, and biosparite. Dolomitization and fossil fragments dissolutions are the two most common diagenetic processes occurring in the Birdbear, hence creating intercrystalline and biomoldic porosities. The reservoir quality analyses show that the Birdbear Formation has decent porosity and permeability but the answer to why the Birdbear is not a prolific producer can be found in the TOC/Rock-Eval analyses.

CHAPTER I

INTRODUCTION

As the quest to explore and exploit more hydrocarbon increases globally to meet the growing energy demand, great attention has been paid in great measures to the Williston Basin. With the advent of horizontal drilling technologies and fracking, this basin has witnessed an unprecedented level of drilling activities in recent times. The Williston Basin to the northeast is bounded by the Canadian Shield, Sweetgrass arch at the north and northwest, Transcontinental arch at the south and southeast, series of Laramide structures like the Mles City arch, Black Hills Uplift, Bowdoin dome, and Porcupine dome to the west and southwest (Figure.1)**,** and deposited over a Precambrian basement. Structurally it is an intracratonic depression with over 16,000 ft. of sediments according to Anna, L.O (2013). The Williston Basin has a wide extent with boundaries in Montana, North Dakota, South Dakota, Saskatchewan, and Manitoba. In the North Dakota this basin, attention has been mostly on the Bakken and the Three Forks Formations having been identified as a prolific producer and as such, great attention has been paid to these two formations as far as research goes. Despite all the work that has been done on these two formations, little attention has been paid to the formation that is stratigraphically below it, the Birdbear Formation (Upper Devonian).

The Birdbear stratigraphically underlies the Three Forks Formation and overlies the Duperow Formation. It is mostly a carbonate-evaporite formation that extends over all the Williston Basin of North Dakota, Montana, Southwest Manitoba and Southern Saskatchewan. It is referred to the Nisku Formation at the Alberta Basin and Montana (Kent, 1968). The formation is easily identified in a wireline log by its sharp kick-outs at the base of the Three Forks Formation (Figure 2). This formation is usually a carbonate member and the middle mostly alternates between carbonates (limestone and dolomites), and anhydrite and at the boundary between the Three Forks and the Birdbear usually starts with a thin layer of anhydrite.

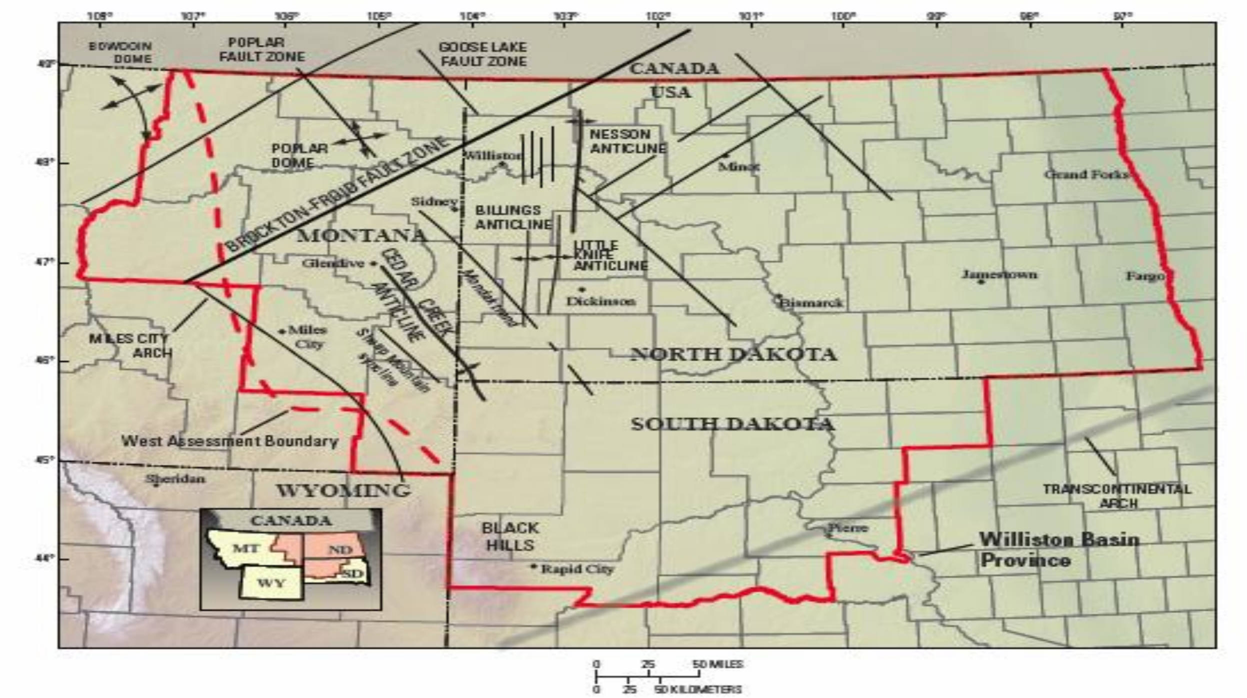

Figure 1. Outline of Williston Basin and major structural features (Anna, 2013).

The Birdbear usually ranges in thickness between 0 to 125 feet. The thin layer of anhydrite at the top of the formation often acts as a barrier or seal for further movement of hydrocarbon that accumulated in the carbonate rocks (Murray, 1964). The anhydrites are present everywhere and are a sign of transition from the Three Forks.

The study area occupies two counties in the Southwestern part of North Dakota, namely the Billings and Golden Counties, Figures 3 and 4.

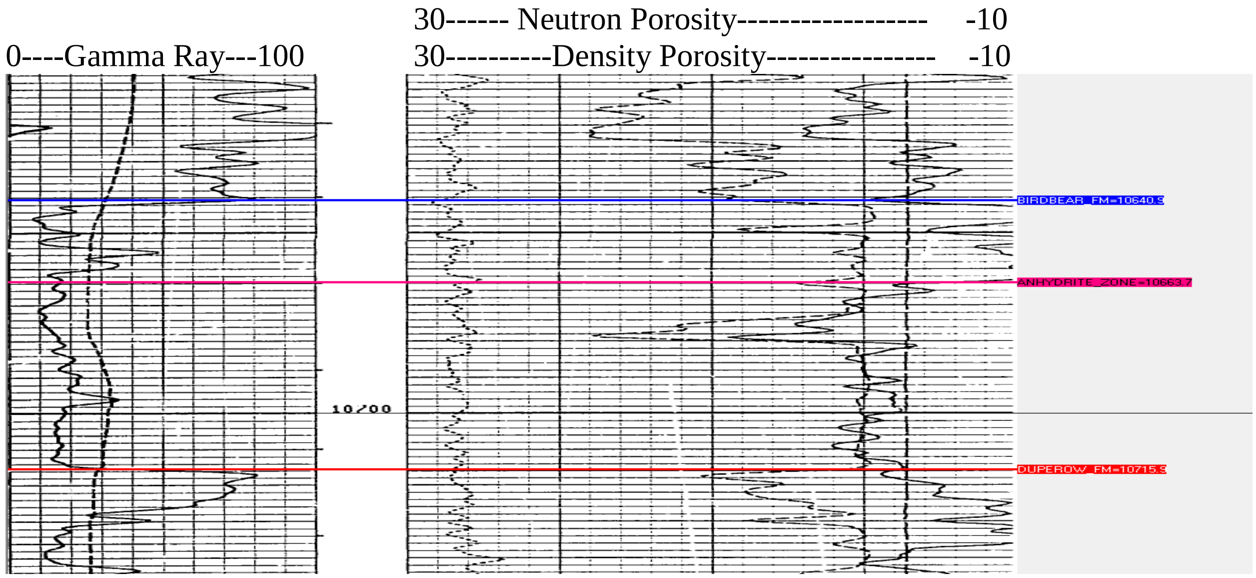

Figure 2. Wireline Log showing the top of the Birdbear with a kick out the top of the Duperow. In-between is the probably anhydrite interval as shown by the point where the density porosity goes off the scale.

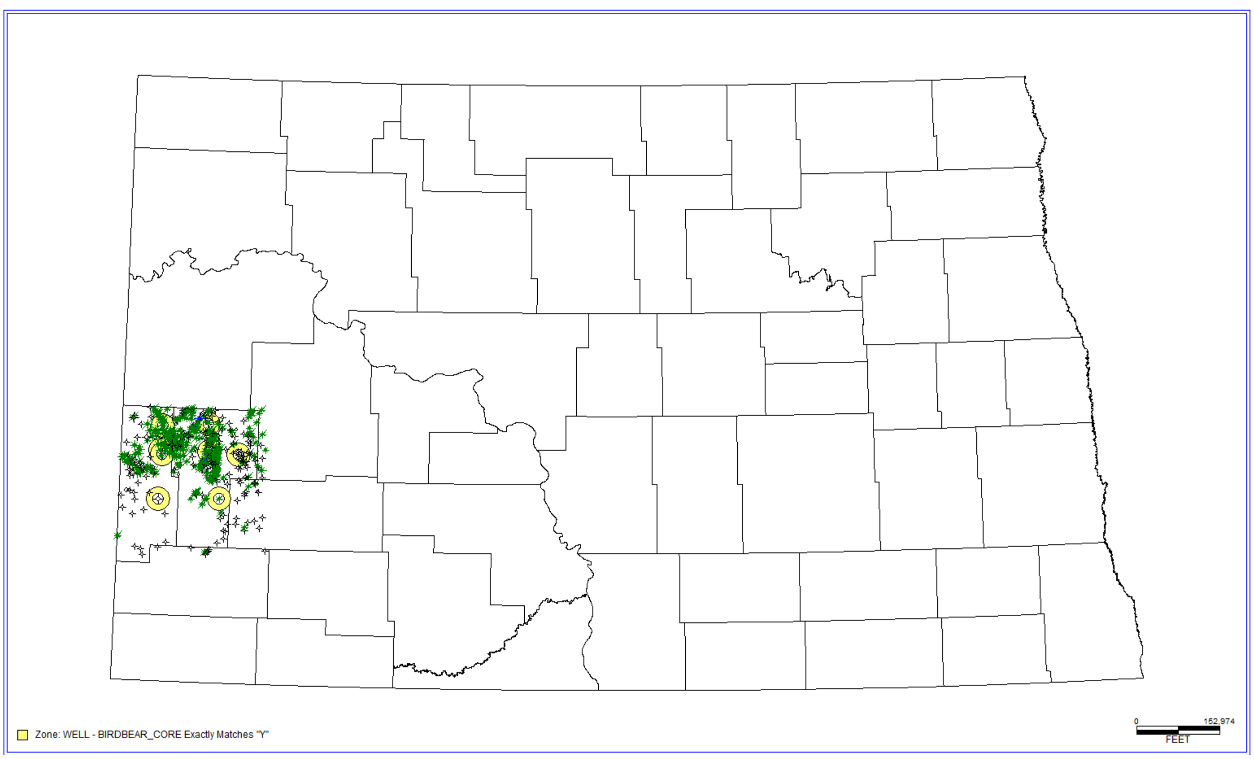

Figure 3. Map of North Dakota with counties showing the area of study and oil wells drilled in the Birdbear.

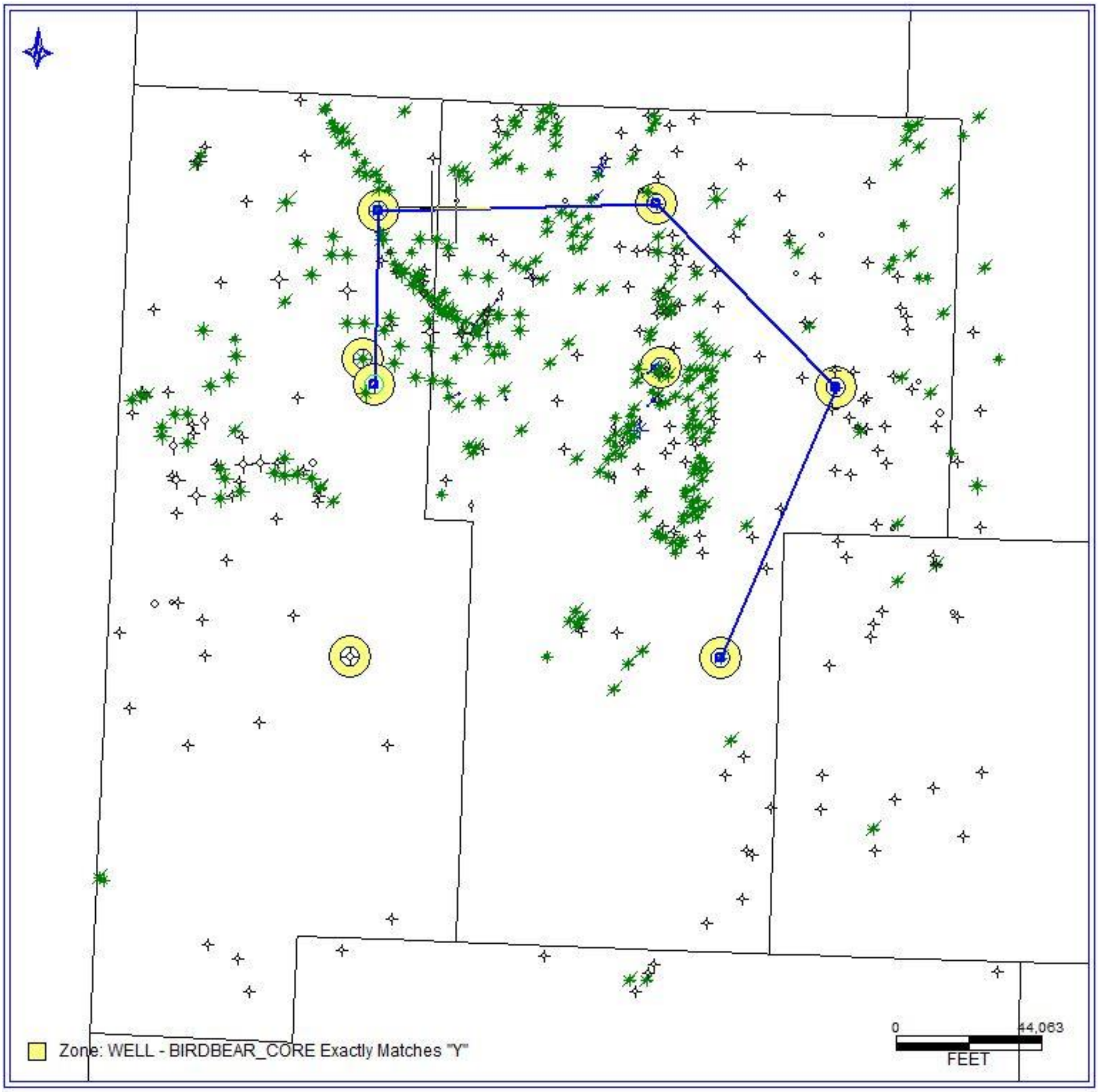

Figure 4. Map of Study area showing the sampled areas in Golden Valley and Billings Counties, oil wells drilled in the Birdbear Formation and the points of cross-section.

1.1 Objectives

The formation has undergone different levels of diagenesis that has significantly affected the reservoir qualities of the formation. These changes reflect on the porosity and permeability of the rocks. This study is to determine how much these diagenetic processes have impacted on the reservoir quality and the lithological changes throughout the formation and how it correlates. This study will look at the reservoir characterization and the quality of the source in the Birdbear Formation. The kerogen type and the stage of the thermal maturation will also be evaluated.

1.2 Methodology

Three basic approaches have been used in this study: cores analysis, thins sections, and wireline logs. Based on availability, only seven cores were used. The cores were analyzed for color, grain size, sedimentary structures, fractures, porosity, and fossil contents using hand lens, color chart, grain size chart. Dilute hydrochloric acid was used to distinguish the limestone from the dolostone. Descriptively, Folk, (1959 and 1962), and the Dunham (1962) classification schemes, were used to name the rocks. Pictures of features of interest were taken from the cores. Thin sections were also examined with the help of a Leica microscope using different magnifications. A total of 105 thin sections were examined to better understand the diagenetic processes and to examine features like porosity, fractures, fossil contents as well as naming the rock types using Folk (1959) and Dunham (1962) classification schemes. Well profiles from the North Dakota Industrial Commission were also used to get some properties of the wells like the porosities, permeability, oil, and water saturation to give further interpretations.

Five hundred and forty wireline logs were used to determine the tops and bottoms of the formation and to identify the anhydrite unit using the PETRA (2014) software. This was done by noting the signatures of the wire line logs as it moves through the different lithology. About 300 wireline logs of neutron-density porosity logs, gamma ray, and sonic logs were digitized and plotted using the SURFER (2013) software to help identify the porosity distribution across the study area as well as the thicknesses of the formation and the anhydrites. Twenty-five rock samples were collected and sent to StratoChem for TOC/Rock-Eval and Pyrolysis to determine richness and maturity stage of the source rock. The rock TOC (Total Organic Carbon) was determined. The rock-Eval method was done by heating and decomposing the samples in the absence of oxygen. The hydrocarbons present in the sample are volatilized and measured and noted as S1. Pyrolysis checks the kerogen present which is recorded as S2, and the CO present is recorded as S3. The Hydrogen Index, Oxygen index and Production Index was calculated from:

HI= S2 (Mg/g) / %TOC x 100 Eq. 1

OI= S3 (Mg/g) / %TOC x 100 Eq. 2

PI= S1 (mg) / (S1 (mg) + S2 (mg) Eq. 3

1.3 Geologic Setting

The Williston Basin is an oval depression (Figure 5) that is on the western edge of the Canadian Shield and stretches to Montana, North Dakota, South Dakota, Saskatchewan, and Manitoba, is known to be part of an embayment stretching through Saskatchewan and Alberta to the open sea beyond, (LeFever, 1999). The repeated flooding of the embayment by changes in sea levels and its decline caused the lower portion of the Birdbear to be predominantly made up of shallow marine limestone and dolostone and the upper portion mainly anhydrites. The largest part of the Williston Basin is in North Dakota which also is where the deepest part of the basin is located (Gerhard et al 1982)

The Birdbear lies on top of the Duperow Formation and below the Three Forks Formation (Figure 6). The anhydrites suggest that North Dakota at a time experienced arid conditions like the sabkha environment. Kissling and Ehrets (1985) noted that the deposition of this Devonian sequence (marine transgressive-regressive sequence), was controlled by three shelf-wide cycles of progressive hypersalinity of which the third cycle deposited the Birdbear,

Figure 6. Hydrocarbon in the Birdbear Formation mostly occurs in the dolomitized stromatoporoid just below the anhydrites. The Birdbear can range in thickness from 0 to 125 ft. and is mainly made up of upper anhydrite layer which acts as a seal for hydrocarbon (Murray, 1964), anhydrite limestone and, dolostone.

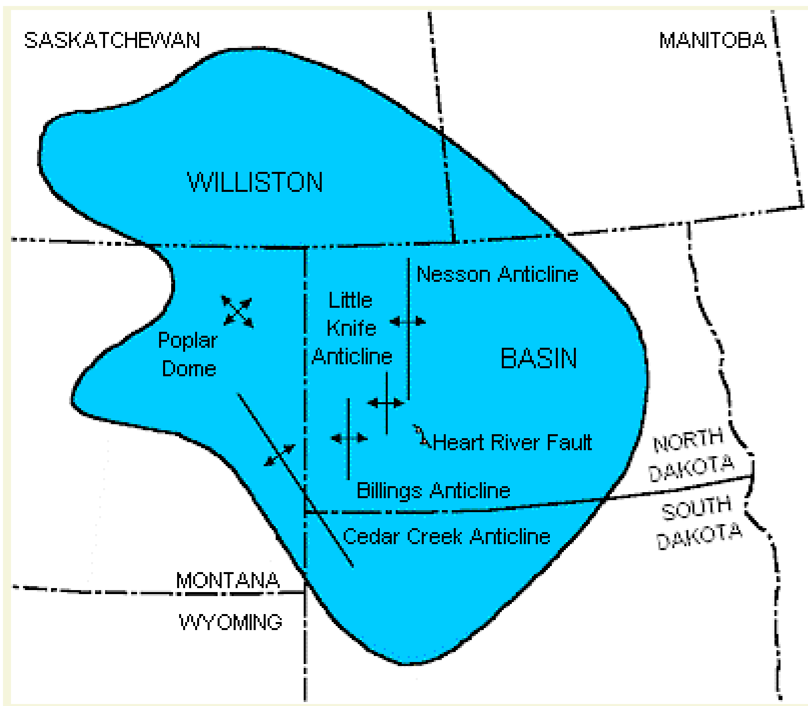

Figure 5. Extent of the Williston Basin with its major structural features.

(www.dmr.nd.gov/ndgs/resources/)

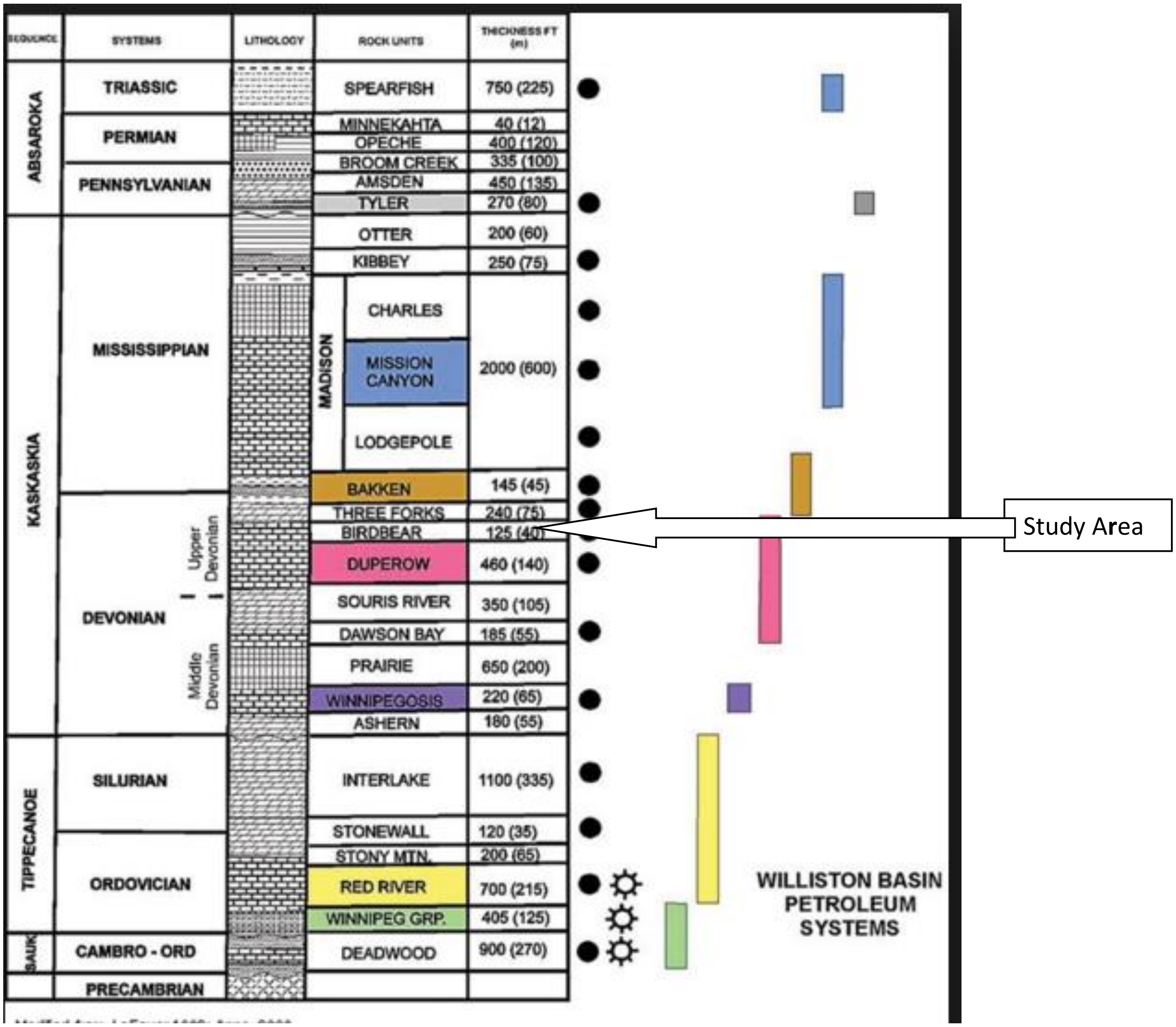

Figure 6. North Dakota Geologic Column. The arrow shows the study area. (Modified from LeFever 1992; Anna, 2009).

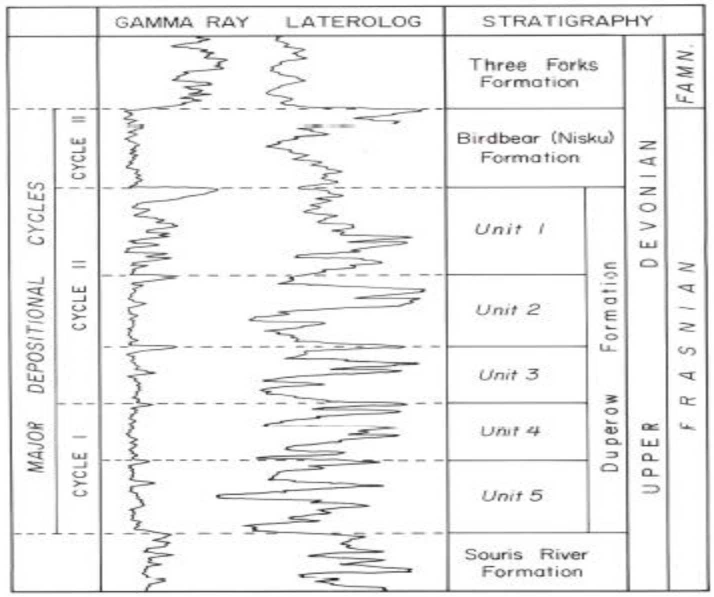

Figure 7. Depositional cycles in the Upper Devonian Stratigraphy with composite log characteristics and subdivisions of the Duperow and Birdbear Formations (Ehrets et al, 1985).

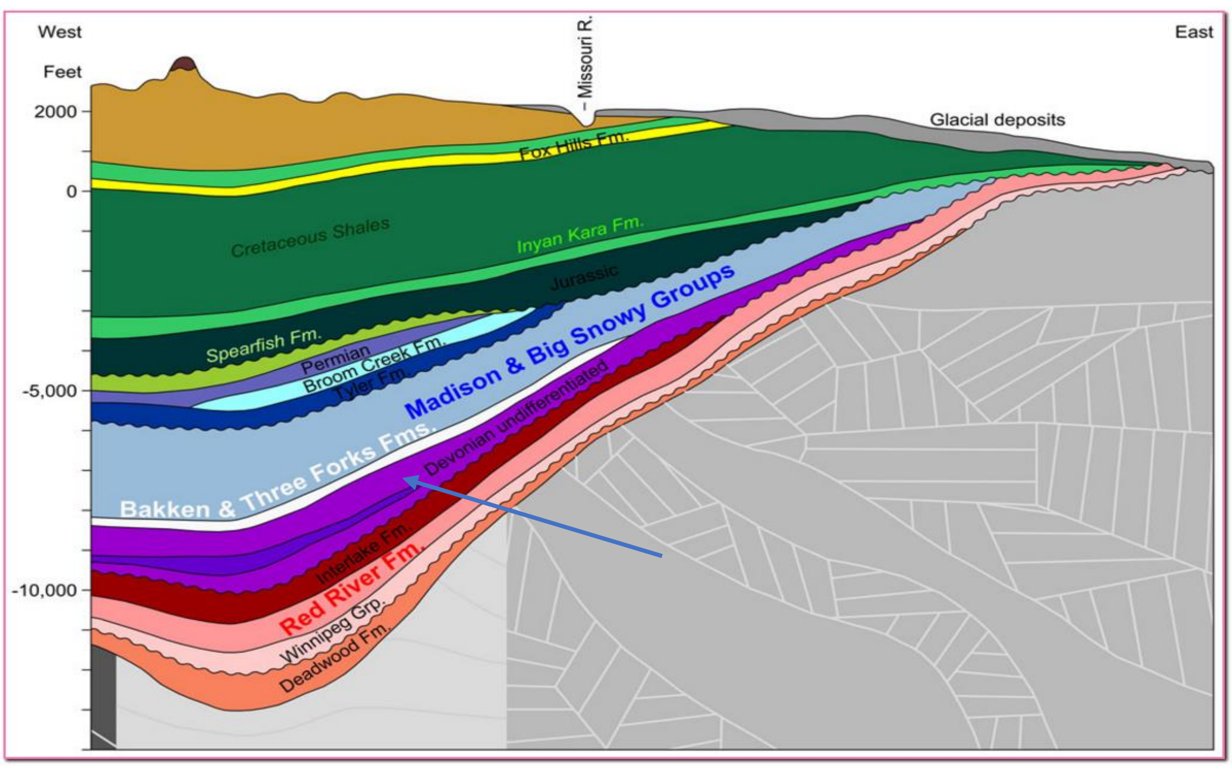

Williston Basin Cross Section: This cross-section of the Williston Basin is to scale and was run from Beach to Fargo, N.D., along Interstate 94.

Photo courtesy of the North Dakota Geological Survey.

Figure 8. Cross Section of the Williston basin from Beach to Fargo, (NDGS).

1.4 Previous Work

A number of work have been done in the Williston Basin as a whole and in some of its formations like the Bakken and Three Forks Formations, which has been the attention of so much exploration activities in recent time, but little work has been done in the Birdbear Formation especially the North Dakota portion of the Birdbear. Most of the work was done on the Canadian portion. The Birdbear Formation was initially defined by Sandberg and Hammond (1958) using the Mobil Oil Producing Company No.1 Birdbear well, c SE1/4NW1/4 Sec.22 T. 149 R. 91W, in Dunn County, North Dakota. Many oil operators still use the name Nisku Formation. The low level of tectonic disturbance, widespread lateral continuity of key beds, and availability of cores and geophysical logs make the Birdbear Formation an excellent rock interval for the development of carbonate depositional and diagenetic models (Halabura, 1982). He also noted that the lower member of the Birdbear shows sediments of marine, low to medium energy deposition. Such sediments are laminated to massive dolomite, nodular bioclastic lime wackestone, bedded to nodular bioclastic lime wackestone to packstone, massive to laminated lime mudstone, partially to completely dolomitization of the original micrite matrix with dolomite crystals sizes ranging from microcrystalline to microsucrosic. Common fossils include brachiopods, gastropods, ostracods, foraminifera, bryozoan and broken intraclasts, Halabura, (1982).

In distinguishing the lower and the upper portions of the Birdbear and its environment of deposition, Halabura (1982) noted that the upper member is supratidal while the lower member is subtidal (Figure 9). It should be noted that many workers have divided the Birdbear into different numbers of units or members depending on what they want to achieve. Kissling (1996) for example divided the Birdbear formation into three members.

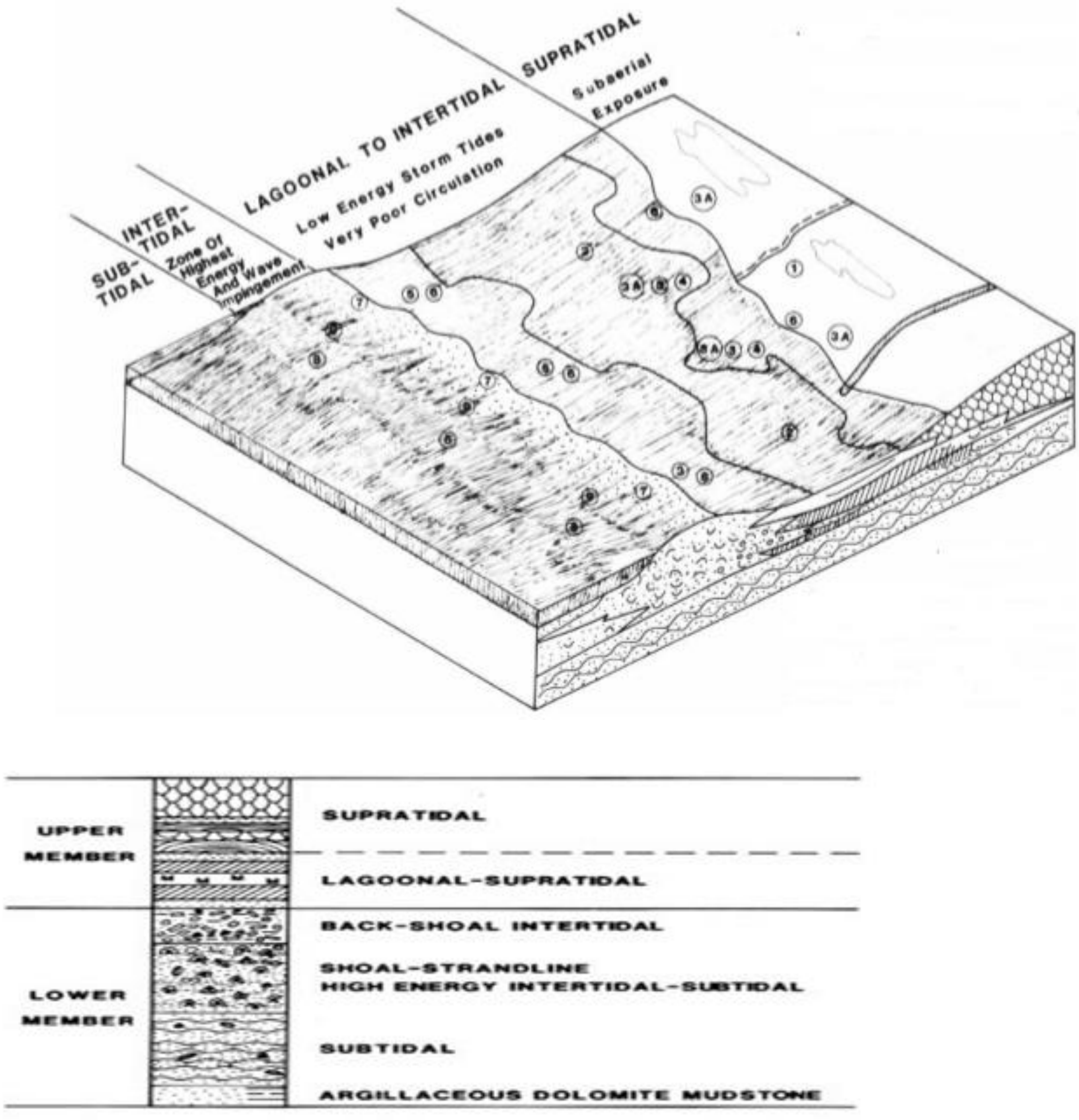

Figure 9. Depositional model for Birdbear Formation in southeast Saskatchewan Halabura and a typical Birdbear depositional cycle. Halabura (1982).

Burke et al (2005) like Halabura (1982) also divided the Birdbear into two units, upper (A) and lower (B) based on gamma ray logs. With the upper part being picked on the gamma ray at the highest reading above the top of the Duperow Formation which also keeps the anhydrite layer within this upper part. This study agrees with this division (Figure 11). He also noted that most of the pay zones are within the part A and that could likely be as a result of stylolite swarms as conduits for the movement of hydrocarbons that helps to drain the large area that accounts for the large production from this zone A. The lower portion of the Birdbear is made up of carbonates, burrow mottled, calcareous mudstone and Wackestone which contains a lot of fossils like gastropods, rugose and brachiopods while the upper portion is mainly cycles of dolostone and anhydrites.

NDGS 10776
PROPEL ENERGY CO.
ANNA LOGOSZ 1
NESW 24-142-99
BILLINGS COUNTY, NORTH DAKOTA

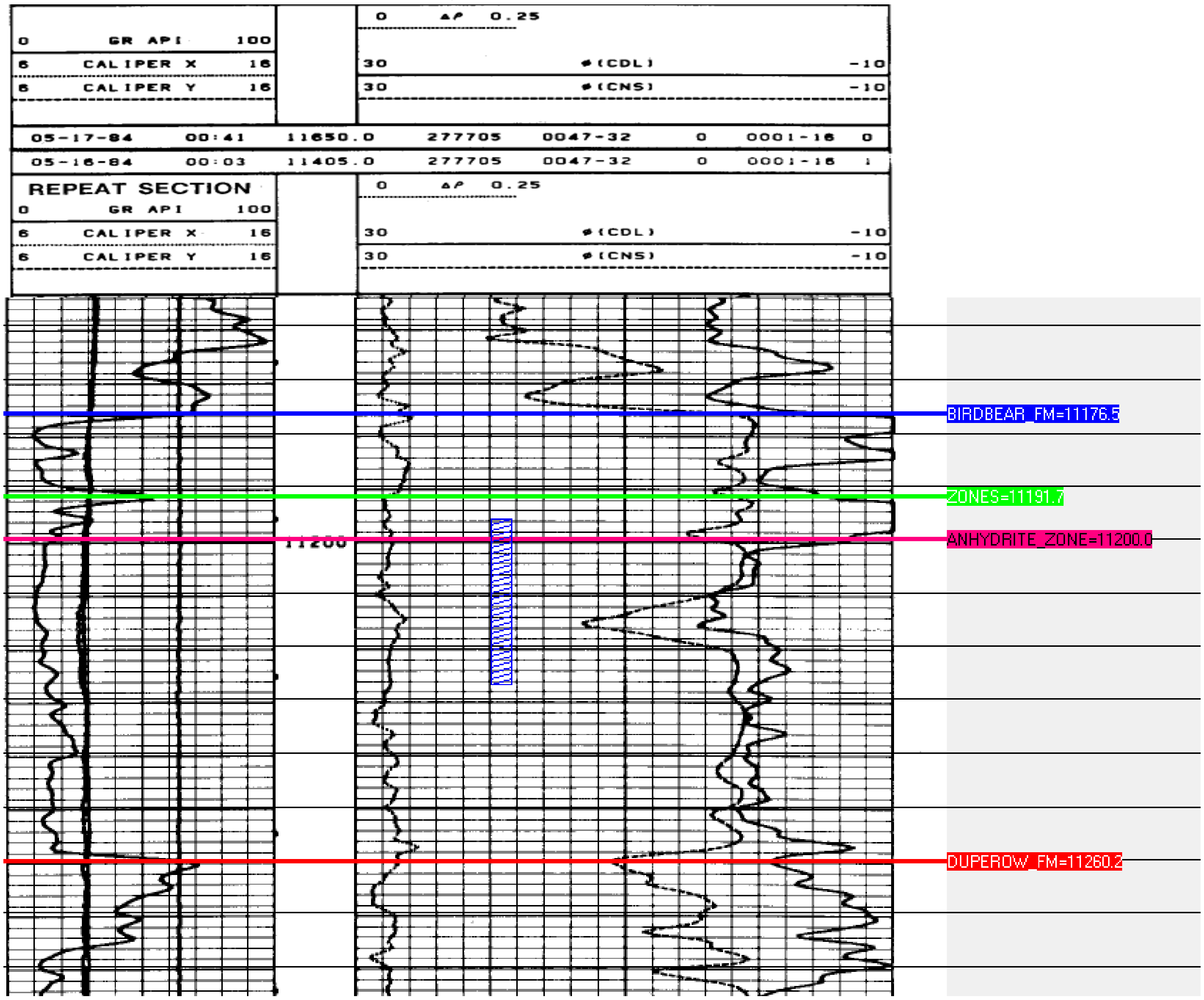

Figure 10. Divisions of the upper and lower zone of the Birdbear and the contact of the anhydrite.

Typically production in the B zone normally comes from the point of structural highs which is also helped by the overlying anhydrite in the A zone acting as a cap rock.

NDGS 6310
Burlington Resources Oil & Gas Company
Federal 6-1
Billings County, North Dakota

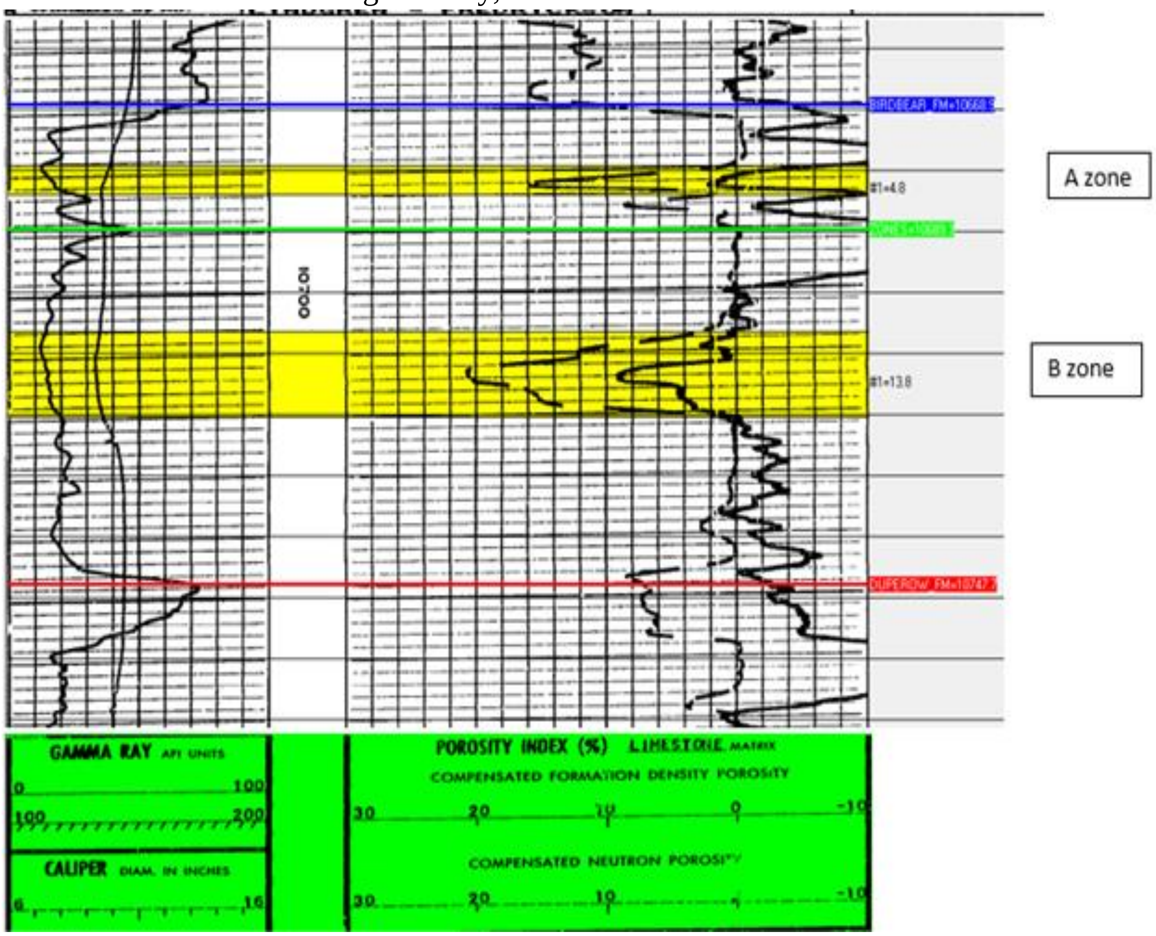

Figure 11. The probable pay zones in both the upper and lower member divisions of the Birdbear formation.

The structural highs and traps in the B zone are as a result of the multistage dissolution and collapse of caverns in the underlying Prairie salts (Clark 2011) and concluded that B zone is a structural play. In his work on the trap mechanics in Nisku Formation of Northeast Montana, Swenson (1967) noted these structural highs are steep sided and less than a mile in diameter and form the B zone reservoirs in northeastern Montana.

The A zone is a thin bed has seen production from about 2 to 4-foot layer of porous dolostone. Most production comes from cycle 2 (LeFever 2009) which is seen as the source rock with an anhydrite overlying it and acts as cap rock. So this is seen as a stratigraphic play. Because of how thin this layer is, horizontal drilling is very common in zone A.
Hans et al (1988) studied the causes of pervasive subsurface dolomitization that is very common in the Birdbear in the Central Alberta where it is referred to as Nisku. They stated that most of the dolomitization ranges from partial to complete and concluded that expulsion of burial compaction water and thermal convection of formation fluids are the driving force for the dolomitization in the Birdbear formation.

Martiniuk et al (1995) identified three reservoir facies within the Lower member including a stromatoporoid and Amphipora bank facies, and a dissolution-related alteration facies.

Cynthia et al (1982) on the diagenesis of the Nisku Formation and the origin of the late-stage cements, interpreted that the sequence of diagenesis is a selective dissolution of fossils, dolomitization, extensive stylolitization, precipitation of calcite cements before, during and after stylolitzation and late-stage anhydrite replacement. In his work on Carbonate Reservoir Models Lucia (1992) noted that dolomite cement systematically grows on the dolomite crystal faces thereby reducing the reservoir qualities.

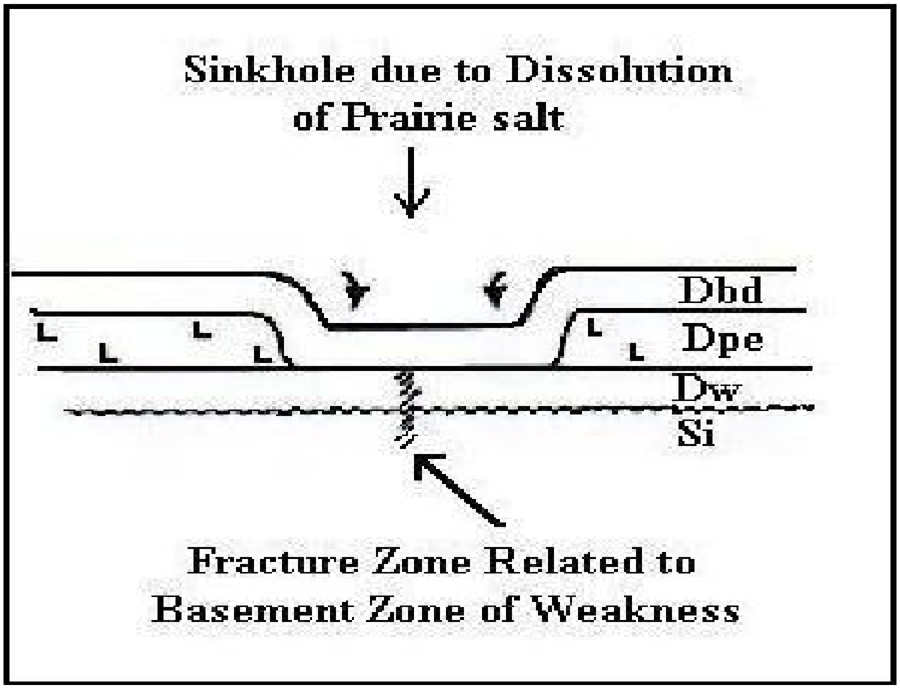

Figure 12. First stage of dissolution of the Prairie salt. Dissolution collapse leads to the formation of sink holes. Dbd=Devonian Dawson Bay formation; Dpe= Devonian Praire evaporate Formation; Dw=Devonian Winnipegosis formation; Si=Silurian Interlake formation. (Source: Swenson, 1967).

Ehrets et al (1985) noted that paleostructural and facies controls were also important to the reservoir development of the Birdbear Formation. While discussing the reservoir characteristics, he noted that the amount of porosity is related directly to the degree of dolomitization, with the completely dolomitized part having the highest porosity, as well as developments of porosity within dolomitized Amphipora and stromatoporoid banks in both Duperow and Birdbear Formations all through the Williston basin.

Fowler (2001) studied the east-central Alberta part of the Birdbear (Nisku) and shows that of the 182 samples subjected to Rock-Eval/TOC analysis, 51 had TOC content greater than 1%, 19 have greater than 2% and 2 have greater than 10%, with the higher TOC samples showing Type II organic matter. Fowler also sampled the Birdbear Formation from Southern

Saskatchewan equivalent to the Birdbear in the North Dakota axis and found that twenty-one out of the forty-one samples have TOC greater than 1%. The type of organic matter for this area shows Type I and Type III. Fowler et al, (2001) sampled the Birdbear Formation from Montana and North Dakota but none showed any hydrocarbon potential.

CHAPTER II

UNIT DESCRIPTIONS AND WELL LOG CORRELATION

The core descriptions were done based on the availability of cores. A total of seven Birdbear cores were described which amounted to a total of about 248 ft. Most of the cores analyzed do not have the entire formation represented making it difficult to have a big picture of the formation of individual wells. Most of them were just a fraction of the entire length of the formation. With that challenge in mind, this work used well logs to reconcile the point of each sampled core. It should also be noted that a comparison of the well logs and the cores show that the well logs were off by a few feet. Going by the informal divisions of a lower B zone and an upper A zone, the cores examined and the thin sections will be used to identify the different lithologies in the formation. Most of the descriptions here are relative and descriptive. A total of 105 thin sections from six cores (one core has no thin section), were examined using the petrographic microscope. More images of the thin sections can be seen in Appendix II.

The core for NDGS 291 was found at the lower end of zone A. Starting from bottom up, the lower unit that has abundant fossil fragments. Most of the fossil fragments found are gastropods, brachiopod stems, ostracod, and bryozoans giving us a biosparite. Most of the fossil fragments can be seen undergoing recrystallization. Stylolites and dissolution seams can be seen thin section. Most of the limestone can still be seen with scattered dolomite crystals. Burrows and amphipora also seen at around 10685 ft. depth. The limestone continues up until at the depth of 10685 ft. where there is more dolomitization taking place. Euhedral dolomite crystals increase the intercrystalline porosity. At the top of this core is an increment in limestone producing an anhydrite limestone. Between 10677 to 10678 ft. is a very short interval of mostly limestone sandwiched by anhydrite limestones on both sides. The rock type up here is mostly packstone.

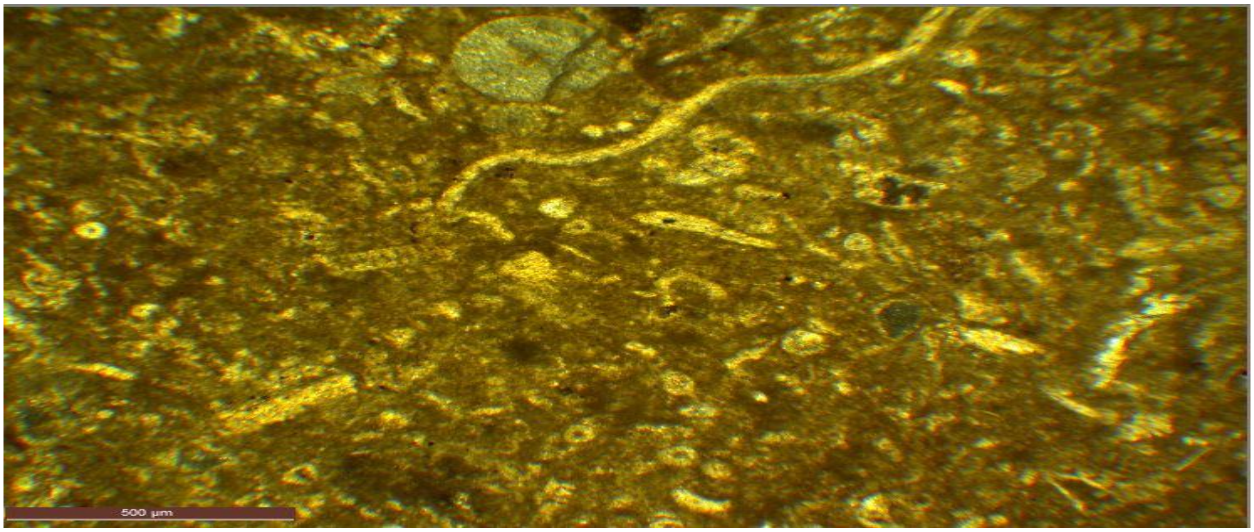

Figure 13. NDGS 291. 10691.5 ft. A packstone with a lot of fossil fragments. The fragments have been calcified and only defined by the micrite envelope. This section gives us a biomicrite.

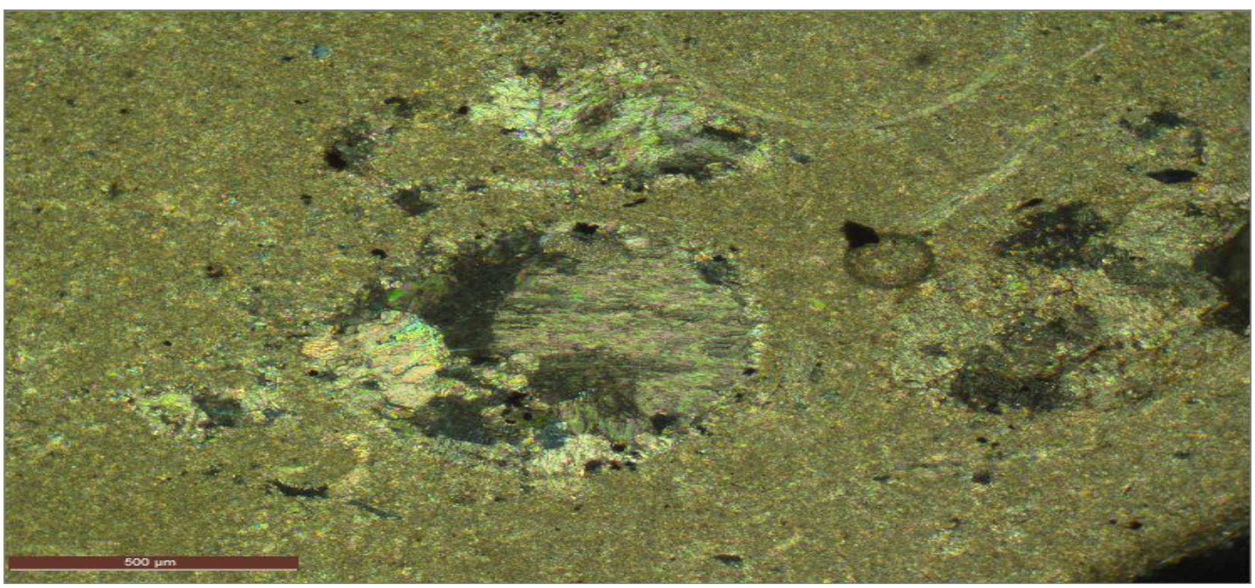

Figure14. NDGS 291. 10699.9 ft. Vug caused by dissolved fossil fragment undergoing recrystallization.

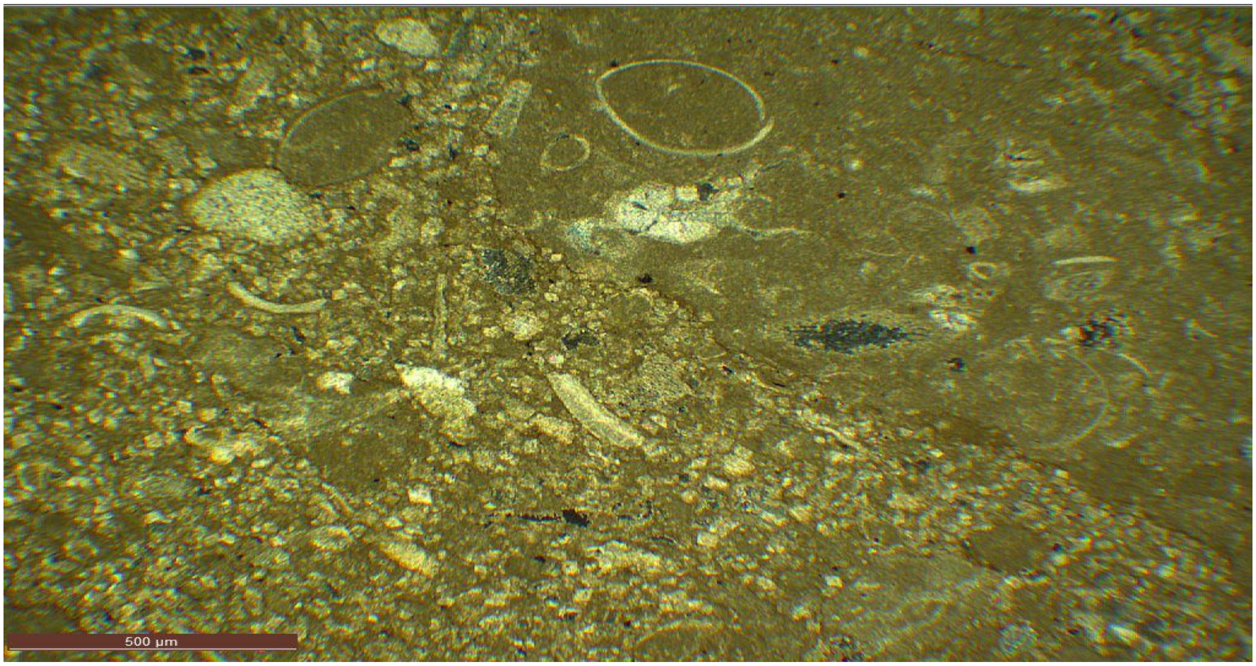

Figure 15. NDGS 291. 10588.8 ft. Progressive Dolomitization. Ostracod on the less dolomitized section as well as fragments of ostarcods and gastropod on the side showing more dolomitization. Beside the whole ostracode is a fivefold structure of echinoderm with recrystallization taking place inside the fossil fragment.

Figure 16. NDGS 291. Depth. 10691-2 ft. A packstone showing biosparite and stylolite.

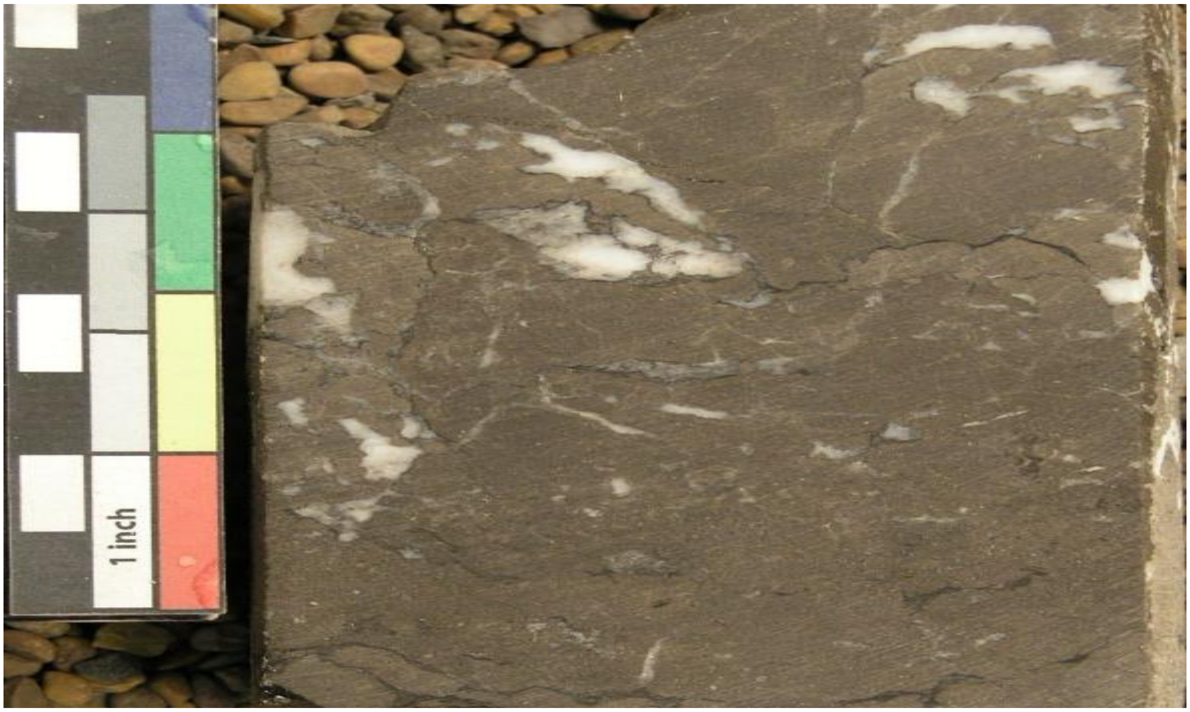

Figure 17. NDGS 291. 10681-5 ft. Patches of anhydrite limestone with fractures.

In NDGS 859, the upper and lower zones are represented. The lower B zone is more of limestone with lots of fossil fragments and different levels of dolomitization. The level of dolomitization in the B zone is more than the A zone.

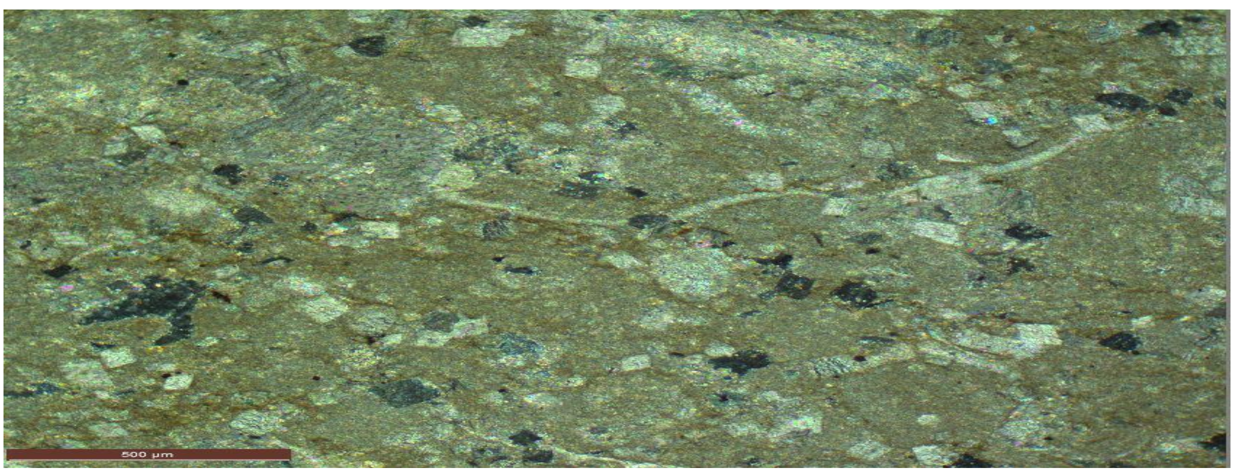

Figure 18. 859. 10957.95ft. Partially dolomitized Packstone. Selective replacement of original micrite by crystalline dolomite. Selective dolomitization.

In zone A, patches of anhydrite becomes very common and more dolomitization. Dissolution seams, fossil fragments, stylolites and calcification of the original aragonites of the fossil fragments are so common. Most of the rock type is biosparite, wackestone and packstone. The anhydrites are invasive in most places. Fossil fragments observed are echinoid spine, brachiopod stem, bivalves, ostracod and bryoazon.

Figure 19. NDGS 859. 10925 ft. Anhydrite limestone.

Within the matrix of this unit is predominantly anhydrites filling the fractures and pores. The dissolved fossil fragments shows recrystallization going on.

NDGS 10776 has no thin section. The cored interval all falls within the B zone. The lower part of it is limestone with abundant burrows and stylolites. Abundant Amphiporas at the lower unit of this core. Apart from this lower limestone layer, the upper part is mainly dolostone with patches of anhydrites.

Figure 20. NDGS 10776. 11226-4 ft. Packstone with burrows.

Figure 21. NDGS 10776.   11214-5 ft. Abundant amphiporas.

In the Golden Valley County, the core of NDGS 15412, fall in the B zone, the cores are highly fractured with anhydrites plugs at intervals. The rock type is mostly dolostone and wackestone. Solution seams at interval and increase in intercrystalline porosity.

Figure 22. NDGS 15412. 10719-0 ft. Highly burrowed with stylolites.

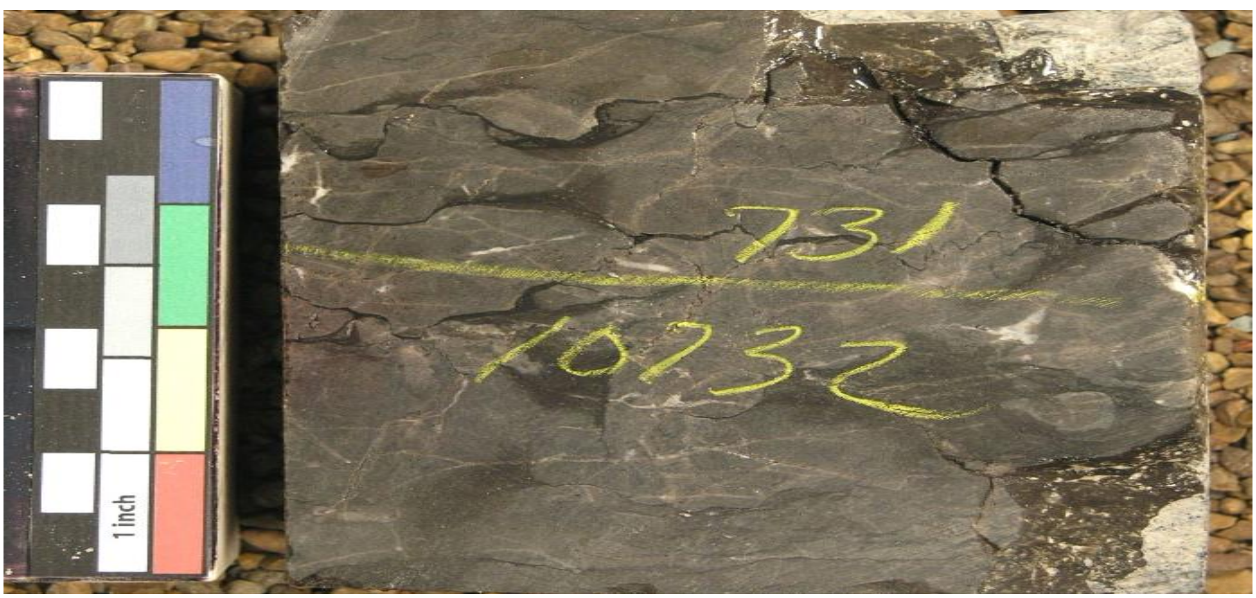

Figure 23. NDGS 15412 ft. highly burrowed wackestone with anhydrite plug.

The A zone is mostly dolomitized with some of the dolomitized areas showing sucrosic textures. It highly porous due to the effect of dolomitization.

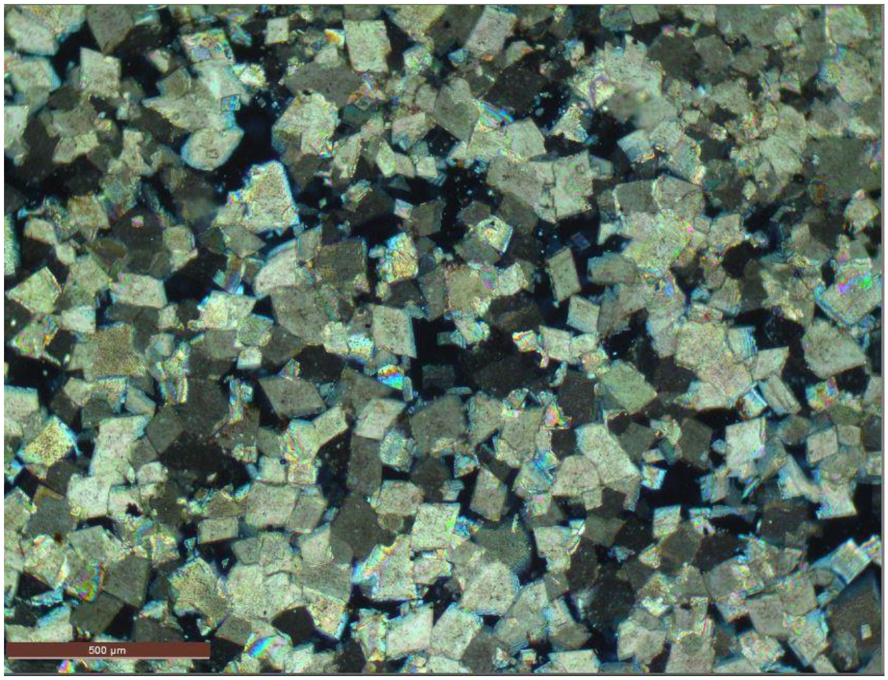

Figure 24. NDGS. 15412. 10710.9ft. Highly porosity due to dolomitization. Sucrosic texture and intercrystalline porosity.

Vugs created due to fossil dissolution adds to the porosity as well. Fractures and stylolites are very abundant. The top of the core interval starts with mudstone and fractures.

Of note in this core is the absence of fossil fragments and biosparite. The core is mostly dolomitized and evidence of possibly dissolved fossil fragments undergoing recrystallization.

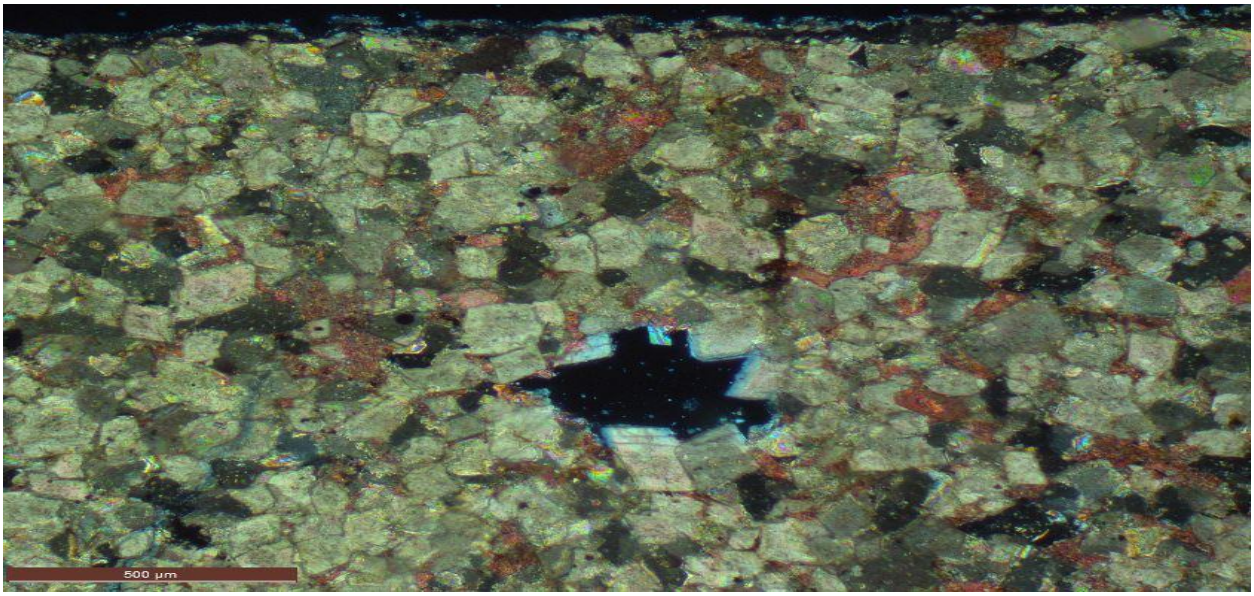

Figure 25. NDGS 15412. 10736.5ft. Dolomitized packstone showing a vug possible created by fossil fragment dissolution and recrystallization.

NDGS 15625 has no well log so it difficult to make a separation between the zones. This happened to be the deepest core interval (12685-12656) of the Birdbear in the study area and is mostly dolostone. Again like the previous Golden Valley county core, this core does not have abundant fossil fragments like the Billing County cores and less of dolomitization process and more of micrite. Another important observation in this core is the persistent anhydrites all through the 29 ft. core. Fractures, stylolites, pressure seams due to depth, recrystallization and vugs remain a common occurrence in this core interval. Highly porous as water poured on the core quickly drains. Most of the original rock is still in place with little evidence of dolomitization.

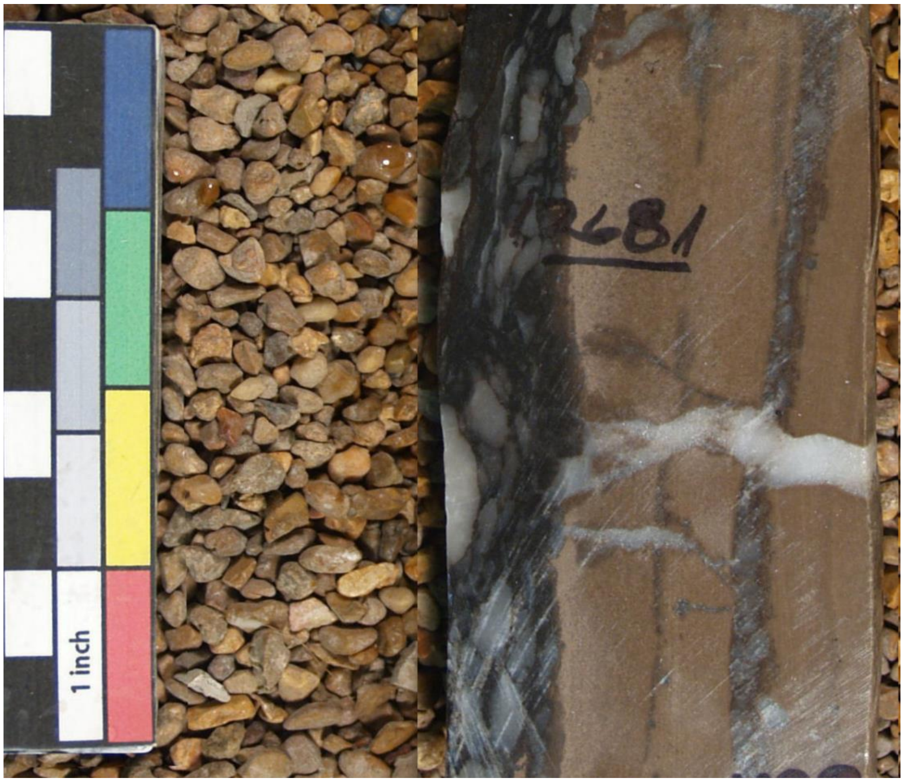

Figure 26. 15625. 12681ft. Anhydrites running through the core.

NDGS 15679 and 21734 are both Golden Valley cores that extends through most of the A zone and parts of upper B zone. Again abundant dolomitization and fewer fossil fragments but not enough to be called a biosparite like those in the Billings County. Different degrees of selective dolomitization, dolomitization fronts, fractures, stylolites, dissolution seams, dissolved fossil fragments, recrystallizations, vugs, dog-tooth spar, anhydrite and mostly highly porous are some of the attributes of this core. The rock type goes from limestone to anhydrite limestone, and from dolostone to dolomitic limestone depending on the percent composition of the different rock types. The areas with limestone is mostly in the upper A zone and dolostone are mostly at the lower B zone. The amphiporas were mostly observed in the lower B zone. Burrows are also a common feature. More images of the features of these cores will be in appendix II.

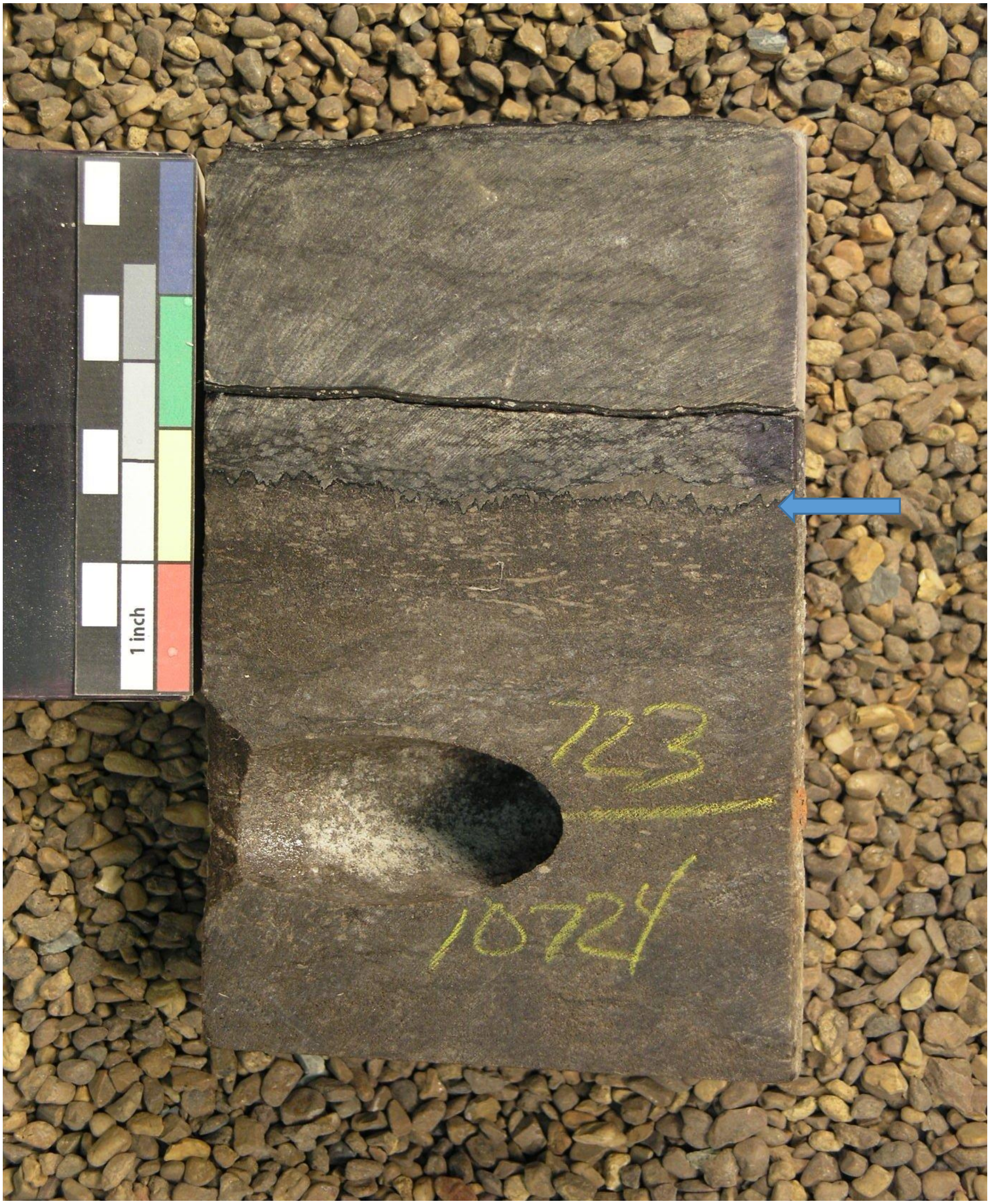

Figure 27. NDGS 15679. 10724-0ft. Contact between an upper limestone and lower dolostone.

Figure 28. NDGS 15679. 10742-3 ft. Highly fractured packstone.

2.1 Well Log Correlation

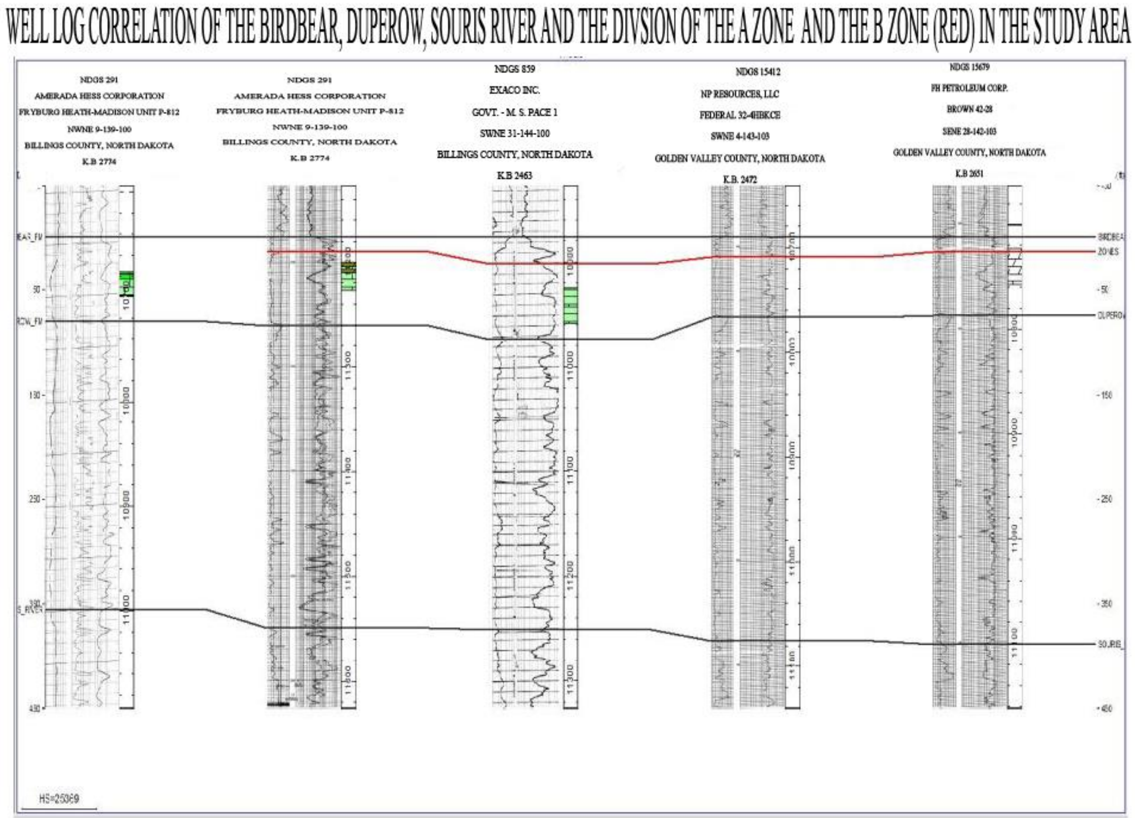

Figure 29. Cross-Section of the Study Area.

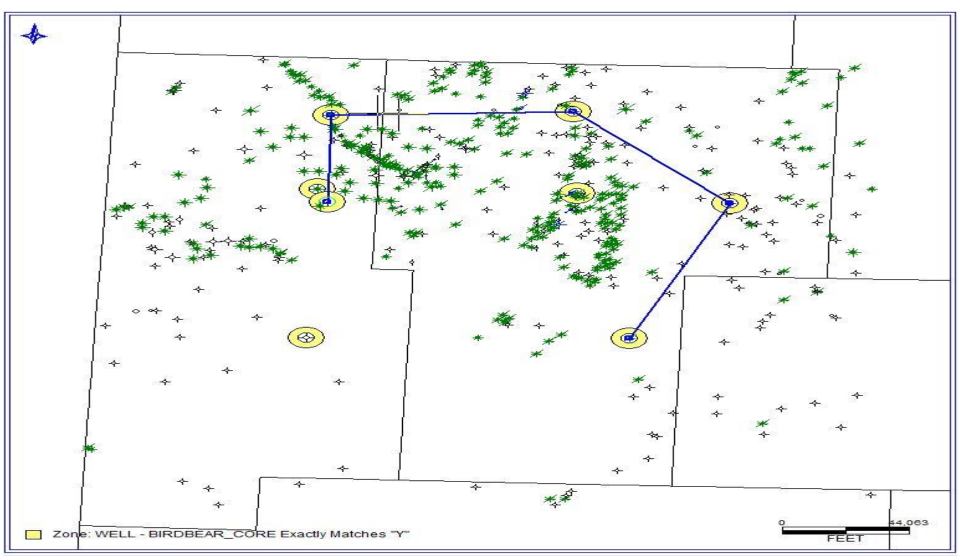

Figure 30. Cross-section and the sampled points in the study area.

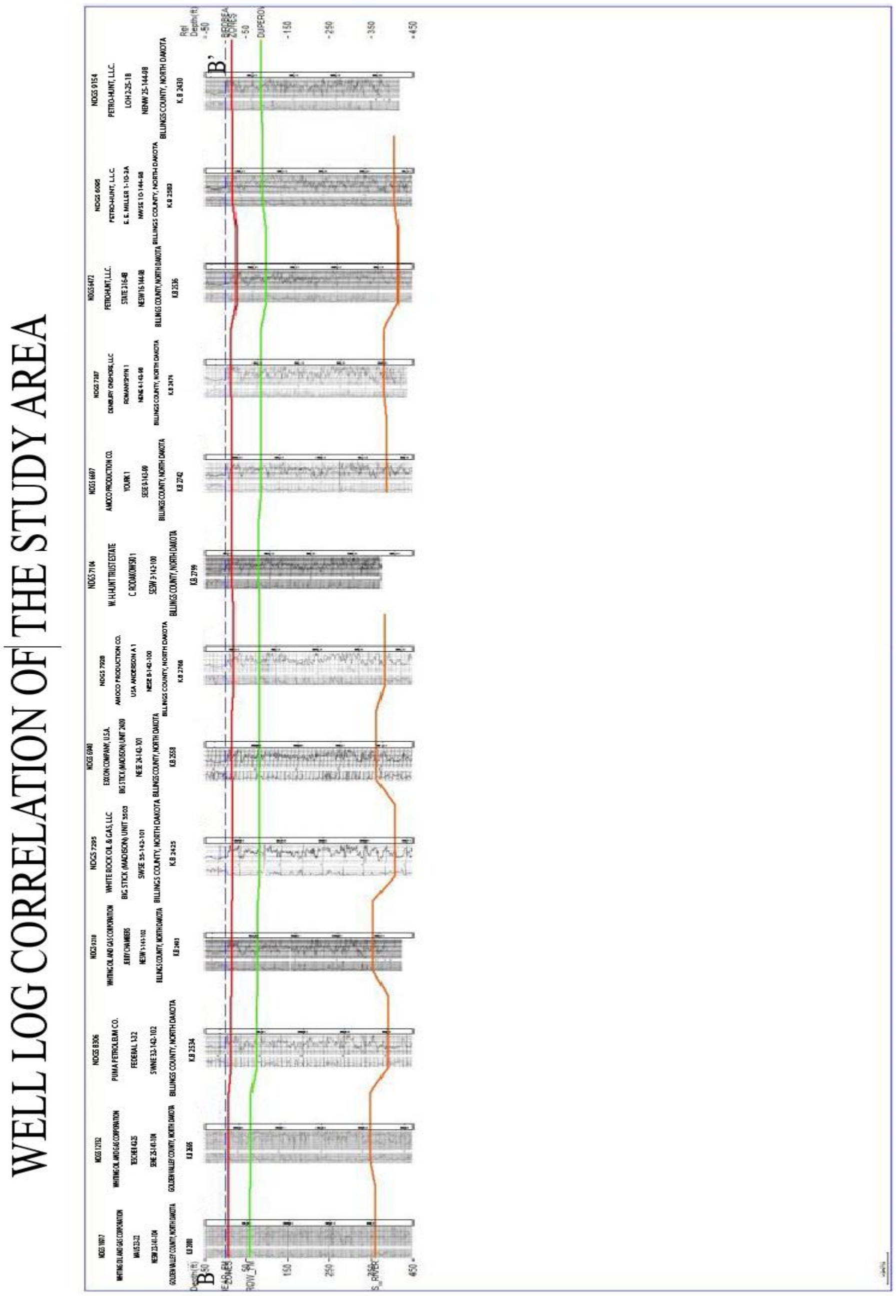

Figure 31. Cross-section of the study area.

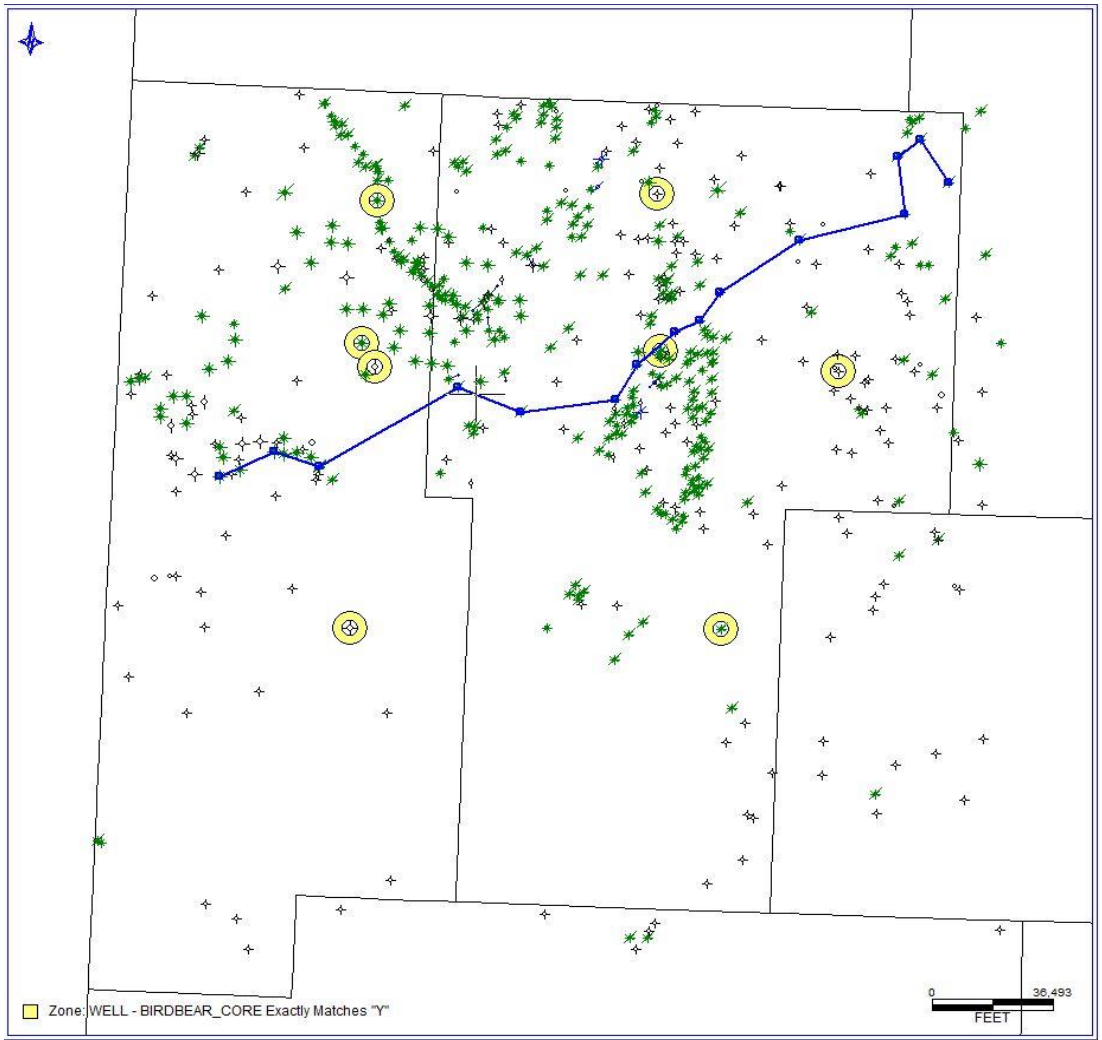

Figure 32. Points of cross-section.

CHAPTER III

DIAGENESIS

Diagenesis can be defined as the alterations that happened and changed the composition and texture of the sediment after the initial sediment has been deposited. The primary deposits include the initial porosity, mineralogy, and grain sized. This alteration can be physical, chemical, and biological. Diagenesis can destroy information about the primary features but can also leave behind vital information about the post-depositional history of the sediment.

Diagenesis in marine sedimentary rocks is divided into two stages: early and late diagenesis. The early diagenesis happens on the seafloor or happens close to the surface of the seafloor. The late diagenesis gives features of marine cements. Most diageneses in the Birdbear Formation occur in early diagenesis as seen by the common occurrence of dolomitization which is a product of the mixing zone.

Diagenesis can decrease or increase permeability and porosity, but mostly decrease them especially with time and depth. An understanding of the diagenetic processes, the processes that brought about them, the factors that affect porosity and permeability are very important in hydrocarbon exploration in a carbonate reservoir. The common diagenetic processes include cementation, dissolution, replacement, recrystallization, physical/mechanical and chemical compaction and fracturing. The Birdbear Formation has undergone significant amount of diagenesis that has affected its reservoir quality. In this chapter, we shall examine how diagenetic processes have affected the reservoir quality with the help of images gotten from thin section study using a microscope.

3.1. Composition and Classification of Carbonate Rocks

Carbonate sediments are produced at or near the site of deposition. The two main rock types found in this Formation are Limestone, $CaCO_3$, and Dolostone, ($CaMg(CO_3)_2$). Most of the shallow marine carbonate sediments are very unstable, especially aragonite and Mg-calcite. Calcite, Mg-calcite, aragonite, and dolomite are all stable under a shallow sea water. Longman, (1981) gave the characteristic of the most common carbonate minerals (Table 1) Limestone is made up of calcite, aragonite, which are either skeletal or nonskeletal constituents from a biochemical or chemical origin. Limestones mostly are characterized by the amount of grains, lime mud (micrite), cement and pores, (Leighton and Pendexter, 1962**), (**Table 2). Limestones can easily be affected by diagenetic processes such as solution, cementation, replacement and recrystallization. Diagenesis affects limestone in a way that most of the primary constituents can be lost giving rise to secondary characteristics. Mostly giving rise to dolomite constituents of limestone with an increase in diagenesis as seen in this study of the Birdbear formation. Folk (1959) attached the name interclasts to the detrital grains which are debris broken from pre-existing rocks. Skeletal grains are those from remains of hard parts of secreted by organisms like crinoids. Pellets are micritic and lack much of internal structures.

Limestone can also be looked at in terms of clastic and biogenic according to Dunham (1962). Below is Folk (1959) Figure 33, and Dunham (1962) Figure 34 classification schemes of carbonate rocks according to depositional Texture. These classifications are based on the percentage of mud content, and grain content as well as the fossil content.

Table 1. Characteristics of the Most Common Carbonate Minerals (Longman, 1981).

ARAGONITE ($CaCO_3$)	
CRYSTAL CLASS:	ORTHORHOMBIC
COMMON SHAPES:	PRISMS AND FIBERS
DIAGENETIC ENVIRONMENT:	MARINE TO HYPERSALINE
SPECIFIC GRAVITY:	2.95
VOLUME CHANGE: (WHEN NEOMORPHOSED TO CALCITE):	8% INCREASE (IN CLOSED SYSTEM)
MG-CALCITE ($Ca_{1-x}Mg_xCO_3$)	
CRYSTAL CLASS:	HEXAGONAL
MG CONTENT:	TYPICALLY 4 TO 18 MOLE PERCENT
COMMON SHAPE:	STEEPENED RHOMBS, FIBERS
DIAGENETIC ENVIRONMENT:	MARINE TO HYPERSALINE
VOLUME CHANGE: (WHEN NEOMORPHOSED TO CALCITE):	INSIGNIFICANT
CALCITE ($CaCO_3$)	
CRYSTAL CLASS:	HEXAGONAL
COMMON SHAPES:	RHOMBS, SCALENOHEDRA, EQUANT CRYSTALS
DIAGENETIC ENVIRONMENT:	FRESH WATER PHREATIC, VADOSE, SUBSURFACE
SPECIFIC GRAVITY:	2.71
DOLOMITE ($CaMg(CO_3)_2$)	
CRYSTAL CLASS:	HEXAGONAL
COMMON SHAPES:	RHOMBS, SUBHEDRAL EQUANT CRYSTALS
DIAGENETIC ENVIRONMENT:	VARIABLE, FRESH WATER TO HYPERSALINE
SPECIFIC GRAVITY:	2.85
VOLUME CHANGE: (WHEN NEOMORPHOSED TO CALCITE):	5 TO 13% (IN CLOSED SYSTEM)

Table. 2. Categories of Grain Types in Limestone (Leighton and Pendexter, 1962).

Major Categories	*Examples*
1. Detrital Grains	Rock fragments Intraclasts
2. Skeletal Grains	Crinoidal, Molluscan, Algal, Foraminiferal } Fragmental and Nonfragmental
3. Pellets	Fecal pellets Grains of micrite
4. Lumps	Composite grains Algal lumps
5. Coated Grains	Oölites and superficial oölites Pisolites Algal- or foraminiferal-encrusted grains

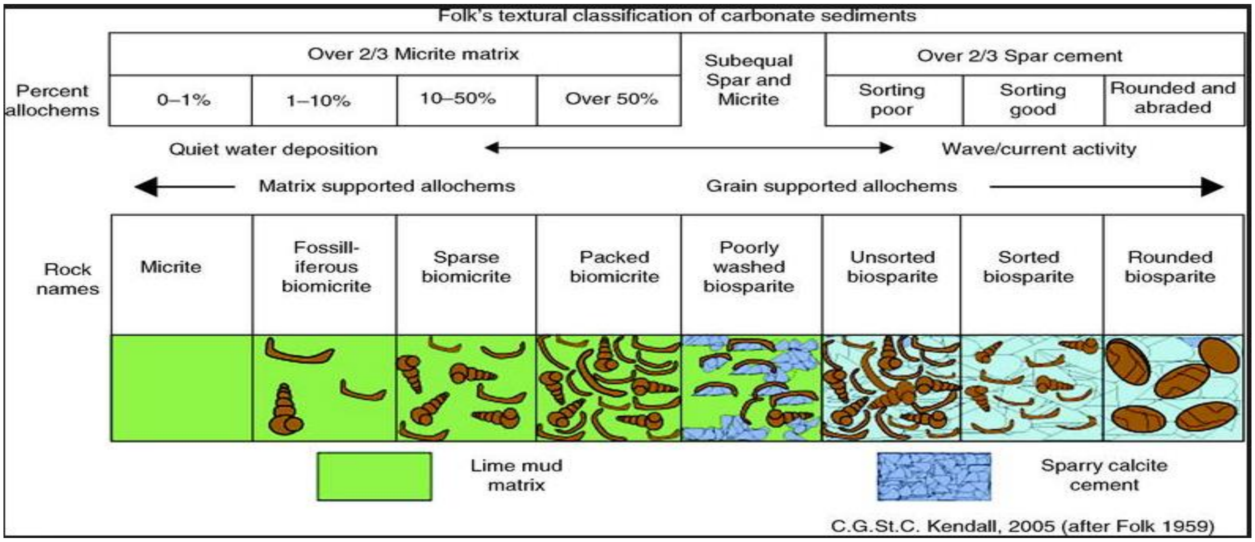

Figure 33. Folk's Classification of carbonate rocks (modified from Folk, 1959).

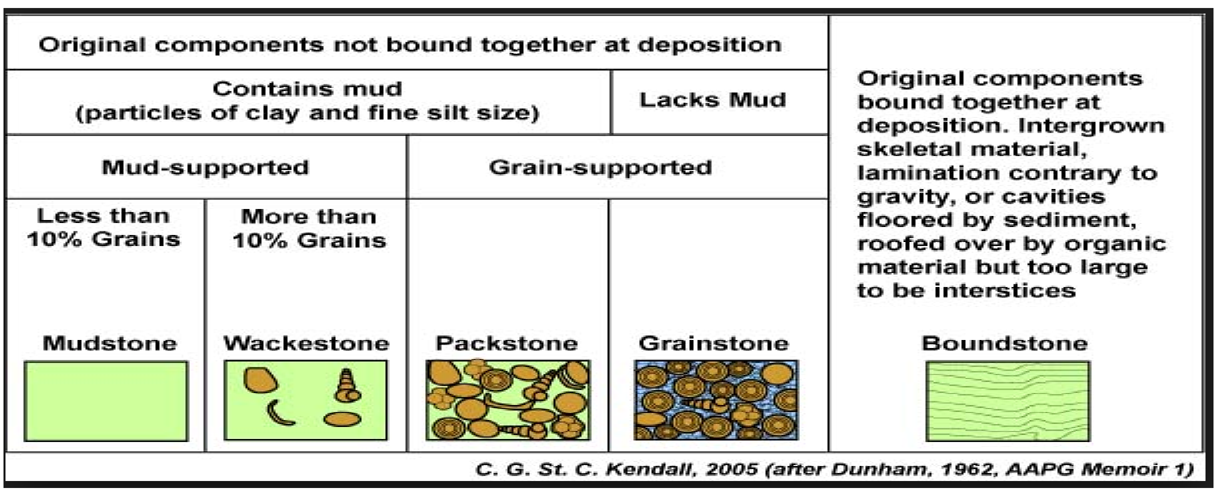

Figure 34. Classification of carbonate rocks according to depositional texture (modified from Dunham 1962).

3.2. Diageneses Environments

Diagenetic environment can be defined as the region in the subsurface where fluid movement, chemistry, nature of the host rock and other factors produce a pattern of diagenesis. All the diagenetic processes that occurred in the Birdbear formation can be used to identify its environment. Interpreting a diagenetic environment can be very complicated due to the abundant diagenetic environments and the different textures and characteristics that they produce. We will attempt to reconcile the numerous diagenetic processes that have been observed in this study and its possible diagenetic environment.

A typical marine sediment during sea level lowering has a sequence that moves from the marine phreatic zone through the mixing zone into the meteoric phreatic and finally into the vadose environment, and the sequence reverses during transgression (Longman, 1981).

The **Marine phreatic zone** represent a zone where all pores in the sediment are filled with normal marine water. Marine **cementation** is common in this zone.

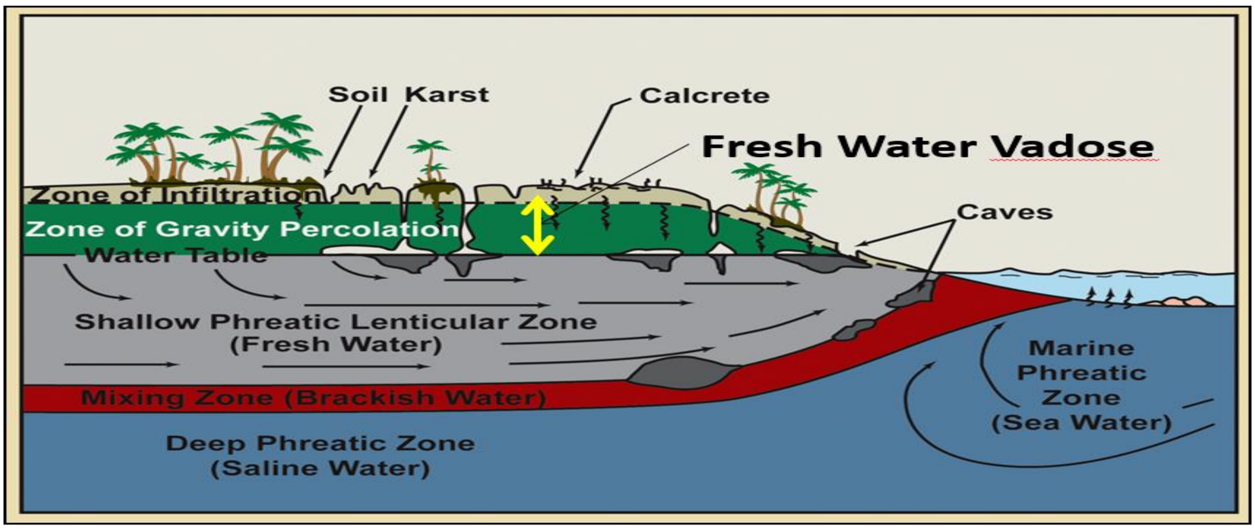

Figure 35. The major subdivisions of a coastal meteoric diagenetic zone. Redrawn from James and Choquette (1984).

The **Freshwater phreatic zone** lies right above the mixing zone and below the water table and the vadose zone. It has all its pore spaces filled with fresh water, mostly meteoric water. Climate and the nature of rainfall is a very important controlling factor in this zone. Common here are both dissolution**s** of fossil fragments that creates secondary porosity as well as cementation by calcite. This zone is very complex because of the different paths of fluid migration, and levels of saturation. Longman 1981 gave five subdivisions of the Freshwater phreatic zone and its characteristics.

Table 3. Idealized Zonation in the Freshwater Phreatic Environment Based on the Assumption that Saturation of Water with Respect to CaCO3 Increases as the Eater Moves Downward. (Longman 1981).

INCREASING SATURATION WITH $CaCO_3$ / INCREASING DEPTH ↓	ZONE	CHARACTERISTICS
	1. ZONE OF SOLUTION OF CALCITE AND ARAGONITE.	FORMATION OF VUGGY AND MOLDIC POROSITY.
	2. ZONE OF SOLUTION OF ARAGONITE.	FORMATION OF MOLDIC POROSITY
	3. ZONE OF ARAGONITE SOLUTION AND CALCITE PRECIPITATION	RAPID NEOMORPHISM OF ARAGONITE GRAINS TO EQUANT CALCITE. CEMENTATION BY EQUANT CALCITE.
	4. ZONE OF NO SOLUTION. PRECIPITATION OF CALCITE.	RAPID CEMENTATION BY EQUANT CALCITE.
	5. STAGNANT ZONE, SATURATED WITH $CaCO_3$	LITTLE OR NO CEMENTATION. SLOW NEOMORPHISM OF ARAGONITE GRAINS WITH PRESERVATION OF SOME STRUCTURES.

Vadose Zone: This environment is lying above the water table with most or all pores filled with water and air. This zone is prone to occasional wetting during rain with much dissolution occurring there. Figures 36 shows the different environments of daigenesis and its associated features.

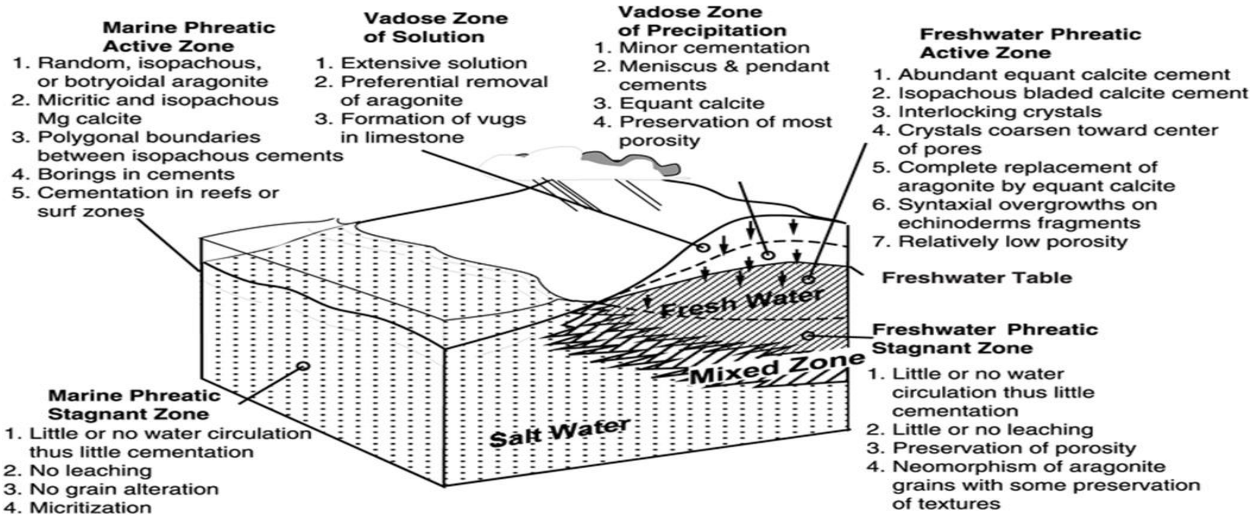

Figure 36. Diagenetic environments and associated features. Beaumont and Hartmann (1999)

The Birdbear Formation is typically deep as far as subsurface depth is concerned. Longman (1981) in his work on the “Carbonate Diagenesis as a Control on the Stratigraphic Traps (with examples from Williston Basin)”, noted nine major diagenetic events that occur during deep subsurface diagenesis: (1) sediment compaction and fluid expulsion; thermal maturation of some minerals and organic material; (3) Stylolitization, (4) dolomitization, particularly along faults and reef margins; (5) calcite cementation, often in proximity to stylolites; (6) fracturing; (7) dolomitization and neomorphism along stylolites; (8) creation of secondary porosity; and (9) oil migration.

3.3. Porosity

Preservation of porosity is very important in hydrocarbon exploration in a carbonate reservoir. At the time of deposition, the porosity is high but with diagenesis, most of the primary porosity is lost. Secondary porosity forms from the diagenetic modifications of the original sediments from the movement of fluids in the pore spaces. Some of the factors that reduce porosity are compaction, early cementation, subsurface cementation, stylolitization. The combination of cementation, leaching, recrystallization, mineralogical stabilization and replacement can provide numerous possible diagenetic paths. Facies which have initial low permeability may be made more permeable through dolomitization or leaching (Scholle, 1979). This study shall attempt to look at some of the factors as it affects porosity. Few images will be used as examples in this section.

3.4. Dolomitization

Dolomite ($CaMg(CO_3)_2$ is a carbonate with calcium and magnesium occupying preferred positions having a rhombohedral shape (Figure 38).

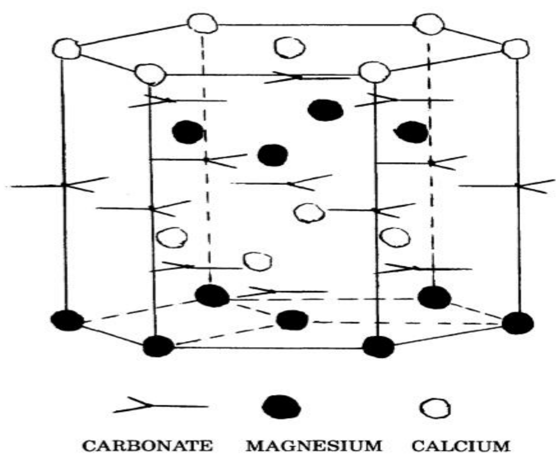

Figure 37. Schematic representation of the crystal structure of dolomite showing the alternation of cation and anion (carbonate) planes, and the alternation of calcium and magnesium planes. (Lynton S. Land, 1982)

3.5. Dolomitization Mechanism

Dolomitization is a selective process where finer carbonate materials like mud are replaced by minerals like crystals.

Dolomites forms by replacing an original carbonate. This happens when fluid imports Mg^{2+} and dissolves the original carbonates, precipitates dolomite and exports Ca^{2+}. The new dolomites nucleate from solution as primary sediment or it will precipitate into pores as cement.

Most models of dolomitization are hydrologic and need the movement of fluid through rocks and a large source of magnesium. Different models of dolomitization models that have been proposed including (1) The Reflux model, (2) the Meteoric Mixing Model, and (3) the burial Diagenesis. (4) Primary precipitation (5) solution-cannibalization (6) subsurface brines and so on. All models have an argument but none is so certain. Figure 38. shows the common dolomite textures exhibited by dolomite.

The Birdbear Formation has witnessed abundant levels of dolomitization and it will be right to see how much this dolomitization has affected the porosity of this formation. They seem to be an argument on how much dolomitization is necessary for good porosity and permeability. In his work to relate the effects of dolomitization with porosity, Wardlaw (1979), noted that the initial stage of dolomitization of between 50 to 70 percent dolomite content, shows the porosity of the host rock to remain the same or only show slight decrease, but with higher dolomite content or dolomitization, the porosity and permeability will show an abrupt increase. But Longman M.W (1982) noted that only intermediate degree of dolomitization is sufficient as too much dolomitization will produce tight dolomites and little will produce scattered dolomite rhombs.

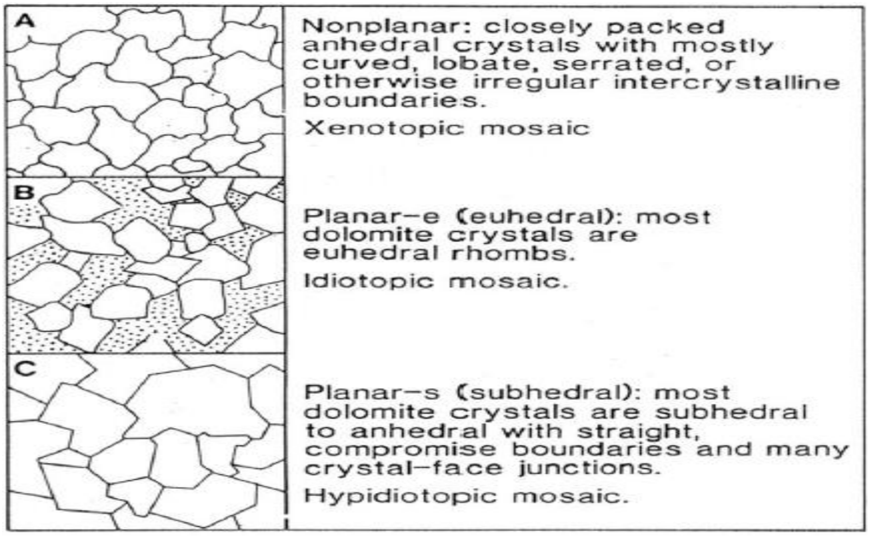

Figure 38. Three common dolomite textures. (A) Non-planar crystals in a xenotopic. (B) Planar-e crystals (e for euhedral) in an idiotopic mosaic. (C) Planar-s crystals (s for sunhedral) in a hypidiopic mosaic. After Sibley & Gregg (1987).

Between the marine phreatic and fresh water phreatic environment is the brackish water which results from the mixing of waters of both environments. The most interesting diagenetic process taking place in the mixing zone is dolomitization but not all mixing zone forms dolomite (Longman, 1981). Dolomitization process requires an abundant supply of magnesium, so if there is a limited supply of magnesium in the mixing zone, we can end up having partial dolomitization and this can account for partial dolomitization in some parts in the study area. The dolomitization is the major source of porosity and permeability in the study area as seen from thin section sections.

Naturally, dolomites have more porosities and permeability because of the differences in sizes, shapes as well as the way the crystals are arranged. Dolomites have a coarser grain size than limestone. These dolomites are better reservoir rocks than most limestones. It should also be noted that it’s not all rocks that have high porosities and permeability will have high hydrocarbon recovery. The study area is highly dolomitized with some areas showing selective dolomitization due to different the prevailing rock type as some are more resistant to dolomitization than others. Others show invasive dolomitization. Some units reveal a well-defined dolomitization front. The dolomitization gives rise to intercrystalline porosity, intergranular porosity, and sucrosic texture. Planar-e and planar-s textures are very common.

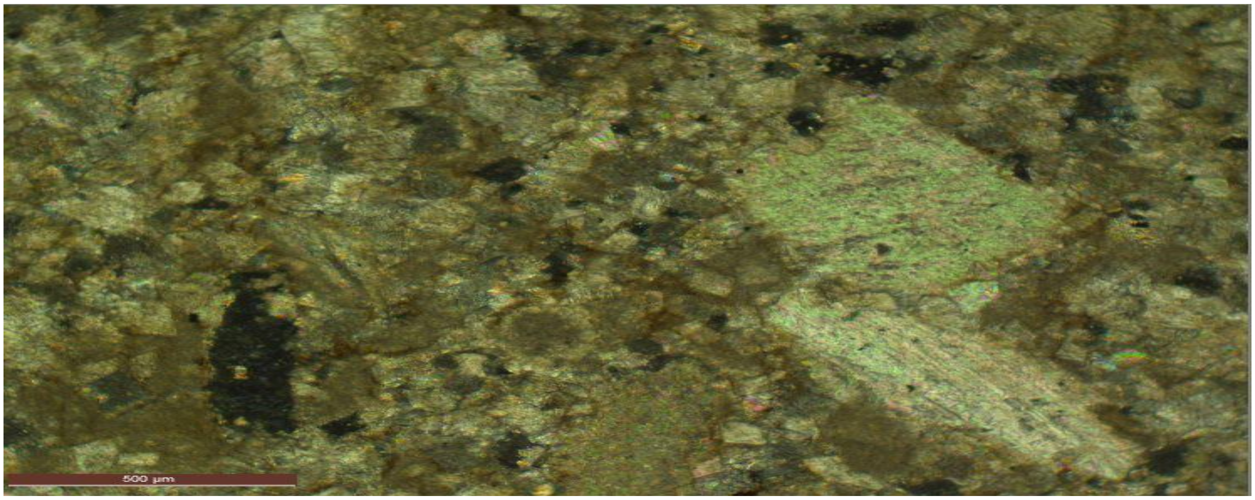

Figure 39. NDGS 291. 10689 ft. Thin section photomicrograph showing a partially dolomitized packstone. Punctuate wall of brachiopod stem on the right.

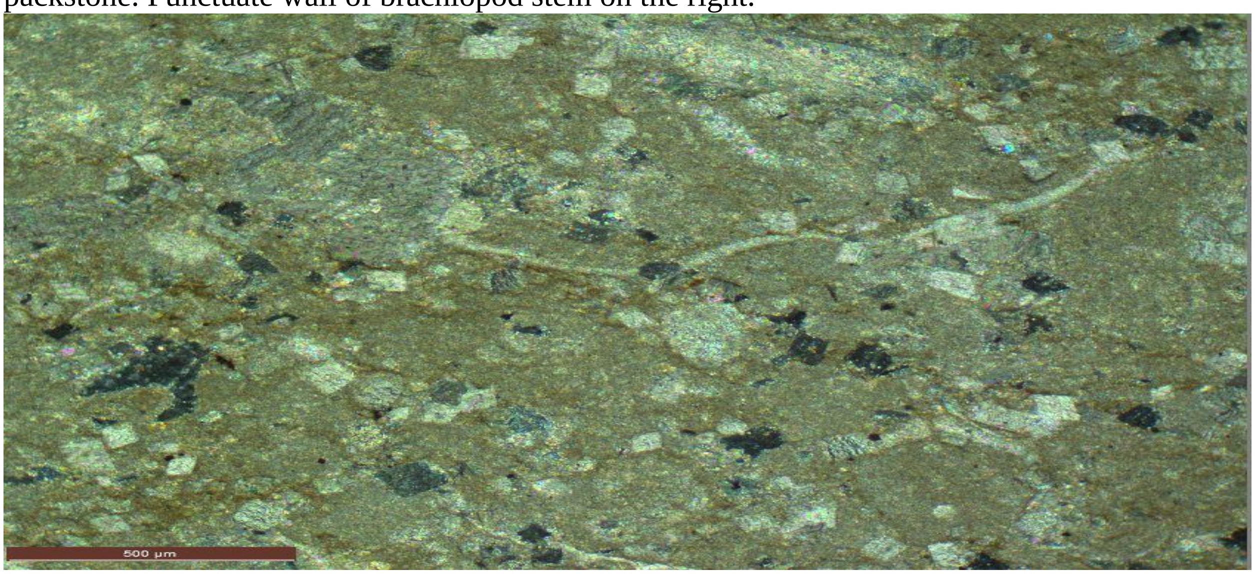

Figure 40. NDGS. 291 10957.95 ft. Thin section photomicrograph the Packstone shows dolomitization process with lots of the original micritic limestone still in place.

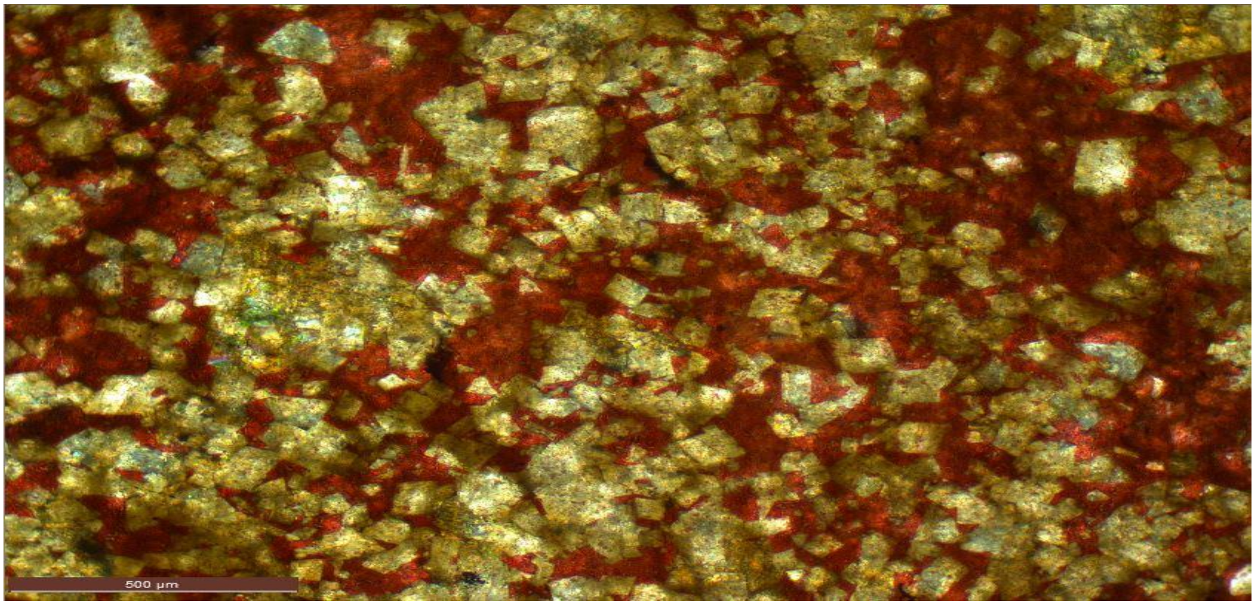

Figure 41. NDGS 15412. 10689.2 ft. Thin section photomicrograph of a packstone. Dolomite crystals from dolomitization showing different dolomite textures and the red stain showing the porosity. The red stains show the porosity developed by the process of dolomitization.

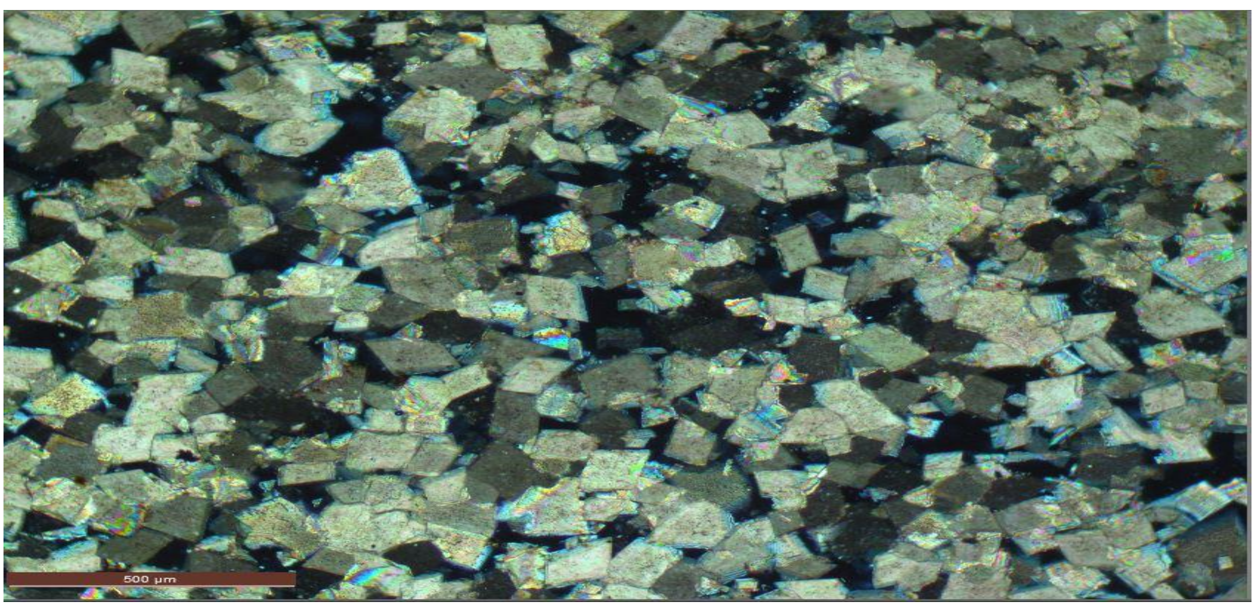

Figure 42. NDGS 15412. 10710.9 ft. Thin section photomicrograph sucrosic structure with euhedral texture of dolomite showing a well-dolomitized layer with intercrstalline porosity. The well-dolomitized zones in the Birdbear can be said to be the most porous.

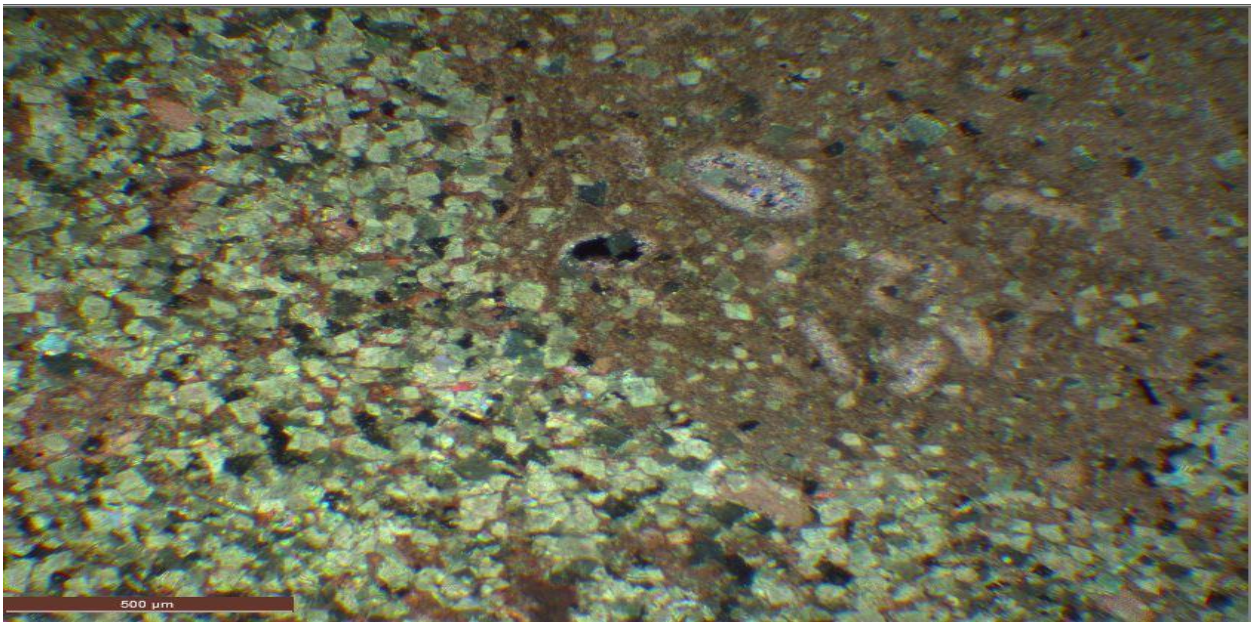

Figure 43. NDGS 15412. 10736.5 ft. Thin section photomicrograph showing a dolomitization front or selective dolomitization. The less dolomitized maybe as a reason of a more resistant material than the dolomitized area.

3.6. Cementation

Chemical precipitate fills in spaces within or between grains. This is a case whereby the open pore spaces created are being filled with precipitated materials. Calcite cement is the most common cement found in carbonate rocks and can assume different shapes like rhomb, coarse blade, radial-fibrous crust, poikilotopic crystals or equants crystals. Cementation is a common process that is common within the marine phreatic zone, especially in the marine active zone and less in the marine phreatic stagnant zone. Cementation mostly occurs on steep slopes or in a shoreface environment like around sediment/water interface. The Birdbear has a lot of cementation processes going on, and these could only be in a marine phreatic (active) zone.

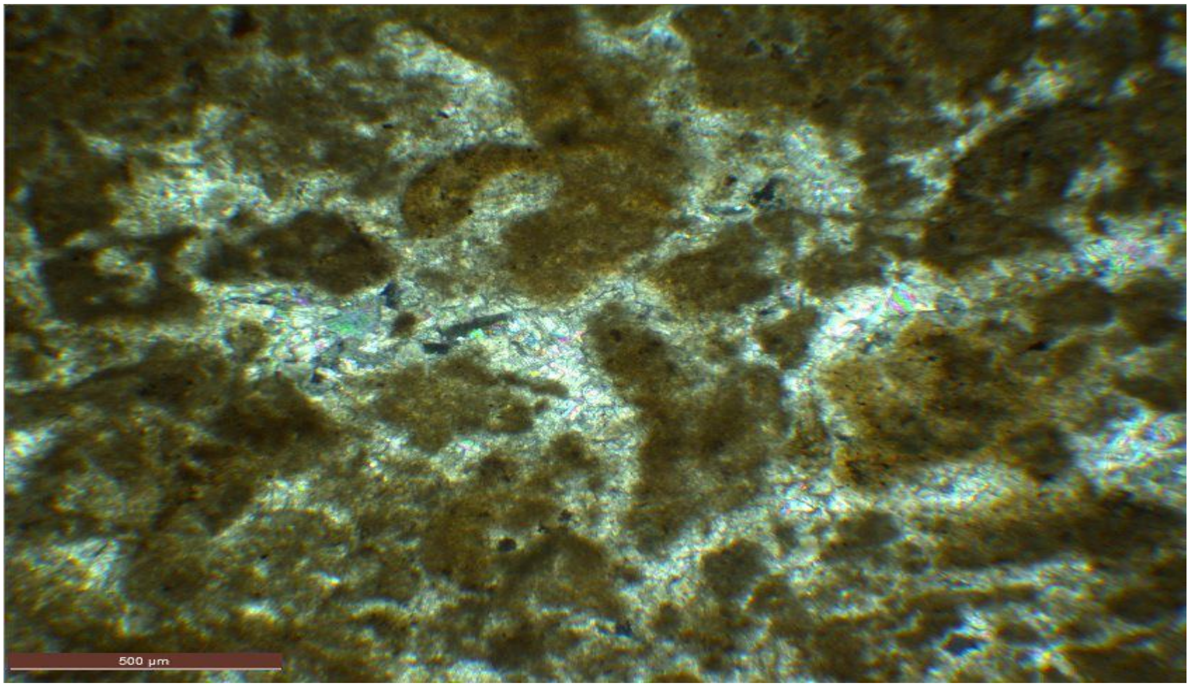

Figure 44. NDGS 15679 10708.9-9.2 ft.. Isopachous cement typical of a marine environment. The calcite cements uniformly close up and reducing the porosity of the reservoir.

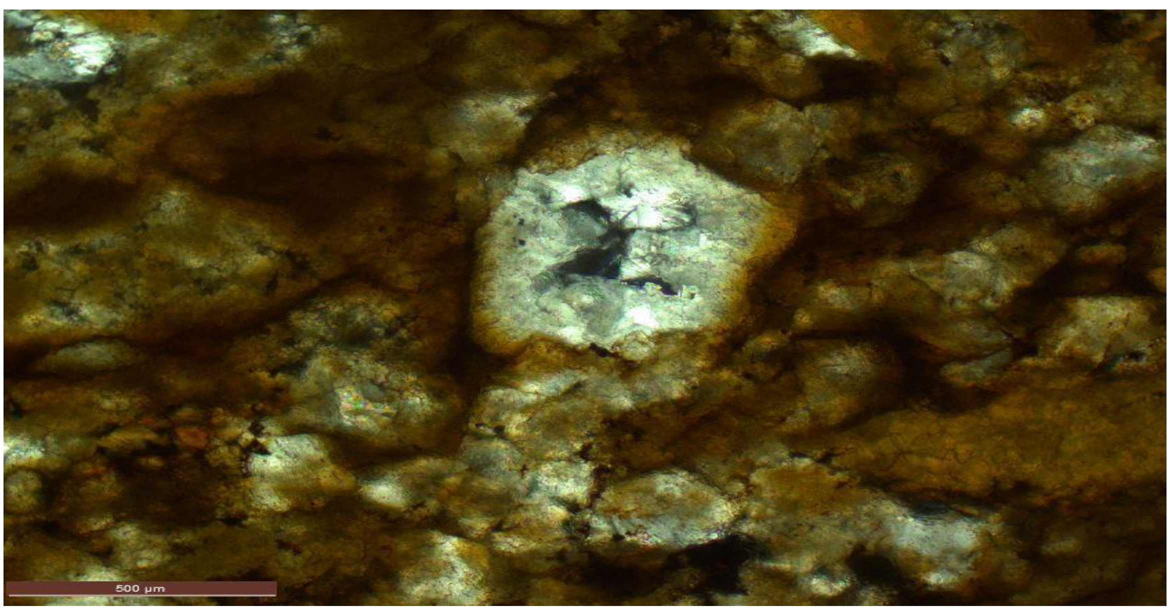

Figure 45. NDIC 15679. 10723-4 ft. Calcite cements growing from the probably dissolved fossil fragments the calcite cement almost closing up the pore space.

3.7. Fossil Fragment Dissolution

This involves the leaching out of unstable minerals thereby giving rise to vugs and secondary porosity. Original aragonites are most often leached. Most dissolutions in the Birdbear Formation were formed by the dissolution of fossil fragments. Most dissolution occurs after deep burial and along stylolites. The vadose zone which lies below the land surface and right above the water table is a zone that is characterized diagenetically by dissolution and removal of aragonite. This is done by solution and precipitation. Pendant cement and equant calcite is another feature of this zone. The Birdbear Formation contains a lot of dissolved fossil fragments. As a matter of fact, dolomitization and fossil fragment dissolution are the major factors responsible for the porosity and permeability in the Birdbear. These dissolutions form vugs in the formation. The vugs add to the porosity as well as the dolomitization.

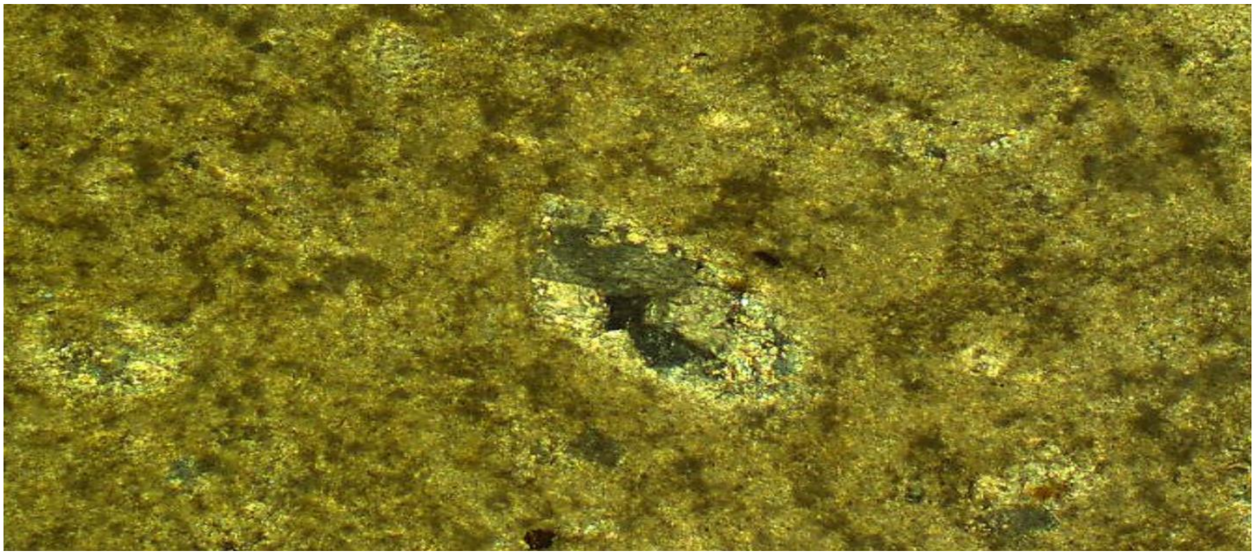

Figure 46. NDIC 291, 10690 ft. Dissolved aragonite shell with calcite precipitation in the center causing biomoldic pores. Equant calcite cementation gradually closing in the vug that has been created.

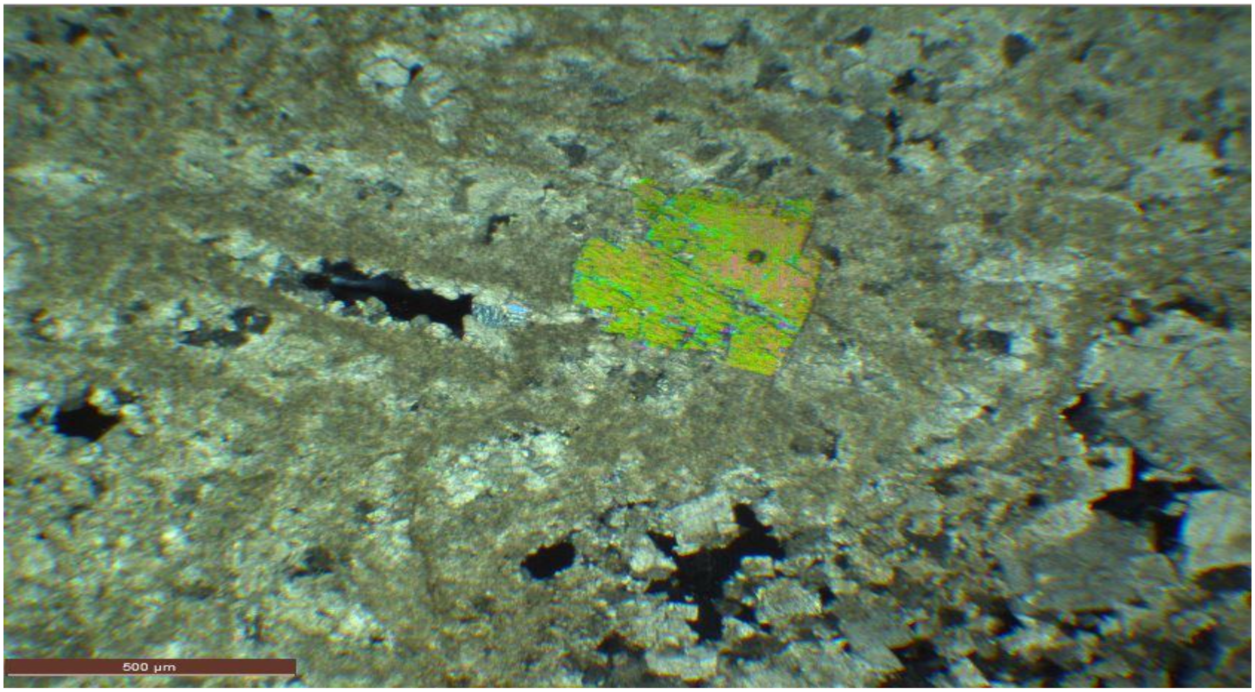

Figure 47. NDGS. 859. 10928-929 ft. Packstone Biomoldic pores as a result of leached fossil fragments and dolomite cements.

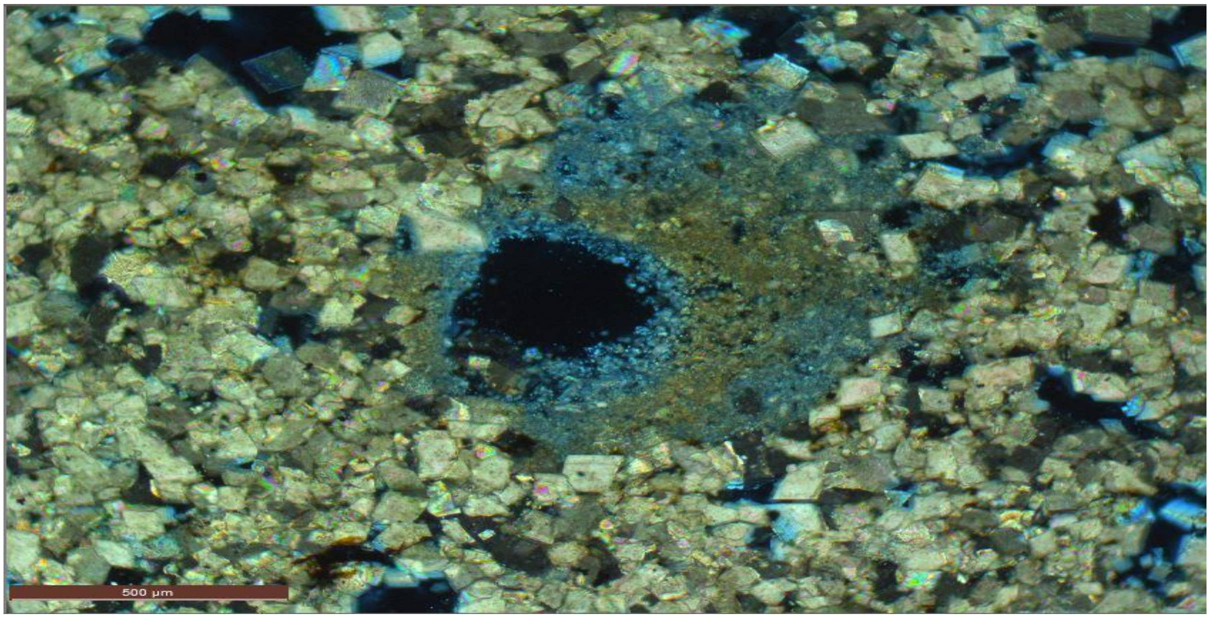

Figure 48. NDGS. 15679. 10730 ft. Thin Section of marine cementation (center) illustrating intergranular cementation. The vugs caused by dissolution can be seen recrystallizing.

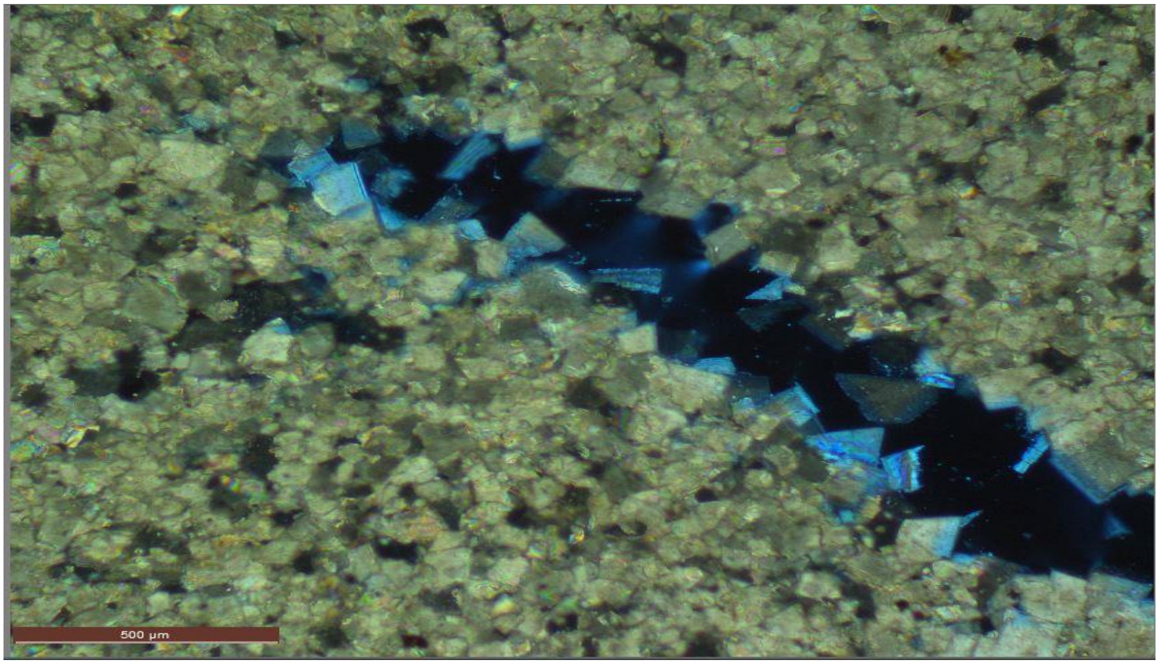

Figure 49. NDGS. 15679. 10736 ft. Coarse crystalline dolomite with interlocking crystals. Around the nuclei is a replacement of the original limestone by dolomite and hollow probably caused by leaching of fossil fragment shows calcite overgrowth by precipitation.

3.8. Physical / Mechanical Compaction

The Birdbear shows a lot of diagenetic attributes that are due to physical compaction. This is not surprising going by the fact that the Birdbear is found at a considerable depth. The overburden acts on this formation giving rise to compactions as well as subsurface fluid migration. These are shown by fracturing and compressing of fossil fragments, alignment of grains in a particular orientation, and dewatering. The type of rock is also a function of the compaction as it has an effect on the destruction of porosity. So dolomites are more difficult to destroy than limestones. Good porosity is present in the deeply buried dolomites in the Williston Basin (Longman, 1981).

From thin sections examined in this work, evidence of mechanical compaction are visible from the fracturing of the fossil fragments.

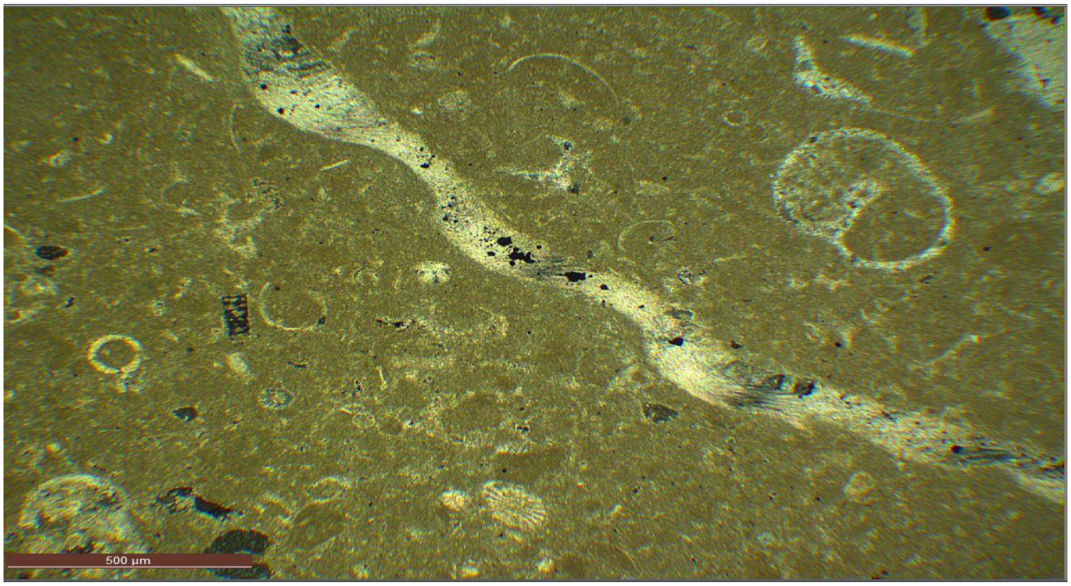

Figure 50. NDGS. 291. 10588.8 ft. Thin section photomicrograph of Wackestone with fossil fragments like echinoids, gastropods, bryozoan, and broken bivalves. It's very important to note that most mechanical evidence happens at great depths in the subsurface as a result of the pressure of overburden.

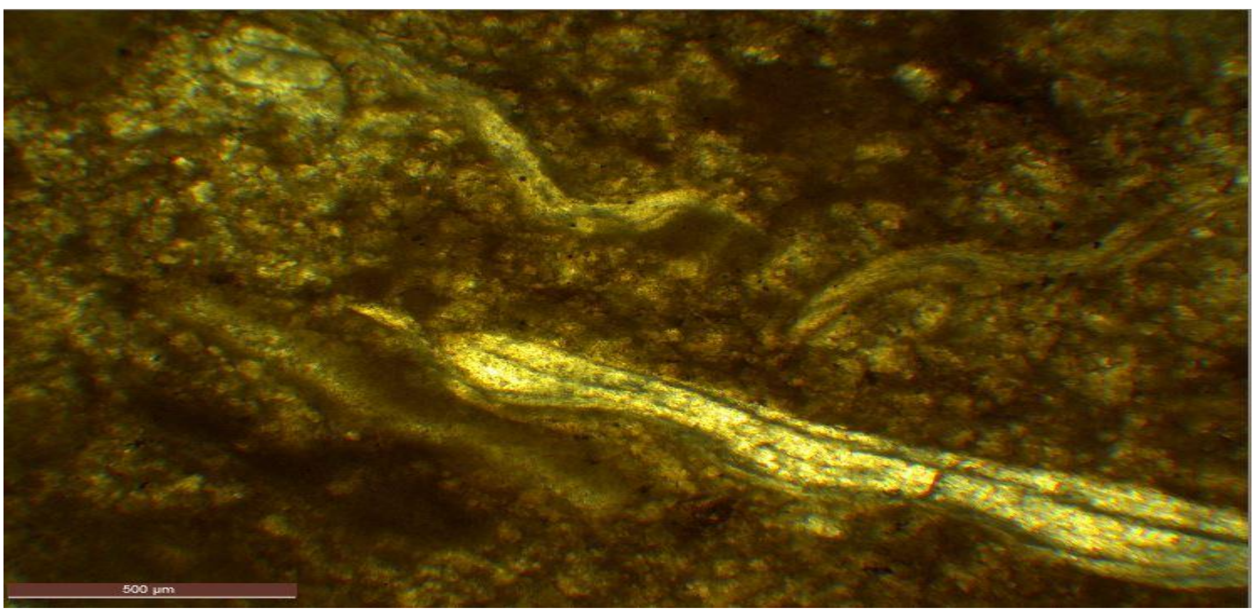

Figure 51. NDGS. 291. 10689.5 ft. Thin section photomicrograph Wackestone with a broken brachiopod stem as a result of the mechanical compaction process.

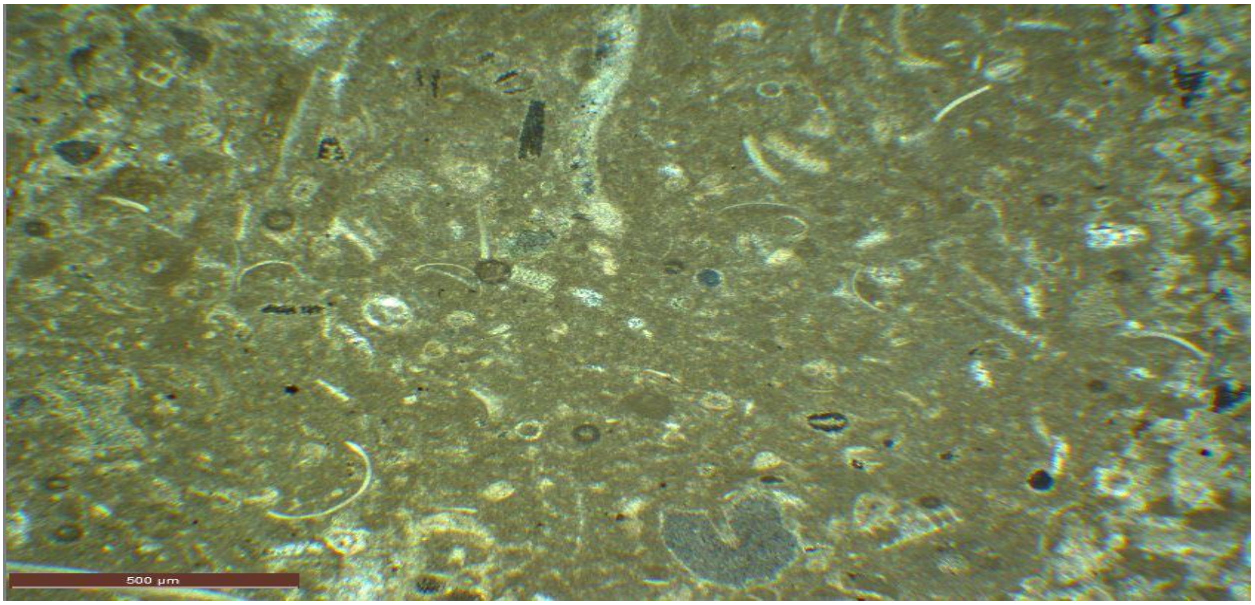

Figure 52. NDGS 859. 10925-26 ft. Packed biosparite showing abundant fragmented fossil fragments.

Going by the depth at which the Birdbear Formation is found, compaction is a common as seen from its effects on the fossil fragments. The type of rock could be a significant factor on the porosity but the porosity in dolomites are less destroyed than in limestone (Longman 1981). This can explain to us why the deeply buried dolomite found in this Formation still retains an appreciable porosity.

3.9. Chemical compaction/Stylolitization

Chemical compaction includes dissolution seams, stylolites and solution seams.

STYLOLITIC: This is porosity that occurs along a pressure solution seam. Stylolites can have a significant porosity that is essential for hydrocarbon exploration. Most stylolites are associated with fractures making stylolites very important diagenetic process.

Stylolites generally occur at a high depth like as seen with mechanical compaction, but this is more chemical in nature. There is no agreed depth at which stylolites typically occur but it is accepted that at depths, large volumes of rock dissolves and the dissolved material are squeezed from the rocks, sometimes through zones of weakness like faults and fractures.

Stylolites are very common in this study area and mostly found at depths of at least 10,000 ft.

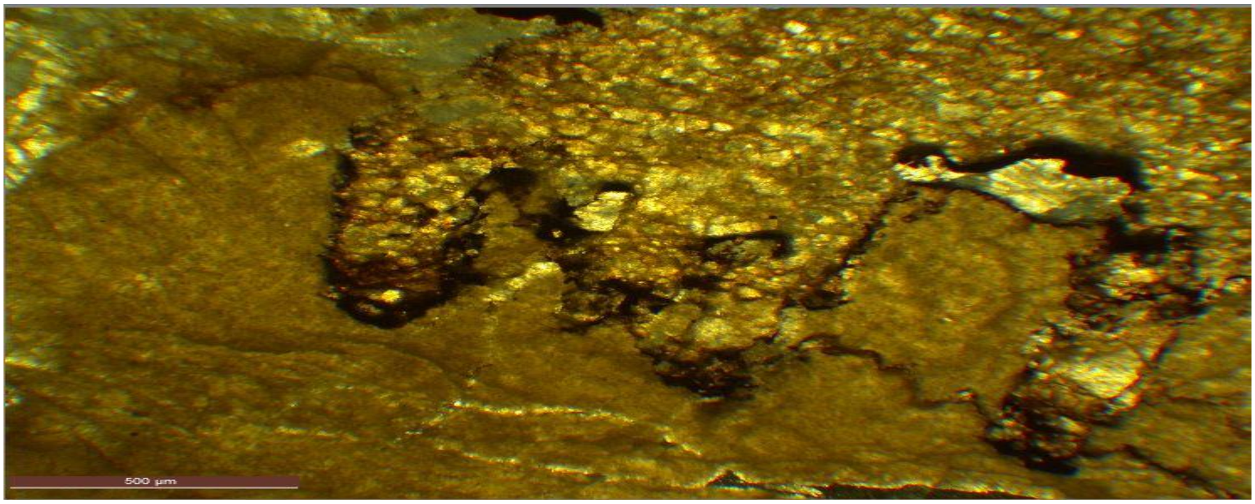

Figure 53. NDGS 291. 10693 ft. Thin section photomicrograph stylolites separating a dolomitized zone from undolomitized zone. The rock materials above are more prone to dolomitization than the ones below and could have resulted to a zone of weakness like a fault from where the dissolution seam precipitate out solutions to form the stylolite.

Stylolites can be useful in providing a part for the migration of hydrocarbon, and creating fractures.

3.10. Fractures

Fractures in the Birdbear Formation can be attributed to the dissolution of the underlying Prairie salt and is instrumental to the formation of the Birdbear reservoir, Swenson (1967). Fractures were observed in the study area, some running extensively. These fractures are also conduits for the migration of hydrocarbon and other fluids in the reservoir. We can say it is another source of porosity in the reservoir.

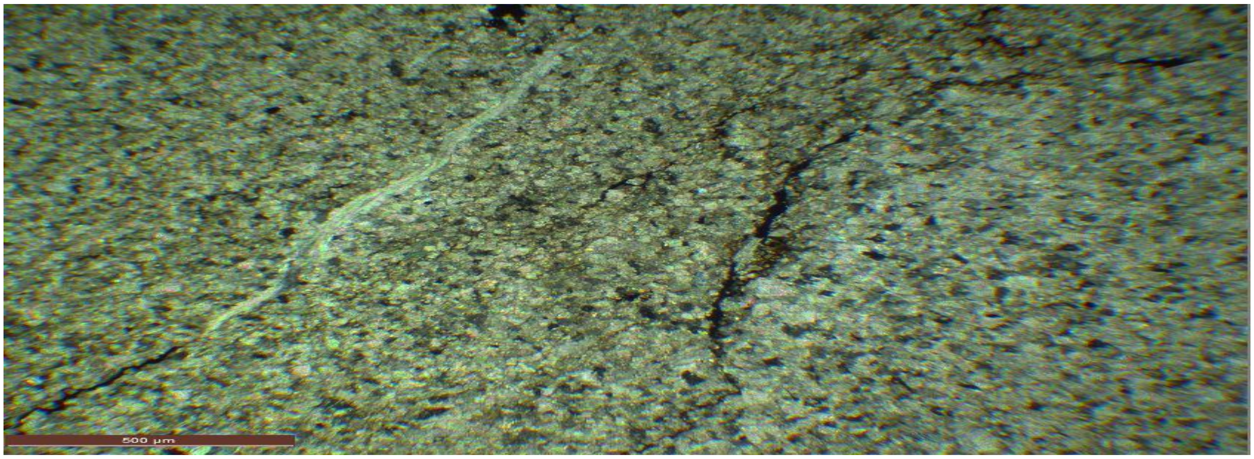

Figure 54. NDGS. 859. 10920-21 ft. Thin section photomicrograph of finely crystalline dolomite with faults. Such fractures can act as a conduit for migration of hydrocarbon.

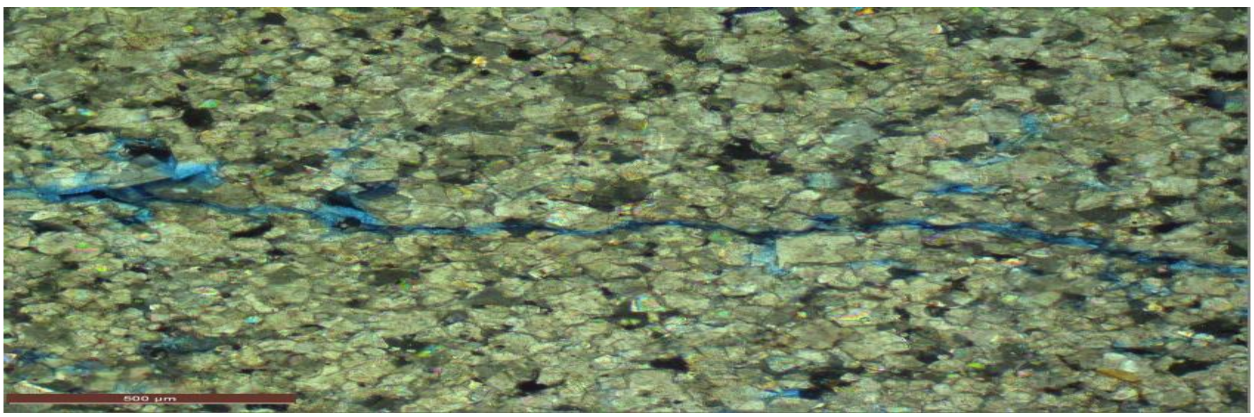

Figure 55. NDGS. 15412. 10716.8 ft. Thin section photomicrograph fractures highlighted by the blue stain.

3.11. Recrystallization/Calcification

This is a change from micrite to microspar. A process where calcite grows to form larger crystals. It is a change in crystal size or geometry without changing the mineralogy.

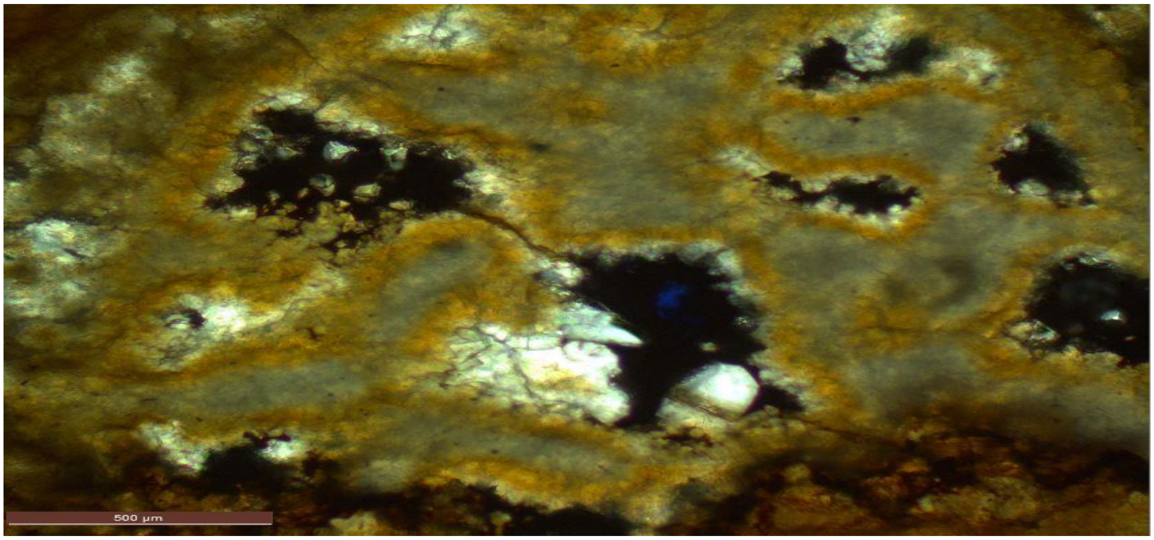

Figure 56. NDGS. 15679. 10723-4 ft. Recrystallization forming calcite cements growing from the dissolved fossil fragments.

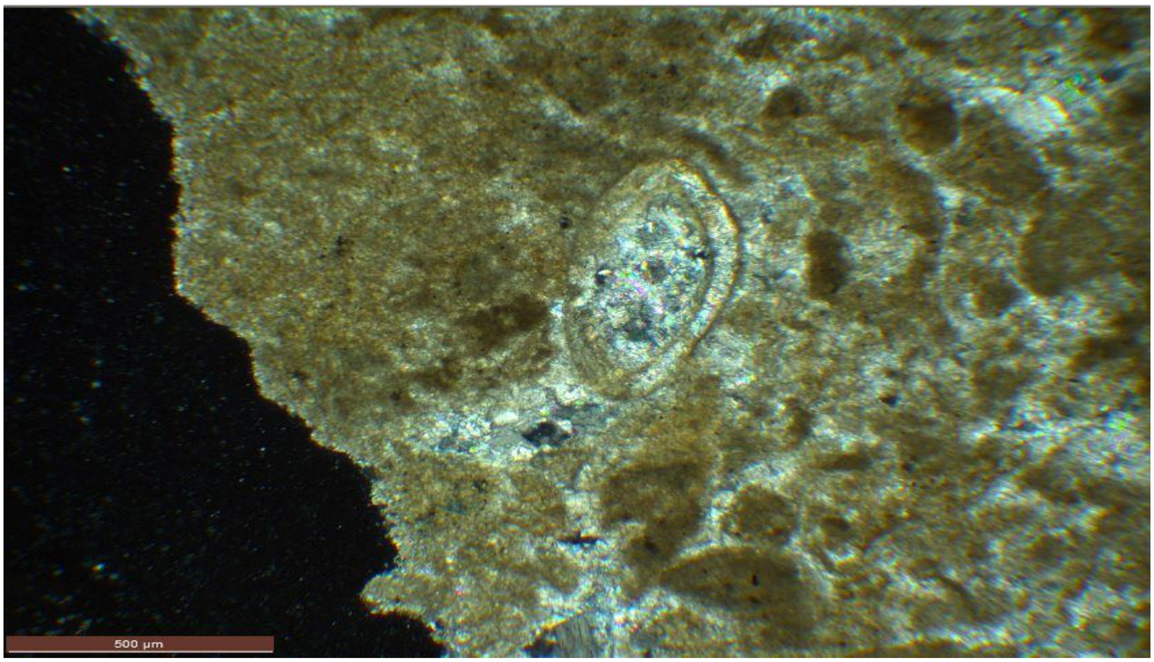

Figure 57. NDGS. 15679. 10708.9-0.2 ft. The bivalve here has been leached and then being recrystallized by dolomite calcites. The outline can only be seen by the micrite envelope.

CHAPTER IV

RESERVOIR CHARACTERISATION

In an attempt to establish the potential characteristic of the reservoir of the Birdbear formation, an emphasis was laid on the porosity and permeability. Using Petra, the tops of five hundred and forty wells were picked. This was done using the gamma ray logs which easily pick the boundary between the Three Forks and the Birdbear Formation. Also picked is the anhydrite interval which is within the A zone. This is indicated by the points where the density porosity goes off the scale. After picking the tops, Petra was again used to digitize about 300 wells. The data from the digitized tops was imported into excel spreadsheet. The thickness of the Birdbear and the anhydrite were calculated. The average value for each thickness and the tops of the well were calculated and plotted using Surfer software. The plot gives a picture of the behavior of each of the parameter across the study area. The Birdbear formation has an average thickness of 75 ft. and an average depth of 10725 ft. across the study location. The anhydrites has an average thickness of about 24 ft. across the area.

The neutron log is used to measure the hydrogen concentration in the formation while the density log is a measure of the electron density of the formation.

The average neutron porosity in the Billings County is 1.1% and 3.0% in the Golden Valley County. The average density porosity in the Golden Valley is -0.135%. Combined average neutron porosity for the counties is 1.9% and the combined density porosity for both counties is -0.31%.

From the limited NDGS well file, the permeability in the Golden Valley averaged 37k.air md, and is far better than those in the Billings County which averaged 0.43 k air md.

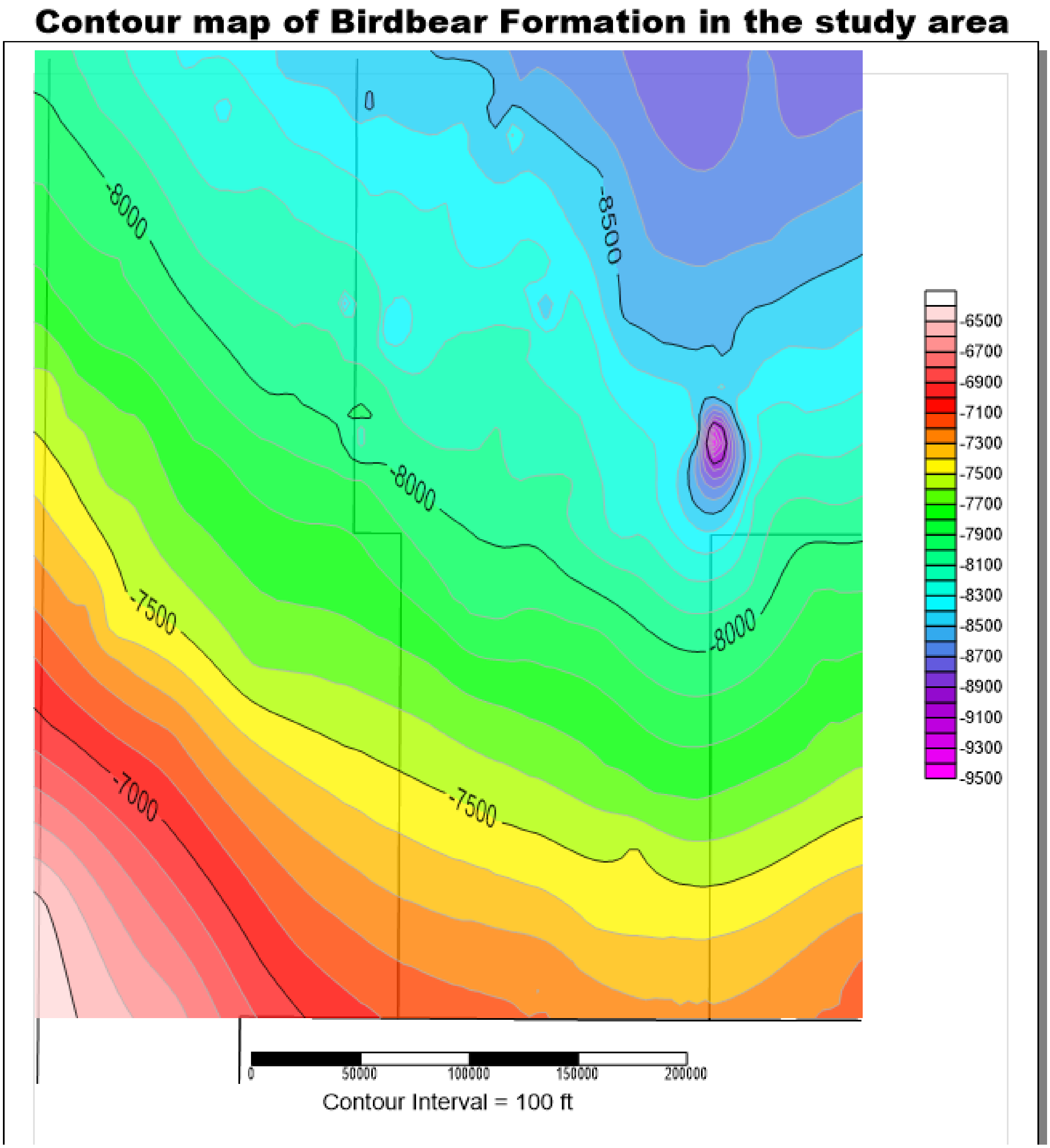

Figure 58. Contour map of the Birdbear Formation in the study area.

The above is a contour map of the area of study. From the figure, it can be seen that the Birdbear gets deeper as we move northeast and least on the southwest towards the Montana boundary.

Table 4. Porosity Values of Sedimentary Rocks (From Schlumberger Log interpretation chart, 2010).

Sediment	Porosity (%)	Permeability
Anhydrite	0	Nil
Limestone, dolomite	5 to 20	Poor to Good
Vuggy limestone	Up to 50	Excellent
Crystalline rock		
Unfractured	0 to 5	Very poor
Fractured	5 to 10	Poor

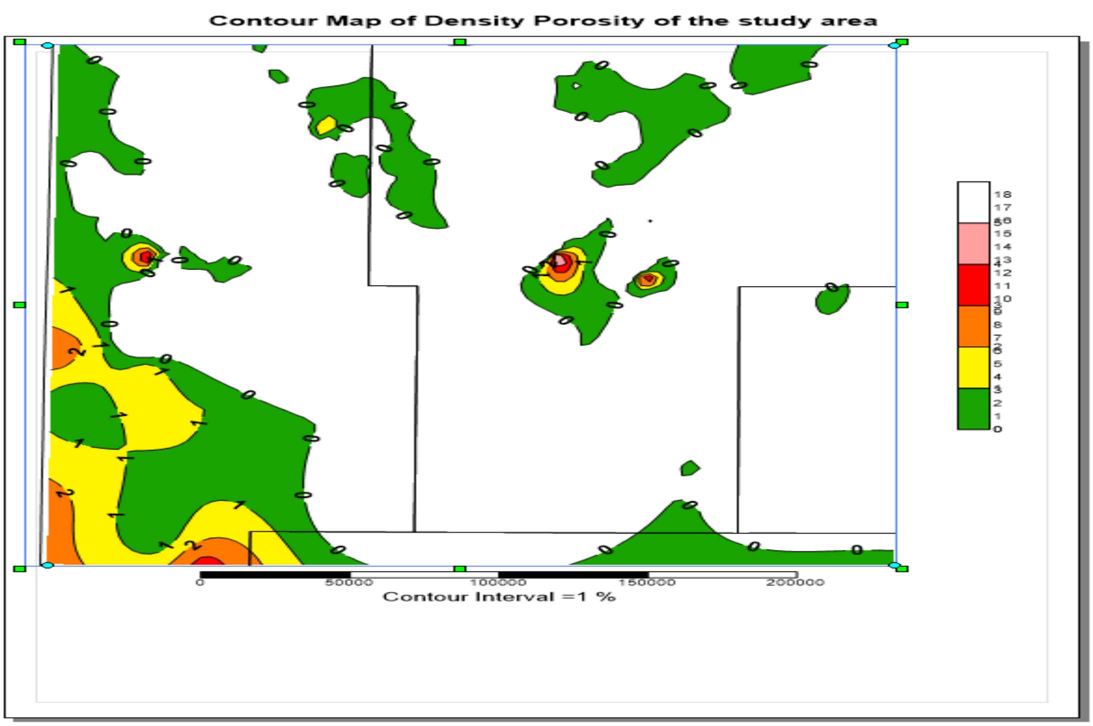

Figure 59. Contour map of the density porosity. The area in white shows no reading or zero porosity.

A plot of the density porosity is an attempt to see the spread of the density porosity across the two counties. This plot shows a lot of areas that has no density. The areas of negative or no density porosity could be as a result of different rock type used in the porosity measurement. If the measurement was calibrated for limestone but runs into dolomite, the values could be in negative or absent. An area northwest of the area in the Montana border has porosity density of between one and two.

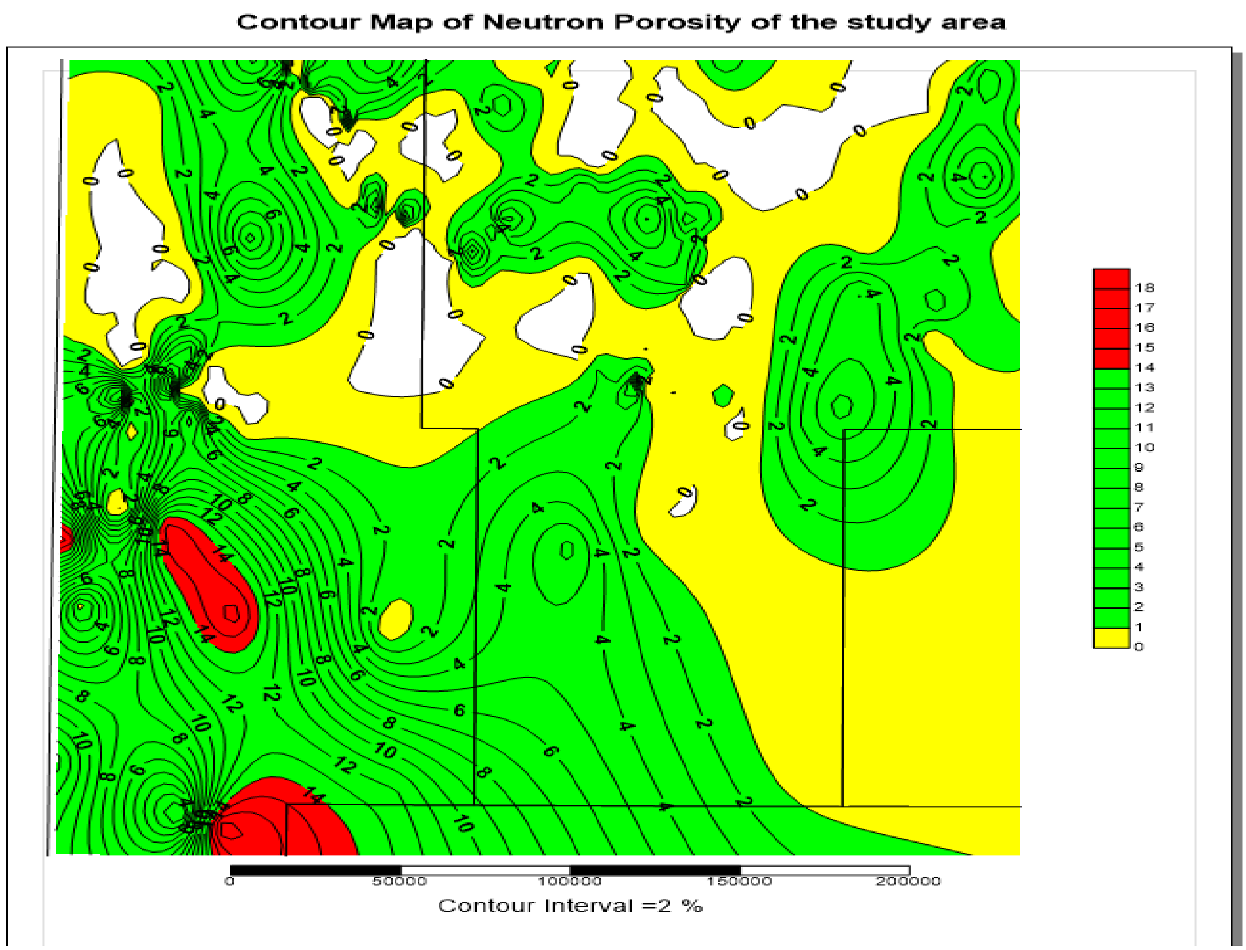

Figure 60. Neutron porosity contour map of the study area.

The average neutron porosity in the entire study area is 1.9% with higher porosity found in the in the southwest part of the area. The Golden Valley having more porosity than the

Billings County. From the middle to the northeast has diminished porosity. From the neutron porosity contour map, the southwest part of the study area has porosity ranging from 2% to 12% which is good for a limestone and a carbonate rock as seen from table 4.

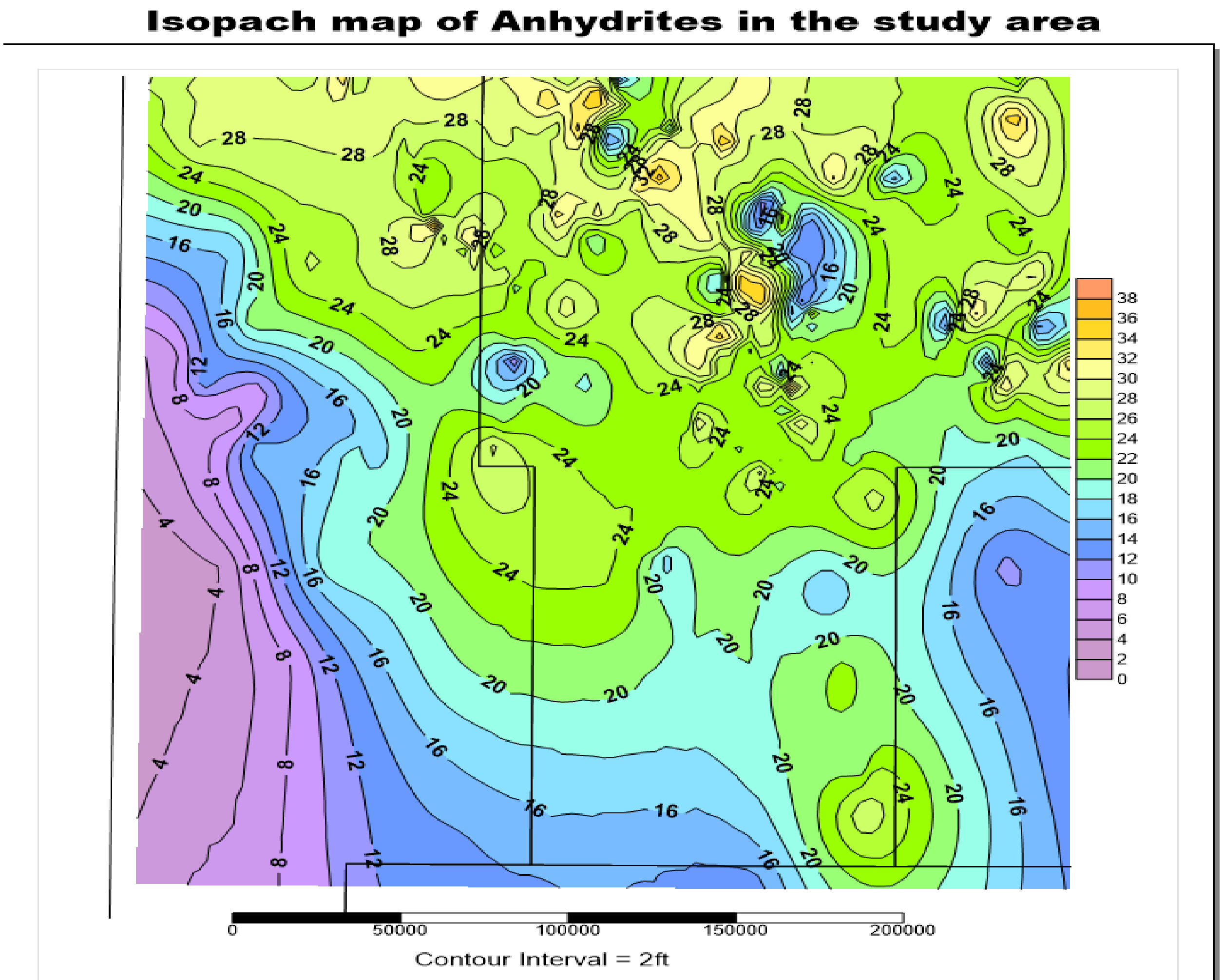

Figure 61. Isopach map of the Anhydrite in the study area.

The anhydrite significantly increases to the north. It shows the southwest towards Montana has lower anhydrites than towards the deeper part of the basin. Going by the fact that the anhydrites act as a seal for the hydrocarbon, the upper part could be that seal needed for the more porous lower part.

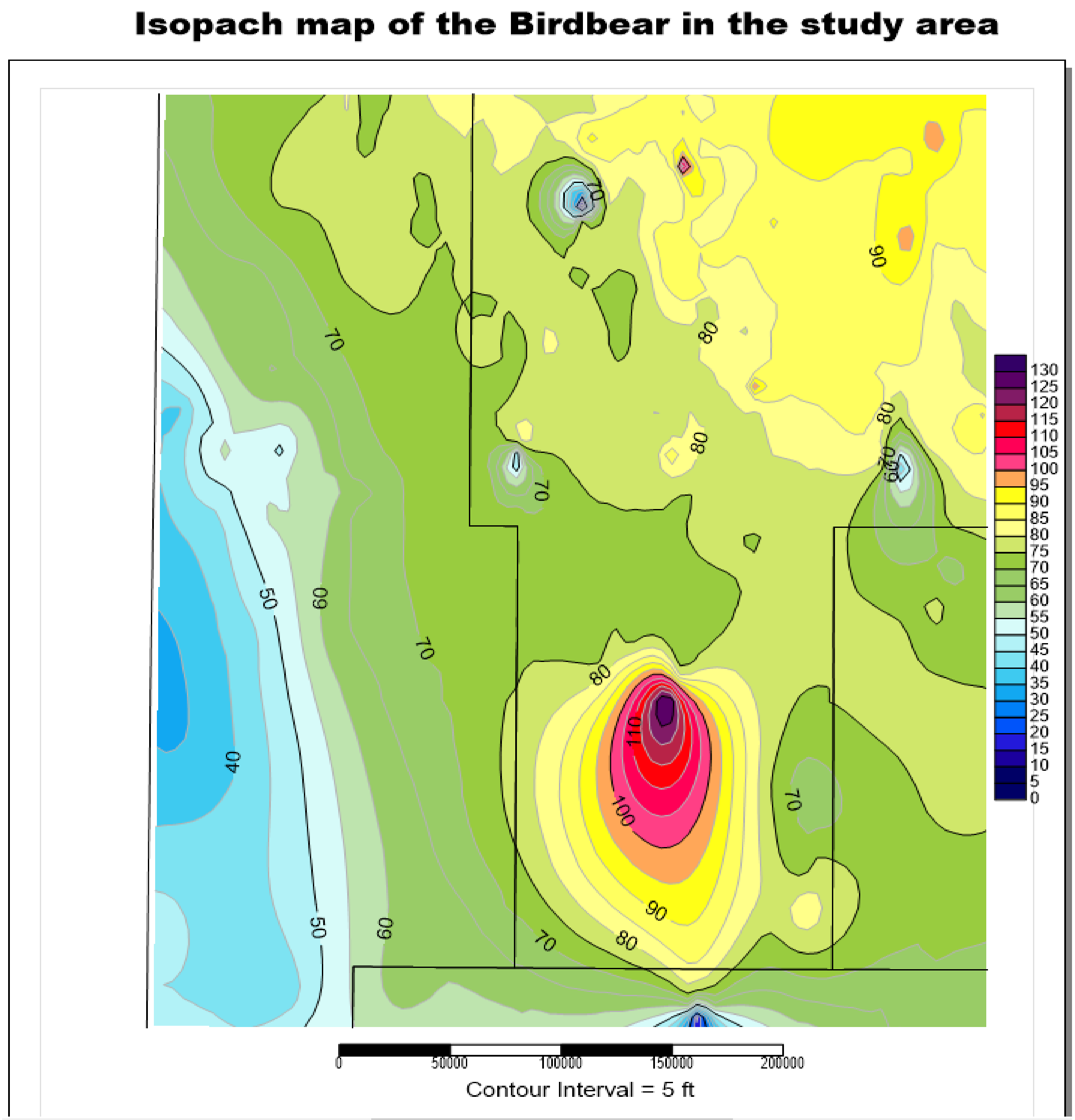

Figure 62. Isopach map of the Birdbear Formation in the study area.

This map is an effort to see the thickness of the formation across the area. Again the formation thickens towards the northeast and least at the southwest. This is an indication that the Birdbear gets deeper towards the McKenzie County which is the deepest part of the Williston basin.

CHAPTER V

HYDROCARBON POTENTIALS

Factors that control source rock richness include the stratigraphic setting, environment of deposition and diagenesis. The use of TOC and Rock-Eval pyrolysis can help us to determine oil and gas zone, kerogen type, the oil window and the stage of oil maturation. Organic matter sources can be brachiopods, ostracod, and other fossil fragments. The parameters screened for in TOC/Rock-Eval are S1, S2, S3, TOC, and Tmax, Figure 63, where S1 is a measure of the free hydrocarbons volatilized at a temperature of about 300^{o}C. The values can be affected or contaminated by drilling mud or fluid. S2 is the kerogen (non-volatile organic matter) presents in the rock and reflects the amount of hydrocarbons that the rock can produce. S2 decreases with depth/burial and is given out at a higher temperature of between 300-550^{o}C at 25^{o}C/min. An S2 value of at least >5 is needed to have a good source rock (Osadetz and Snowdon, 1986). The third parameter S3 is a measure of the organic CO_2 from the kerogen at fast heating of about 300-390^{o}C at 25^{o}C a min. Tmax is the temperature at which S2 is maximum, this is measured in Celsius (^{o}C). Tmax is an indication of the level of the kerogen maturation. S1-S3 are measured in mg/g while TOC is in wt. %. From the TOC/Rock-Eval Pyrolysis analyzes, other measurements can be derived. HI: Hydrogen Index (HI= (S2/TOC) X 100. This ratio gives the measure of hydrogen richness of a source rock. A plot of HI against OI will give us a rough idea of the generative potential of the petroleum. OI is the oxygen potential: (S3/TOC x 100) measures the richness of oxygen in the source rock. Most researchers consider OI greater than 50 as immature oil window but this is very unreliable. Production Index, PI= S1/S1+S2, is the ratio of the already generated hydrocarbon to the potential hydrocarbon. This work will go with K.G. Osadetz and L.R. Snowdon (1995) standard and Peters and Cassa, 1994 in interpreting the results of the TOC and Rock-Eval pyrolysis.

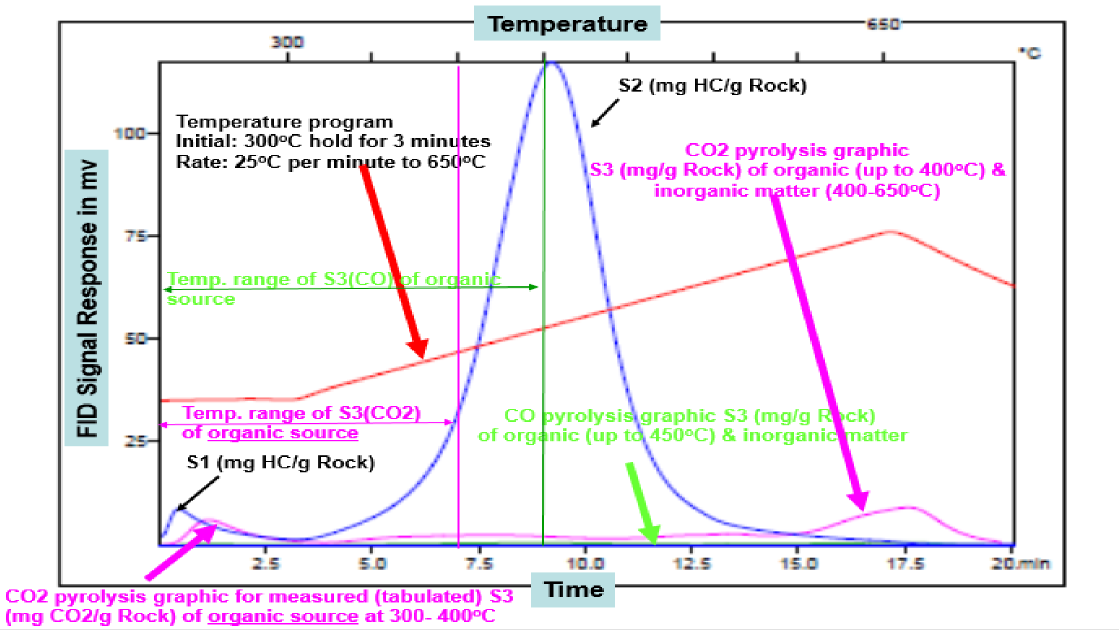

Figure 63. Explanation of parameters analyzed in TOC/Rock-Eval.

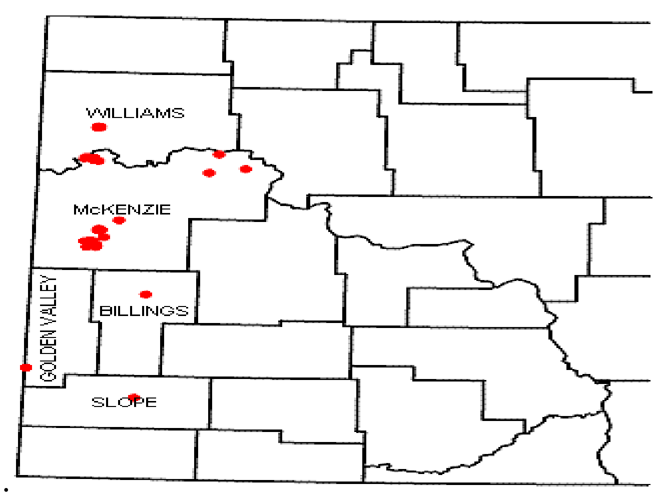

Figure 64. Partial distribution of oil and gas wells producing from the Devonian Birdbear Formation. www.dmr.nd.gov/ndgs/Resources/

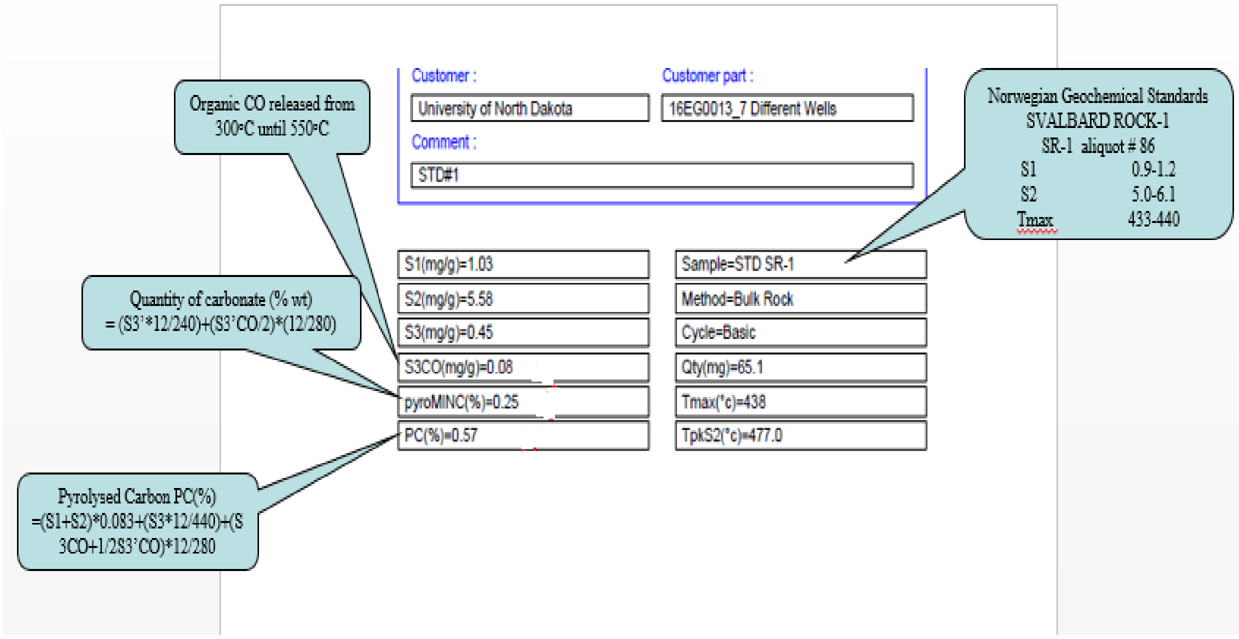

Figure 65. Key to some of the parameters and standards.

Osadetz et al (1986) notes that TOC of ≤ 0.3% has questionable significance in all other parameters, Oxygen Index (S3/TOC) has questionable significance if TOC is ≤ 0.5%, and Tmax and Production Index (PI=S1/(S1+S2)) is questionable if S1 and S2 are ≤ 0.2, and all these could mean no potential, they observed. Though generally speaking good source rock can depend on the TOC content and its kerogen type, but a high TOC content can sometimes compensate for its poor Kerogen type. The organic geochemistry images for the samples analyzed will be in the appendix III.

A total of twenty-five samples were collected from the available cores. Even distribution of sampled points was taken into consideration in order to have a good representation of the different zones of the Birdbear formation from the available cores. An average of four samples were obtained from each of the seven available cores. The logs and the points of sample collection can be seen in the Appendix. The samples were sent to StratoChem Services for TOC (total organic carbon) and Rock-Eval pyrolysis analyses. Table 5 shows the results obtained and some associated well information of the samples. Three cores were from the Billings county area and the other four core were gotten from the Golden Valley County. K.G. Osadetz and L.R. Snowdon (1995) noted that most Paleozoic rocks in the Williston have no or little petroleum source rock potential and that organic matter associated with carbonate rocks have more hydrogen and are easily changed thermally than fine-grained siliciclastic hence a different criteria for rating potential carbonate source rocks as shown in Table 5.

Table. 5. Results of TOC/Rock-Eval.

STRATOCHEM SERVICES

TOTAL ORGANIC CARBON and ROCK-EVAL PYROLYSIS

Company: UNIVERSITY OF NORTH DAKOTA — Project #: 16EG0013

Client ID	WELL NAME	Lab ID	Sample Type	Depth	Prep	TOC Wt. %	S1 mg/g	S2 mg/g	S3 mg/g	Tmax	HI	OI	S1/ TOC	PI	Formation
	291	UDEG000001	CORE	10677.0 FT	NOPR	0.68	2.65	0.93	0.36	405	137	53	391	0.74	
	291	UDEG000002	CORE	10679.0 FT	NOPR	0.45	1.36	0.55	0.41	398	123	92	304	0.71	
	291	UDEG000003	CORE	10690.0 FT	NOPR	0.19	0.08	0.07	0.48	436	36	247	41	0.53	
	291	UDEG000004	CORE	10696.0 FT	NOPR	0.26	0.12	0.12	0.25	444	47	98	47	0.50	
	859	UDEG000005	CORE	10927.0 FT	NOPR	0.27	0.15	0.18	0.55	426	66	202	55	0.45	
	859	UDEG000006	CORE	10935.0 FT	NOPR	0.18	0.07	0.06	0.28	431	33	154	38	0.54	
	859	UDEG000007	CORE	10957.0 FT	NOPR	0.21	0.09	0.11	0.42	429	53	201	43	0.45	
	10776	UDEG000008	CORE	11197.0 FT	NOPR	0.13	0.04	0.03	0.81	428	24	643	32	0.57	
	10776	UDEG000009	CORE	11204.0 FT	NOPR	0.80	0.15	0.88	0.46	447	111	58	19	0.15	
	10776	UDEG000010	CORE	11211.0 FT	NOPR	0.25	0.12	0.19	0.39	439	76	155	48	0.39	
	10776	UDEG000011	CORE	11217.0 FT	NOPR	0.23	0.10	0.18	0.50	595	77	215	43	0.36	
	15412	UDEG000012	CORE	10689.0 FT	NOPR	0.37	0.39	0.43	0.37	437	117	101	106	0.48	
	15412	UDEG000013	CORE	10700.0 FT	NOPR	0.33	0.31	0.39	0.38	437	120	117	95	0.44	
	15412	UDEG000014	CORE	10708.0 FT	NOPR	0.33	3.21	0.47	0.54	435	143	164	976	0.87	
	15412	UDEG000015	CORE	10725.5 FT	NOPR	0.17	0.95	0.18	0.60	413	107	357	565	0.84	
	15625	UDEG000016	CORE	12663.0 FT	NOPR	0.09	0.07	0.05	0.37	412	55	405	77	0.58	
	15625	UDEG000017	CORE	12681.0 FT	NOPR	0.08	0.05	0.04	0.41	318	49	503	61	0.56	
	15679	UDEG000018	CORE	10709.5 FT	NOPR	0.53	0.50	0.90	0.63	437	171	120	95	0.36	
	15679	UDEG000019	CORE	10717.7 FT	NOPR	0.40	2.94	0.53	1.59	296	133	399	739	0.85	
	15679	UDEG000020	CORE	10723.2 FT	NOPR	0.19	0.26	0.21	0.40	430	112	213	138	0.55	
	15679	UDEG000021	CORE	10741.2 FT	NOPR	0.22	1.34	0.34	0.62	421	152	278	601	0.80	
	15679	UDEG000022	CORE	10745.7 FT	NOPR	0.21	1.67	0.44	0.54	407	210	257	795	0.79	
	21734	UDEG000023	CORE	10494.0 FT	NOPR	0.23	0.05	0.15	0.19	440	66	84	22	0.25	
	21734	UDEG000024	CORE	10498.0 FT	NOPR	0.13	0.07	0.10	0.34	432	77	262	54	0.41	
	21734	UDEG000025	CORE	10500.0 FT	NOPR	0.13	0.06	0.11	0.82	606	83	617	45	0.35	

5.1. TOC/Rock-Eval Result and Interpretations

5.1.1. Source Rock.

Using the Osadetz and Snowdon (1986) criteria for rating potential source rocks, most of the samples analyzed fall between fair to good, with just two samples indicating very good (table 6). Four samples were taken from NDGS Well no. 219 and has TOC values of good to very good. All samples were taken from the upper A zone as this core interval does not get to the B zone. NDGS well number 859 has three samples all from the lower B zone with two showing fair and the one closest to the A zone indicating good. NDGS well number 10776 samples were all from Zone B indicating fair, good and very good which is different from the observed trend. NDGS Well number 15412 has all good TOC in the A zone with the one fair TOC in the B zone. NDGS well 15625 all shows poor TOC. This well has no well log. Again NDGS Well number 15679 followed the same trend, but NDGS Well number 21734 samples all taken from A zone shows fair TOC. In all, 2 samples were classified poor, 13 samples were classified as fair, 7 were good, and just 3 as very good in terms of source rock.

Table 6. Standard Criteria for Rating Potential Source Rocks (Osadetz and Snowdon, 1986).

Rating	%TOC in shales	%TOC in carbonates
Poor	0.00–0.50	0.00–0.12
Fair	0.50–1.00	0.12–0.25
Good	1.00–2.00	0.25–0.50
Very good	2.00–4.00	0.50–1.00
Excellent	>4.00	>1.00

S2 Value (mg of HC/g of rock)

Rating	S2 Value
Poor	<2.00
Fair	2.00–5.00
Good	>5.00

A Dembicki (2009) plot of S2 against TOC, for source rock classification Figure 67, shows that the source rocks of the study area are between poor and fair with the majority in the poor category.

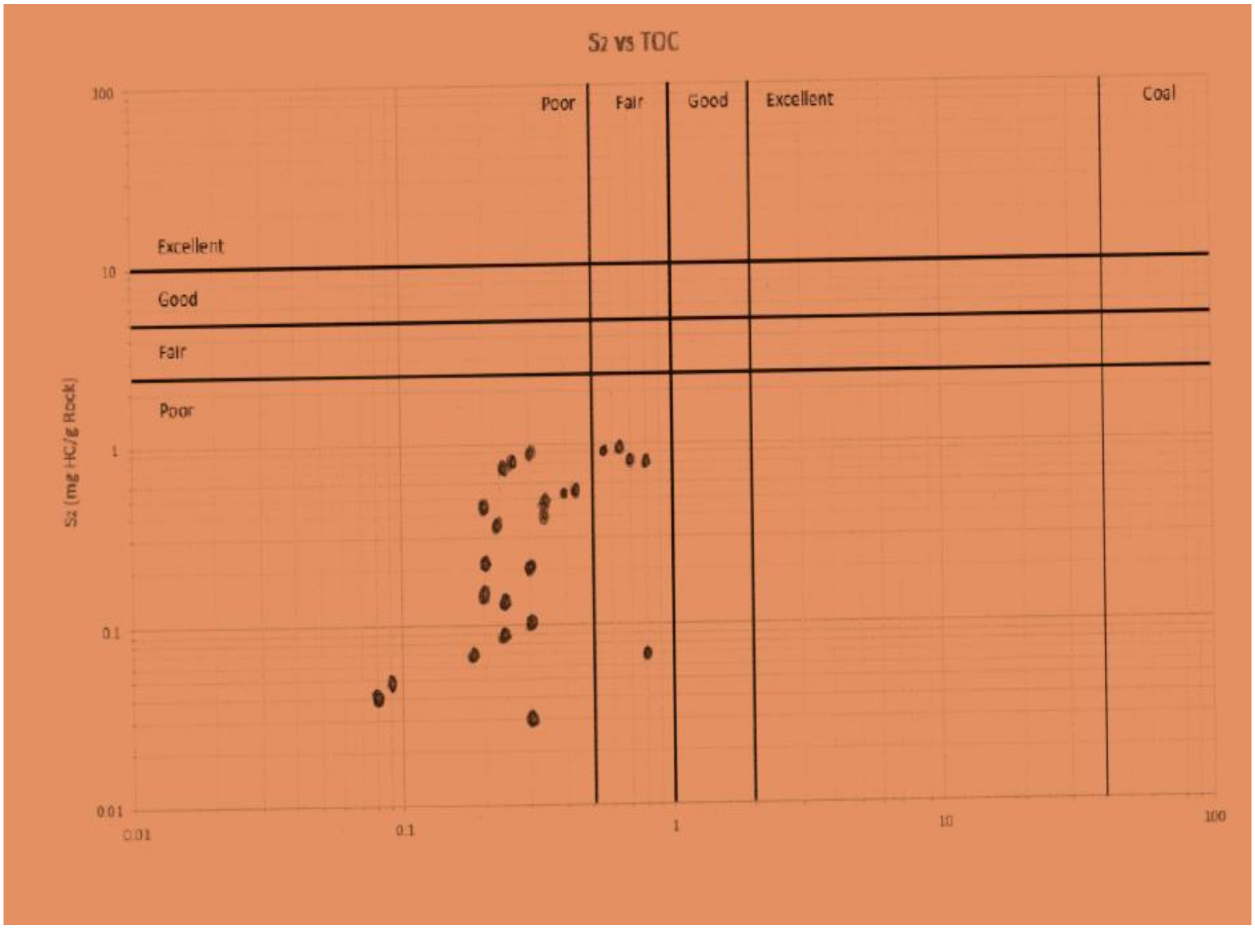

Figure 66. A Dembicki (2009) plot of S2 against TOC.

5.1.2. Kerogen Type.

From the derivatives in the Rock-Eval and pyrolysis, the Kerogen type was made. Using Peters et al (1994), (Table 7), and considering the HI, it will be noticed that the HI values from this area are between 24 to 210.

Table 7. Geochemical Parameters Describing Kerogen Type (Quality) and the Character of Expelled Products (Peters et al 1994).

Kerogen Type	HI (mg HC/g TOC)	S_2/S_3	Atomic H/C	Main Expelled Product at Peak Maturity
I	>600	>15	>1.5	Oil
II	300–600	10–15	1.2–1.5	Oil
II/III[b]	200–300	5–10	1.0–1.2	Mixed oil and gas
III	50–200	1–5	0.7–1.0	Gas
IV	<50	<1	<0.7	None

Five out of the twenty-five readings falls below the value fifty which is considered as Kerogen Type IV with no hydrocarbon. One point is above 210 considered as Type II, which is a mixture of oil and gas but the rest 19 readings (majority) is between 50-200, considered as Kerogen Type III (gas prone).

A van Krevelen plot of the HI vs OI (Figure 67), also reflects the point that the Kerogen Type is mainly Type III and few Type II, with some in the boundary between Type II and Type III. This shows that the Kerogen type is mainly gas with few still in the oil window.

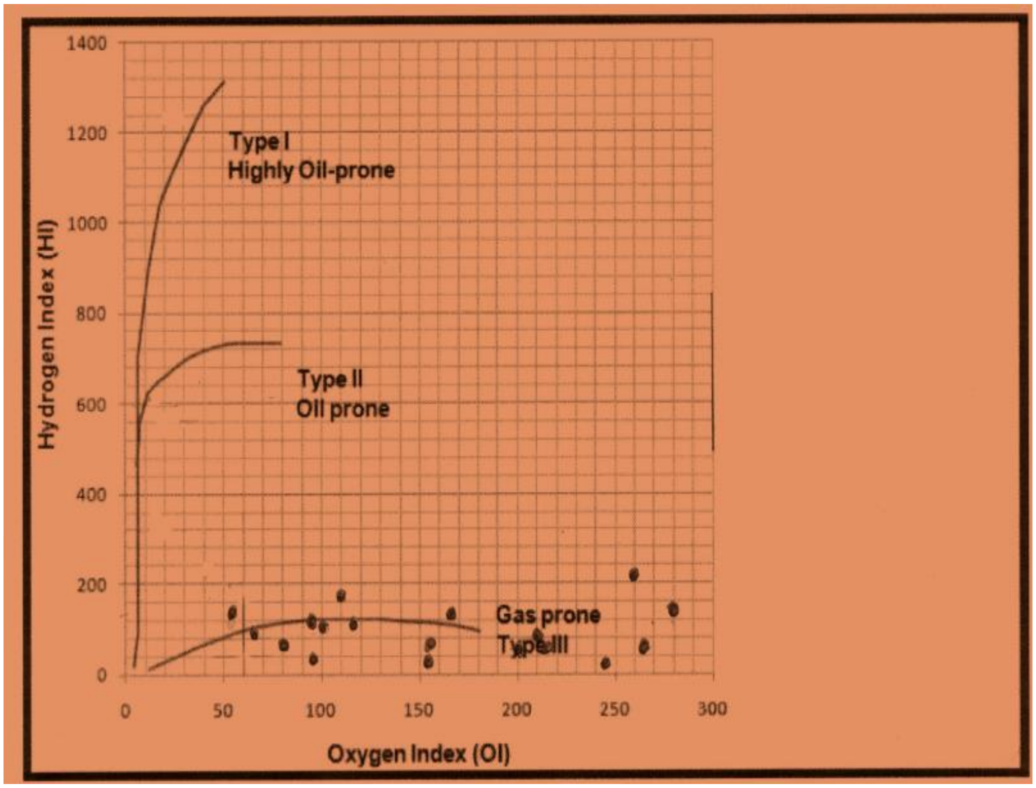

Figure 67. A Van Krevelen plot of HI vs OI.

5.1.3. Thermal Maturation.

The thermal stage of a reservoir is also very important in determining the thermal maturation of the reservoir. This tells us if the source rock is in the oil window or past the oil window.

Considering the Tmax and Production Index of the study area against Peters and Cassa (1994) levels of thermal maturation, Table 8, shows that most of the thermal maturation of the study area are mainly in the mature category especially in the of late mature category. A plot of the Hydrogen Index against Tmax on a modified pseudo-Van Krevelen plot also reveals that most of the source rock are Type III and thermally matured but with a handful in the immature category, (Figure 68).

Table 8. Level of Thermal Maturity (Peters and Cassa, 1994).

Level of Thermal Maturity						
Stage of Thermal Maturity for Oil	Maturation			Generation		
	R_o (%)	T_{max} °C	Thermal Alteration Index (TAI)	Bitumen/TOC	Bitumen (mg/g rock)	Production Index $[S_1/(S_1 + S_2)]$
Immature	0.2-0.6	<435	1.5-2.6	<0.05	<50	<0.10
Mature						
Early	0.6-0.65	435-445	2.6-2.7	0.05-0.10	50-100	0.10-0.15
Peak	0.65-0.9	445-450	2.7-2.9	0.15-0.25	150-250	0.25-0.40
Late	0.9-1.35	450-470	2.9-3.3	---	---	>0.40
Postmature	>1.35	>470	>3.3	---	---	---
From Peters and Cassa, 1994						

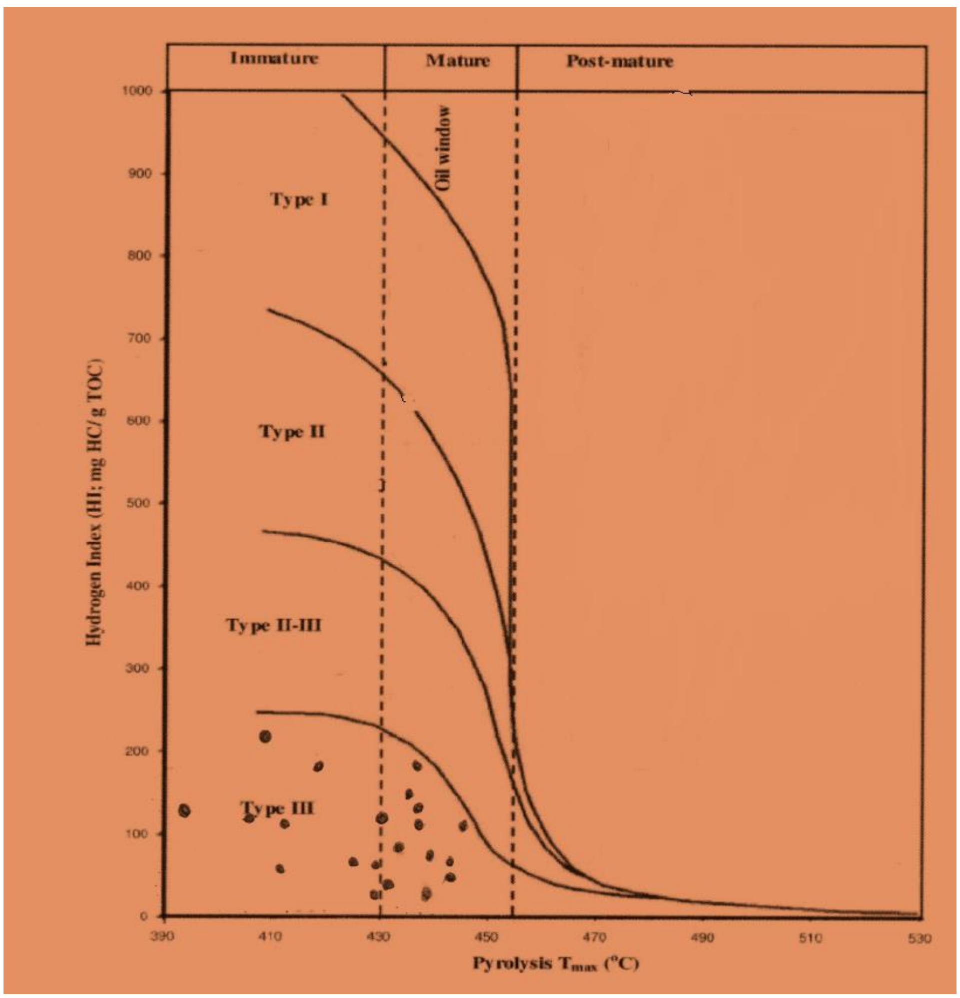

Figure 68. Modified pseudo-Van Krevelen plot of Hydrogen Index against Tmax.

Table 9. TOC/Rock-Eval Including the Well Status and Well Bore Type.

WELL NAME	Depth	TOC Wt. %	S1 mg/g	S2 mg/g	S3 mg/g	Tmax	HI	OI	S1/ TOC	PI	Well Status
291	10677.0 FT	0.68	2.65	0.93	0.36	405	137	53	391	0.74	PA/1967
291	10679.0 FT	0.45	1.36	0.55	0.41	398	123	92	304	0.71	PA/1967
291	10690.0 FT	0.19	0.08	0.07	0.48	436	36	247	41	0.53	PA/1967
291	10696.0 FT	0.26	0.12	0.12	0.25	444	47	98	47	0.50	PA/1967
859	10927.0 FT	0.27	0.15	0.18	0.55	426	66	202	55	0.45	DRY/1955
859	10935.0 FT	0.18	0.07	0.06	0.28	431	33	154	38	0.54	DRY/1955
859	10957.0 FT	0.21	0.09	0.11	0.42	429	53	201	43	0.45	DRY/1955
10776	11197.0 FT	0.13	0.04	0.03	0.81	428	24	643	32	0.57	DRY/1964
10776	11204.0 FT	0.80	0.15	0.88	0.46	447	111	58	19	0.15	DRY/1964
10776	11211.0 FT	0.25	0.12	0.19	0.39	439	76	155	48	0.39	DRY/1964
10776	11217.0 FT	0.23	0.10	0.18	0.50	595	77	215	43	0.36	DRY/1964
15412	10689.0 FT	0.37	0.39	0.43	0.37	437	117	101	106	0.48	*
15412	10700.0 FT	0.33	0.31	0.39	0.38	437	120	117	95	0.44	*
15412	10708.0 FT	0.33	3.21	0.47	0.54	435	143	164	976	0.87	*
15412	10725.5 FT	0.17	0.95	0.18	0.60	413	107	357	565	0.84	*
15625	12663.0 FT	0.09	0.07	0.05	0.37	412	55	405	77	0.58	ACTIVE
15625	12681.0 FT	0.08	0.05	0.04	0.41	318	49	503	61	0.56	ACTIVE
15679	10709.5 FT	0.53	0.50	0.90	0.63	437	171	120	95	0.36	TA/2015
15679	10717.7 FT	0.40	2.94	0.53	1.59	296	133	399	739	0.85	TA/2015
15679	10723.2 FT	0.19	0.26	0.21	0.40	430	112	213	138	0.55	TA/2015
15679	10741.2 FT	0.22	1.34	0.34	0.62	421	152	278	601	0.80	TA/2015
15679	10745.7 FT	0.21	1.67	0.44	0.54	407	210	257	795	0.79	TA/2015
21734	10494.0 FT	0.23	0.05	0.15	0.19	440	66	84	22	0.25	DRY/2013
21734	10498.0 FT	0.13	0.07	0.10	0.34	432	77	262	54	0.41	DRY/2013
21734	10500.0 FT	0.13	0.06	0.11	0.82	606	83	617	45	0.35	DRY/2013

Conclusion

The Birdbear formation can be divided into two informal units: the lower B zone and the upper A zone. The A zone is made up of dolomites, limestone, and abundant anhydrites. Its environment is supratidal while the lower part is made up of dolomite, limestone, amphiporas and stromatoporoids. Its environment of deposition is subtidal. The rock types are wackestone, packstone, grainstone, biosparite, micrites and biomicrites. The potential pay zone in the A zone is stratigraphic caused by the anhydrite patches in this zone while the pay zone in the B zone is structural due to the salt dissolution in the Prairie Formation. The formation is mainly made up of dolomite and limestone. The formation has undergone some significant diagenetic activities and the most common of those diagenetic processes are dolomitization. Most of the sediments have undergone different levels of diagenesis ranging from moderate to completely dolomitized depending on how much of the original sediment have been dolomitized. This process took place in the early diagenesis stage in the marine environment in a mixing zone. The Mg^{2+} needed in the mixing zone for dolomitization to occur was from the salt from the Prairie Formation. The dolomitization process gave rise to secondary intercrystalline porosity and sucrosic texture. The total dissolution of fossil fragments also is a significant diagenetic process in the formation giving vugs and biomoldic secondary porosity while some of the porosity have been closed up by calcite cement and recrystallization. Selective replacement, mechanical compaction and chemical compaction like stylolites and dissolution all added to the changes that have affected the reservoir quality.

From the contour map, the Birdbear Formation in the study area has the shallow part in the southwest Golden Valley and gets deeper in the northeast part of Billings County. Density porosity in the study area, though low but better in the southwest of Golden Valley going into

Montana. The Neutron density porosity increases from the middle of Billings County to southwest Golden Valley, with patches of other high areas of neutron porosity in the western Billings and northern Golden Valley Counties. In general, most of the area has a good porosity. Isopach map of the anhydrite shows that it is increasing in southwest to northwest trend from Golden Valley to Billings Counties with more anhydrites in the Billings County. The thickness of the Birdbear Formation increases in the study area in a southwest to northeast trend, getting thicker towards the deeper part of the Williston basin.

The study area shows that the source rock ranges from poor to fair and the Kerogen Type is Type III. This means that the area is gas prone. Most of the “good” source rock are found within the A zone while most of the “fair” source rocks are in the B zone. The source rock also was discovered to be mostly mature and few immature using the thermal maturation index. The results above could explain why most of the well drilled in this area are either dry, permanently abandoned, or temporally abandoned.

Out of the seven cores examined, three were dry well, one permanently abandoned, two temporally abandoned and with just one active well.

APPENDICES

APPENDIX I

CORE AND THIN SECTION DESCRIPTION

NDGS 291
AMERADA HESS CORPORATION
FRYBURG HEATH-MADISON UNIT P-812
BILLINGS COUNTY, NORTH DAKOTA
FRYBURG FIELD
CORE INTERVAL: 10676-10699.7

TS: 10,588.8:	Micro-vugs with the pore spaced recrystallizing. Fossil fragments. Invasive and progressive dolomitization. Horse tail stylolites. Dissolution seams separating the more dolomitized part from the less dolomitized. U-shaped Crinoid arm plate which goes into extinction on rotation. Ostracod. Five-fold structure of echinoids with recrystallization inside the fossil fragments. Broken brachiopod fragments. Biserial foraminifer. Intraclastic limestone. Compacted bryozoan
10676'-10677':	Anhydritic Limestone. Penetrative anhydrites embedded in the limestone with mild effervescence. Interlaminate laminae. Fractures that runs deep.
TS: 10,676:	Anhydrites riddled the dolomite crystals. Packstone
10677'-10678':	Limestone. Dark brown. A very short interval of pure limestone sandwiched by the anhydritic limestone below and above. Intercrystalline porosity. Visible fractures.
TS: 10,678:	Highly dolomitized with dissolution seams. Large dolomite crystals.
TS: 10680:	Ostracod embedded in a dolomitized background. Abundant anhydrites. Fractures showing high porosity.
TS: 10682:	Well dolomitized with high porosity.
10678-10684:	Anhydritic Limestone. The anhydritic limestone returns as the first unit. The nodular anhydrites runs deep into the core. Intercrystalline porosity and fractures and increases as we go down the core. . Most of the fractures show recrystallization. Some areas have vugs.
TS: 10684.8:	Euhedral dolomite crystals well dolomitized. Fractures are recrystallized. More replacement of the limestone by medium to coarsely crystalline intercrystal porosity.

TS: 10685:	Brachiopod running through a dolomitized area. Most of the pore space is filled with dissolution seam
10685-10699:	Limestone. This section is mainly limestone with the liminess increasing as we go deeper. Fractures continue to run both vertically and horizontally. Stromatoporoids are abundant. At 10687 ft is a gastropod. Lower down this section we have burrows and abundant fossil fragments between 10693 ft-10694 ft.
TS: 10689:	This section shows less diagenesis in some parts as most of the original micritic envelopes are still intact with most of the original sediment still in place. Lots of compacted foraminifer with other fossil fragments. Fractures and broken brachiopod stem.
TS: 10690:	Most of the original limestone are still in place except for the fossils outlines re-precipitated to form a dog-tooth spar.
TS: 10691.5:	Mostly fossil fragments forming a biosparite.
TS: 10693-10693.5:	Stylolite separating a dolomitized portion from non-dolomitized. Abundant crinoids, gastropods and bryozoan in a less dolomitized allochem.
10699.6-10699.7:	Accumulation of fossils and fossil fragments. Gastropods and brachiopods. Again is another recrystallized impression of gastropods.
TS: 10699.9:	Less dolomitized than upper members with abundant of fossil fragments giving us a biosparite. Brachiopod stem, bryozoan, ostracod, lots of stylolite and dissolution seams and fractures with precipitation occurring in the fossil fragments almost closing up the pore spaces. Most of the structures showing effects of deep burial as compaction is very common.

NDGS 859
TEXACO INC.
GOVT. - M. S. PACE 1
BILLINGS COUNTY, NORTH DAKOTA
MAGPIE FIELD
CORE INTERVAL:10925-10958

TS: 10920-21: Fractures and well dolomitized. Packstone.

TS: 10921-922: Partially dolomitized. The fossil fragments have been recrystallized with a faint Outline of the original deposits with evidence of micrite envelop. Ostracod. Most of the porosity has been partially covered by calcite cement.

TS: 10925-26: Trilobites. Echinoid spine, ostracod, ooids, and bryozoans rich limestone. This unit is filled with many fossil fragments with most of the crystals found in the fossil fragments and most of the original sediments still in place. The rock type is Biosporite.

10925-10926: Anhydritic Limestone. Yellowish gray. Intergranular. Packestone. Here the anhydrites acts as the matrix and also fills the fractures (cements). The anhydrites are invasive in nature and runs in a West East direction. Stromatoporoids. Stylolite intrudes the 10926 ft. section.

TS: 10928-929: Fossil dissolutions produces a lot of vugs and pore spaces that increase porosity. Calcite cement precipitating from the dissolved fragment and causing most of the vugs to be partially covered. The rest of the unit still retains its primary deposition. Dissolution seams abundant.

TS: 10929-30: Mostly dolomitized. An enlarged view of brachiopod. Curved and fibrous wall structured.

10927-10933: Limestone. Almost absence of anhydrites. Fractures. The fractures runs in an east-west direction. Lots of dolomite crystals in magnification lens.

TS: 10933-934: Evidence of progressive dolomitization with the un-dolomitized portion filled with fossil fragments like brachiopod stems, and ostracods.

TS: 10940-41: Partially dolomitized with evidence of the original depositional history intact. Showing selective dolomitization and fractures. Fossil fragment recrystallization with pore spaces.

10934-10943: Limestone. Vertical fracture. At 10943 ft. are some gastropods shells. Dissolution seams increase as well as anhydrite patches. Going down to 10938 ft. dolomitization process increases and at 10939 ft. is a stylolite. At 10940 ft. mark is a huge bivalve, Brachiopod.

TS: 10943-10944: Fossil fragments like ostracod, brachiopod stems, gastropods, and the flower-like echinoid spine distinguished by its micritic infill. Less dolomitized.

TS: 10946-10947:	More fossil fragments and less to no dolomitization. The echinoid spine compacted, as well as lots of broken brachiopod, and micritized fossil fragments.
TS: 10948-10949:	Little to no dolomitization. Most of the original deposit still very much together. Abundant echinoids, brachiopods, ostracod. Fractures.
10944-10949:	Limestone. Starts with stylolite and lots of stromatolite. Fractures. Lots of brachiopod shells. Soft sediment deformations. Dissolution seams. Abundant broken brachiopod stems indicting the effects of pressure.
TS: 10950-10955:	Abundant Stylolites, crinoids, gastropods, echinoids (some compacted), brachiopod. The fossil fragments recrystallization. Abundant dissolution seams
10950-10958:	Limestone. At 10950 ft. is a highly anhydritic layer but ends as we enter 10951 ft. Fractures increase at 10952 ft. and continue down the core. At the 10958 ft. mark returns the massive accumulation of brachiopod stems and bivalve brachiopod fossil.
TS: 10957.95:	Dolomitized and less fossil fragments. Dissolution seams.

NDGS 10776
PROPEL ENERGY CO
ANNA LOGOSZ 1
BILLINGS COUNTY, NORTH DAKOTA
WILDCAT
CORE INTERVAL: 11196-11202

11196-11199:	Dolostone. Pale brown in color. Visible pores. Pockets of anhydrite, stylolite. Laminated. Very fine grained. From 11198 ft. fine grained mudstone and soft sediments. Fractures.
11199-11200:	Limestone. A short interval of Limestone. Light gray color with pockets of calcites align in a uniform direction running from east-west.
11200-11202:	Dolostone. A short Anhydritic dolostone. Pale brown. Dissolution seams.
11202-11227:	Limestone. Light (olive) gray color. Highly porous with lots of burrows. Abundant Stylolites, vertical fractures. Highly effervescence. Abundant amphipora giving this interval a spotted appearance. Stromatoporoids. Recrystallization taking place in the fractures. At 11220 ft. the amphipora reduces but stromatoporoids extend all the way.

NDGS 15412
WHITING OIL AND GAS CORPORATION
FEDERAL 32-4HBKCE
GOLDEN VALLEY COUNTY
BICENTENNIAL FILED
CORE INTERVAL: 10690-10739 (49ft).

Comparing the core with the log, the log was noted to be about 24ft off. The core was also not deep enough to make a contact with the Duperow Formation below. The core interval 10700-10730 is highly oil stained.

TS: 10682-10689.2:	Micrite. Fractures with anhydrite running through the pores. Recrystallization taking place in the line of the fractures. Most of the sediments shows very low degree of dolomitization. Very porous as shown by the stained thin section.
10690-10692:	Light gray, poorly sorted and coarse grained intraclast packstone. White nodular-mosaic anhydrites.
10692:	a mixture of peloids-pisolites with intercalations of fine grained mudstone and siltstone.
10693-10700:	The mudstone intercalations show signs of deformations with fractures of the bands increasing. Stromatolites also observed. The peloids-pisolites features returns at 10695 ft. depth
10700-10707:	Limestone. Poorly sorted, medium grained and dark gray. Abundant amphipora (Amphipora packstone) with fractures that have been recrystallized and then pockets of anhydrites. 10703 ft. shows amphipora and stromatoporoids increases with stylolite noted at 10703 ft.
10708:	Dolomite. Lots of stylolite and solution seams. Burrows abundant. Floatstone, fractures, nodular mosaic.
TS: 10710.9-10720.5:	Completely dolomitized with lots of anhydrites. Vugs. The original sediments almost completely changed to dolomite crystals. Fractures with signs of recrystallization.
TS: 10722.5-10738.5:	Still highly dolomitized with abundant stylolite running through the unit. Certain points are less dolomitized than the others but still highly dolomitized. Patches of anhydrites. Vuggy areas showing recrystallization more like the dog-tooth spar. At point 10736.5 ft. shows how dolomitization can actually close up a pore space thereby affecting porosity and the reservoir quality.
10708-10724:	Limestone, slightly anhydrite and slightly laminated.

10724-10728:	Dolomite. Nodular-bedded Wackestone with platy stromatoporoid boundstone. Abundant burrows, with increase in porosity. Solution seams at intervals.
10730-10733:	Dolomitic Limestone. More limy shown by increased effervescence. Momentary patches of amphipora that ends at 10731 ft. Stylolite penetrates the wackstone at 10736 ft.
10733-10735:	Dolomite. Anhydrite plugs the pores in the wackestone. Fractures and stromatoporoids abundant.

NDGS 15625
FH PETROLEUM CORP.
STATE 14-16
GOLDEN VALLEY COUNTY
COOKS PEAK FIELD
CORE INTERVAL: 12656-12685

12656-12657:	Dolomite. Peloids. Both vertical and horizontal fractures. Calcite acting as the cementing materials in the multiple fractures. Patches of anhydrites. Stromatolites.
TS: 12657.8:	Completely micritic fine grained.
TS:12667.5-12667.6:	Fractures with recrystallization taking place in the fractured area and spreading inward from the fractures. The other areas still have the dolomite envelope. Patches of anhydrites and selective onset of dolomitization and recrystallization happening in dissolved fossil fragments. Dissolution seams.
12657-12665:	From 12657 ft. the anhydrites are greatly diminished and just scattered. Presence of microlaminae. Vertical fractures. Peloids. The anhydrites still filled in the fractures. This central vertical fractures that ran almost all through this core some places where not filled by anhydrite but some places as dissolution seam.
12665-12668:	Anhydrite crystals increase but not as massive as the first unit. The central running fractures make the central part of this core more porous than the other parts of the core. As we get to the lower part of this unit, the dolomitization increases considerably.
12668-12672:	Dolomite: This section begins with lots of embedded anhydrite. Brachiopods stems very common at 12668 ft. Widespread stylolite seam which extend from the corner but goes to the center from point 12669 ft. This centrally running stylolite at some points thins out but quickly reappears at the center of the core. Cross laminae continue to attend this core as well as fractures. Water poured on the core quickly drains through the central stylolite. At 12670 ft. saw nodular anhydrites recrystallizing from the fractures and the stylolite. Stromatoporoids at 12672 ft.
12672-12679:	Dolostone. From 12673 ft. the huge stylolite covered the entire surface of the core and the calcite crystals increases in abundant making the core more light colored. Fractures with pressure seams. A bivalve impression (brachiopod) seen at 12674 ft. More fractures as we go down the core and cross laminae. At 12677 ft. is peloidal grainstone as we move back to abundant fractures with patches of anhydrites.

12680-12685: Anhydritic Dolostone. Peloidal grainstone. Fractures with recrystallization occurring in the fractures. The anhydrites being massive at some points and at other time nodular. Stylolite.

NDGS 15679
FH PETROLEUM CORP.
BROWN 42-28
GOLDEN VALLEY COUNTY
WILDCAT FIELD
CORE INTERVAL: 10700-10758 (58ft).

10700.1-10700.8:	Anhydrites. Stromotoporoidic Mudstone. Thick wavy dark black thin beds of mudstone covering the nodular anhydrites.
10701-10702.5:	Nodular-mosaic anhydrites with veins of fine grained mudstones. Peloids-pisolites also present.
1072.5-10703:	Limestone. This small interval is a short limestone interval. Highly effervescence. Stromatoporoids. Anhydrite runs through the unit as it recrystallizes the fractures acting as the cementing materials in the matrix.
10703-10704:	Dolostone. Pale yellowish brown. Stromatoporoids. Veins of anhydrite plugs abundant until 10704 ft. Fractures recrystallizes by white anhydrites.
TS: 10704.2-6:	Progressive dolomitization with lots of patchy anhydrites. Most of the original dolostone still so much in place without changes.
TS: 10705.4-5.8:	Abundant dissolution seams with scattered dolomite crystals.
TS: 10708.9-9.2:	Invasive dolomitization gradually eating through the original fabrics. The dolomite crystals acting as cementing materials covering the pore spaces. Ostracod shell recrystallized. Some pores created by dissolved fossil fragments.
TS: 10709.2-9.5:	Here the bivalve shows alteration of the original aragonite shells that has been dissolved and precipitated by more stable calcite spar. This is only recognized by the outline of the shape by the micrite envelopes. Dolomites show interlocking of dolomite crystals.
TS: 10709.5-10:	Pressure induced dissolution seams with scattered crystals. Onset of dolomitization process, mostly selective. Fractures running through some of the areas. Crinoid showing five-fold symmetry with micrite infilling with cementation within the pores and pressure solution in the grain margins.
10704-10723:	Dolomitic anhydrite. Slightly shaly. Intercalations of anhydrites embedded at intervals. Fractures at 10704.5 ft. Solution seams. Peloid Packstone. At 10707.1 ft. dissolution seams and mosaic anhydrite. The anhydrite cuts through the pisolite-peloid matrix. At 10708.1 ft. are layers of tiny mudstone showing signs of soft sediment deformations. Intervals of mudstone with soft sediment deformation showing fractures and hence solution seams. At 10722 ft. stromatoporoids become abundant and diminishes at 10722.6 ft. with a stylolite acting as a boundary.

TS: 10723-4:	Coarsely crystalline subhedral, zoned, nonferroan replacement of dolomite. The primary fabrics are being gradually replaced by the crystals acting as a cementing material. Though pores have not been completely filled by the calcite so still have high porosity. Dissolution seams in the area with lesser replacement.
10723-10725:	Limestone: Dusky brown color. Stylolite 10723.7 ft. The two stylolite seems to bind this limestone.
TS: 10728-10730:	From this point we see a more dolomitized units. The dolomites have dark and cloud cores and clear rims. Completely dolomitized with crystal interlocking growths.
TS: 10735-37:	Dolostone: Wackestone. The crystal growths gives rise to scattered dog-tooth spars. Fine to coarse grained. Greater than 10% grains Fractures. Vugs caused probably by fossil dissolution. Leached bivalve shells adds to the porosity. This secondary porosity has been reduced by cementation by calcite in the interior of the mold.
10725-10739:	Dolostone: slightly limy. Yellowish gray color. Nodular bedded wackestone. Intercalations of anhydrites at intervals. Fractures at intervals. At 10726.3 ft. burrows where noted and continued being abundant through this unit. Stylolite become very common.
10739-10747:	Dolomitic limestone. This interval becomes more limy than the previous unit. Abundant here are solution seams and nodular anhydrites. Wackestone. 10741 ft. the core becomes highly fractured with high porosity.
TS: 10755-57:	Stylolites. Grain-supported. Dissolution seams mostly on the limestone parts. Anhydrite patches. Crinoid columns. Scattered penetrating dolomite with the limestone matrix. Invasive dolomitization showing a dolomitization front, selective in some areas. The more dolomitized are more porous than others. Stylolite separating the dolomitized from the non-dolomitized areas.
10748-10758:	Limestone. Highly fractured packstone, recrystallized fissures, amphibopora, burrows, peloids-pisolites,

NDGS 21734
CHESAPEAKE OPERATING, INC.
OLSON 12-139-104 A 1H
GOLDEN VALLEY COUNTY
WILDCAT FIELD
CORE INTERVAL: 10494-10550

TS: 10493.8	Botryoidal anhydrites penetrating the limestone with few dolomite crystals. Micritic with evidence of faults.
10494-10497:	Anhydrite. Light to medium (N7, N6, N5) gray nodular anhydrite with areas of soft sediments running across the face.
10498-10499:	Limestone. Pure limestone with strong effervescence. Medium gray, interparticle porosity. Have high porosity. Stromoporoids. Fault running east-west.
10499-10501:	Dolomitic limestone. Slightly dolomitic. Pale Greenish Yellow (10Y8/2). Fine grained soft sediments of mudstone bands running across the core at intervals giving it a dark and light color bands. Peloids and desiccation features so abundant.
10502-10509:	Anhydritic Limestone: This section starts with pure massive nodular anhydrite then at 10503 the anhydrites turns grayish orange pink (10R 8/2). At intervals, the anhydrite seems to be covered by soft sediments with desiccation features and peloids with laminated bedding.
TS: 10509.2:	Anhydritic Limestone. Micrite envelopes. The anhydrites form a band that is compacted due to pressure. Micritic.
10510-10513:	Dolomitic Limestone: The anhydrites is reduced to tiny bull eye patches on the surface of the core. Abundant peloids. Peloidic limestone. Stromaporoids. Floatstone. Stylolite at 10514 and at 10516. Desiccation features. Abundant fractures.
TS: 10521:	Dolomite. Grain-supported. Packestone. More dolomitized than the upper units. More of an invasive dolomitization. The blues stains to show the porosity.
10514-10550:	Dolomitic Limestone: Medium Light Gray (N6). Good porosity. Abundant amphipora. Abundant burrows, Anhydrites acting as floatstone, Wackstone/packstone. Stromatolites. Abundant fractures. Stylolite at 10517 and 10520. Peloids. Brachiopod stems.

APPENDIX 2

THIN SECTION IMAGES

NDGS 291

AMERADA HESS CORPORATION

FRYBURG HEATH-MADISON UNIT P-812

BILLINGS COUNTY, NORTH DAKOTA

FRYBURG FIELD

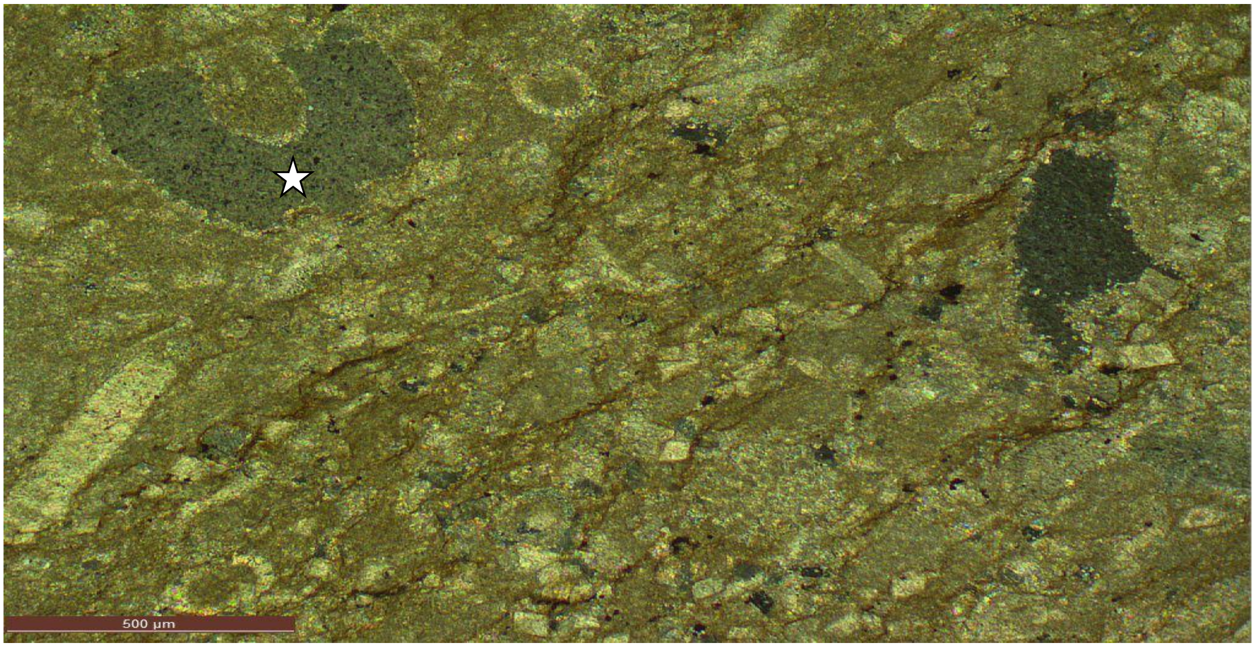

291 (10,588.8 ft.). Packstone showing selective dolomitization, dissolution seams and horse tail stylolites. Crinoid arm plate (stared)

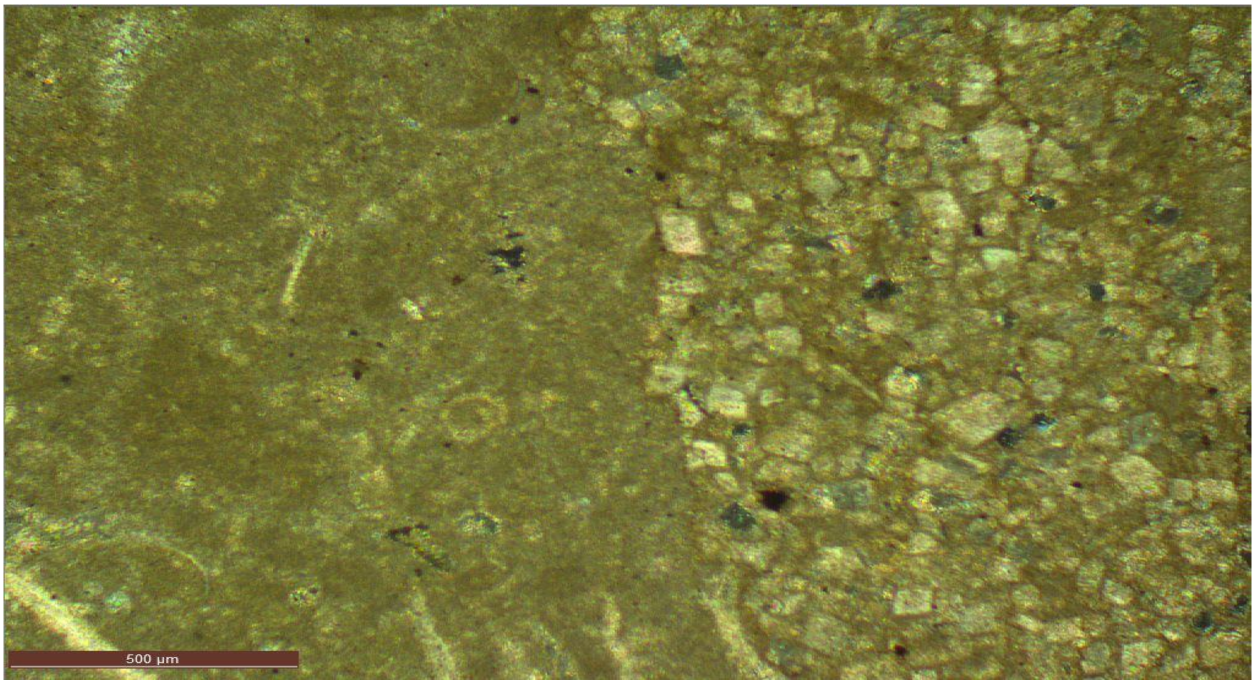

291 (10599.8 ft.) Dolomitization front moving from right (packstone) to left (wackestone). This preferential dolomitization showing that the rocks at the right are more prone to dolomitization than those on the left.

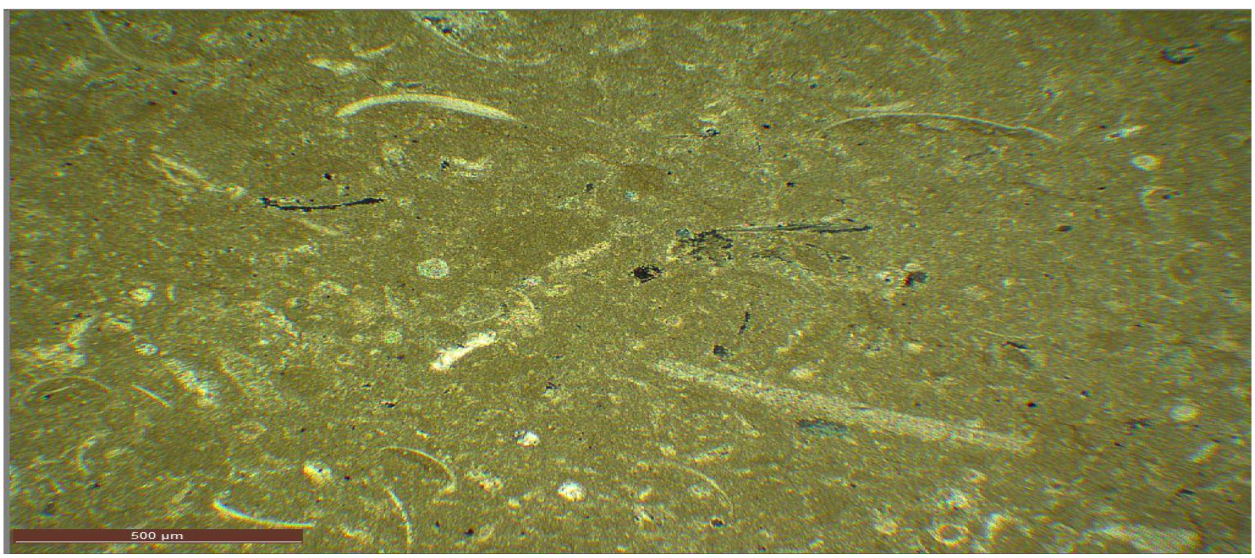

291 (10588.8 ft). Packstone showing a bioclast. This section still have the original limestone still largely not dolomitized.

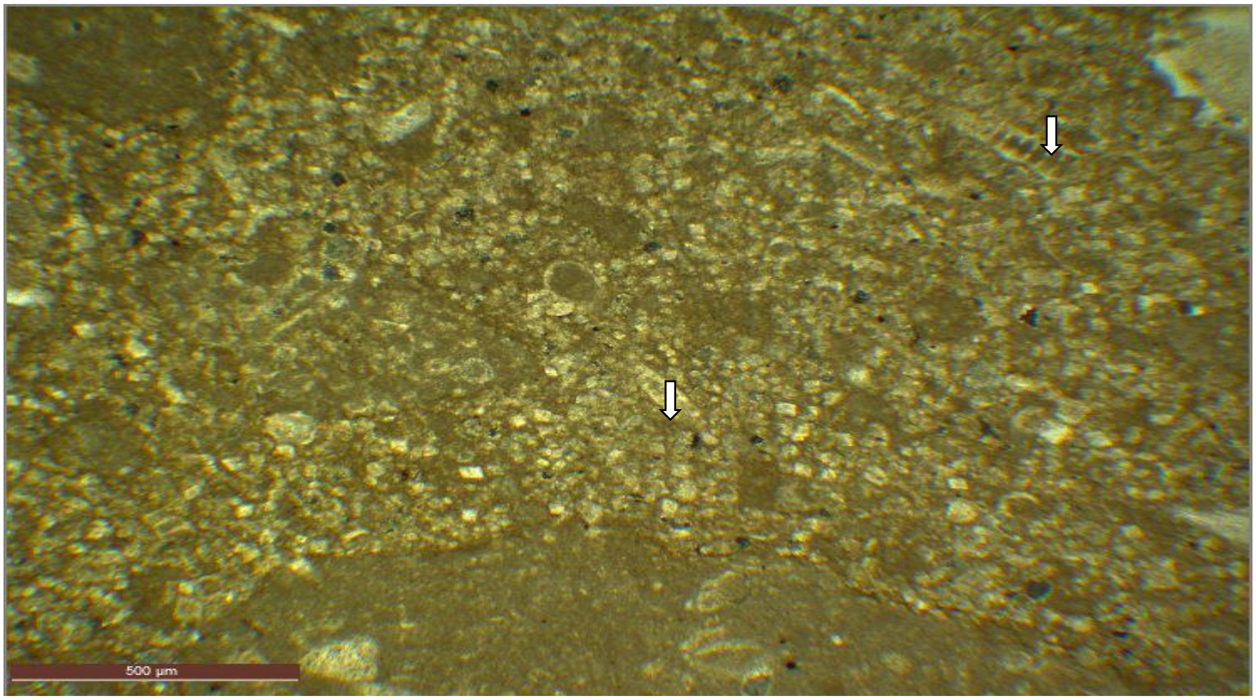

291 (10,588.8 ft.) selective dolomitization with Biserial foraminifer (arrows).

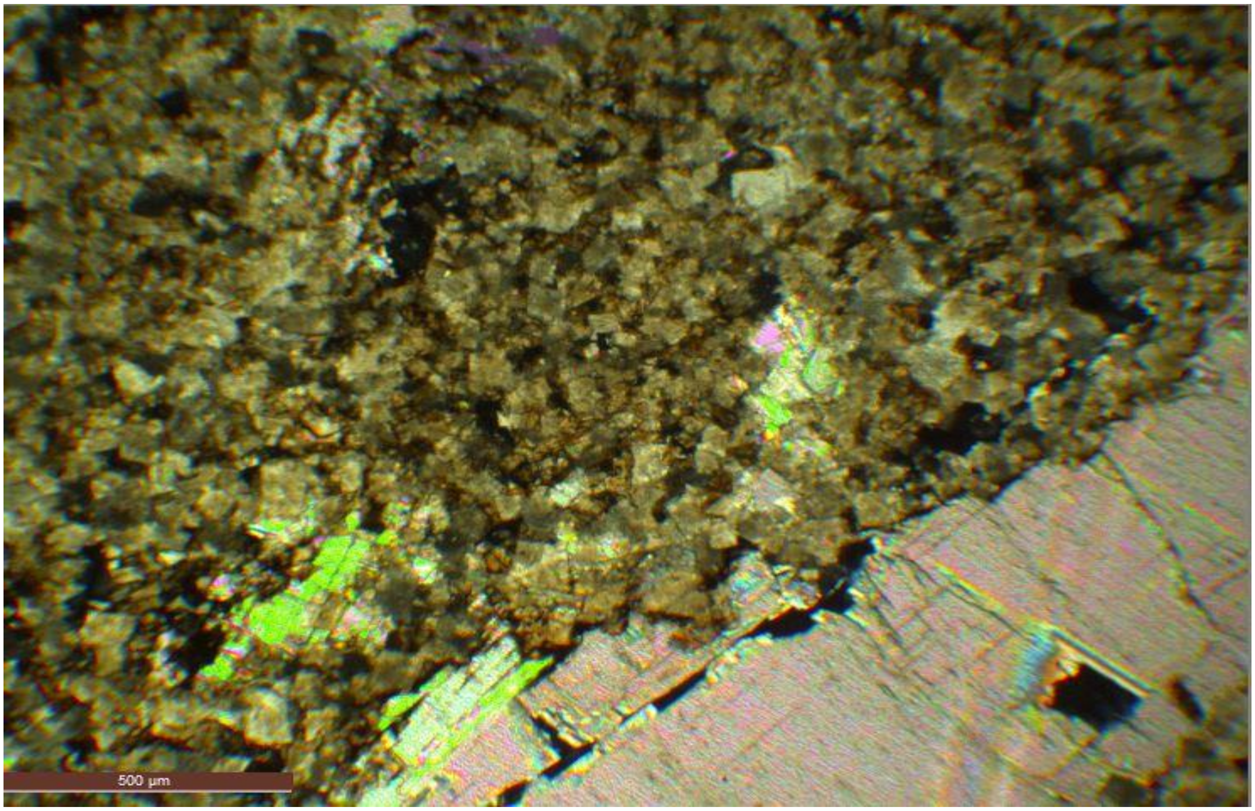

291 (10,676 ft.). Dolomite crystals with patches of anhydrites.

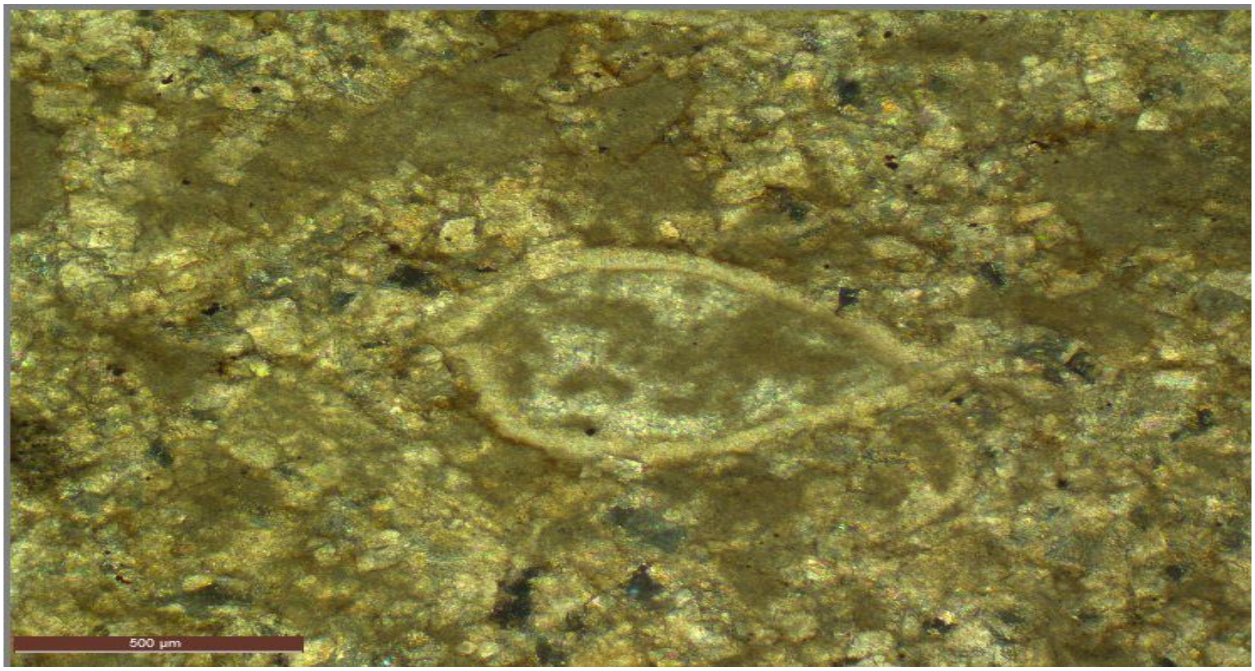

291 (10680 ft.). Packstone with dolomite crystals and a bivalve that has been calcified with its original outline only able to be identified by the micrite envelope.

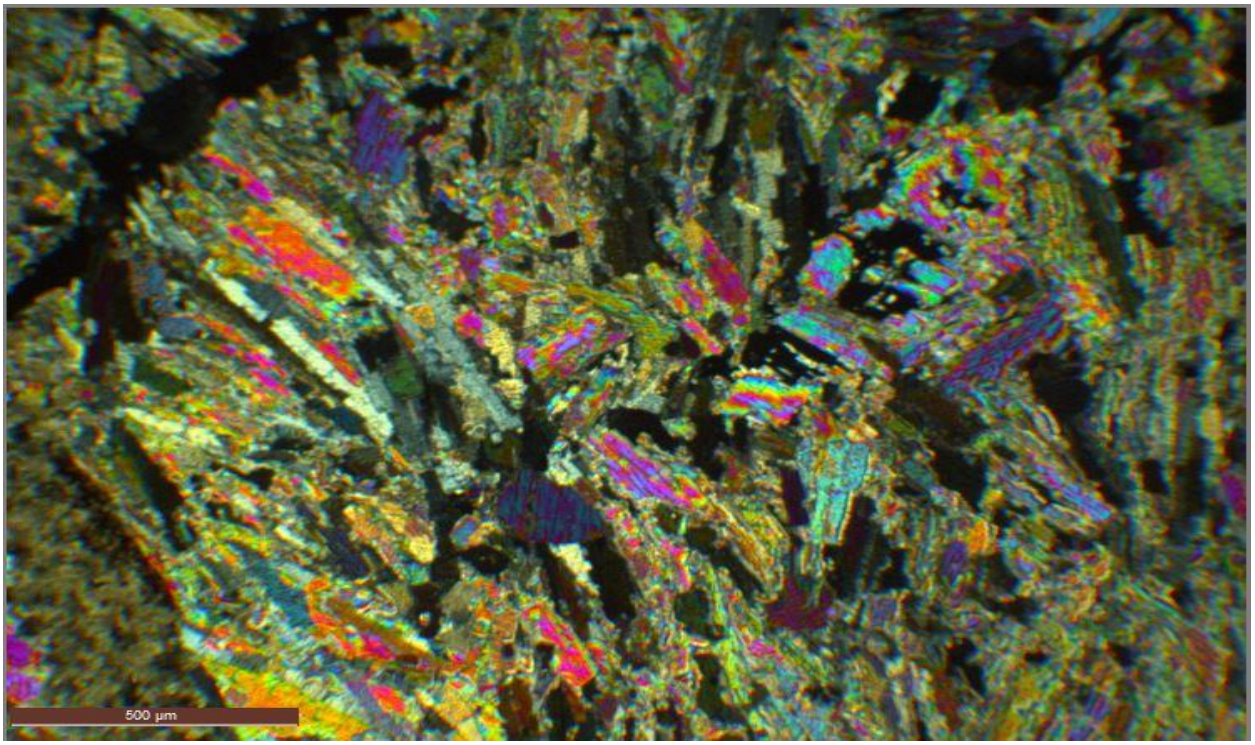

291 (10680 ft.) Large bladed anhydrites displaced and replacing the original carbonate material. These anhydrites occludes the porosity

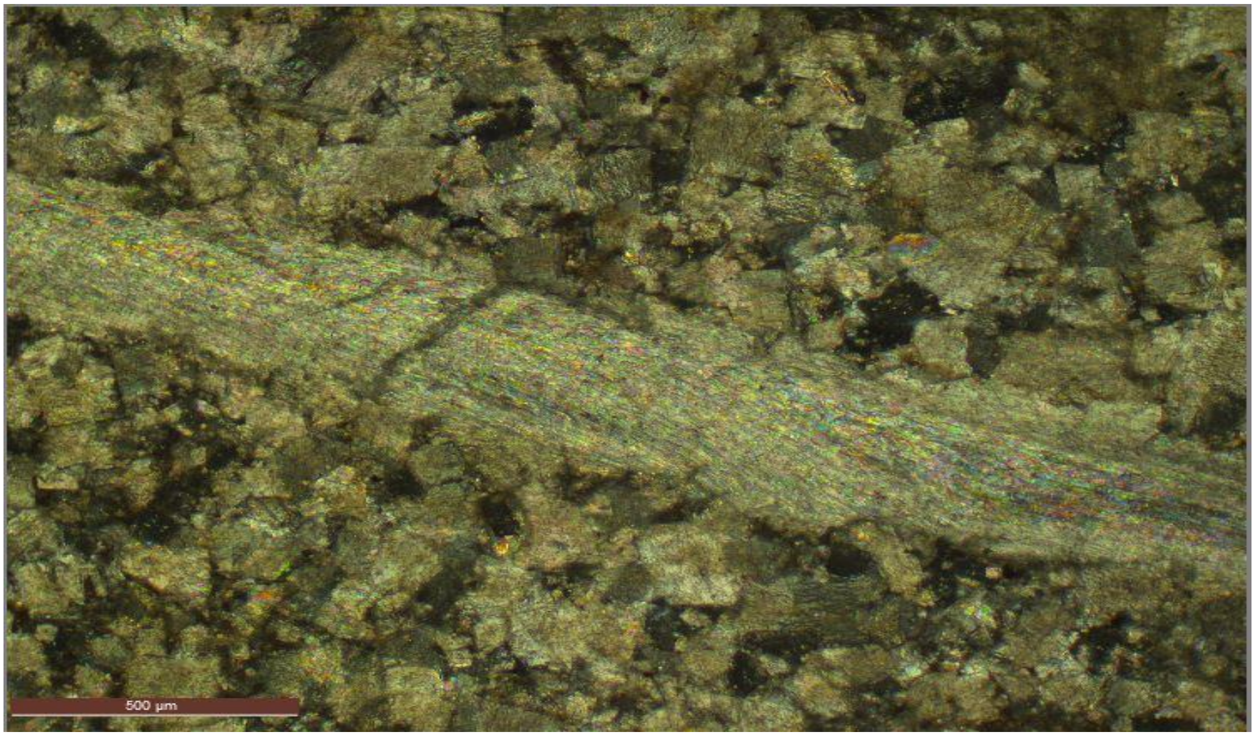

291 (10685 ft.) Punctuate brachiopod stem filled with anhydrites.

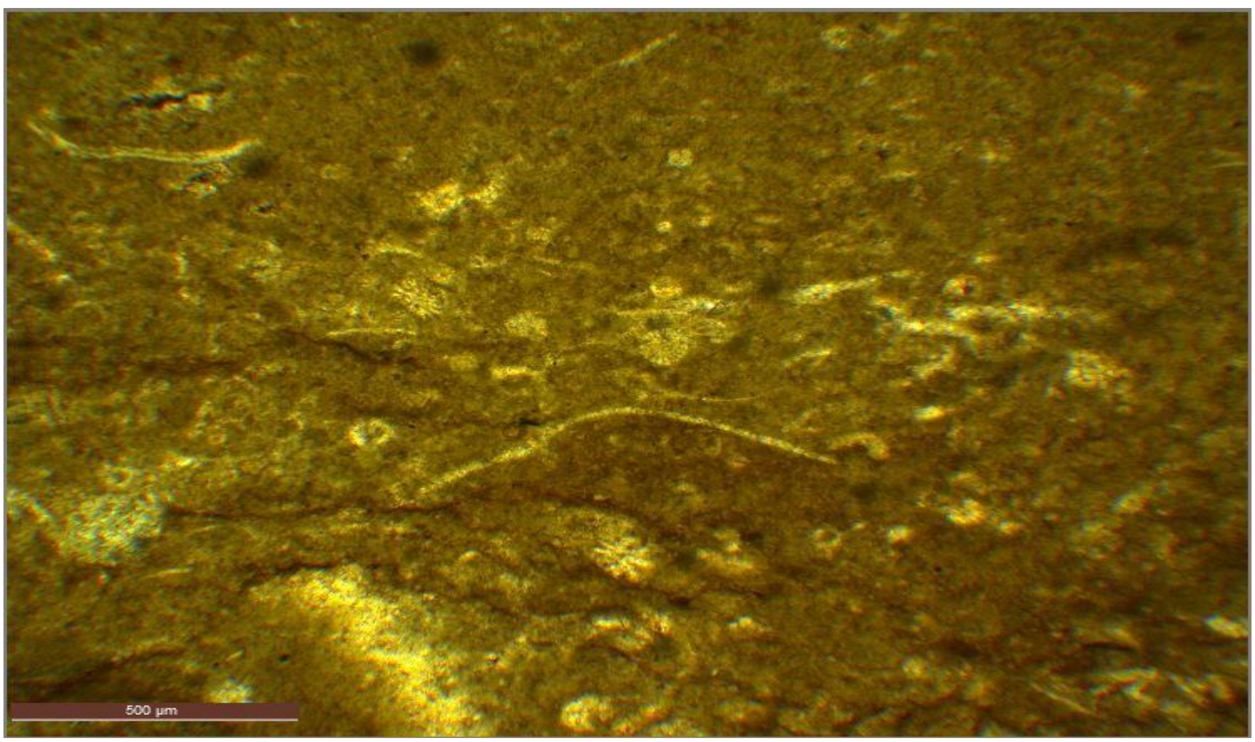

291 (10689 ft.) Wackestone with fragment like echinoids and bivalves that has been calcified.

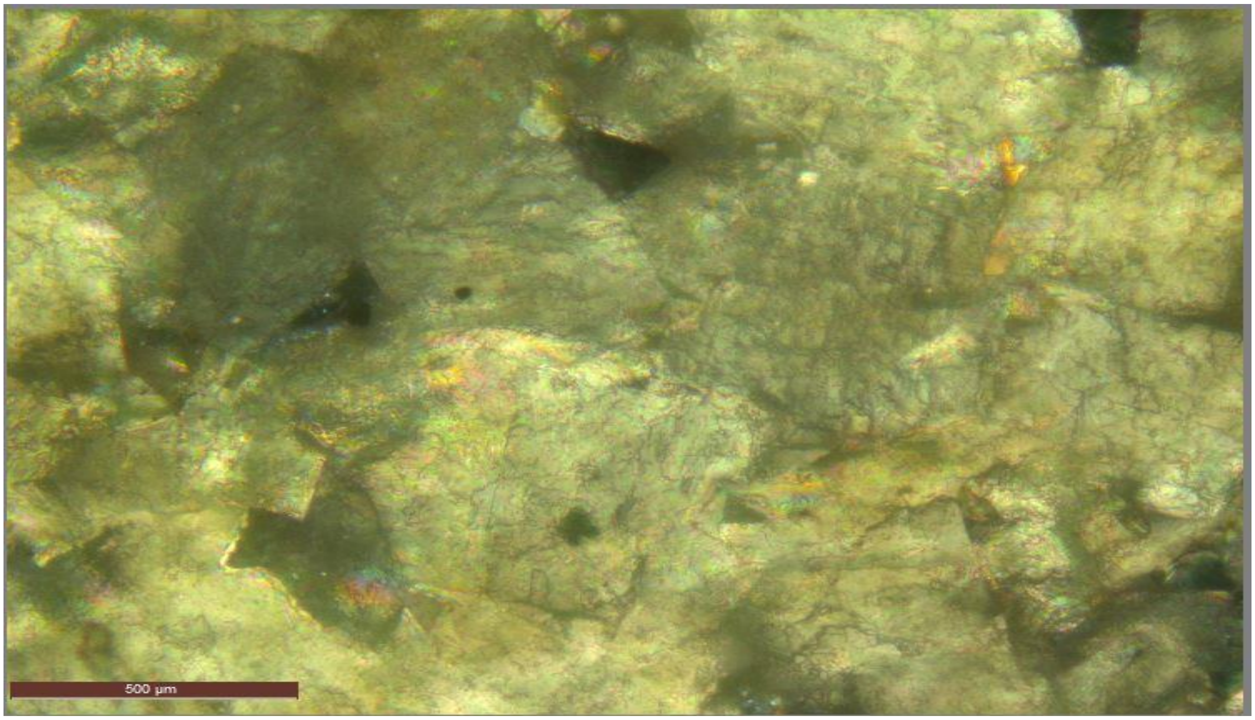

291 (10684.8 ft.) Dolomite crystals chemically being sutured together hence reducing porosity.

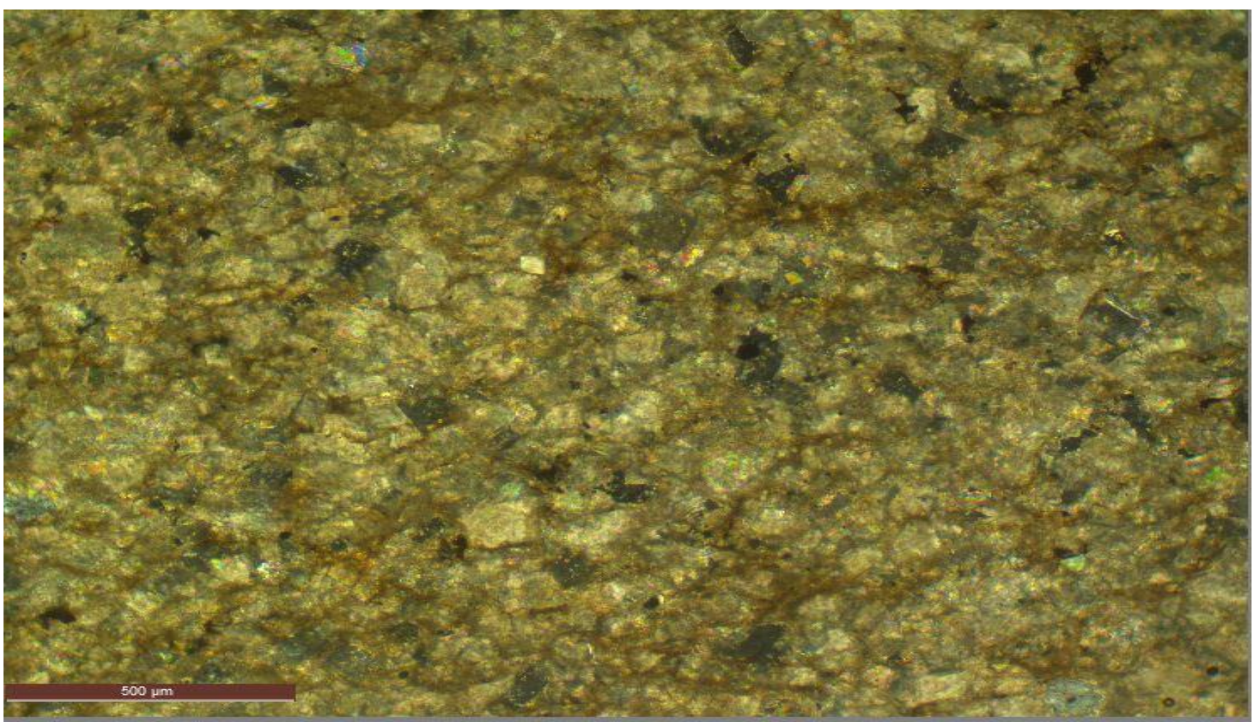

291 (10685 ft.) Packstone partially dolomitized but with lots of the “ghost” of the original sediment visible by the micrite envelops.

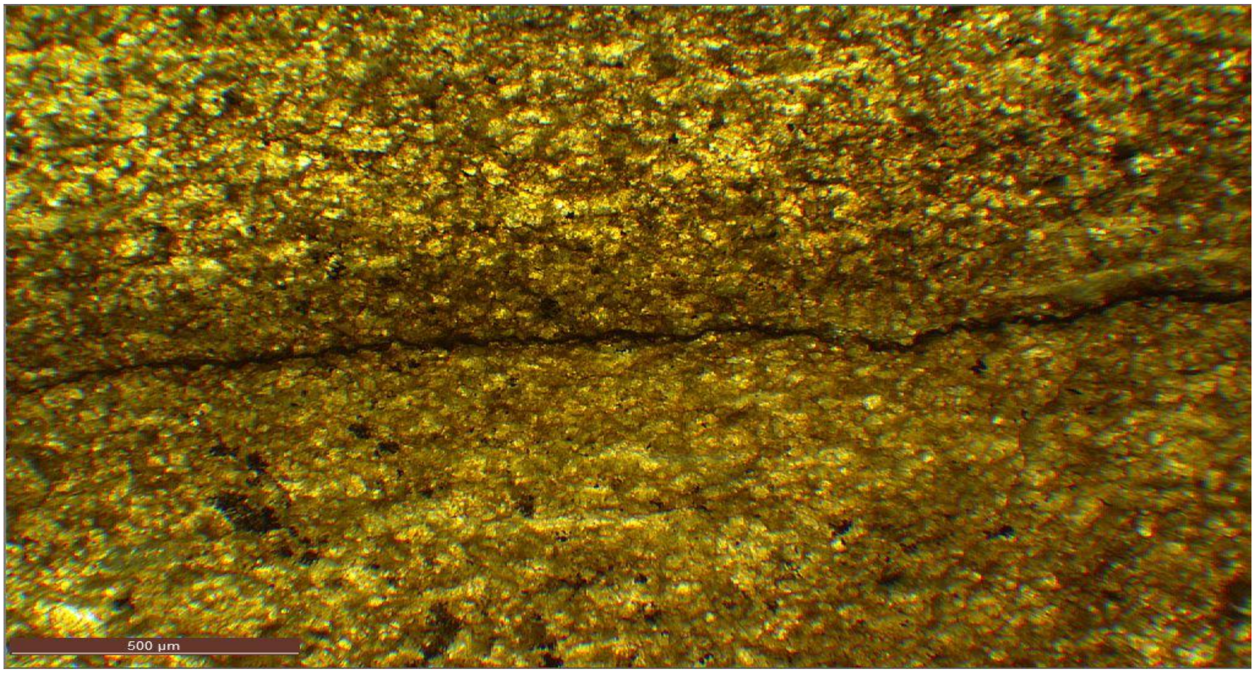

291 (10689 ft.) Fine dolomite crystals with fracture running over it.

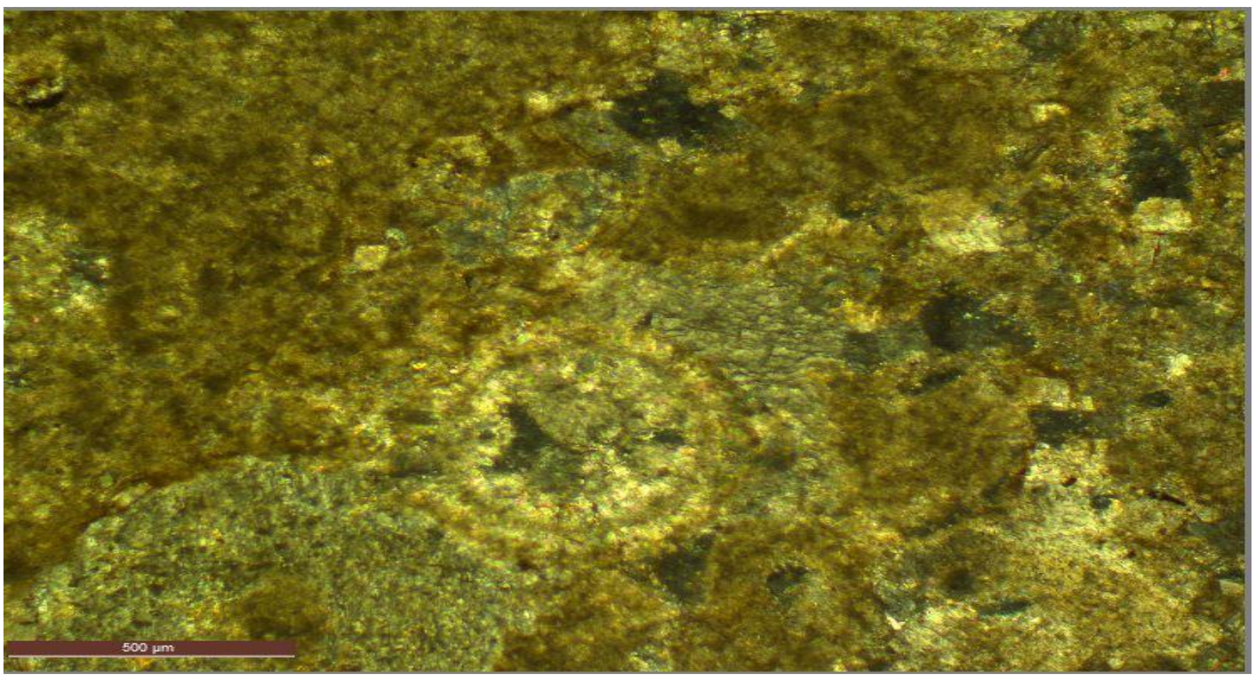

291 (10690 ft.) Dissolved aragonite shell with calcite precipitation in the center causing biomoldic pores.

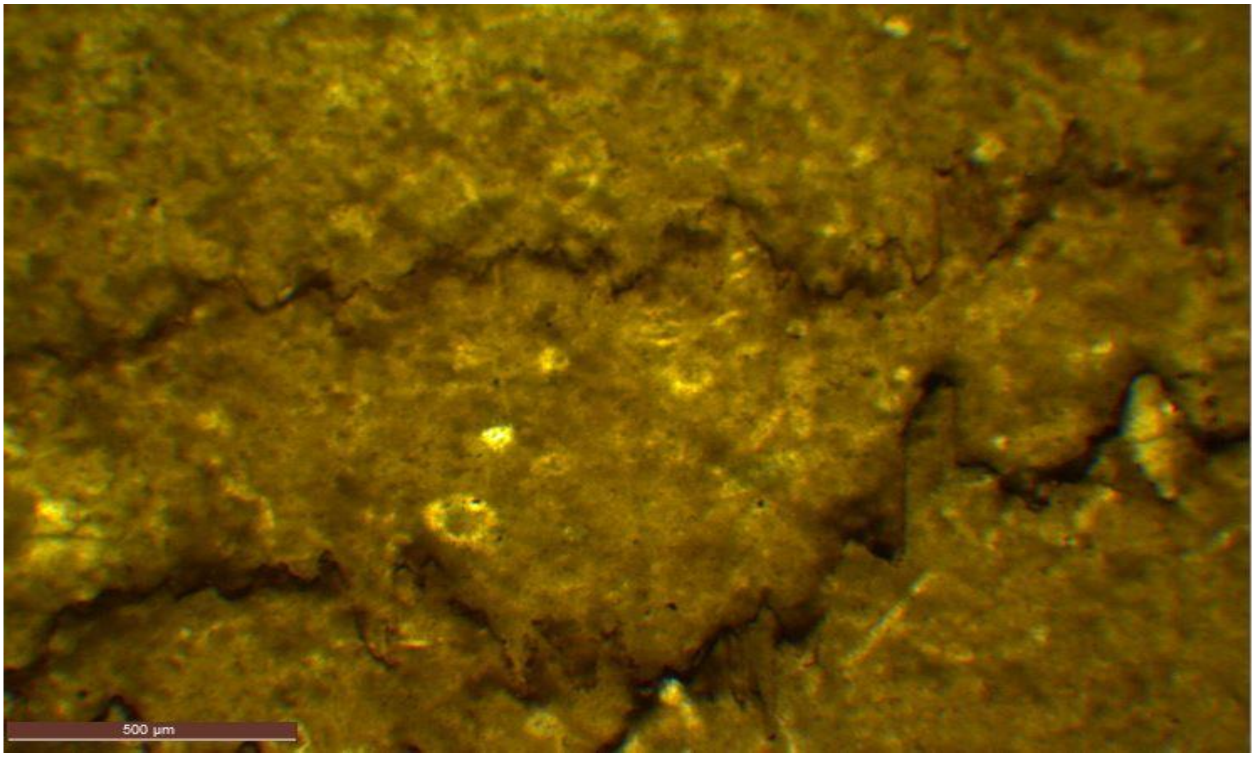

291 (10693.5 ft.) Stylolite.

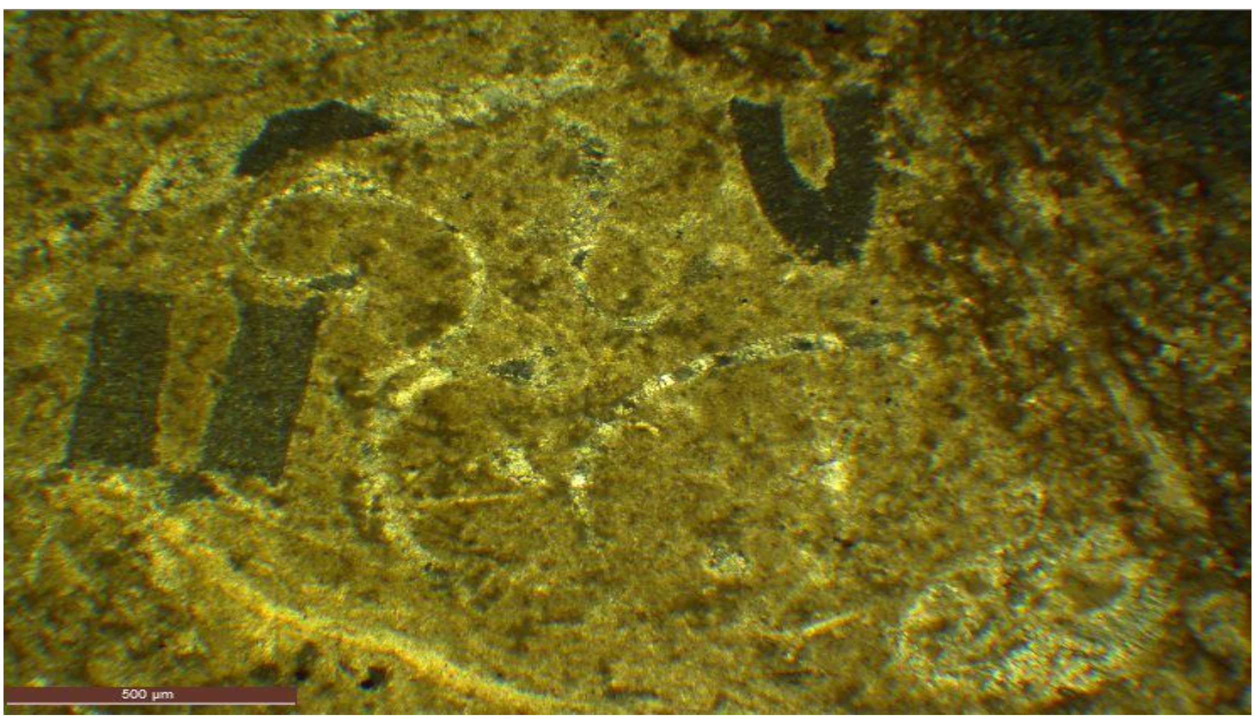

291 (10693.5 ft.) Wackestone with crinoids, gastropods, and bivalves outlined by the micrite envelope.

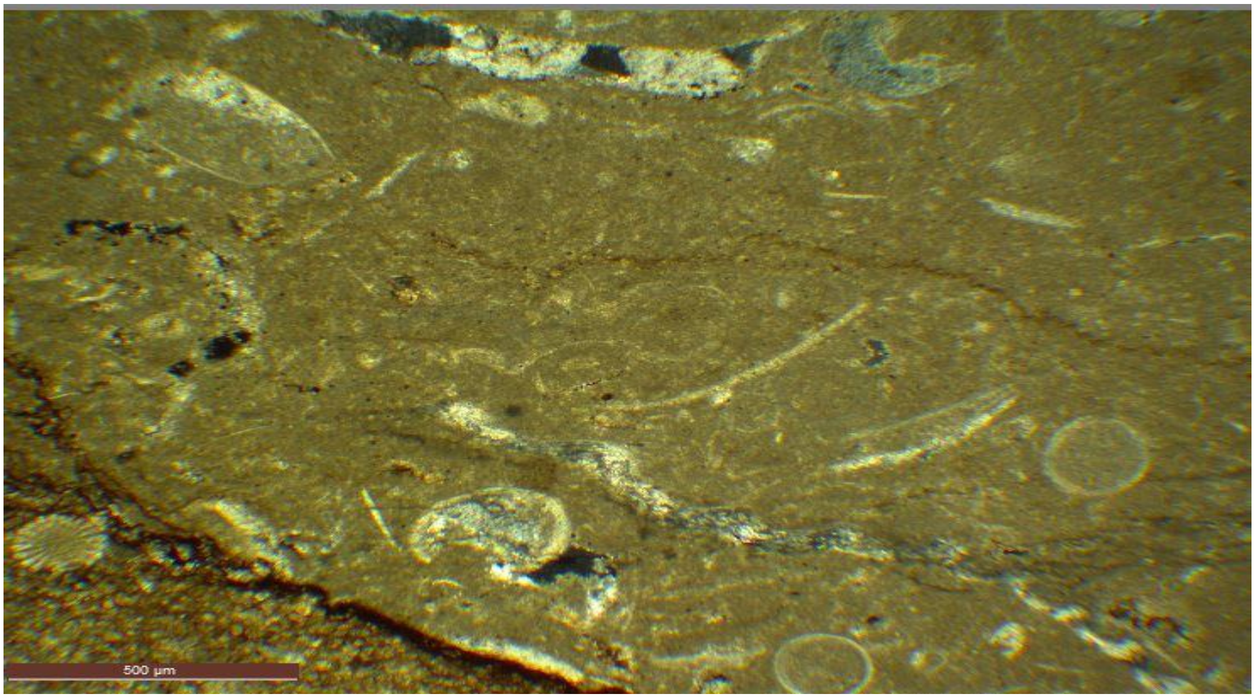

291 (10699.9 ft.) Wackestone with lots of fossil fragments making up the allochem and constituting a biosparite.

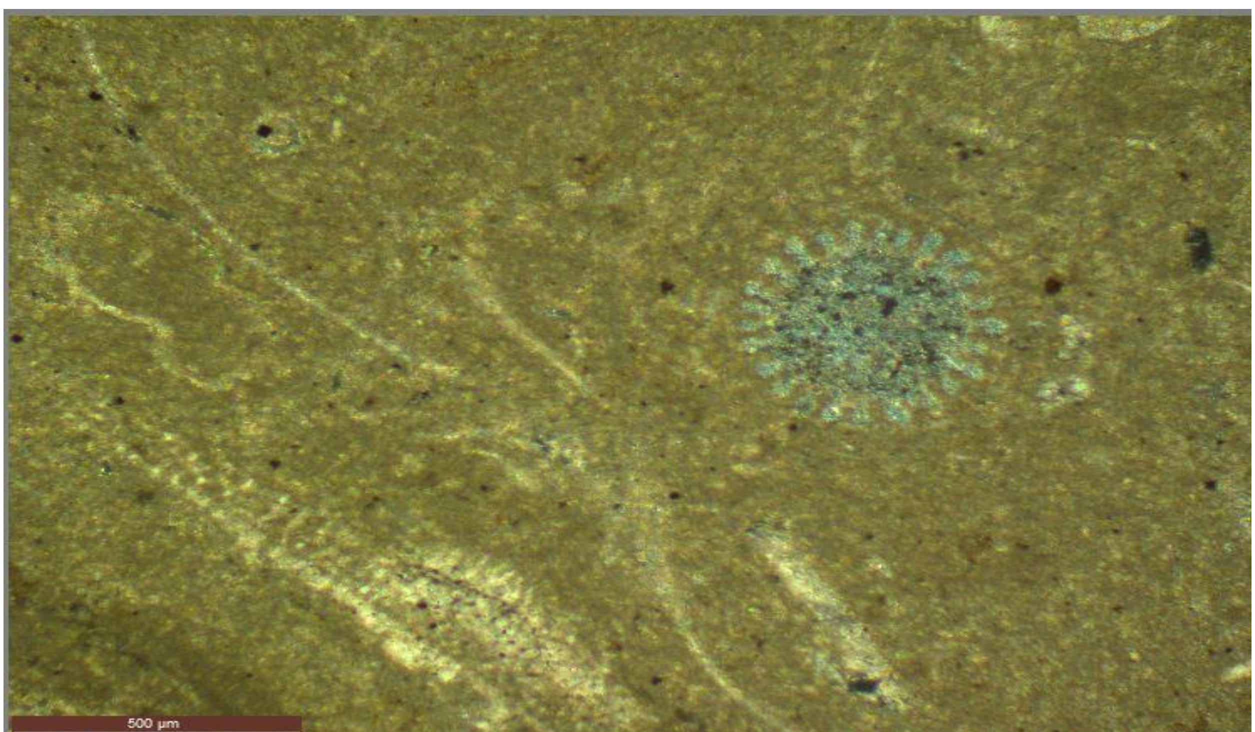

291 (10699.9 ft.). Echinoid, brachiopod and other fragments making up this Wackestone.

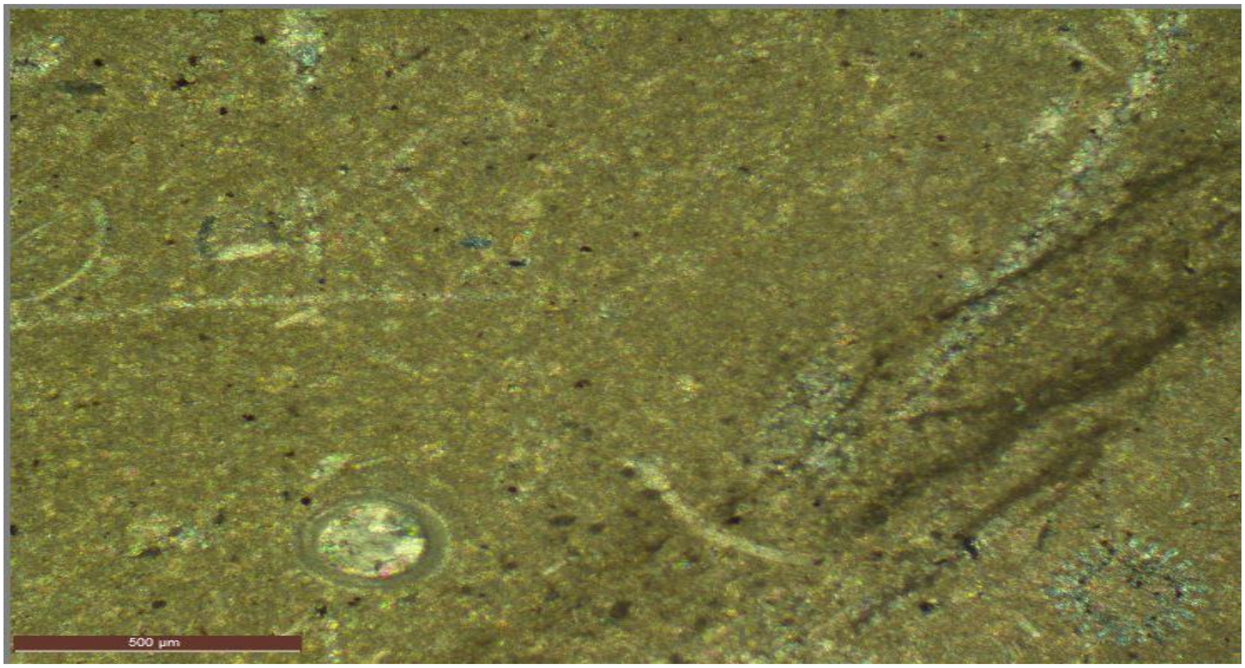

291 (10699.9 ft.) The ooid at the lower section of this wackestone, as outlined by the micrite envelope has been filled by calcite thereby closing what could have been a good source of porosity. Also seen are other fragments like echinoid and broken bivalves.

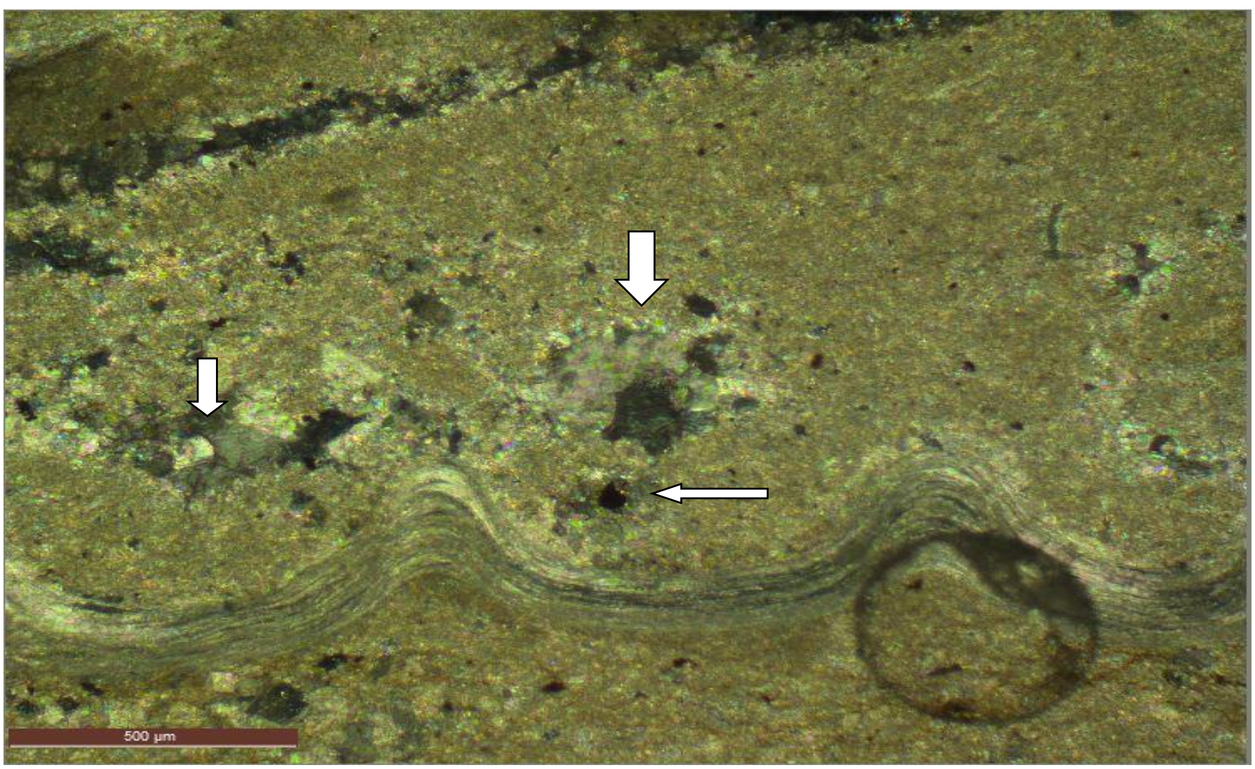

291 (10699.9). Moldic pores formed by fragment dissolutions(arrows), though the vugs created can be seen to be undergoing calcification.

THIN SECTIONS IMAGES FROM
NDGS 859
TEXACO INC.
GOVT. - M. S. PACE 1
BILLINGS COUNTY, NORTH DAKOTA
MAGPIE FIELD

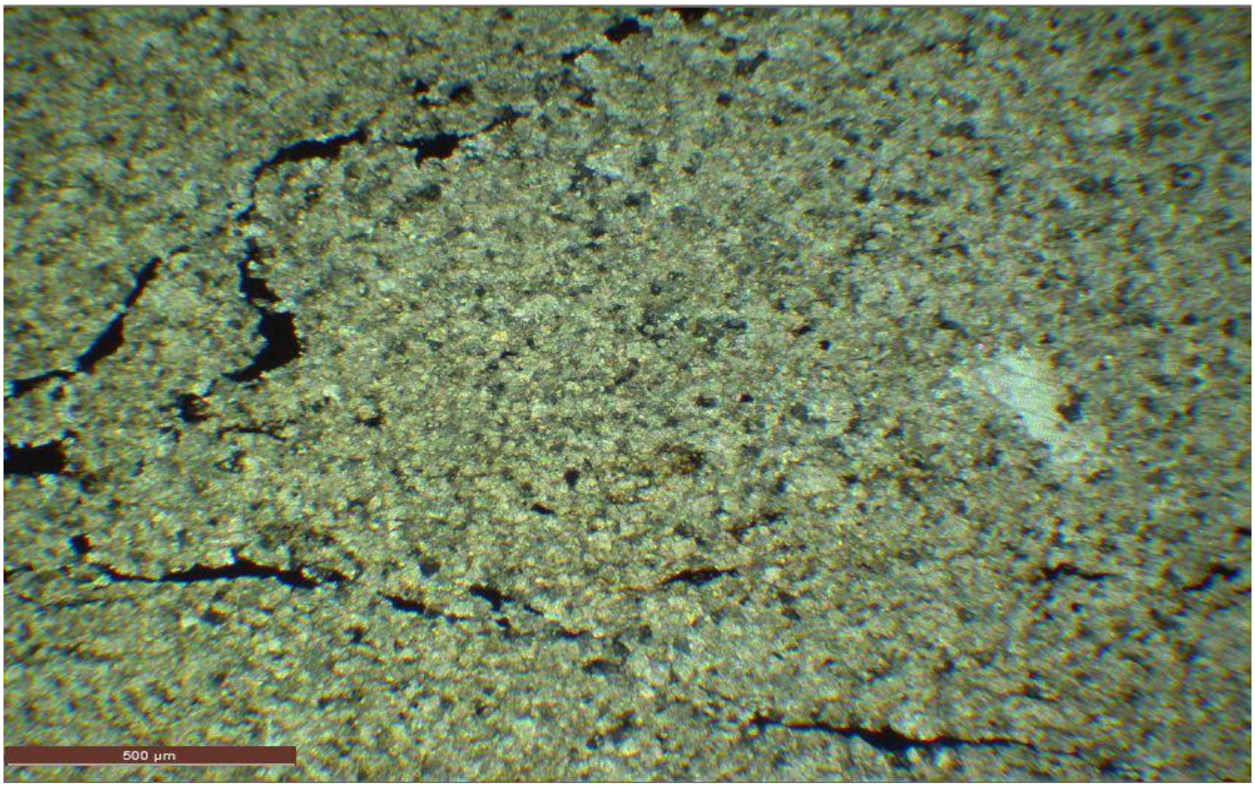

859 (10920-21 ft.) Finely crystalline dolomite with faults

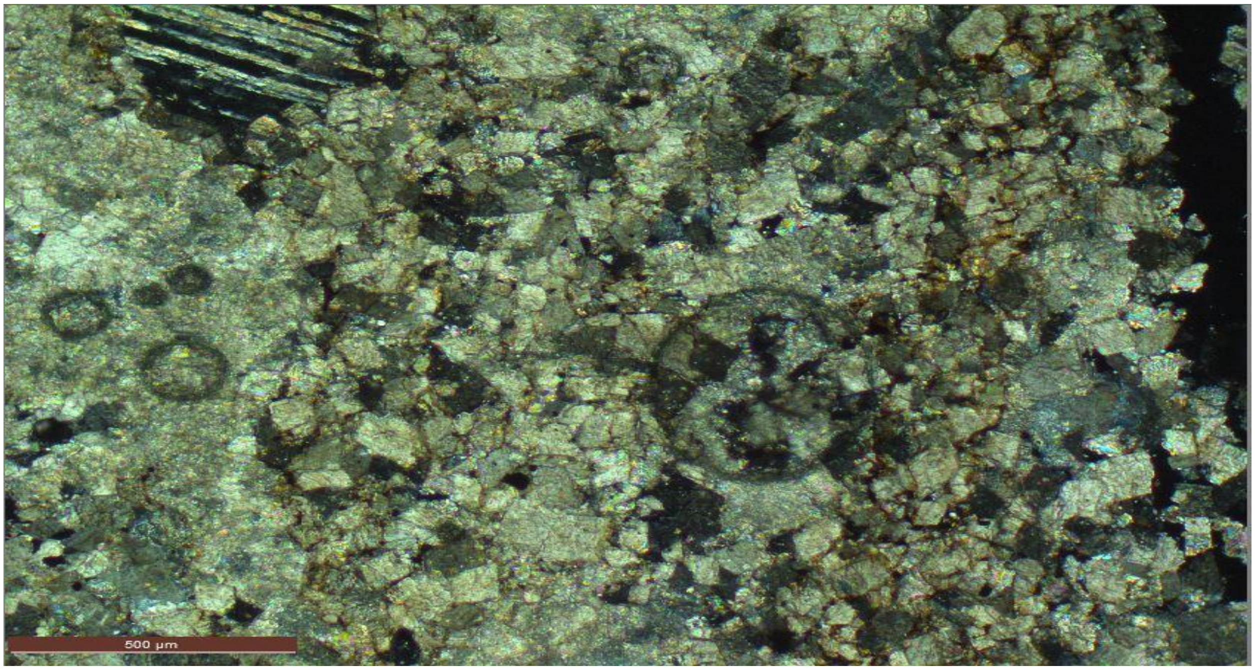

859 (10921-922 ft.) Packstone with selective dolomitization and dolomite cements in the fossil fragments. Leaching has taken place in the fragment forming a biomoldic pores.

859 (10925-26 ft.) A packstone showing bivalve, echinoid and brachiopod forming a biosporite with micrite envelopes projecting the outline of the original structures.

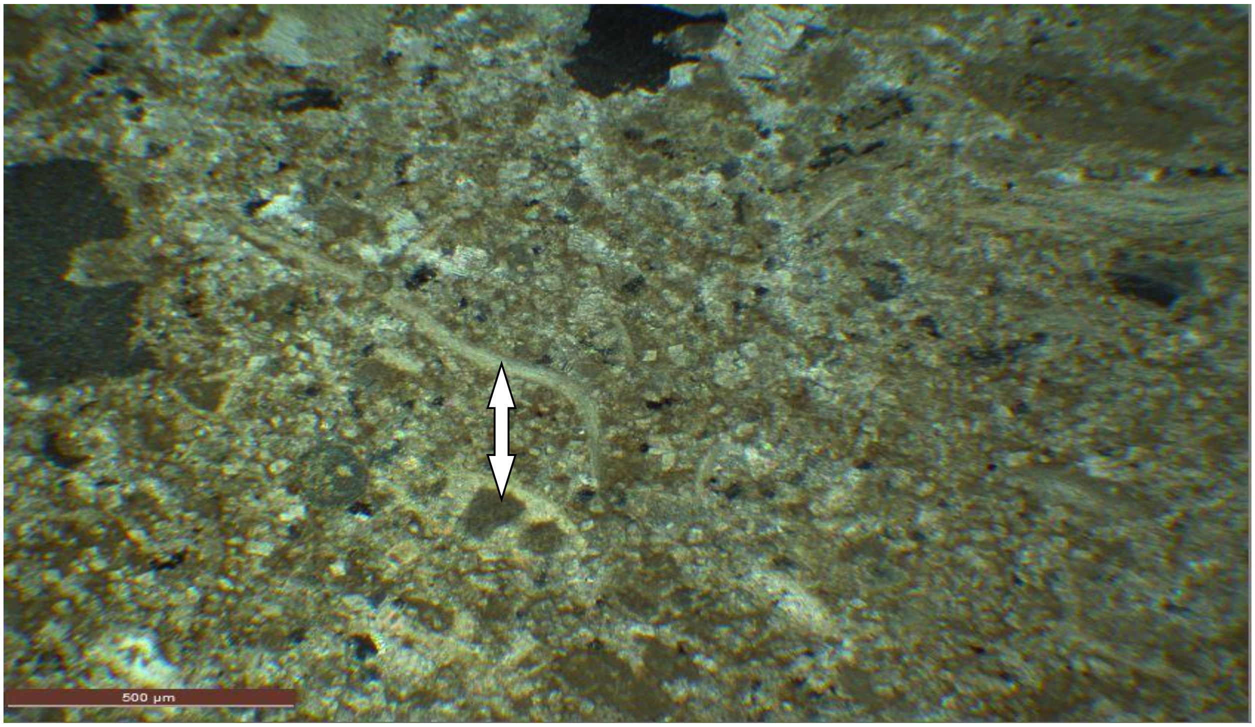

859 (10925-26 ft.) This packstone shows gastropod and brachiopod fragments embedded in a limestone with dolomite crystals

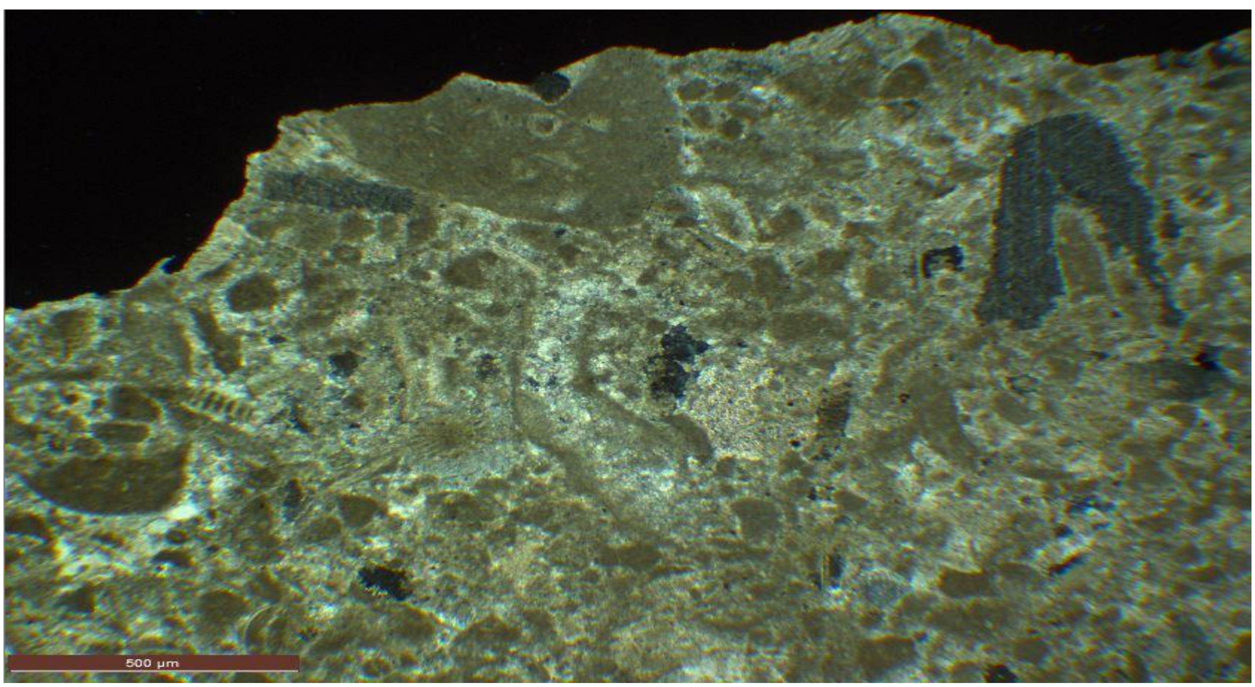

859 (10925-26 ft) Wackestone/Sparse biomicrite with different fossil fragments that can only be recognized by the micrite envelops. Most of the fragments have been calcified.

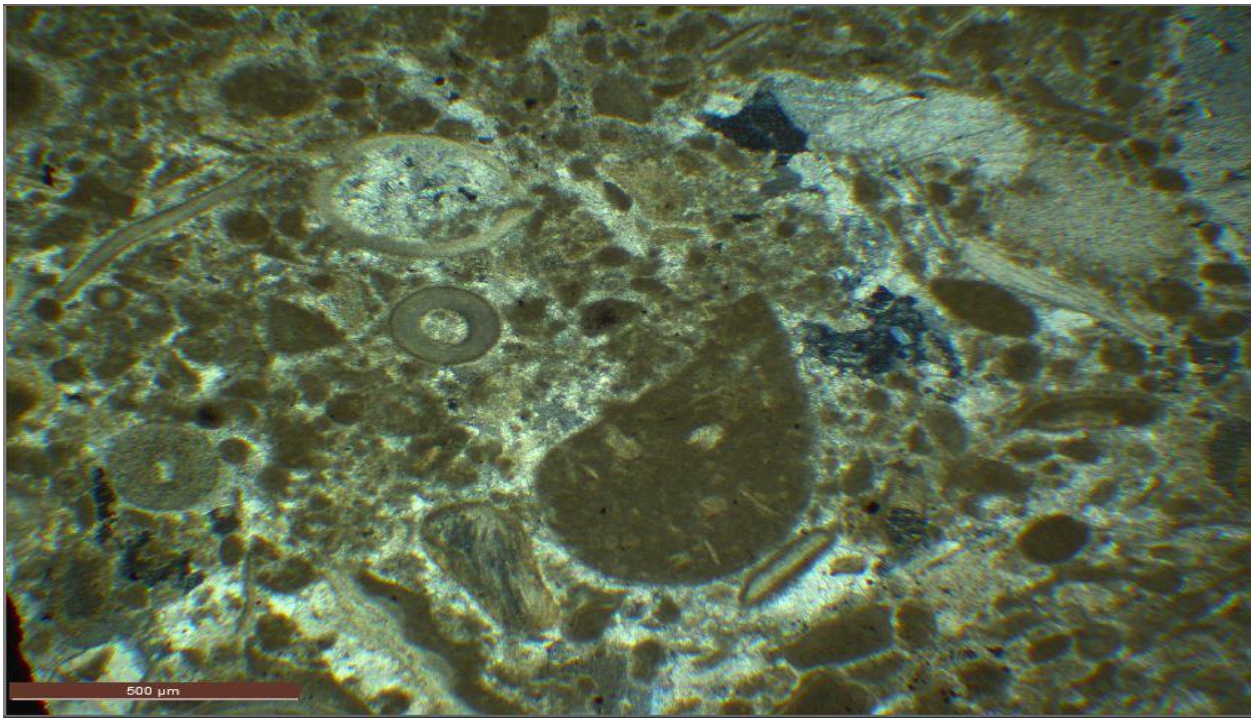

859 (10925-26 ft.) This packstone/biosparite shows isopachous cement showing a marine with a variety of fossil fragments as a contributor to the sediment. The soft arogonites from the bivalves and the ooids has been dissolved but the outline can still be seen with calcite crystals growing in the middle.

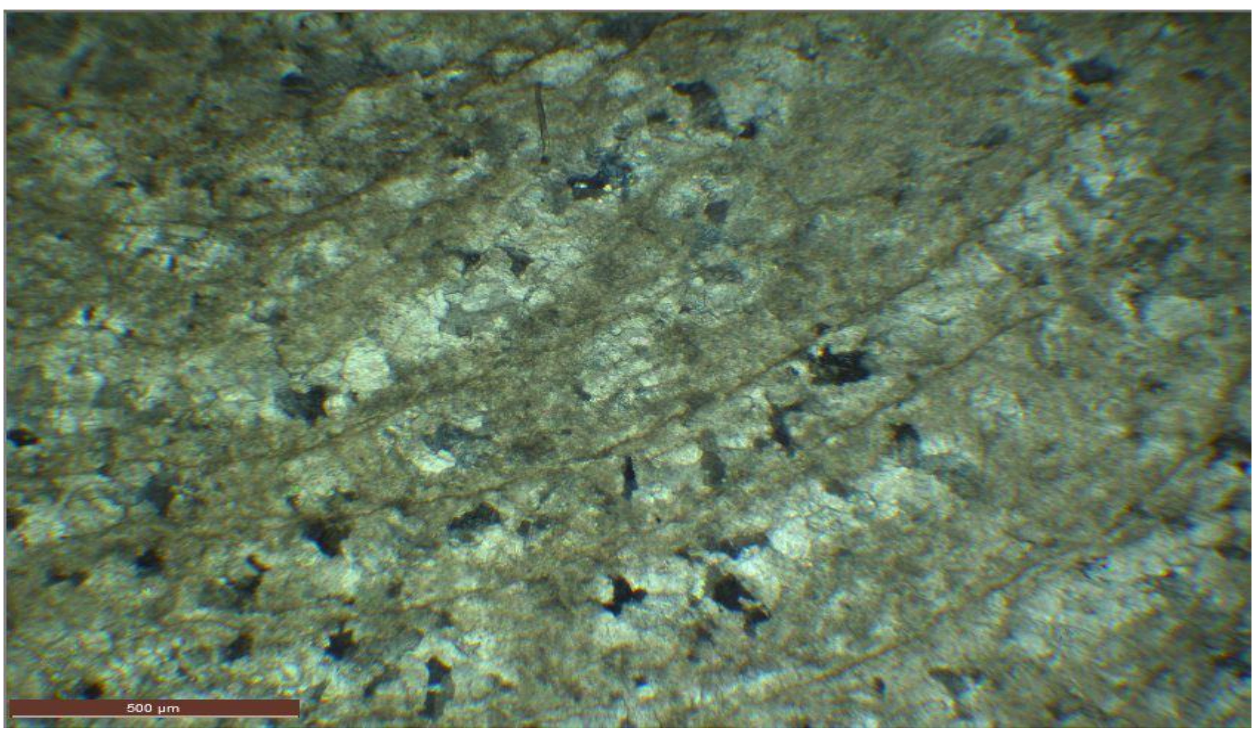

859 (10928-929 ft.) Selective Dolomitization but the original sediment can still be seen.

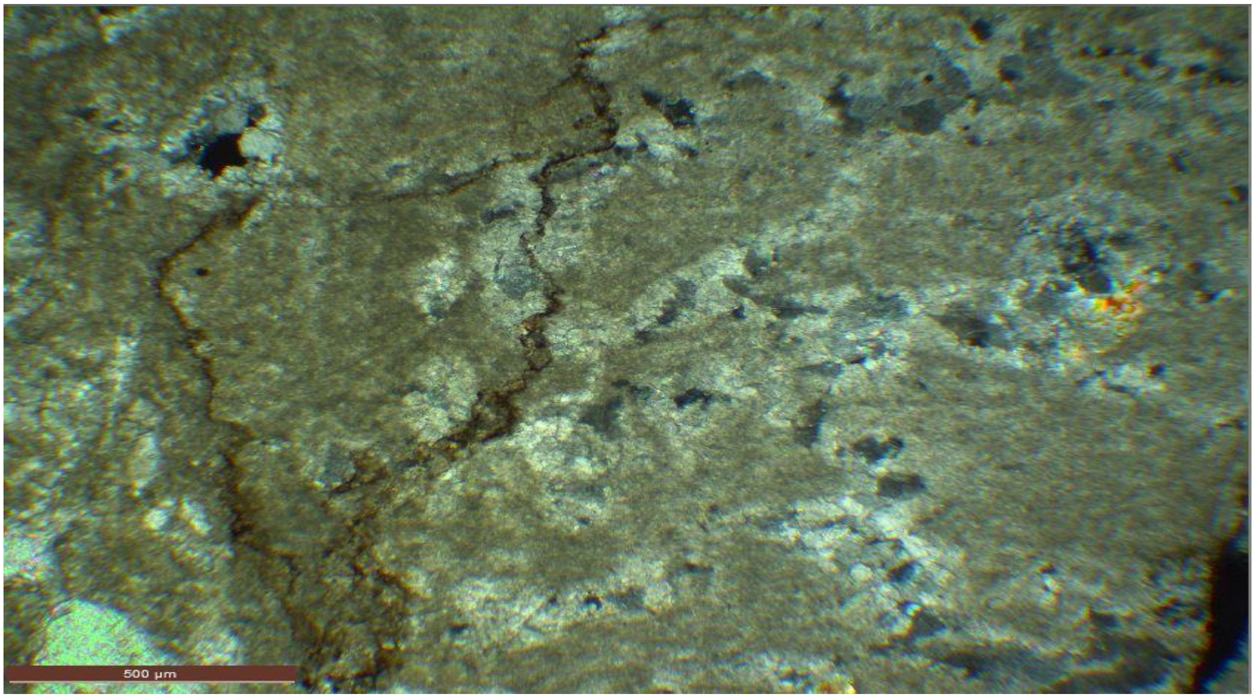

859 (10928-929 ft.) Packstone with dissolution seam running through the unit. The dissolved fossil (upper left) produces a vug with recrystallization taking place within. Scattered dolomite crystals and anhydrite at the bottom left.

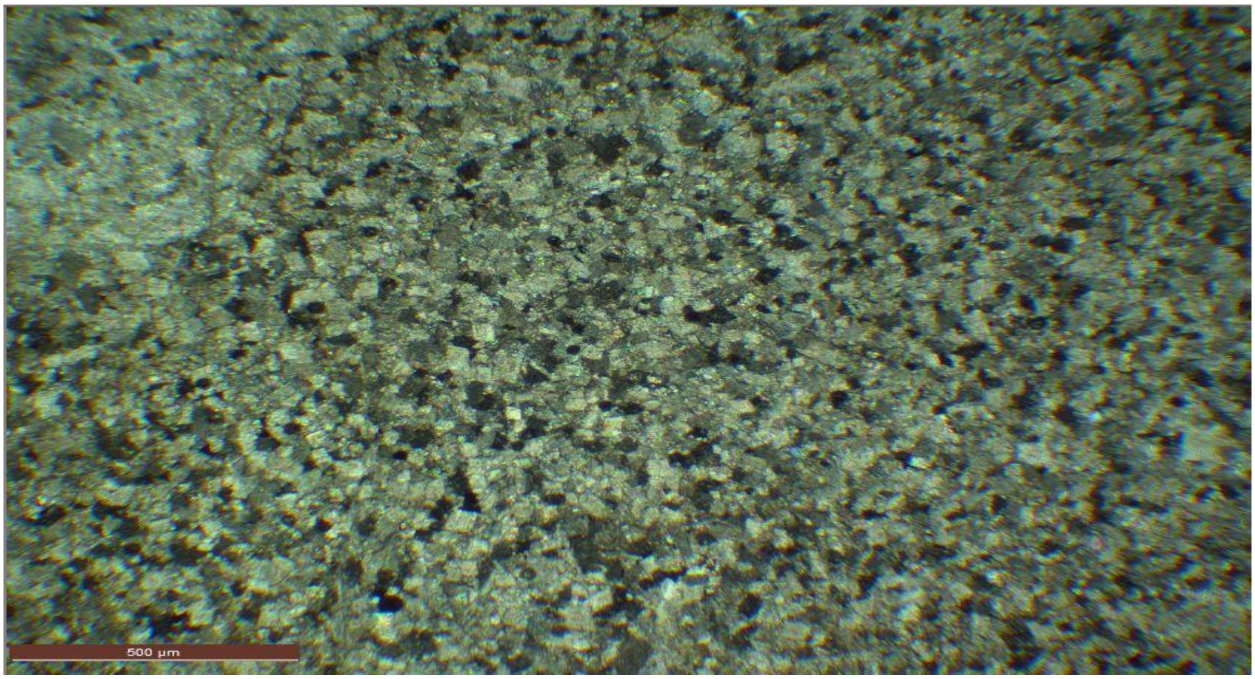

859 (10928-929 ft.) Dolomitization causing high porosity.

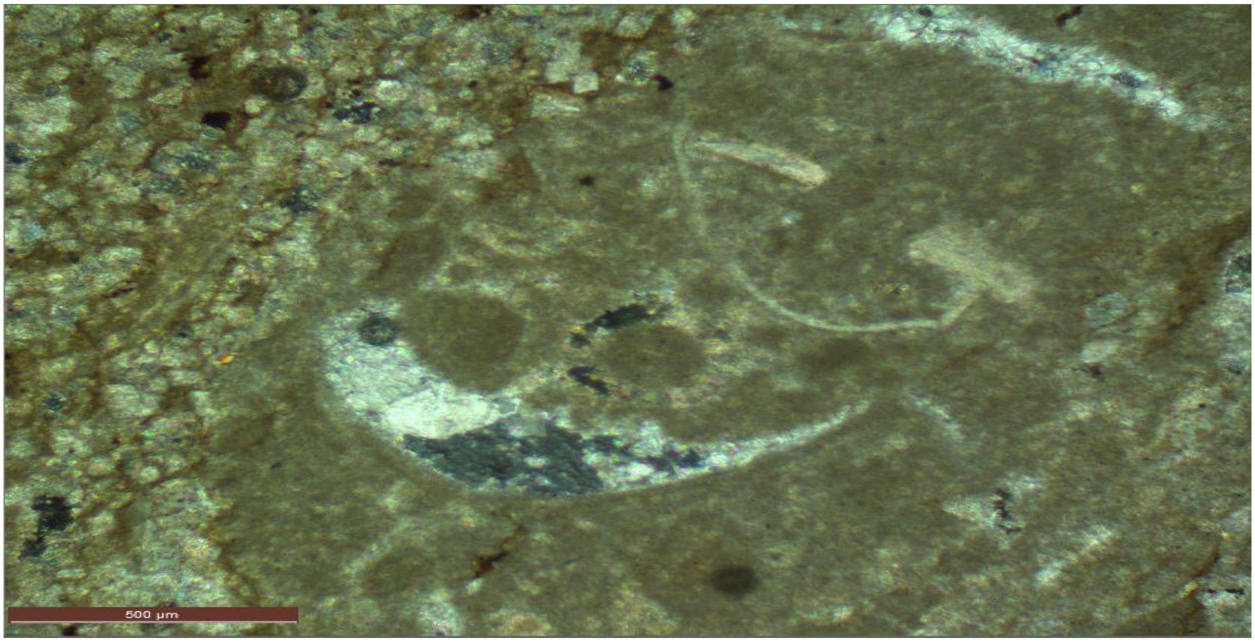

859 (10933-934 ft.). Dolomitization front showing probably a more resistant material to the right with recrystallized fossil fragments projected by the micrite matrix.

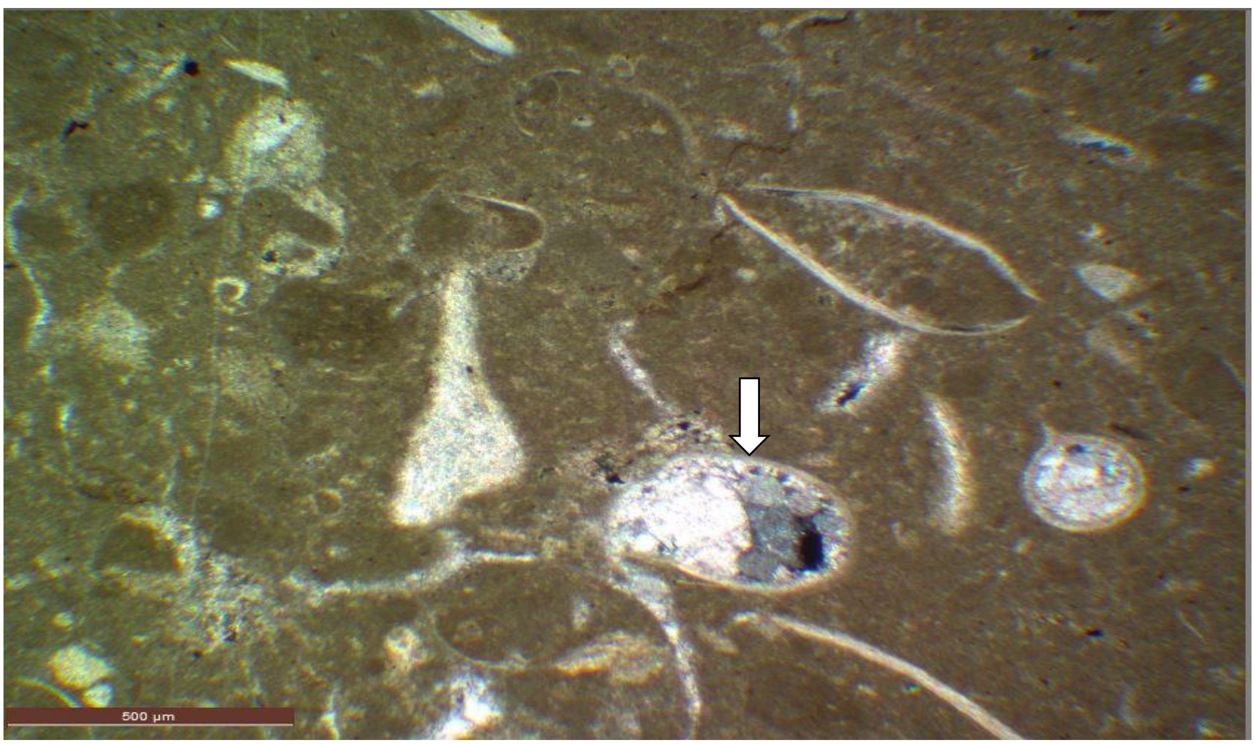

859 (10933-934 ft.) Packstone/biosparite. Abundant fossil fragments calcified. The bivalve shows a geopedal structure (arrow)

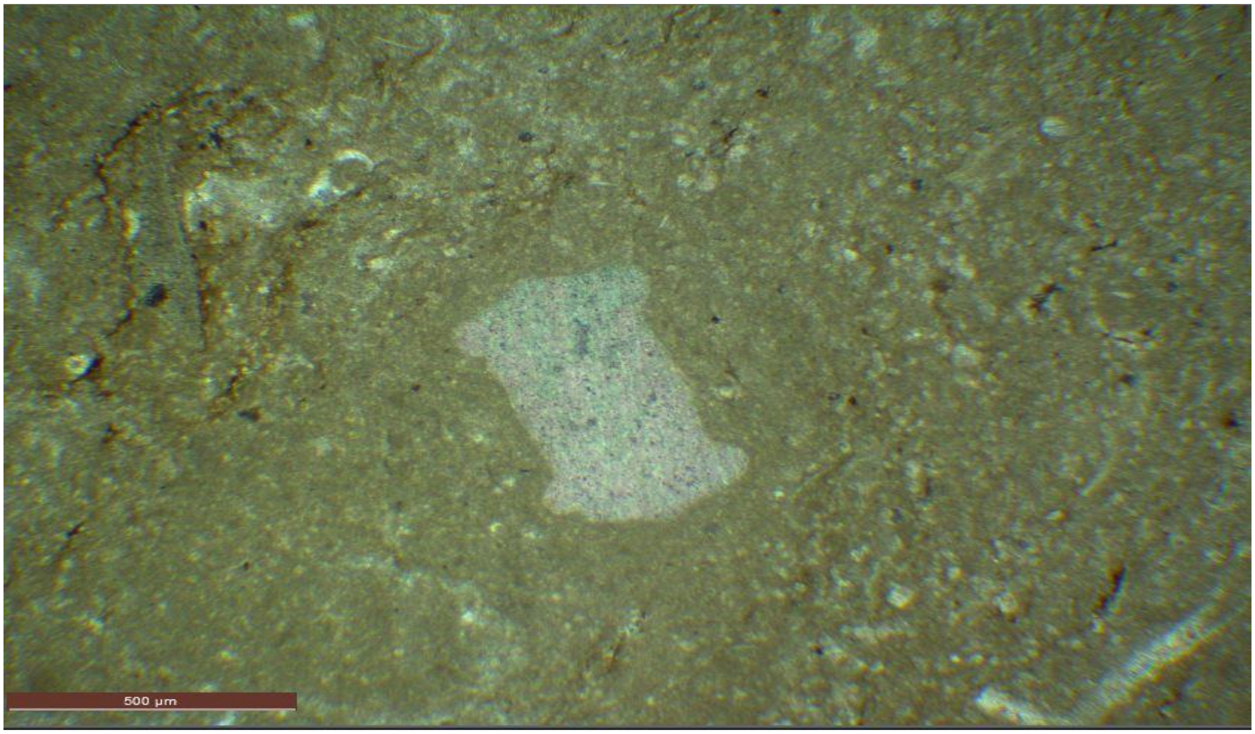

859 (10943-944 ft.) Wackestone with crinoid

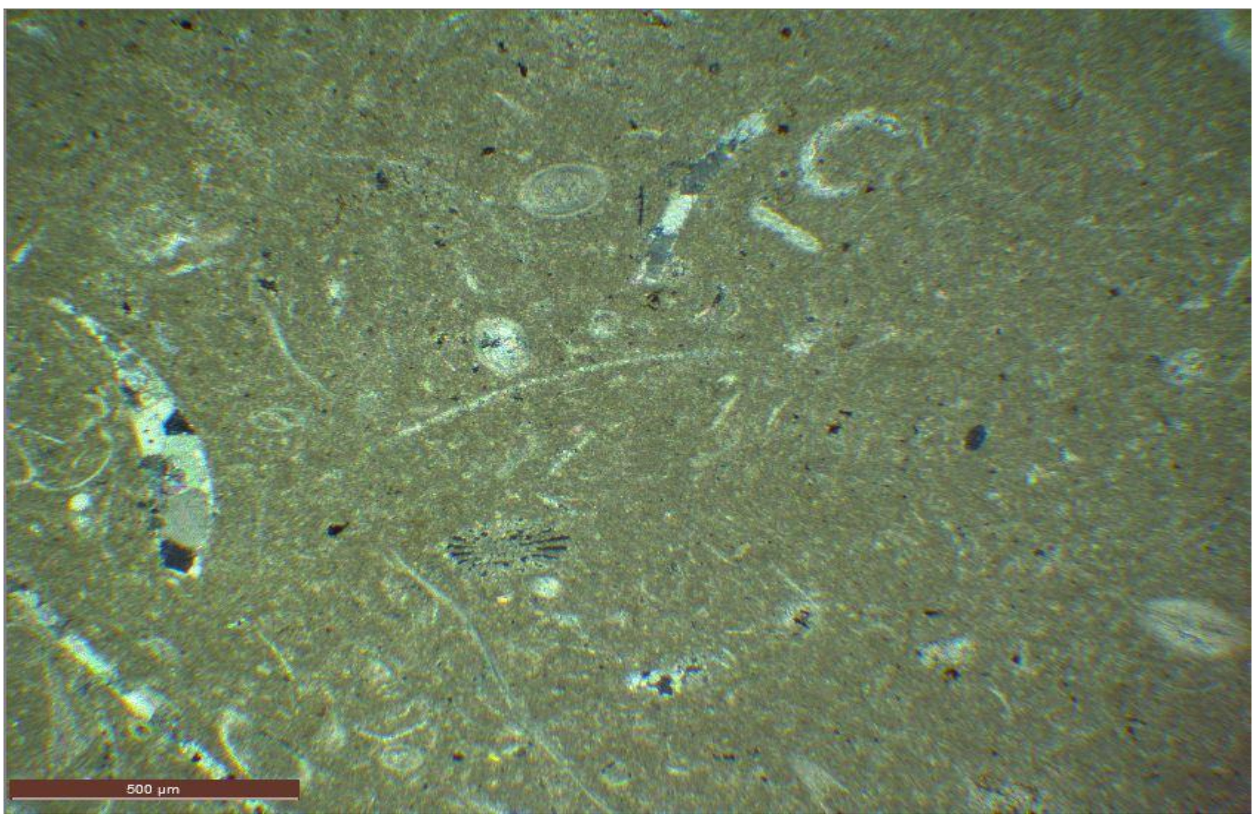

859 (10946-947 ft.) Wackestone/biomicrites. Fossil fragments.

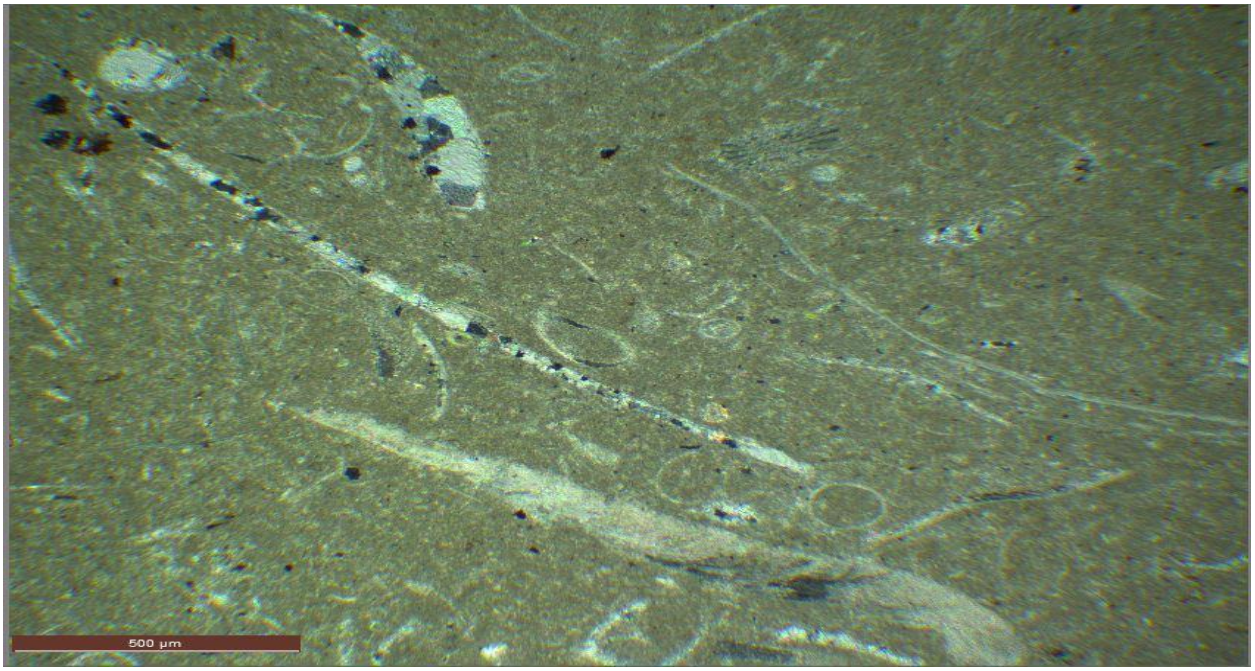

859 (10946-947 ft.) Wackestone/biomicrites. Fossil fragments.

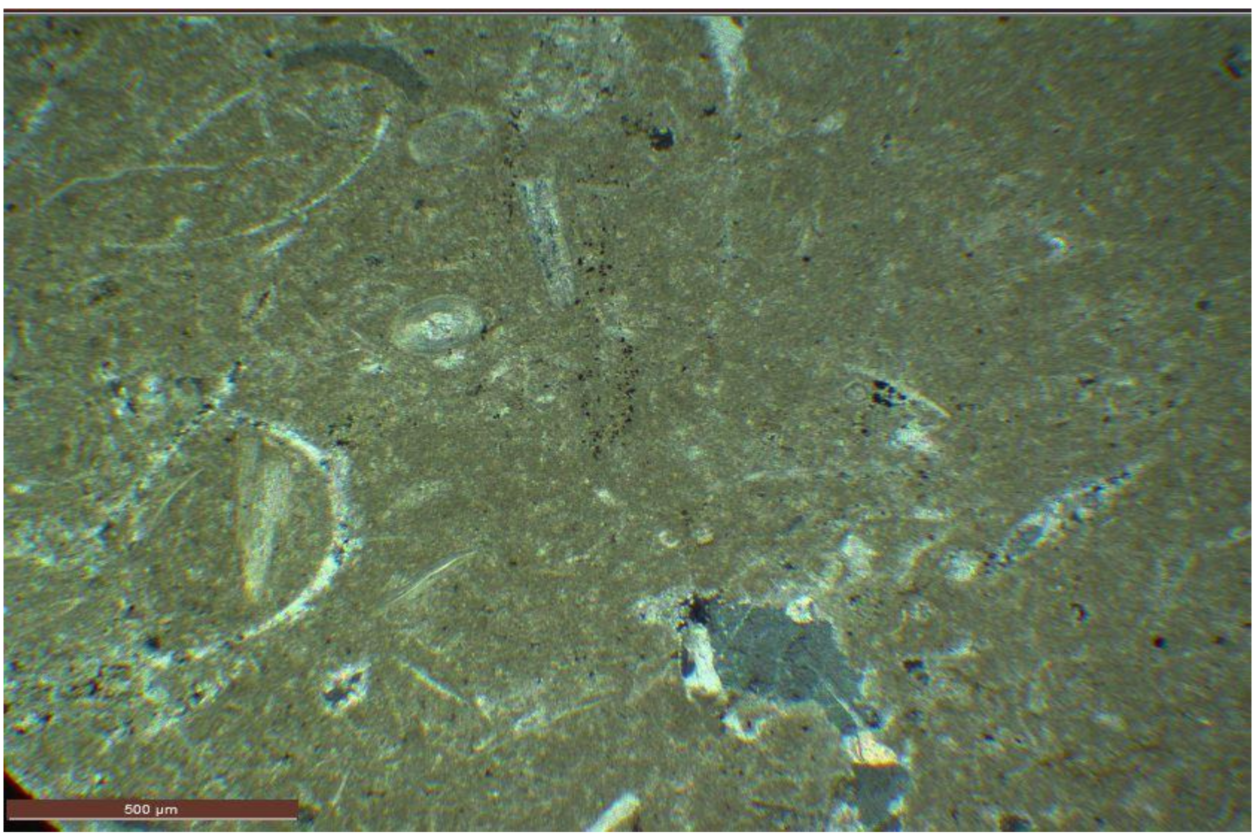

859 (10946-947 ft.) Wackestone/biomicrites. Fossil fragments.

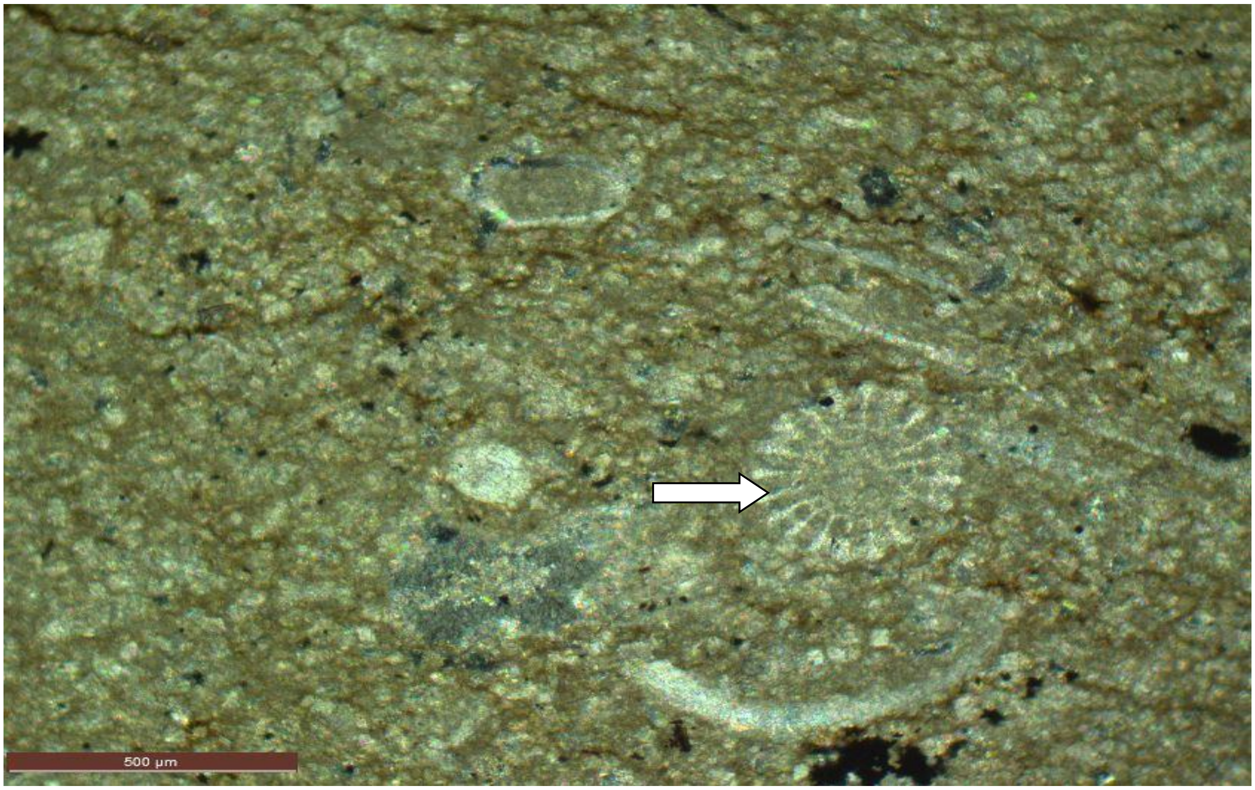

859 (10948-949 ft.) Transverse section of single echinoid spine (arrow) with the flower pattern and lobate outline.

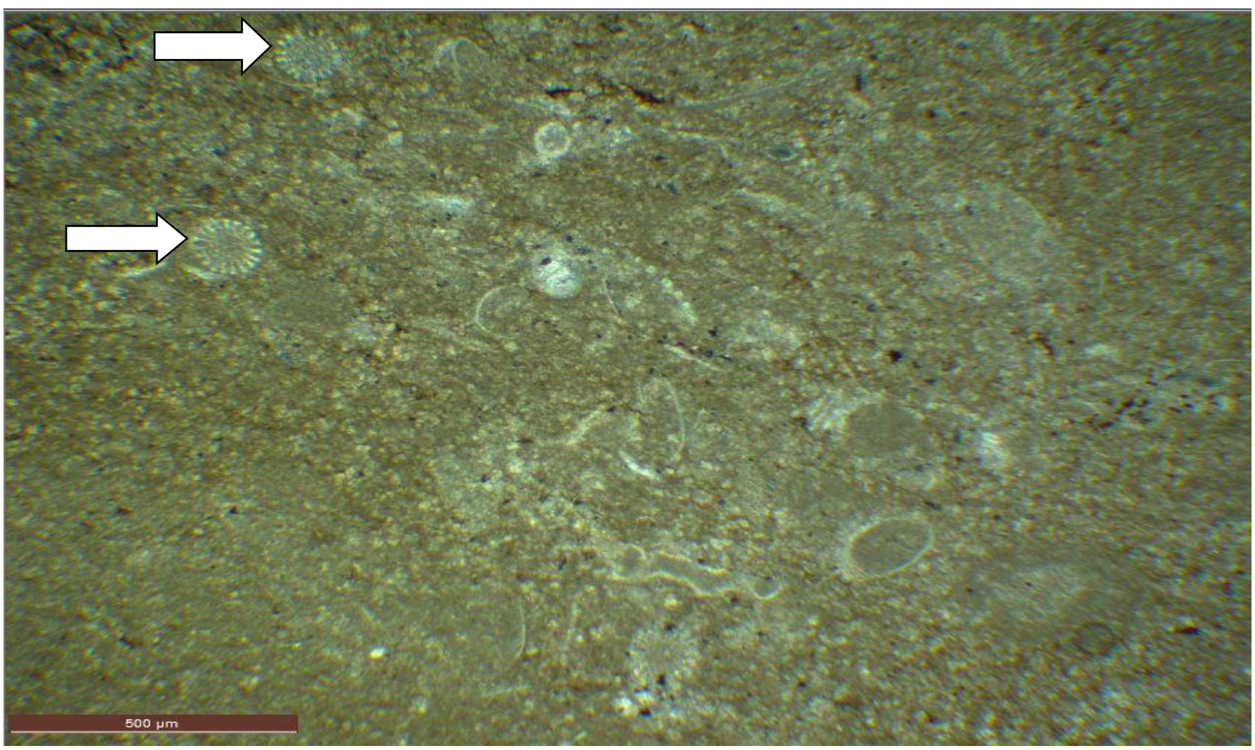

859 (10948-949 ft.) Echinoid stems (arrow) and other fossil fragments.

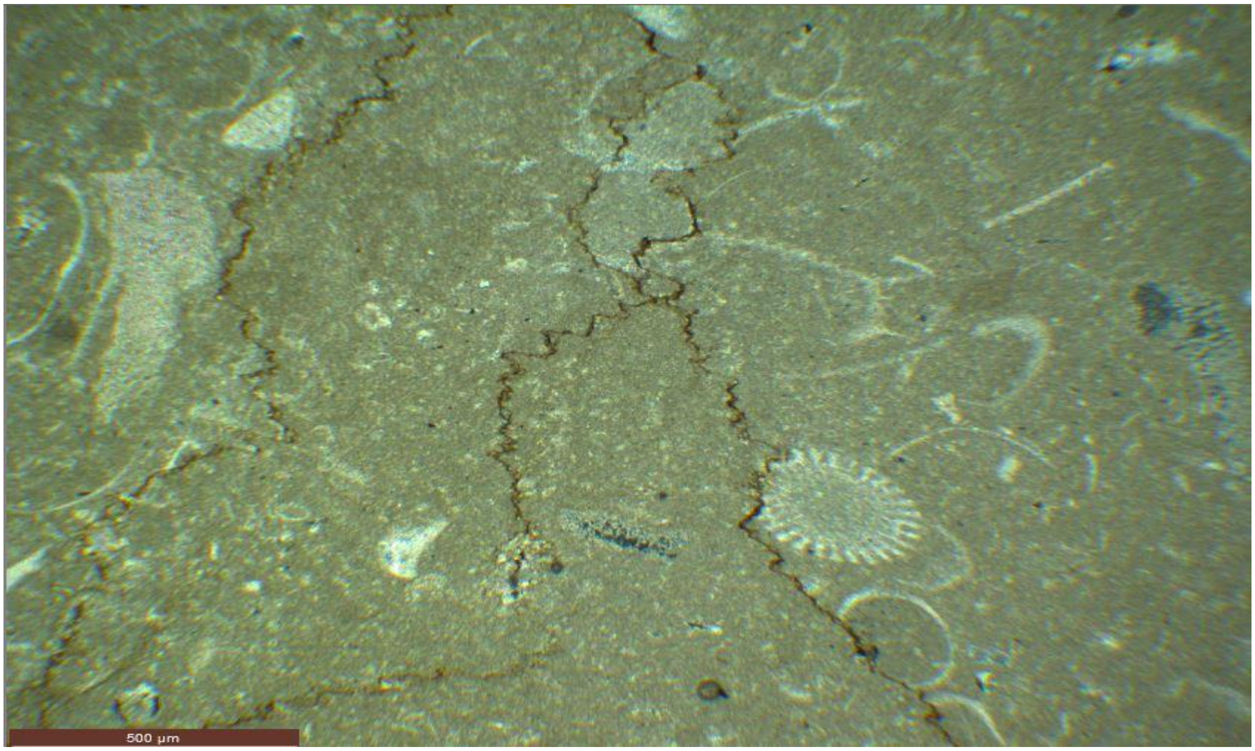

859 (10950-51 ft.) echinoid spine with stylolites running through it.

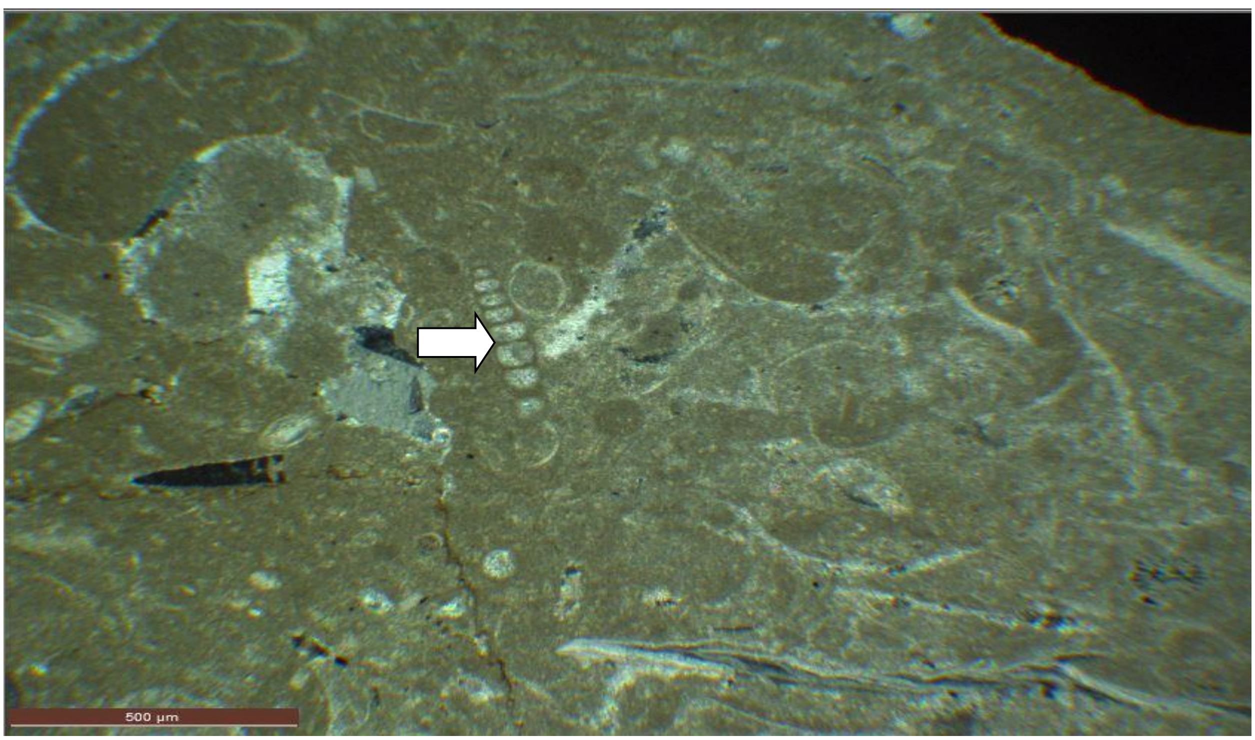

859 (10950-51 ft.) Biosparite. Foraminifera (arrow)

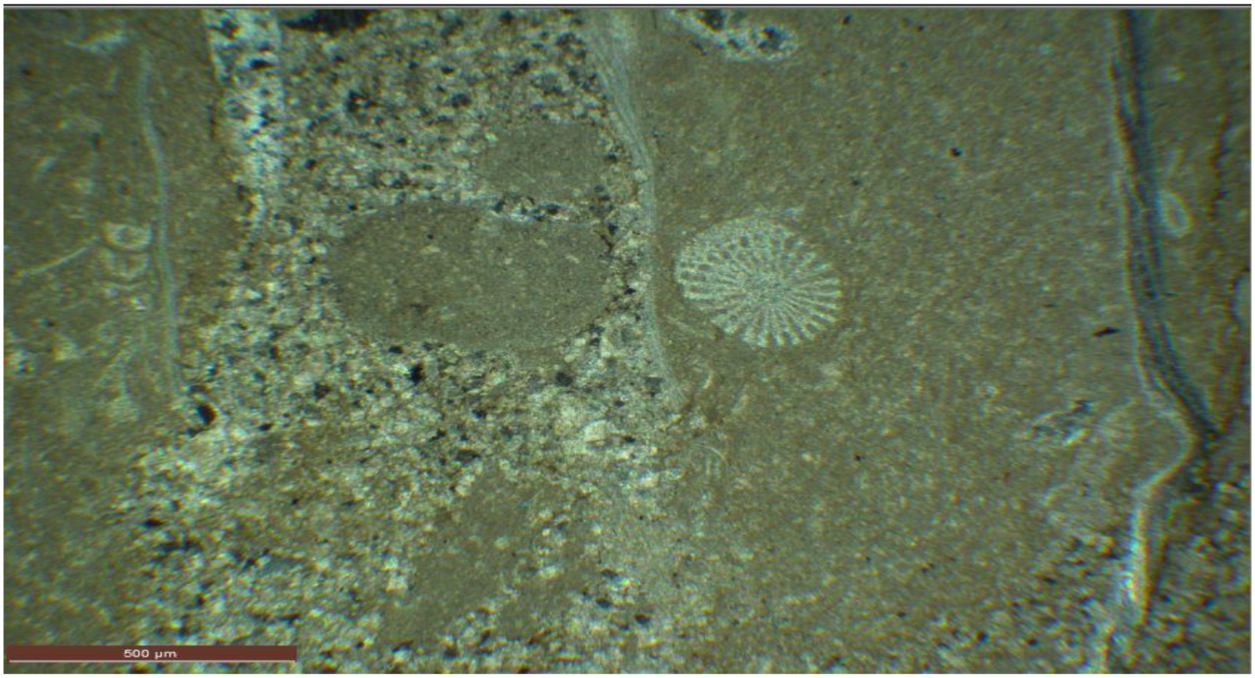

859 (10950-51 ft.) Selective dolomitization inside a fossil fragment and echinoid spine by the side.

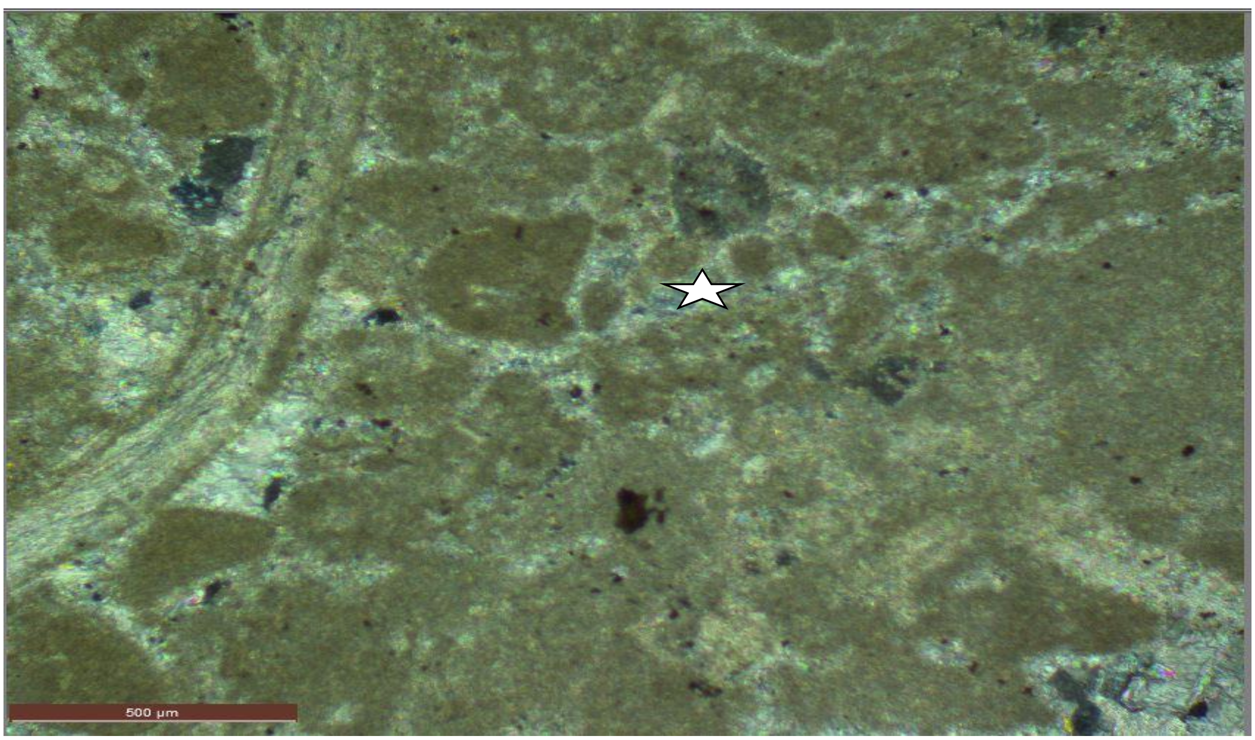

859 (10955.9 ft.). Foraminifera (stared) and brachiopod stem in this wackestone

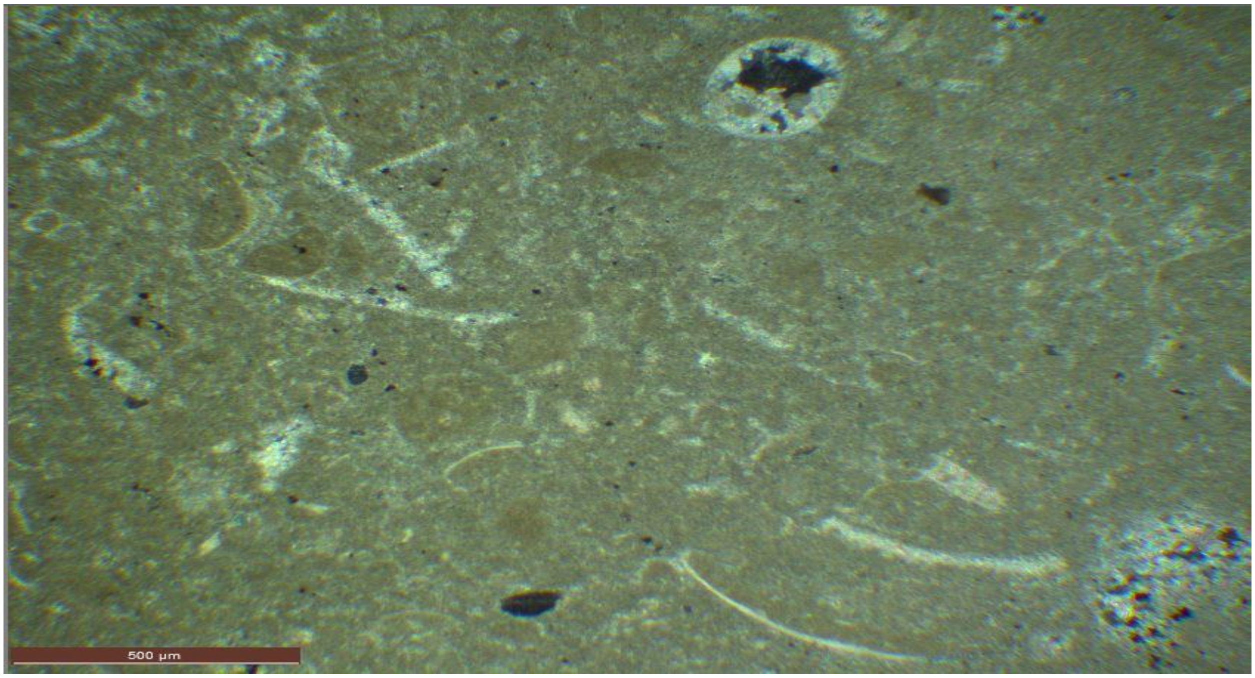

859 (10955.956 ft.) Fossil fragments and a vug being recrystallized (above) in this wackestone.

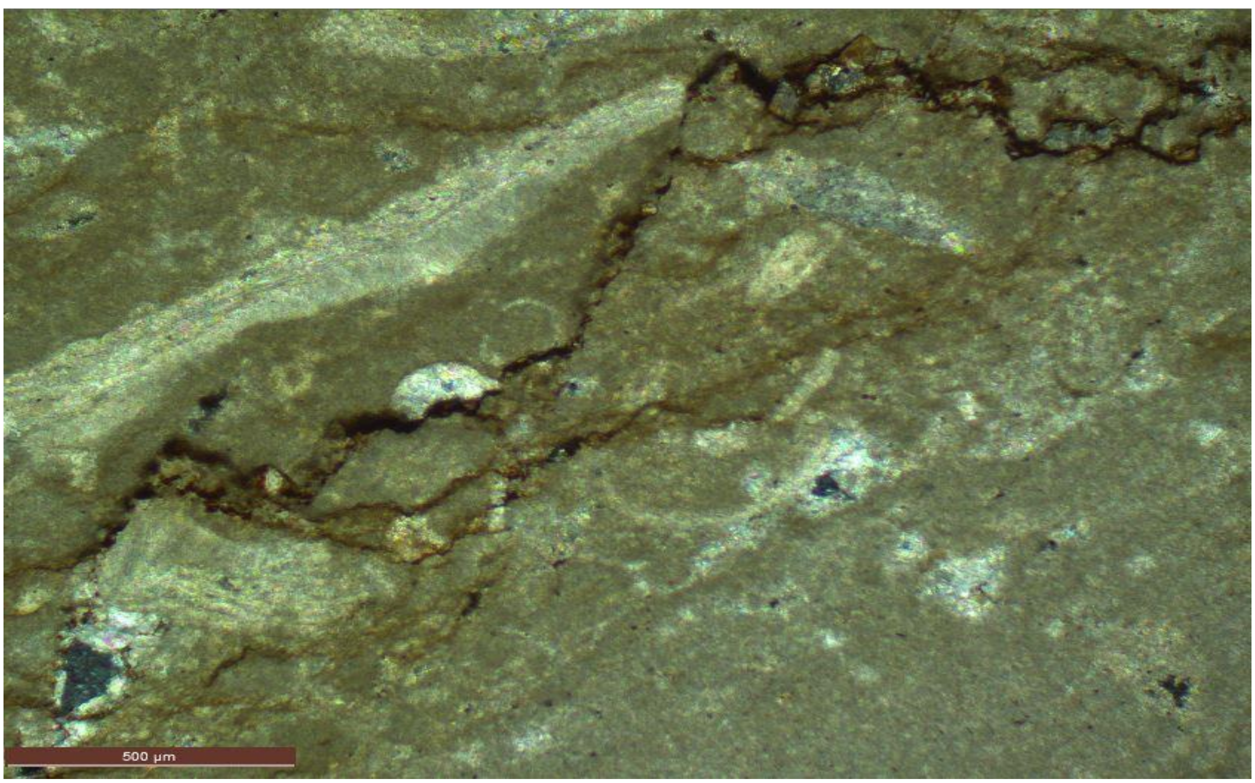

859 (10955.956 ft.). Broken brachiopod stem at the top with solution seam

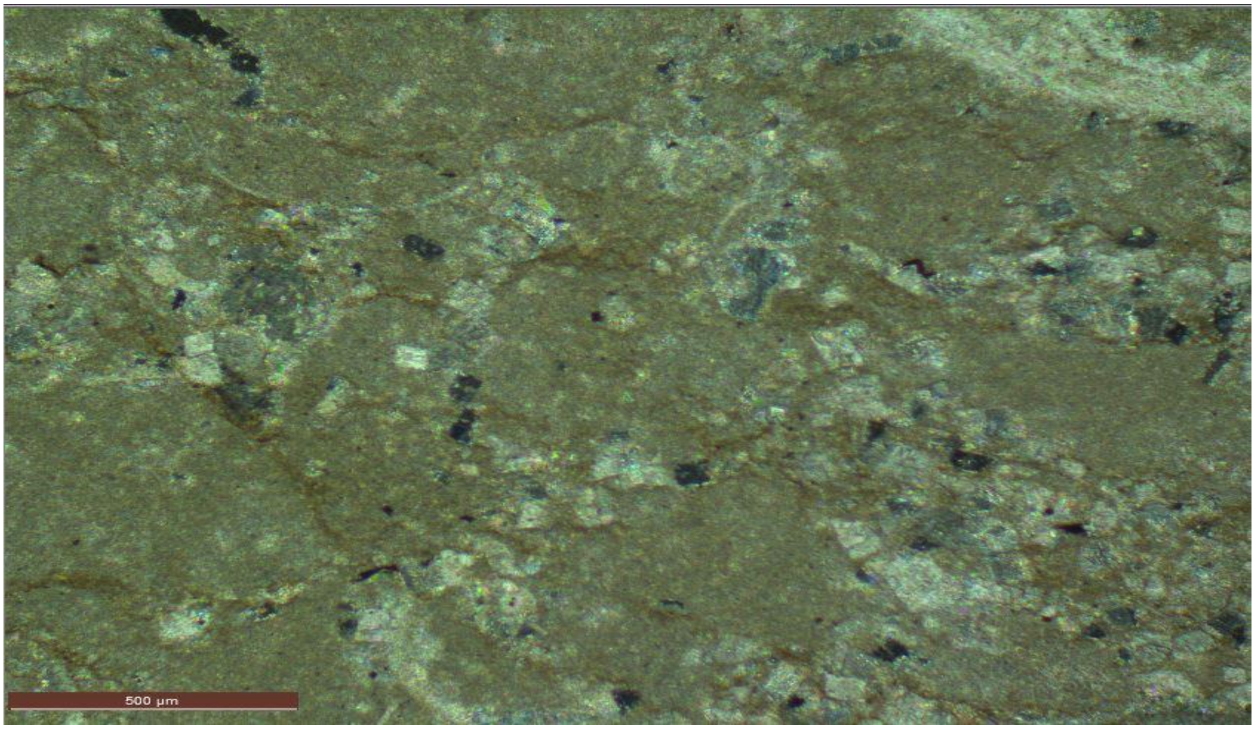

859 (10957.95 ft.). Selective replacement of original micrite by crystalline dolomite.

THIN SECTION IMAGES FROM
NDGS 15412
WHITING OIL AND GAS CORPORATION
FEDERAL 32-4HBKCE
GOLDEN VALLEY COUNTY
BICENTENNIAL FILED
CORE INTERVAL: 10690-10739 (49ft).

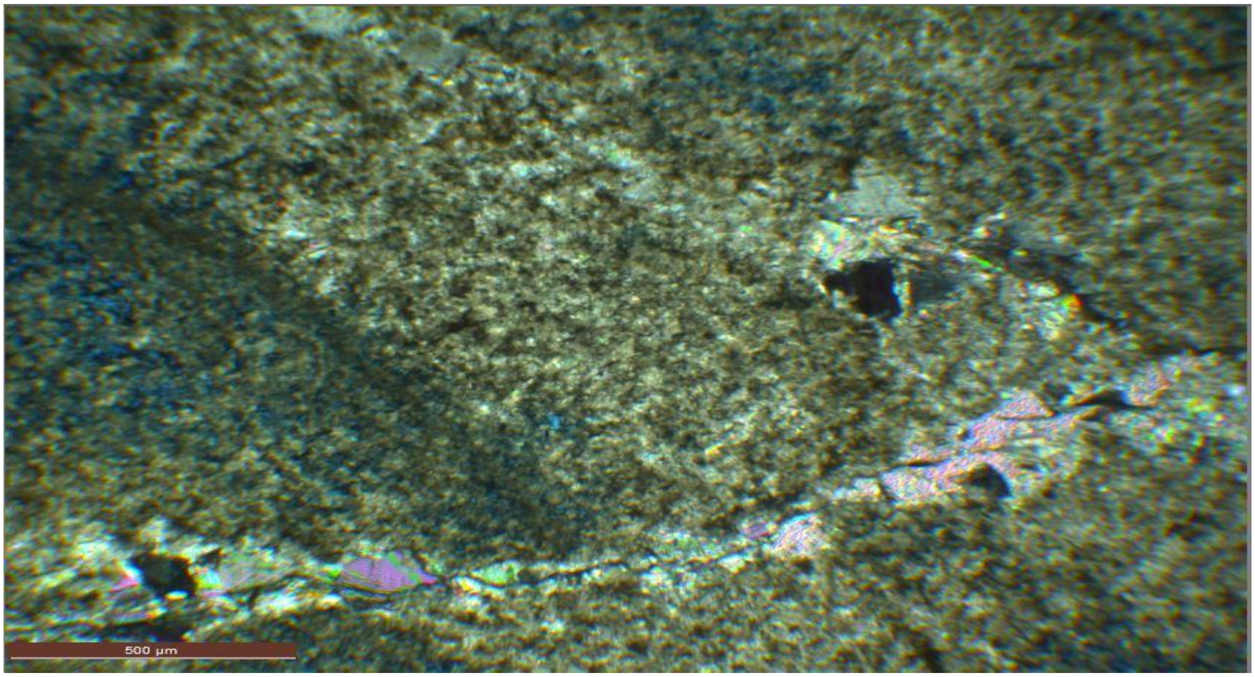

15412 (10682 ft.). Anhydrite precipitating through the fault. Vug due to fragment dissolution

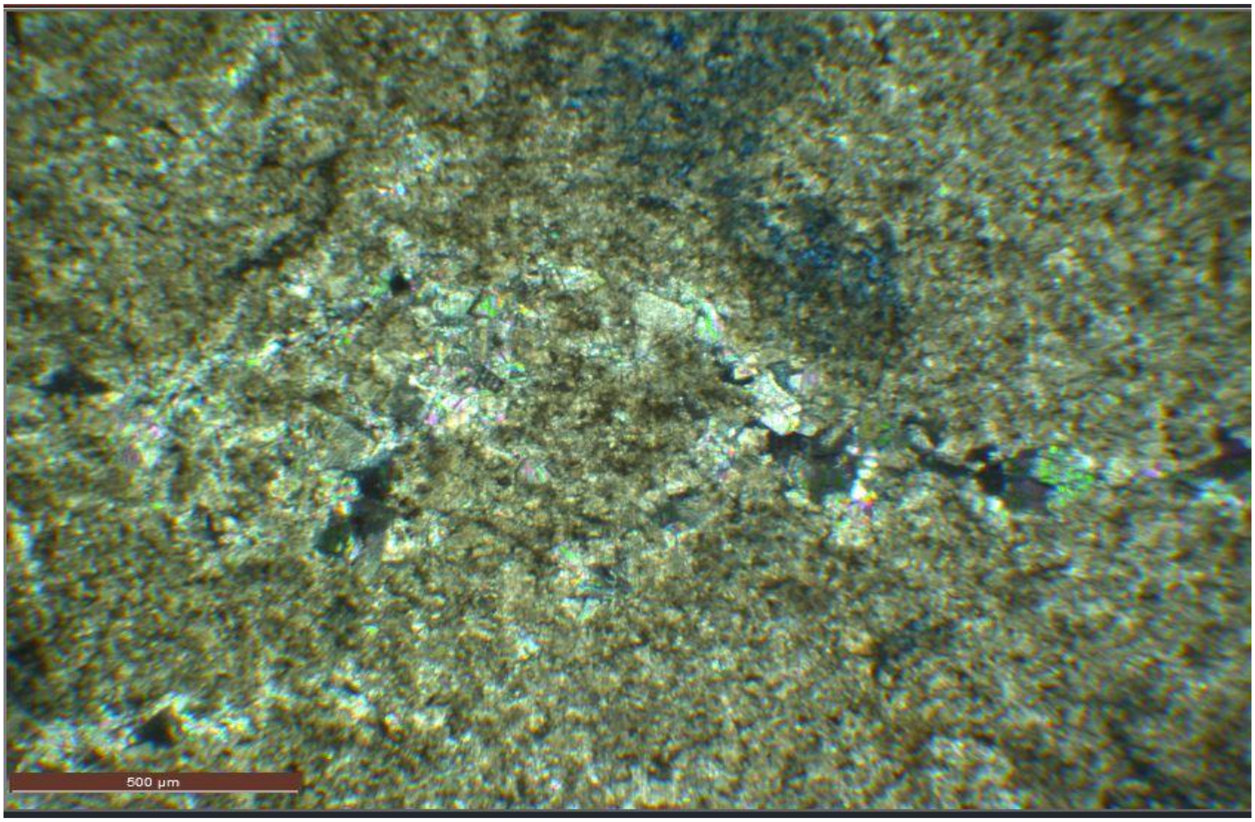

15412 (10682 ft.). Patches of anhydrites in the fractured areas.

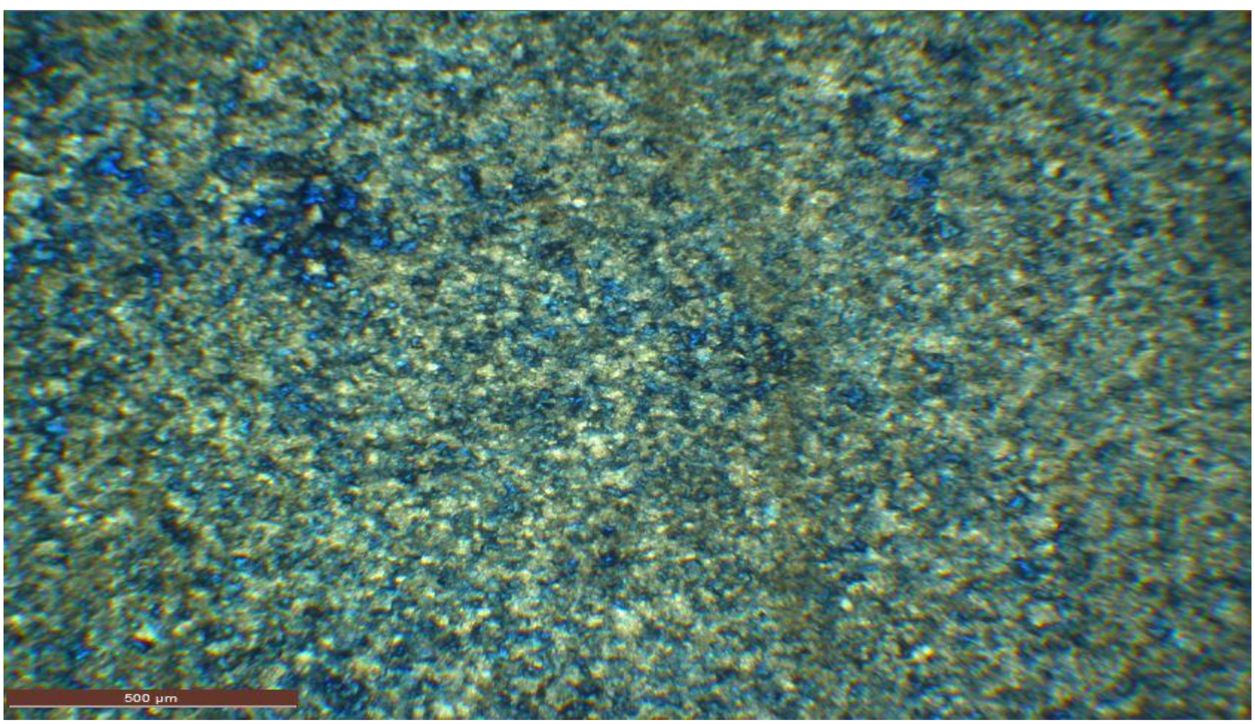

15412 (10682 ft.). Fine dolomite crystals with the blue stains showing the porosity.

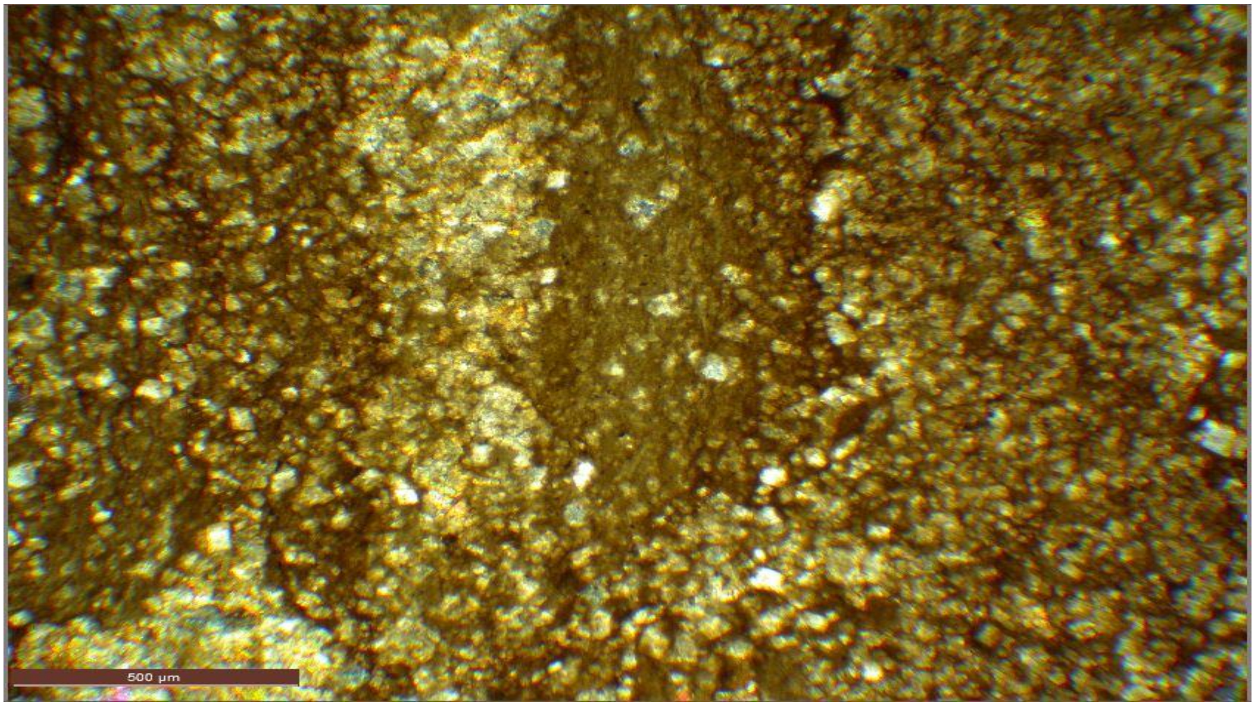

15412 (10689.2 ft.) The white dolomite crystals replacing the original matrix.

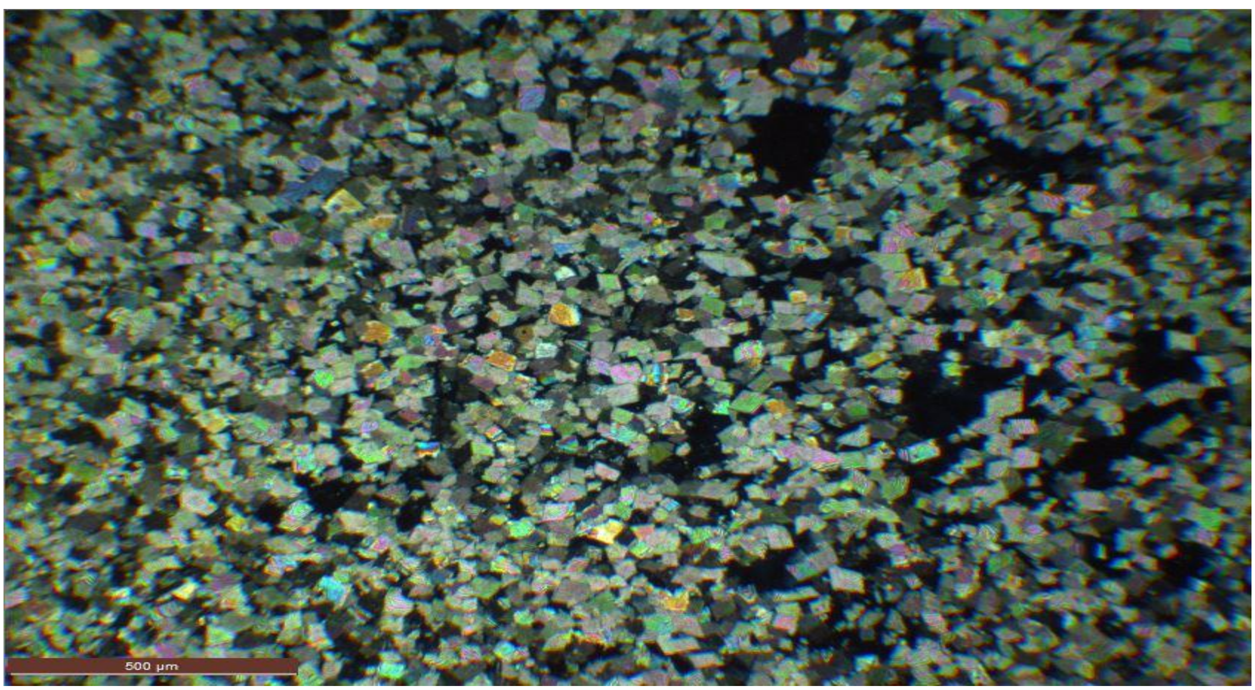

15412 (10710.9 ft.) A mixture of dolomite crystals and anhydrites patches.

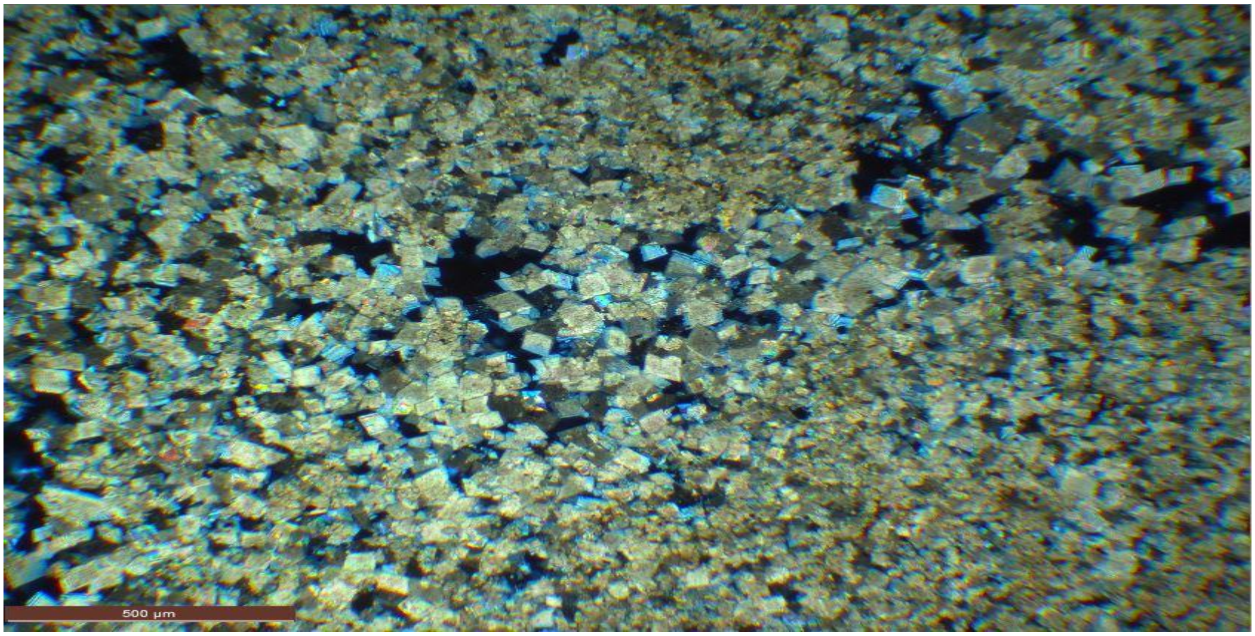

15412 (10712.5 ft.) Invasive dolomitization with areas of dissolved fossil fragments now vuggy with recrystallization taking place creating a biomoldic pore spaces.

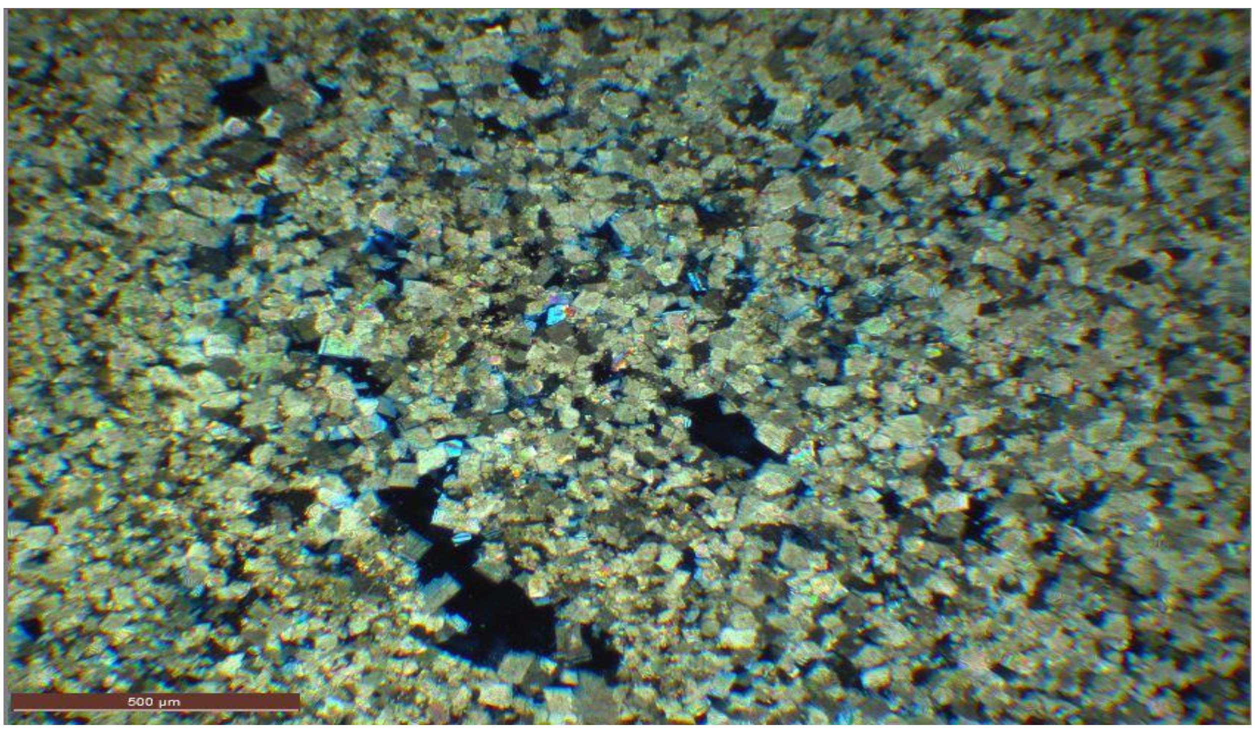

15412 (10714.4 ft.) Areas of dissolved fossil fragments now vuggy with recrystallization taking place creating a biomoldic pore spaces.

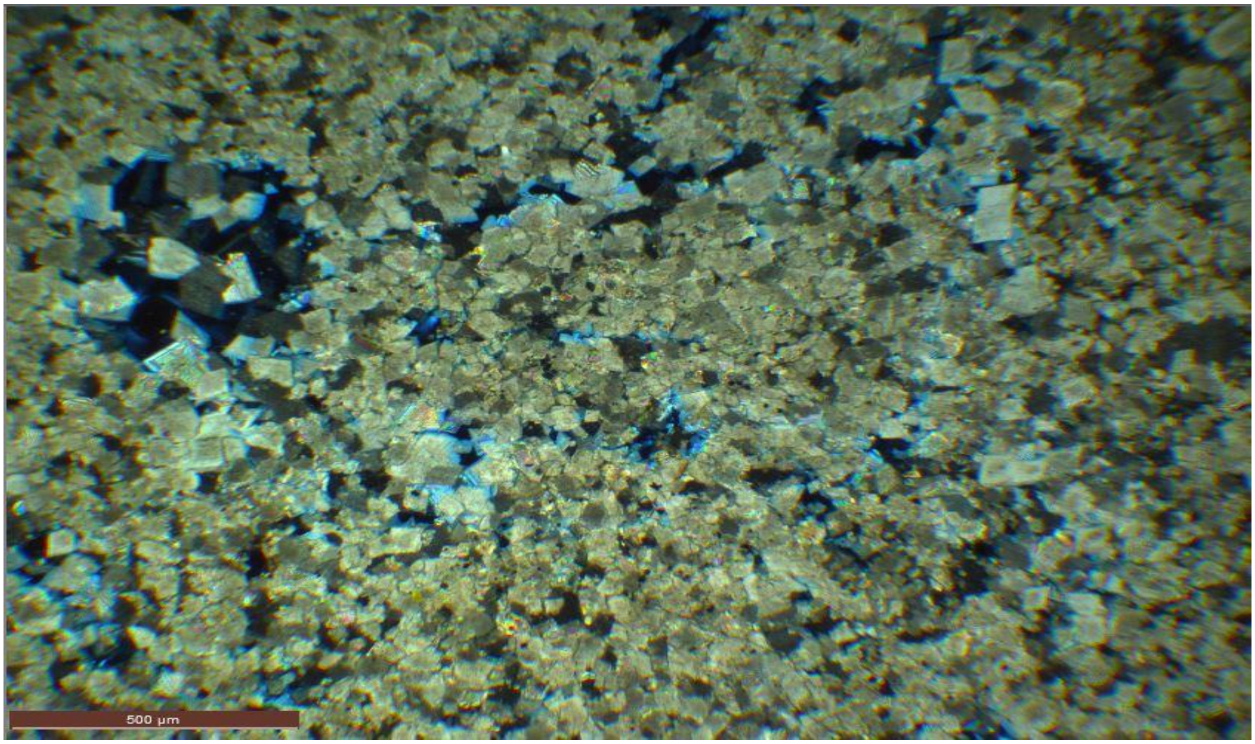

15412 (10720.5 ft.) Areas of dissolved fossil fragments now vuggy with recrystallization taking place creating a biomoldic pore spaces.

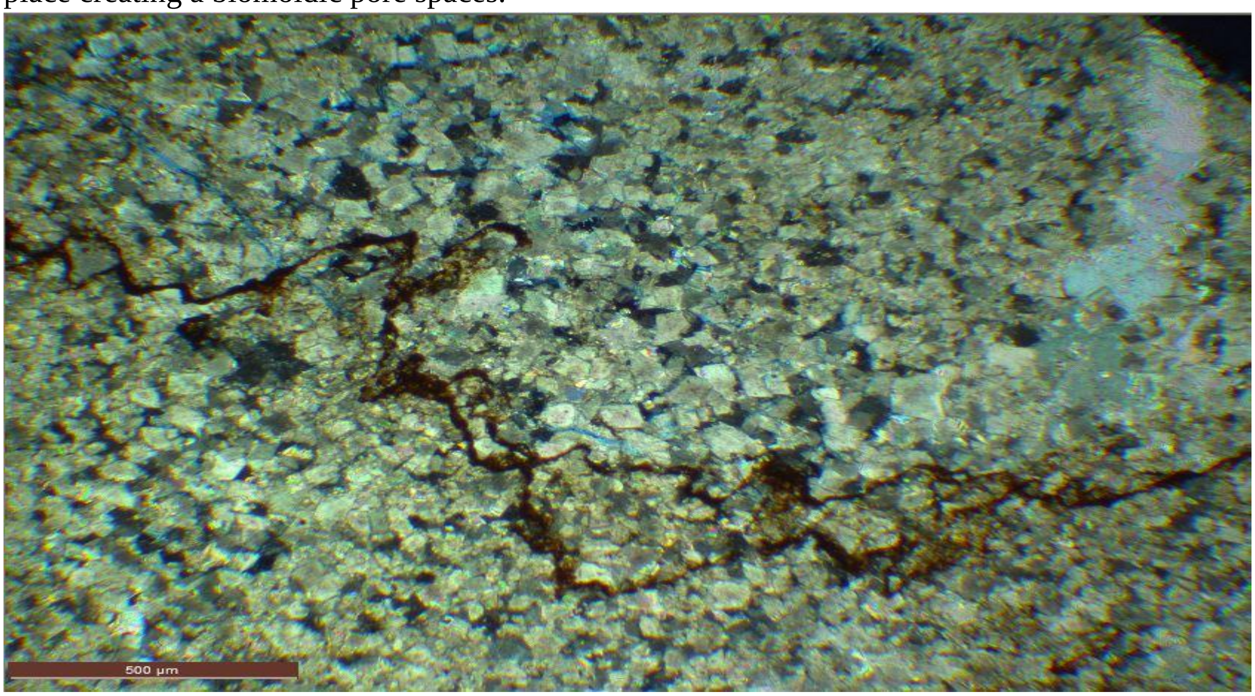

15412 (10722.5 ft.) Styloite running through this dolostone.

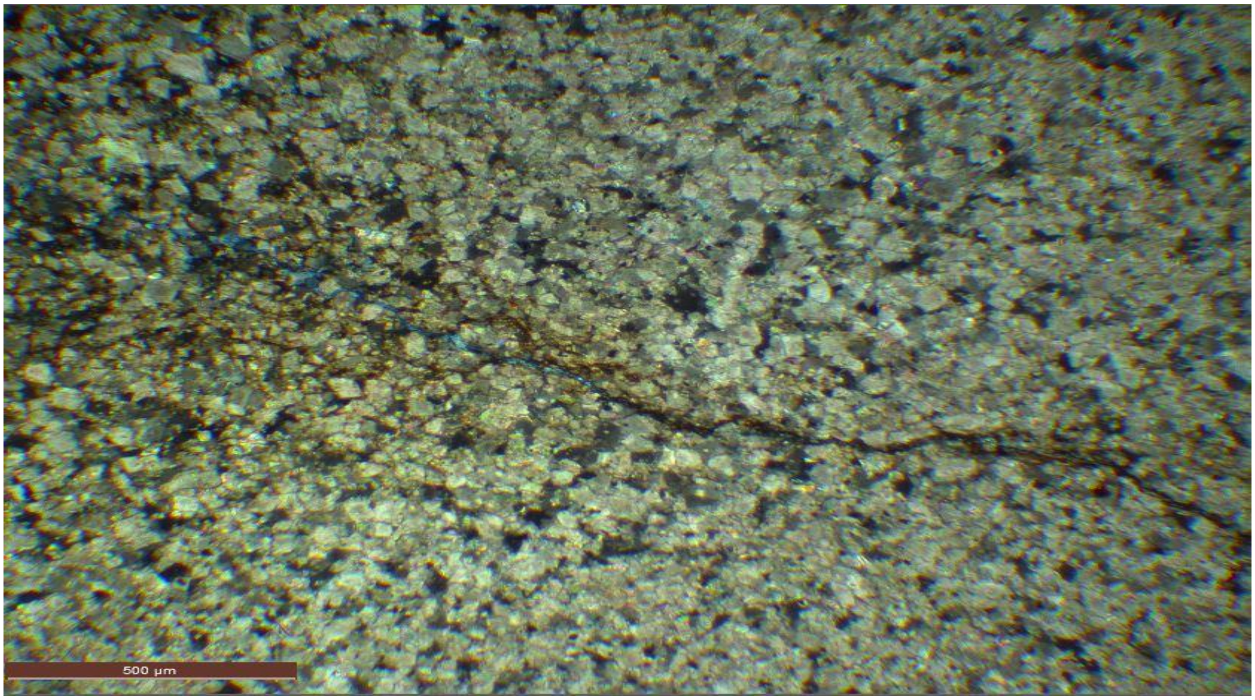

15412 (10728.5 ft.). Fractures.

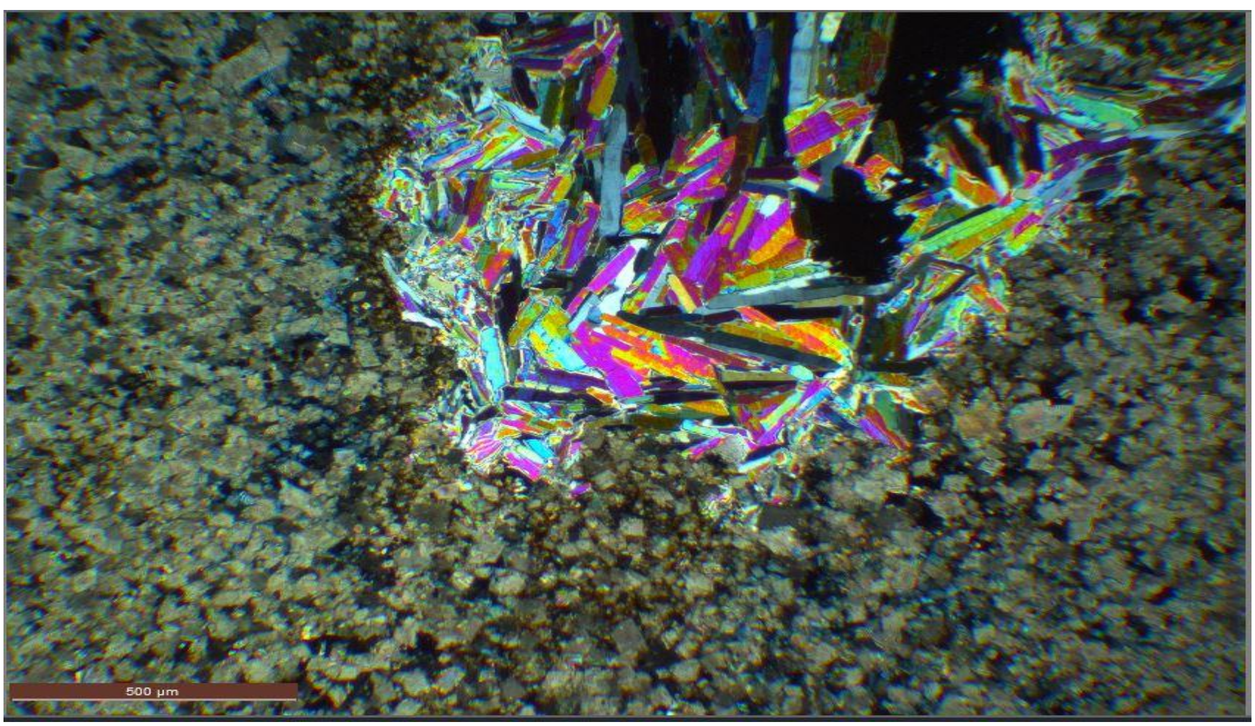

15412 (10728.5 ft.) Large bladed anhydrites displaced and replacing the original carbonate material. These anhydrites occludes the porosity

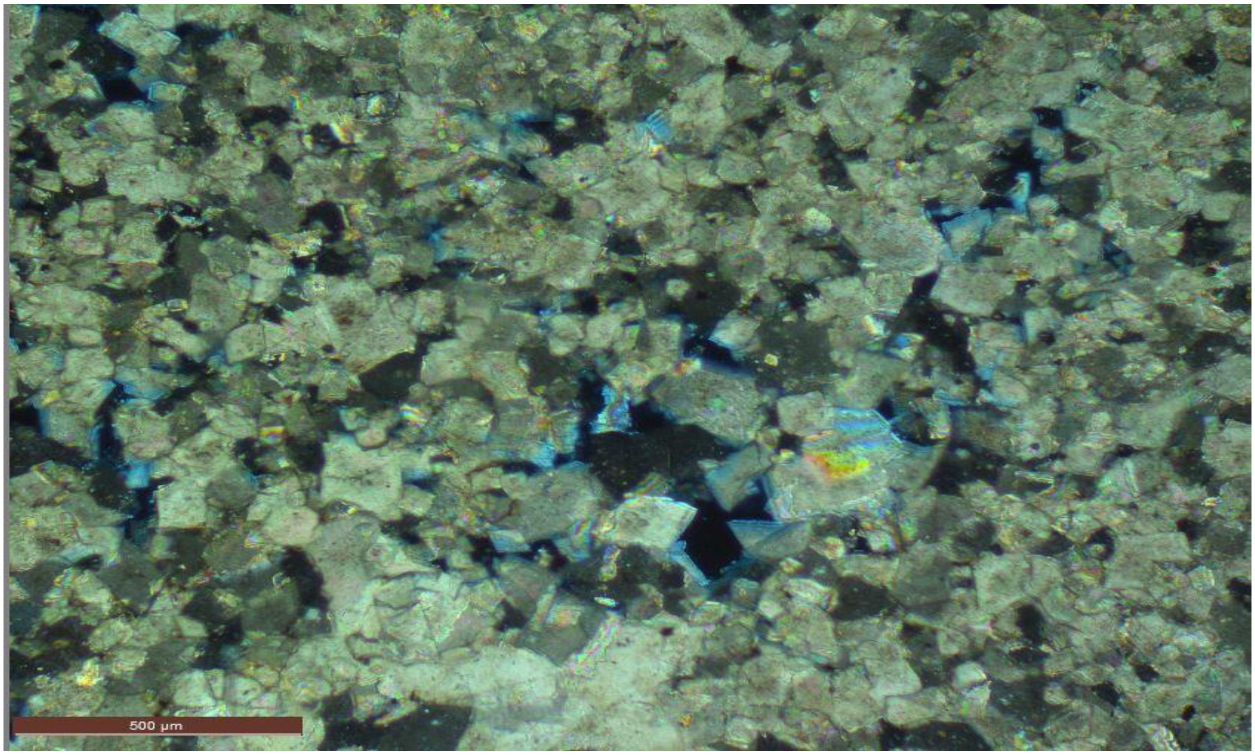

15412 (10728.5 ft.) Moldic porosity caused by vugs in the packstone

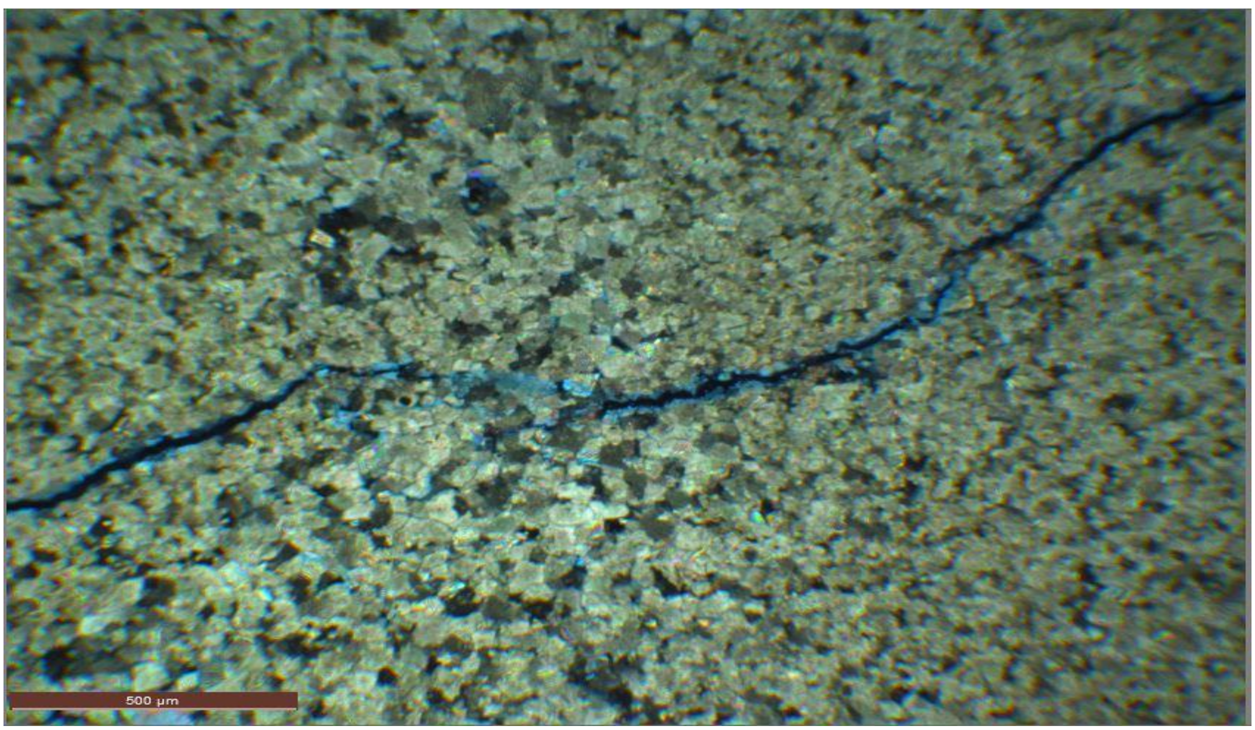

15412 (10733.3). Red stain showing fracture

THIN SECTION IMAGES
NDGS 15625
FH PETROLEUM CORP.
STATE 14-16
GOLDEN VALLEY COUNTY
COOKS PEAK FIELD

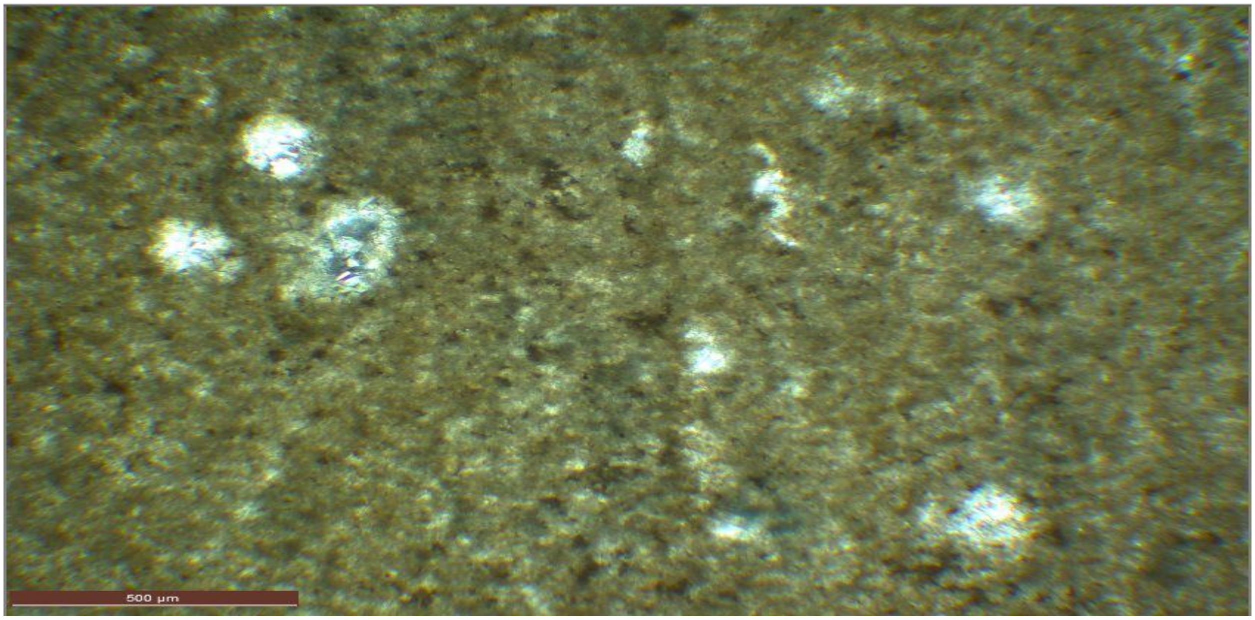

15625 (12667.5 ft.) Fossil fragment that has been calcified shows a contrast from the original sediment.

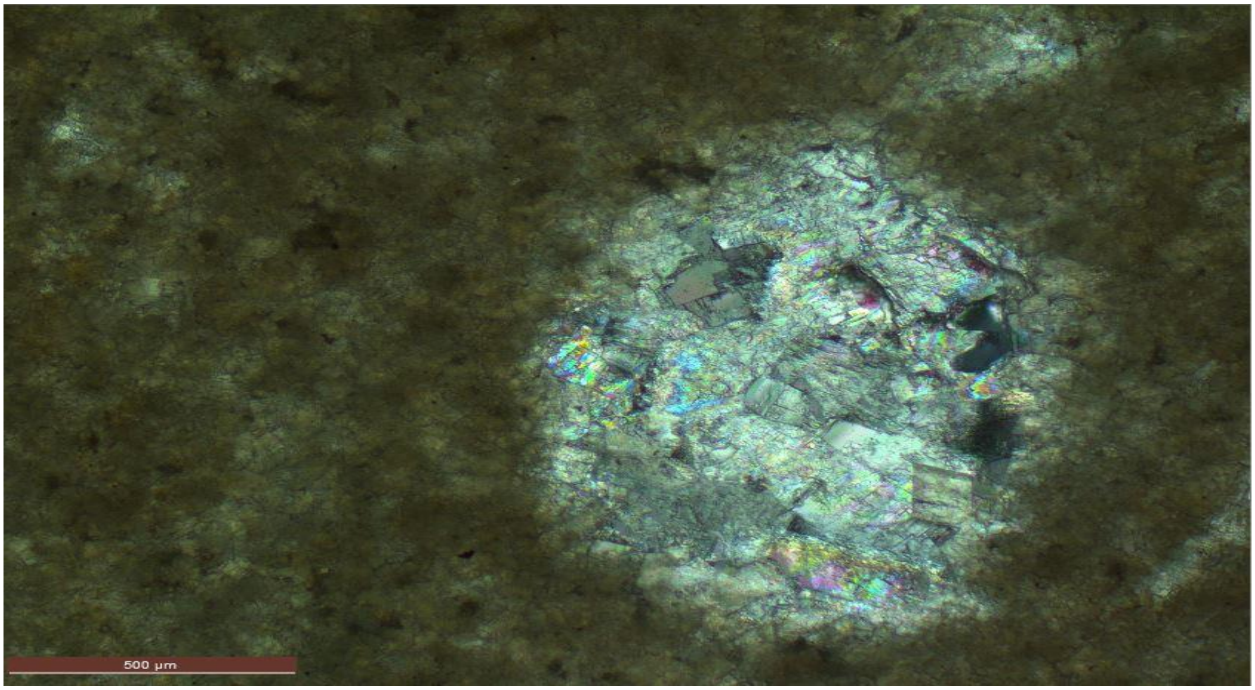

15625 (12667.5 ft.) This moldic pore space has been almost completely closed by dolomite calcite cement.

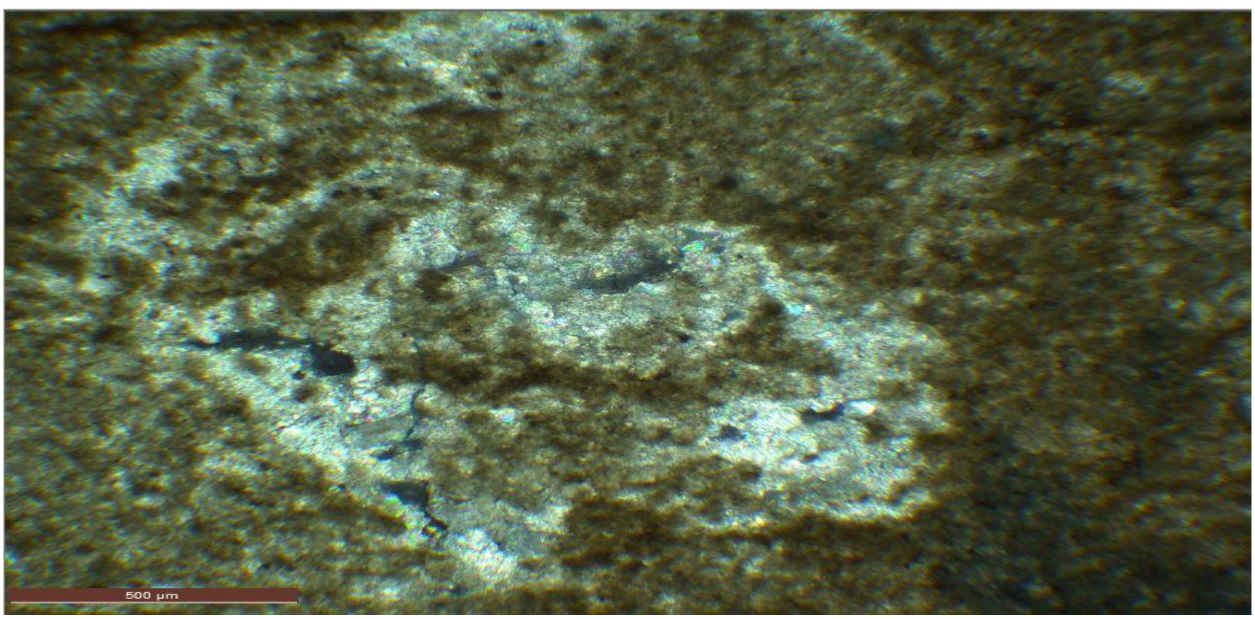

15625 (12667.6 ft.) Fossil fragment undergoing recrystallization.

THIN SECTION IMAGES FROM
NDGS 15679
FH PETROLEUM CORP.
BROWN 42-28
GOLDEN VALLEY COUNTY
WILDCAT FIELD
CORE INTERVAL: 10700-10758 (58ft).

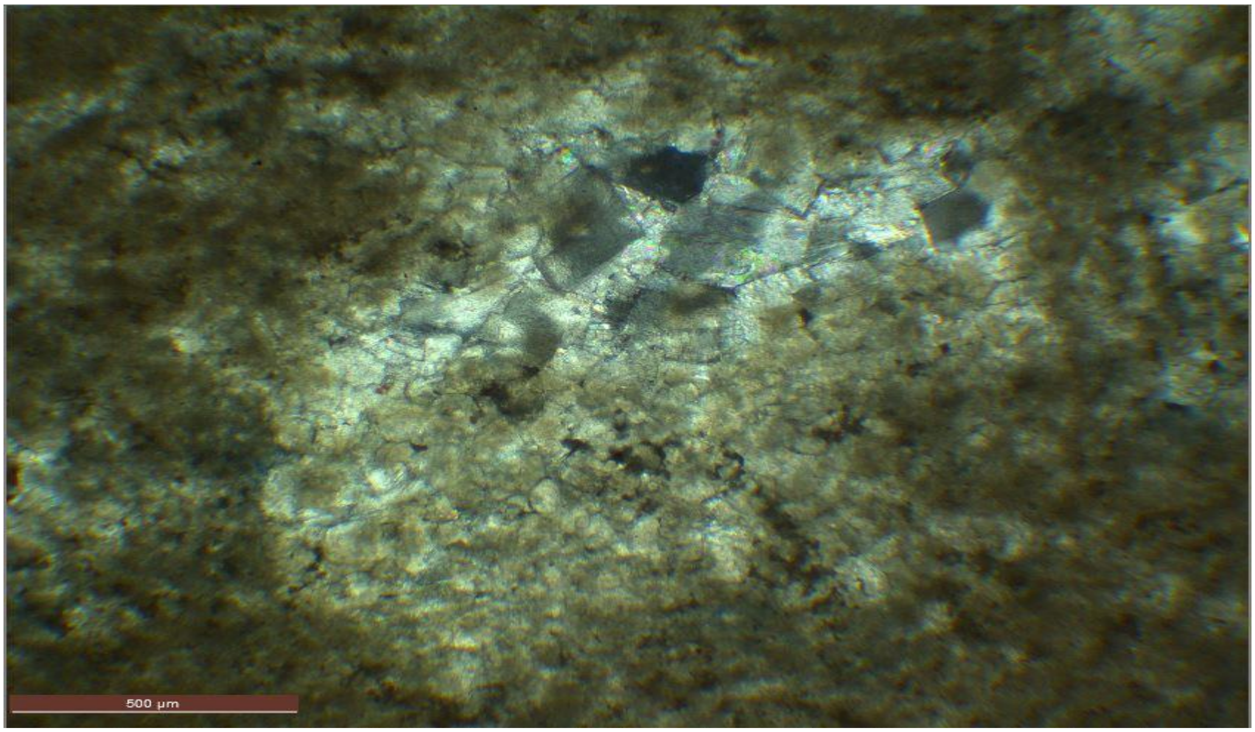

15679 (10704.2-6 ft.). Calcite cement closing up the pore space. This affects the porosity of the reservoir.

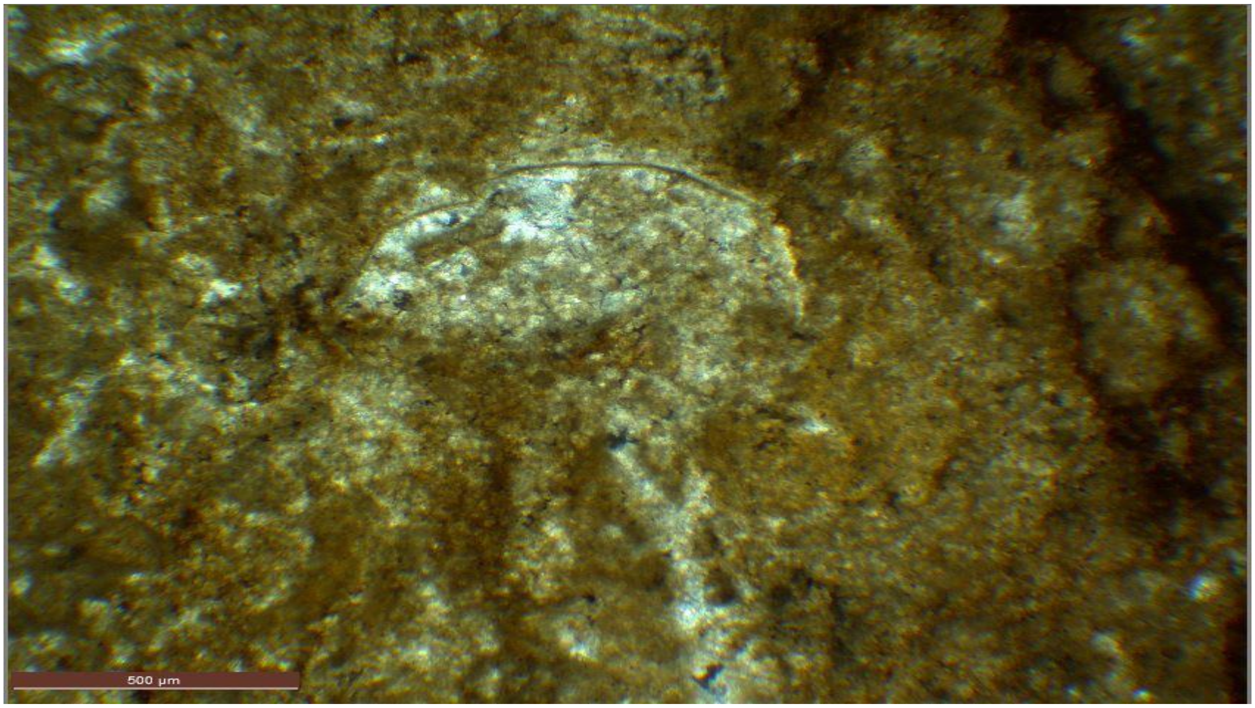

15679 (10709.2-9.5 ft.) The bivalve here has been leached and then being recrystallized by dolomite calcites. The outline can only be seen by the micrite envelope.

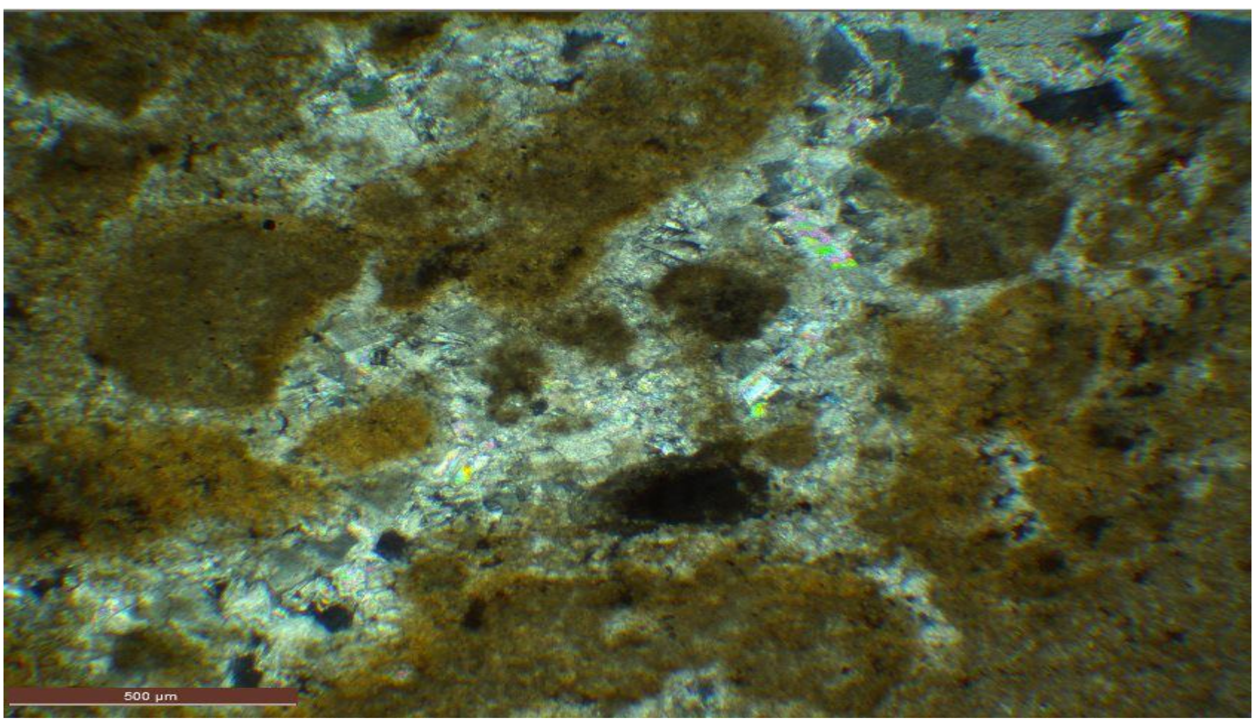

15679 (10709.2-9.5 ft.) Isopachous cement typical of a marine environment. The calcite cements uniformly closes up and reducing the porosity of the reservoir.

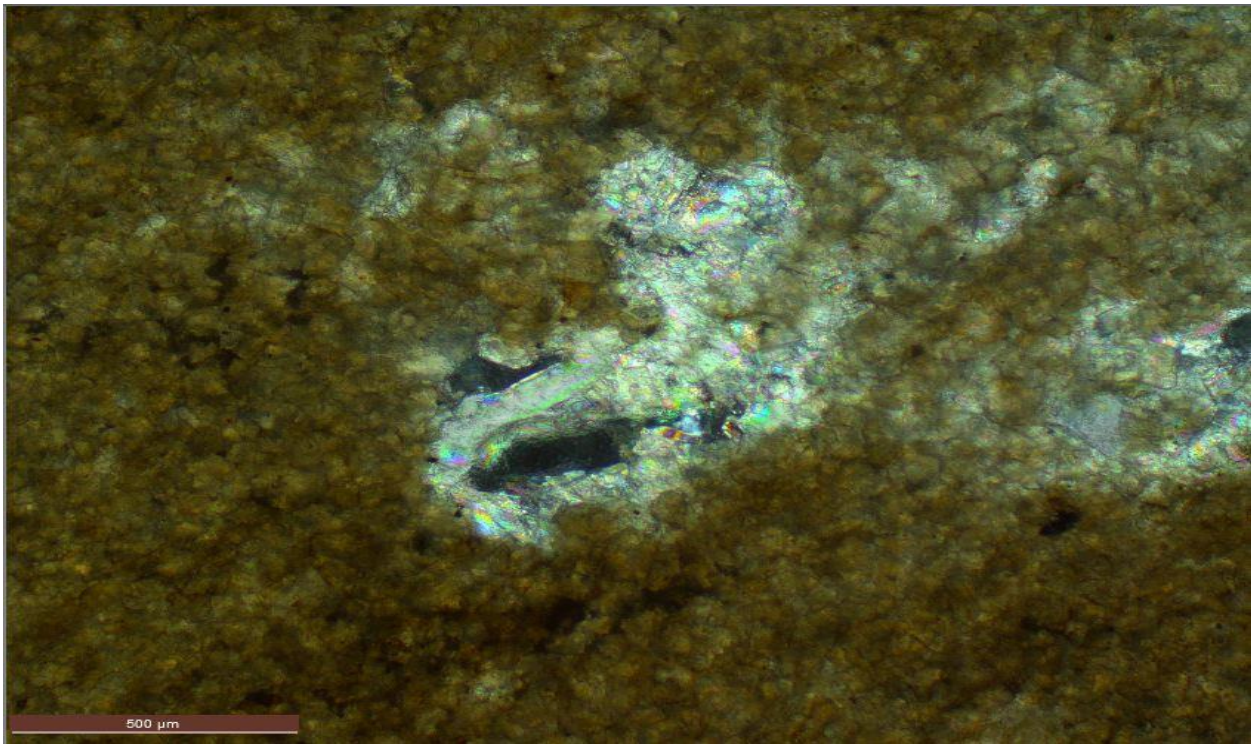

15679 (10709.5-10 ft.). Dolomitization going on through the dissolved fossil fragment. Most of the original matrix is still in place.
15679 (10709.8-10 ft.). Solution seams

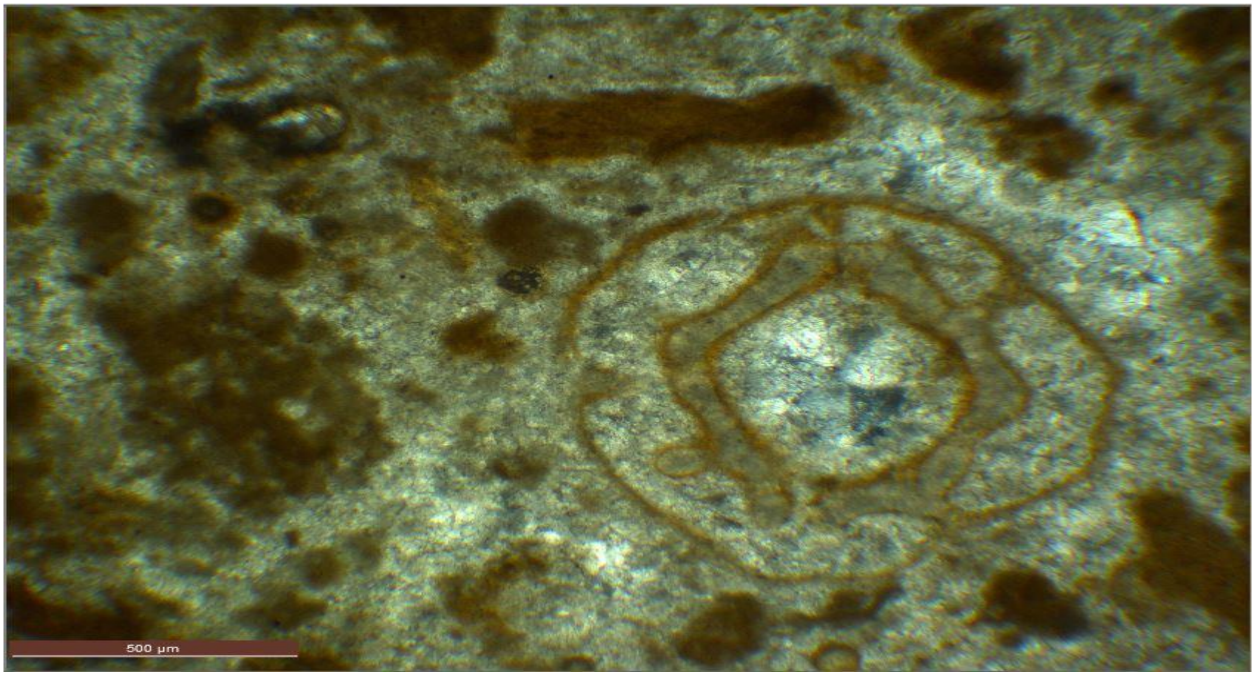

15679 (10723.4-7 ft.) Packstone shows Echinoid with its five-fold symmetry. Arogonitic micrite shows the original outline that has been replaced by sparry calcite.

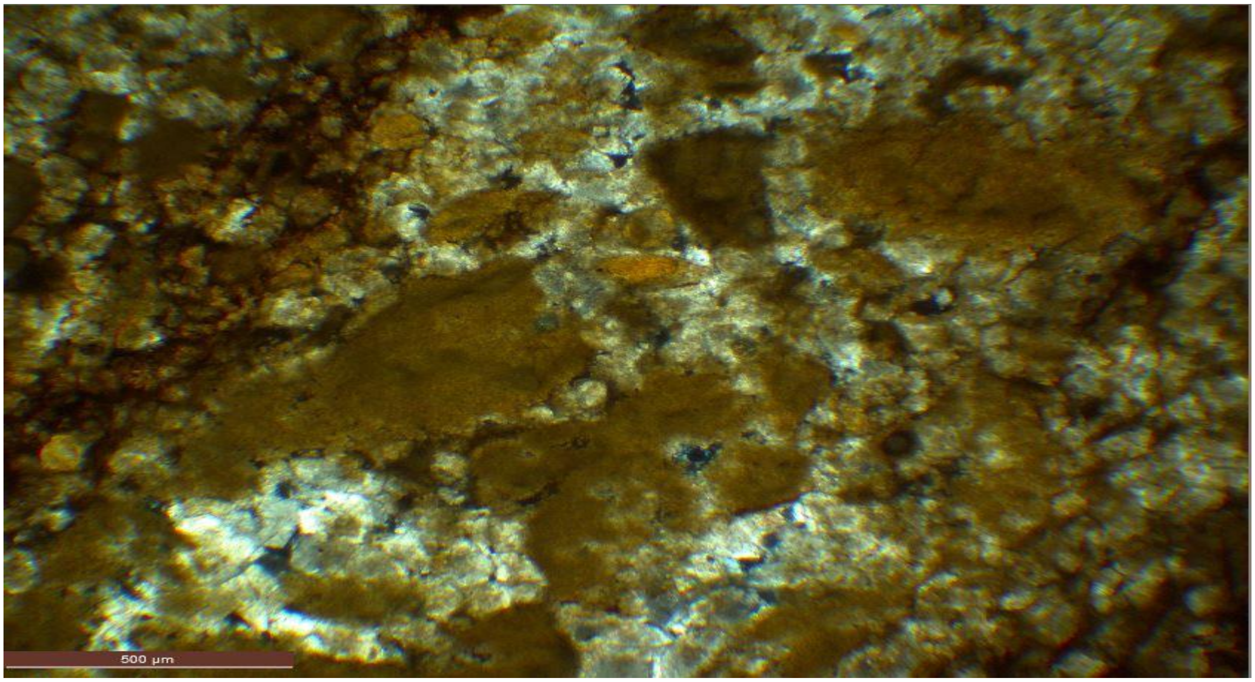

15679 (10723-4 ft.). Calcification of the original matrix

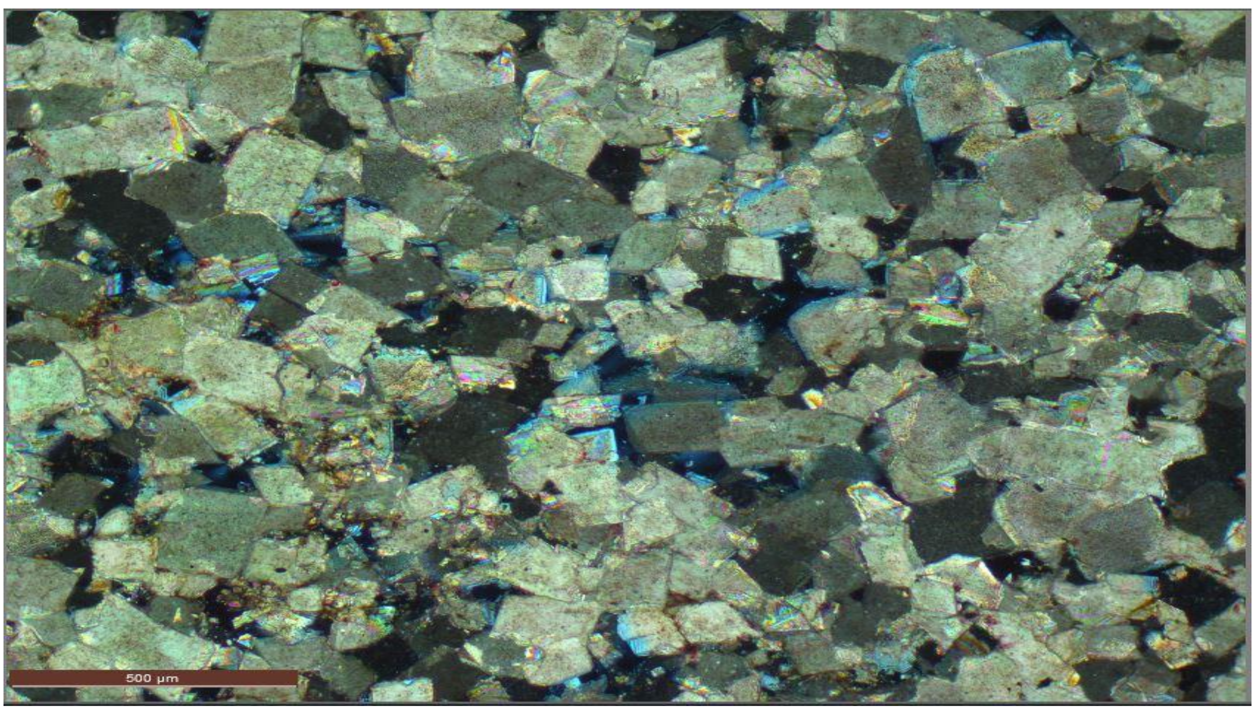

15679 (10728 ft.)The dolomites have dark and cloud cores and clear rims. The cloudy cores we can interpret to mean a mixing zone condition. A shift to marine condition gives the limpid dolomite outer zones that could be the cement.

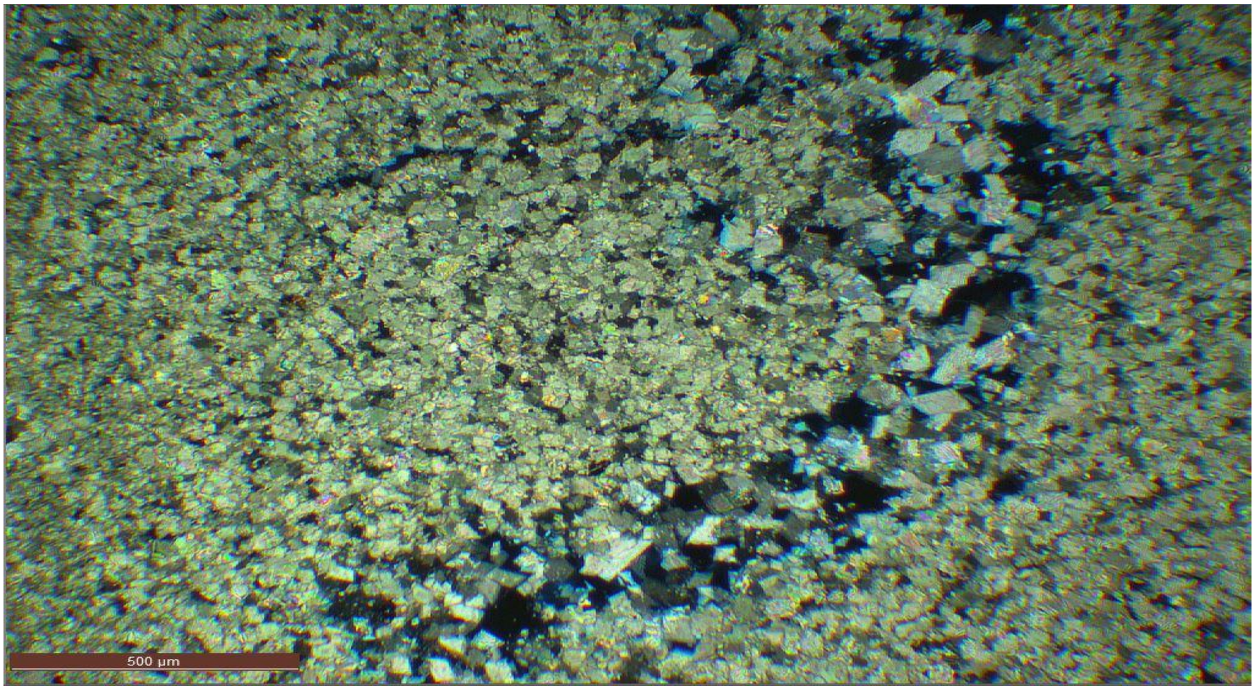

15679 (10736 ft.). Coarse crystalline dolomite crystals in a probably burrow.

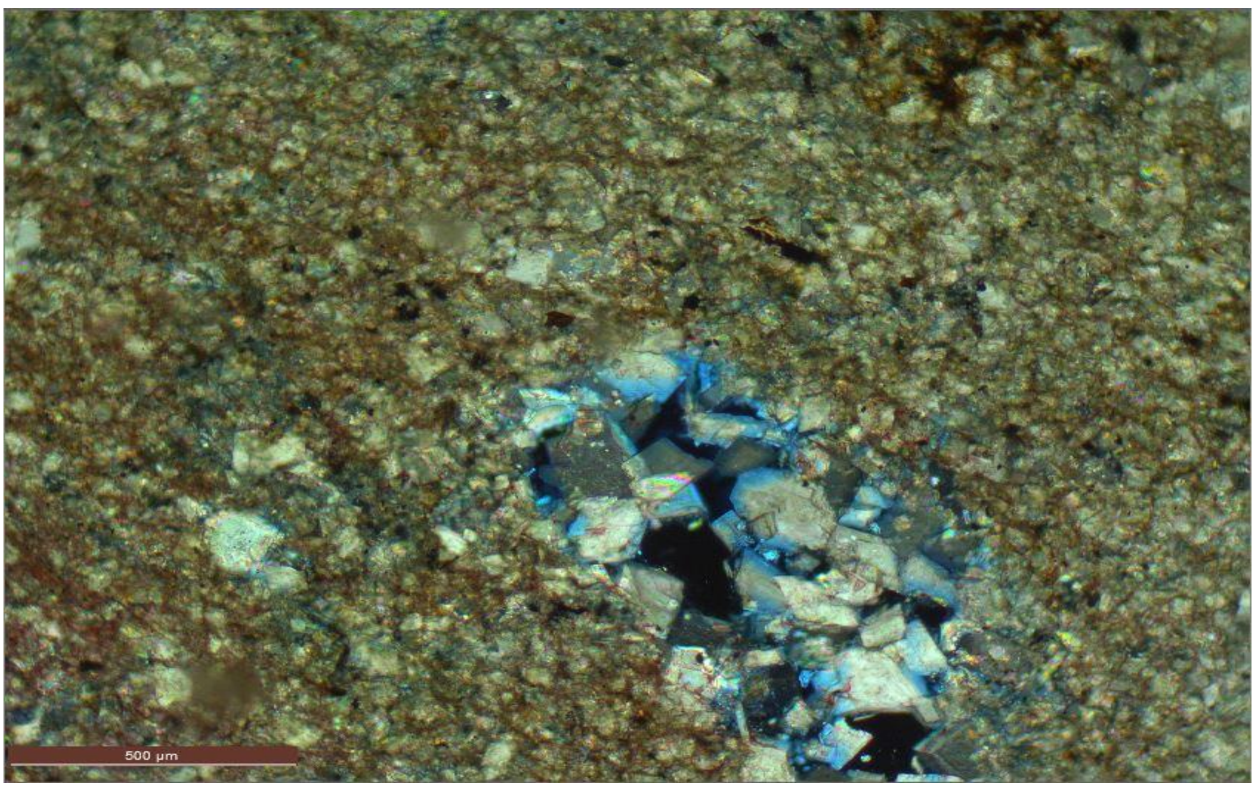

15679 (10736 ft.) Coarse crystalline dolomite with interlocking crystals. Around the nuclei is a replacement of the original limestone by dolomite and hollow probably caused by leaching of fossil fragment shows calcite overgrowth by precipitation.

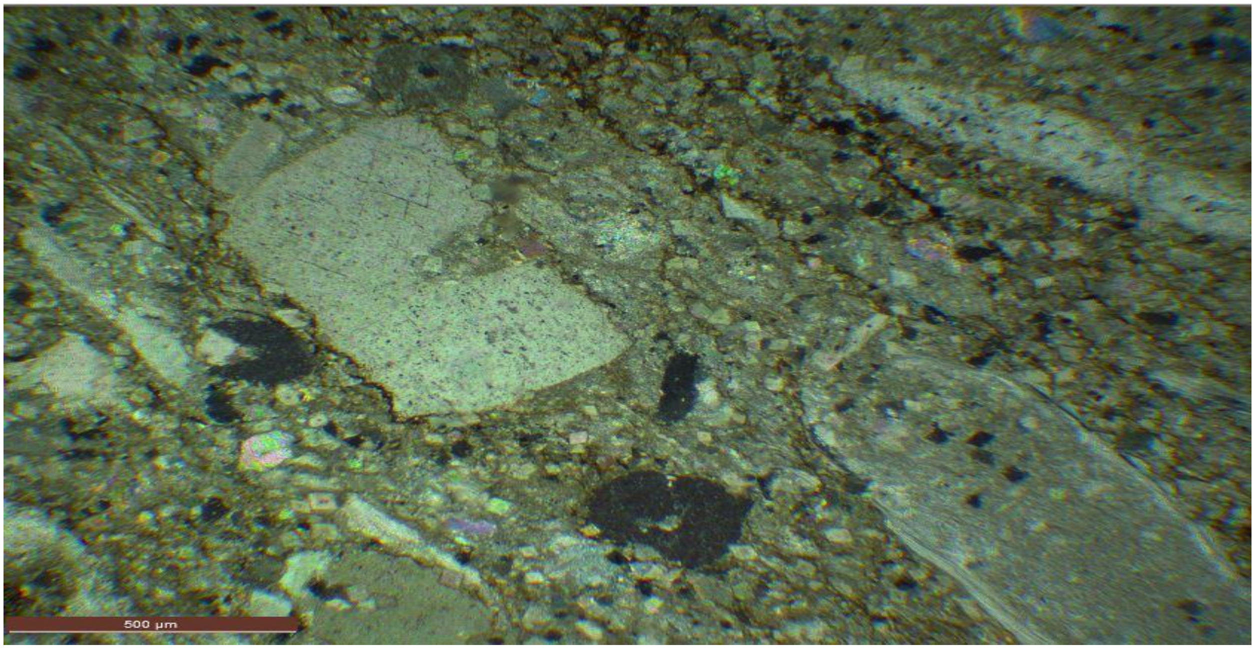

15679 (10755 ft.). Crinoids in a partially dolomitized packestone

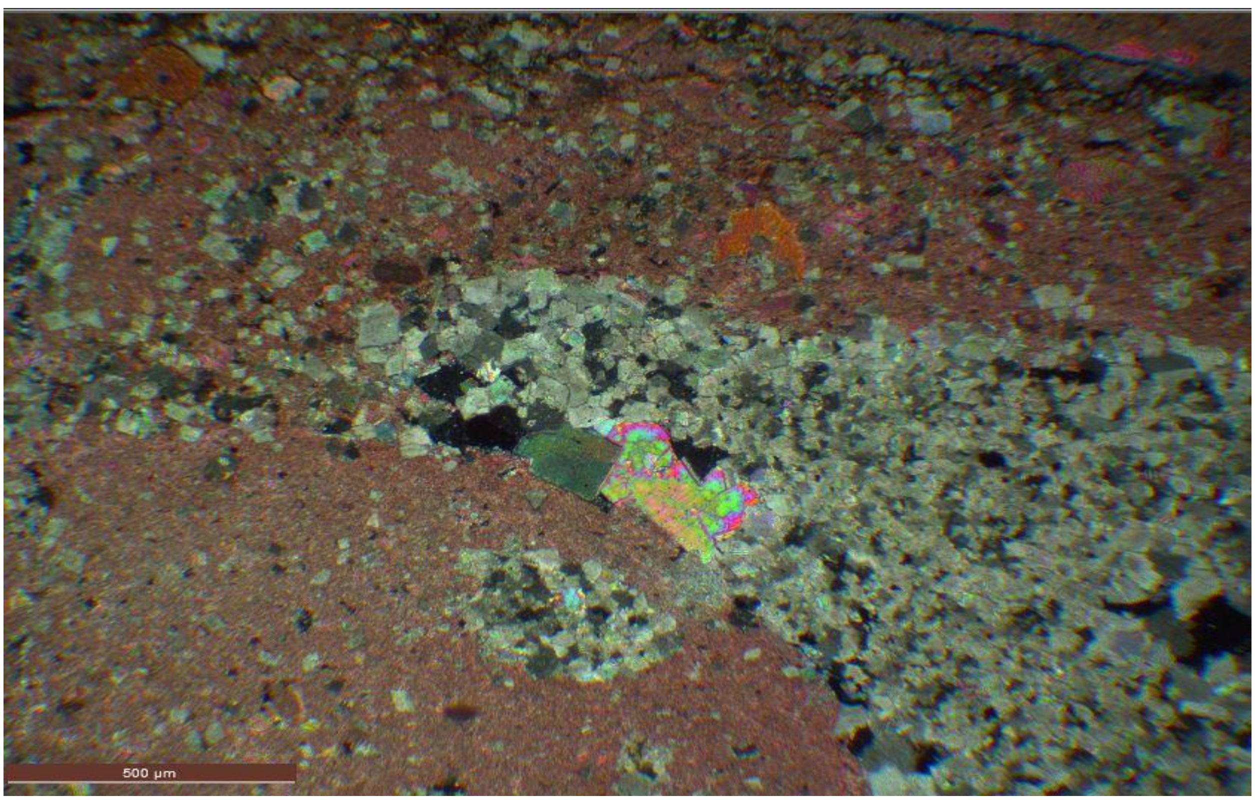

15679 (10755 ft.). Invasive and selective dolomitization

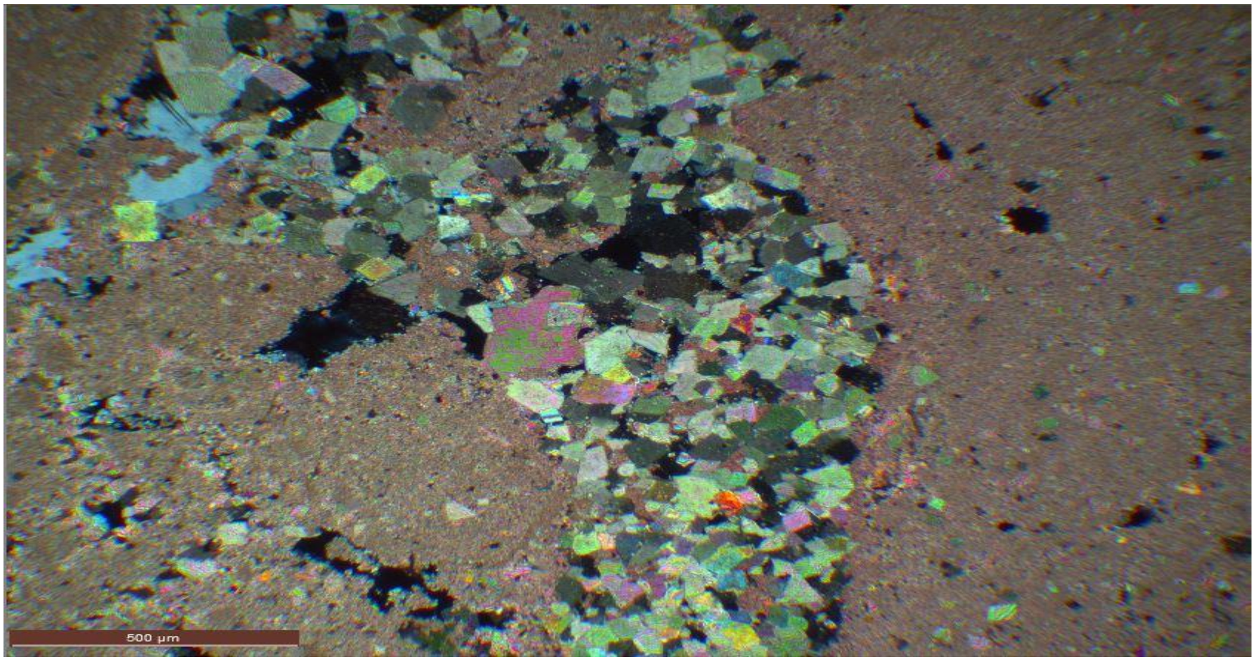

15679 (10757 ft.). Primary sedimentary like this burrow remains open until filled by probably sparry calcite cement. Open burrows are normally loosely packed and can add to the porosity of the reservoir.

THIN SECTIONS FROM
NDGS 21734
CHESAPEAKE OPERATING, INC.
OLSON 12-139-104 A 1H
GOLDEN VALLEY COUNTY
WILDCAT FIELD

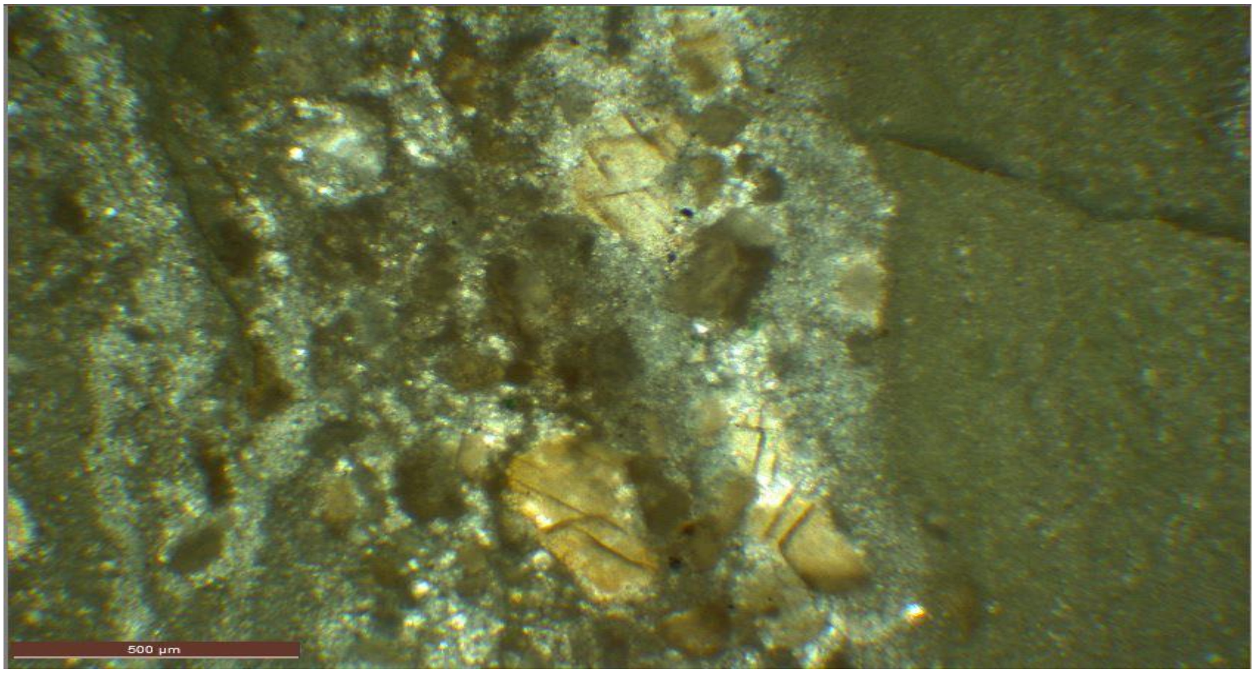

21734 (10493.8 ft.). Bathryodal anhydrites embedded in this limestone

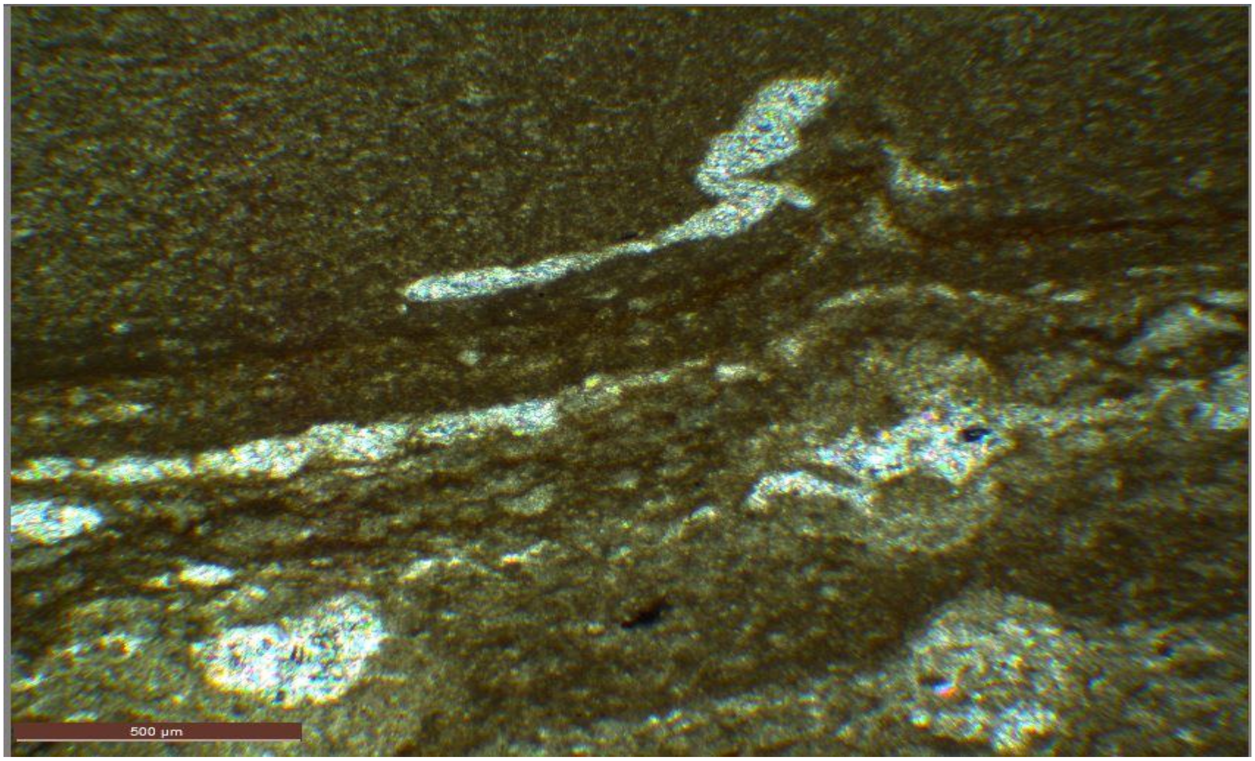

21734 (10509.2 ft.) Anhydrite running through this limestone. The anhydrite bands shows evidence of physical deformation possibly due to pressure.

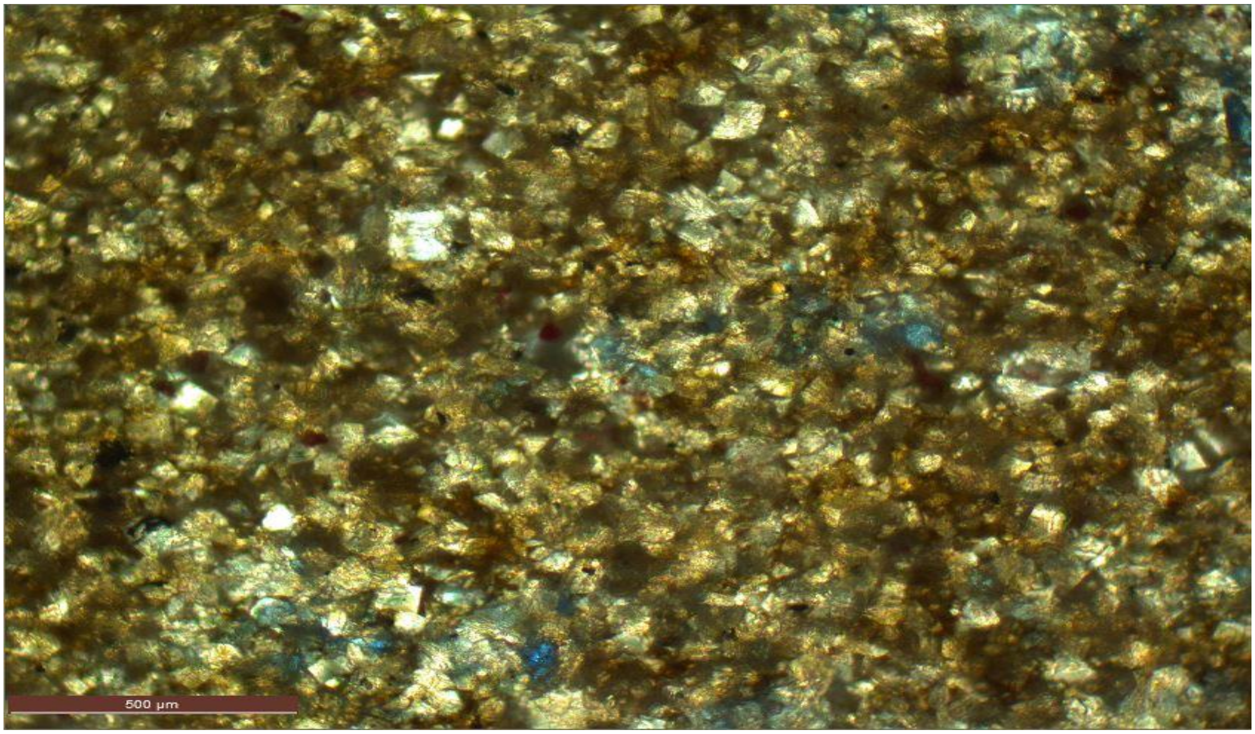

21734 (10521 ft.) Partially dolomitized packstone.

APPENDIX III

DIVISIONS OF THE A AND B ZONE WITH THE CORE INTERVALS OF THE POINTS OF TOC/ROCK-EVAL SAMPLES

The following are well logs showing the divisions of the A and B zones, the core intervals, and the points from where the samples for TOC/ Rock-Eval analyses where taken.

NDGS 291
AMERADA HESS CORPORATION
FRYBURG HEATH-MADISON UNIT P-812
NWNE 9-139-100
BILLINGS COUNTY, NORTH DAKOTA

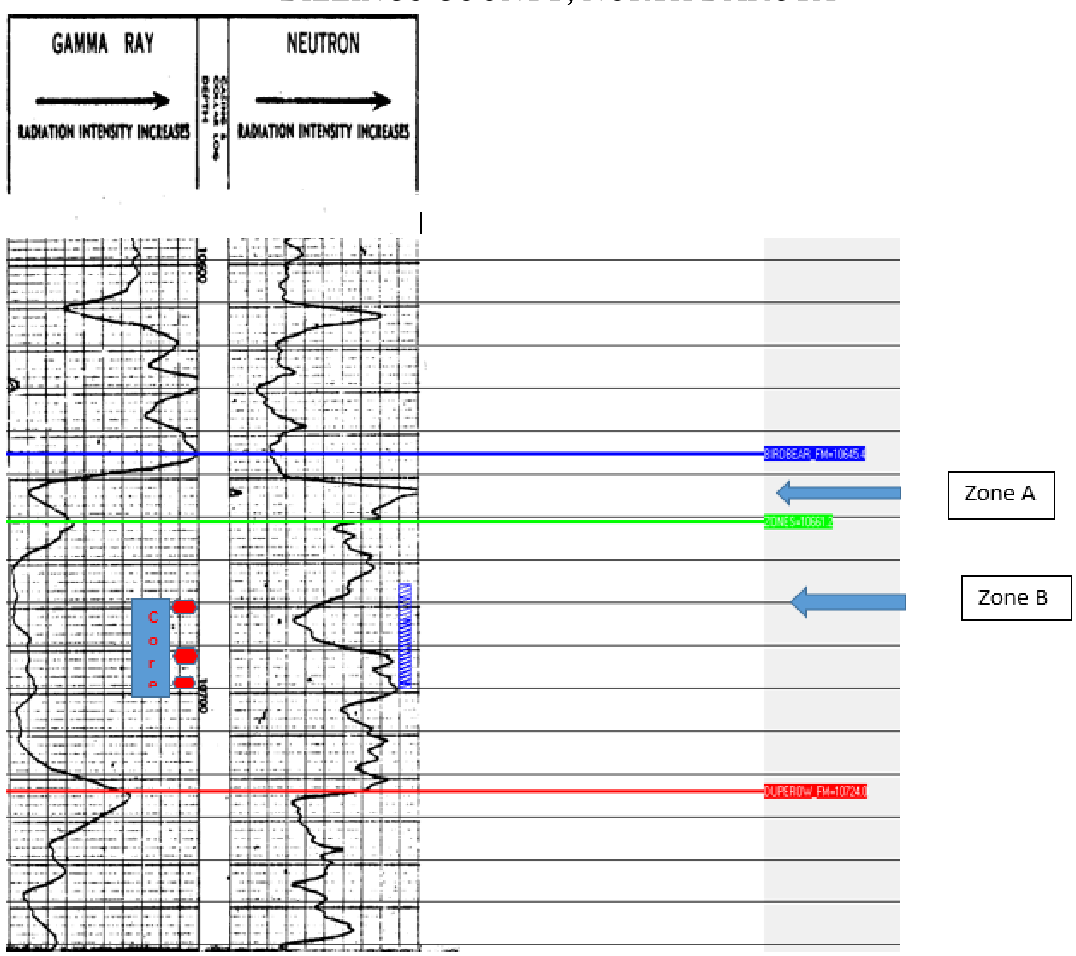

NDGS 859

EXACO INC.

GOVT. - M. S. PACE 1

SWNE 31-144-100

BILLINGS COUNTY, NORTH DAKOTA

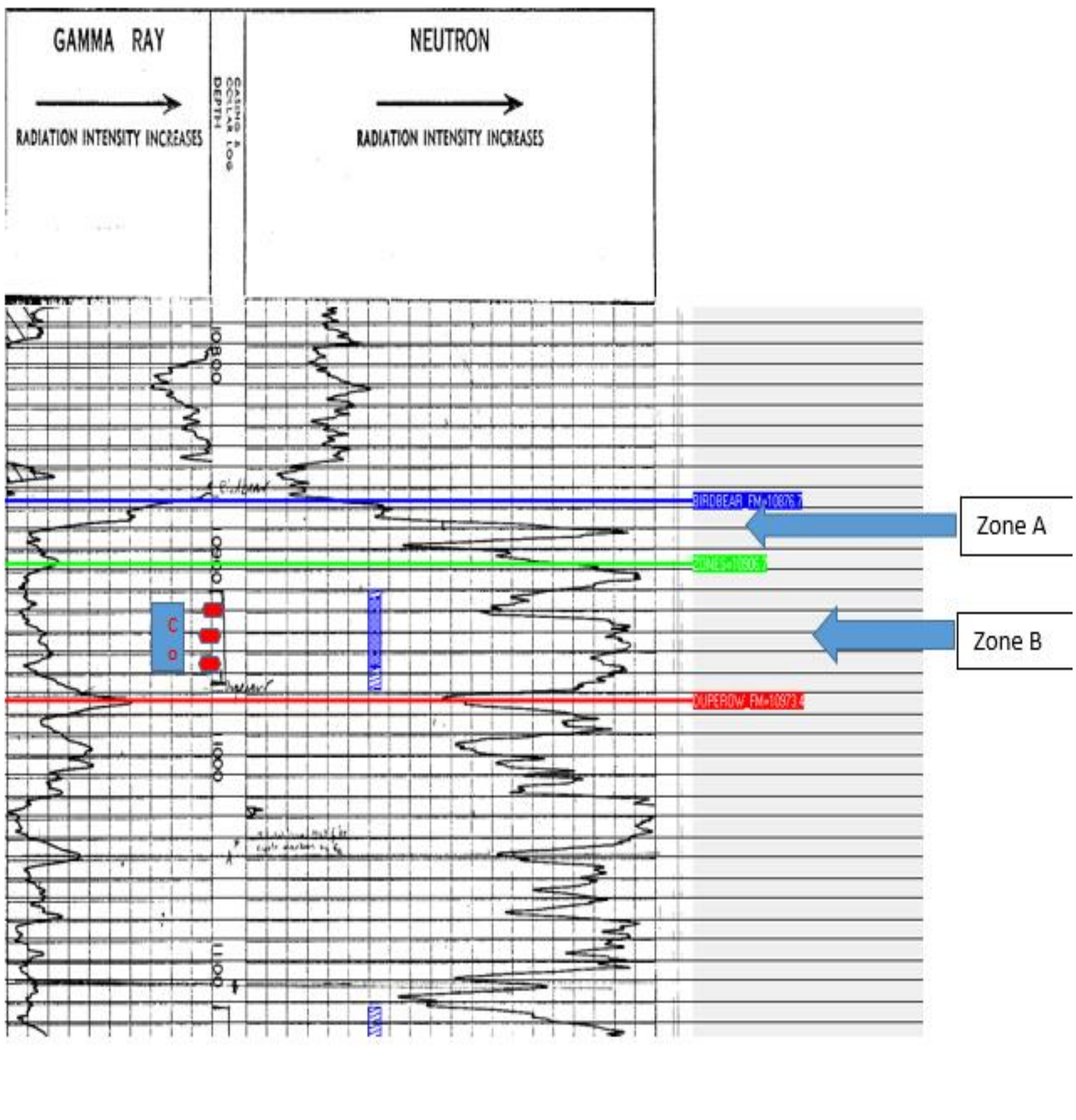

NDGS 15412
NP RESOURCES, LLC
FEDERAL 32-4HBKCE
SWNE 4-143-103
BILLINGS COUNTY, NORTH DAKOTA

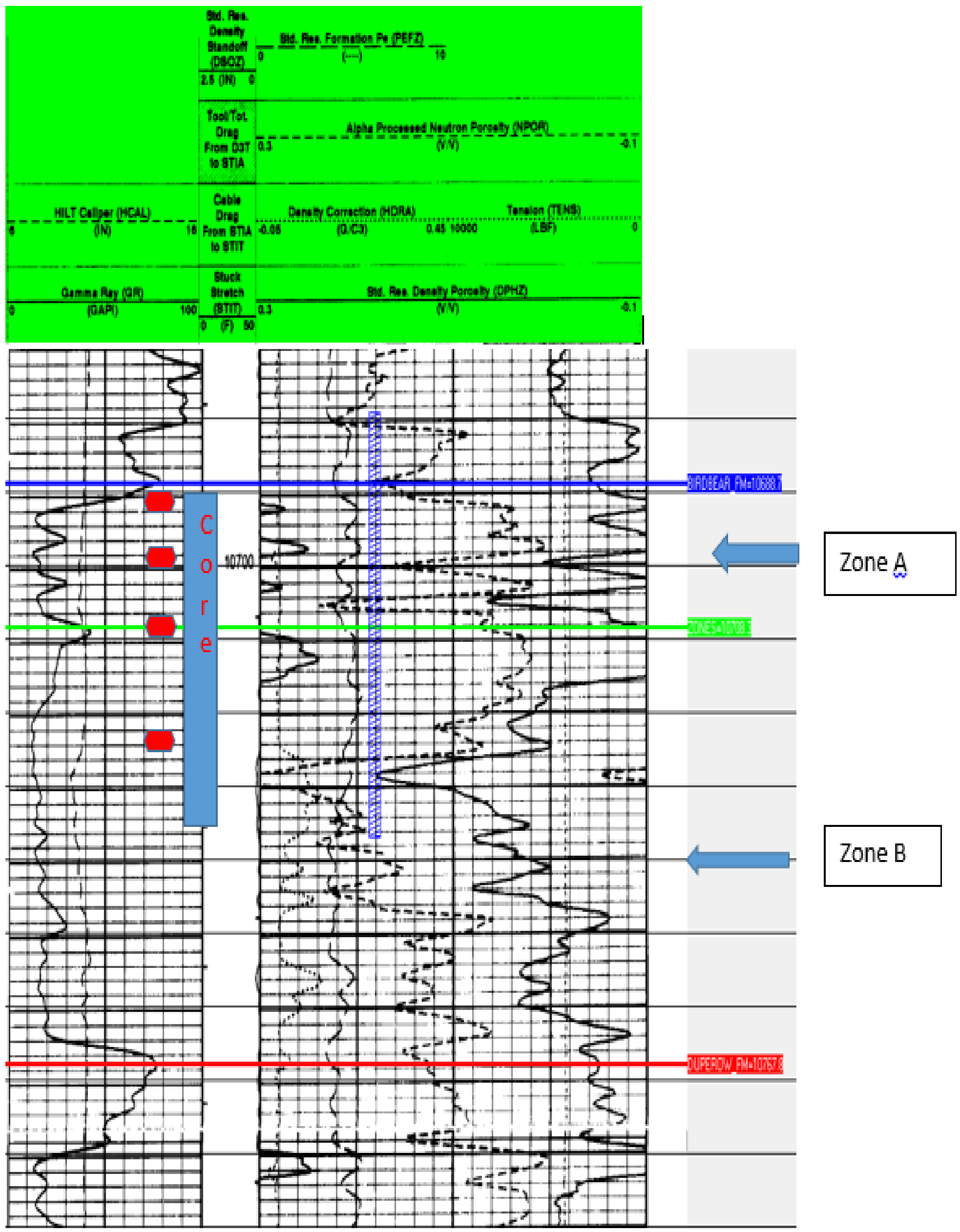

NDGS 15679

FH PETROLEUM CORP.

BROWN 42-28

SENE 28-142-103

GOLDEN VALLEY COUNTY, NORTH DAKOTA

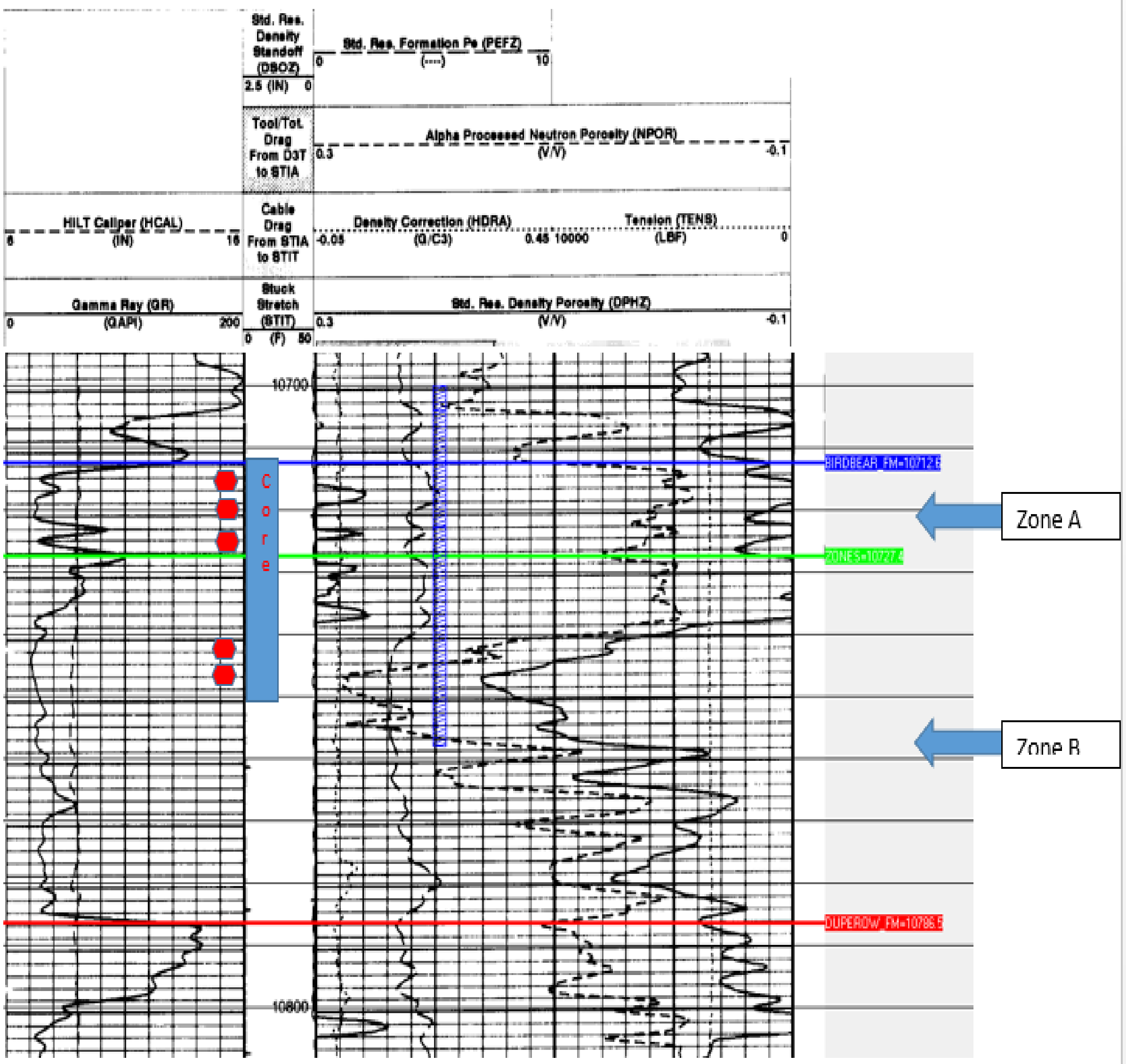

APPENDIX IV

TOC/ROCK-EVAL ANALYSES GRAPHS

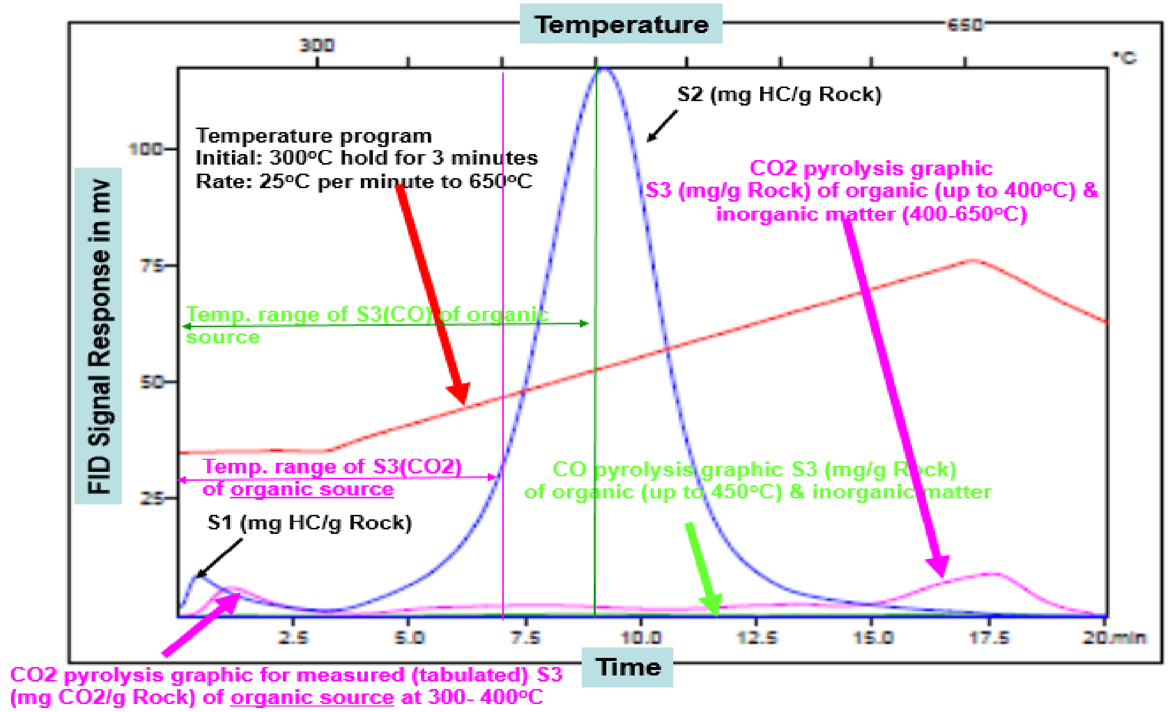

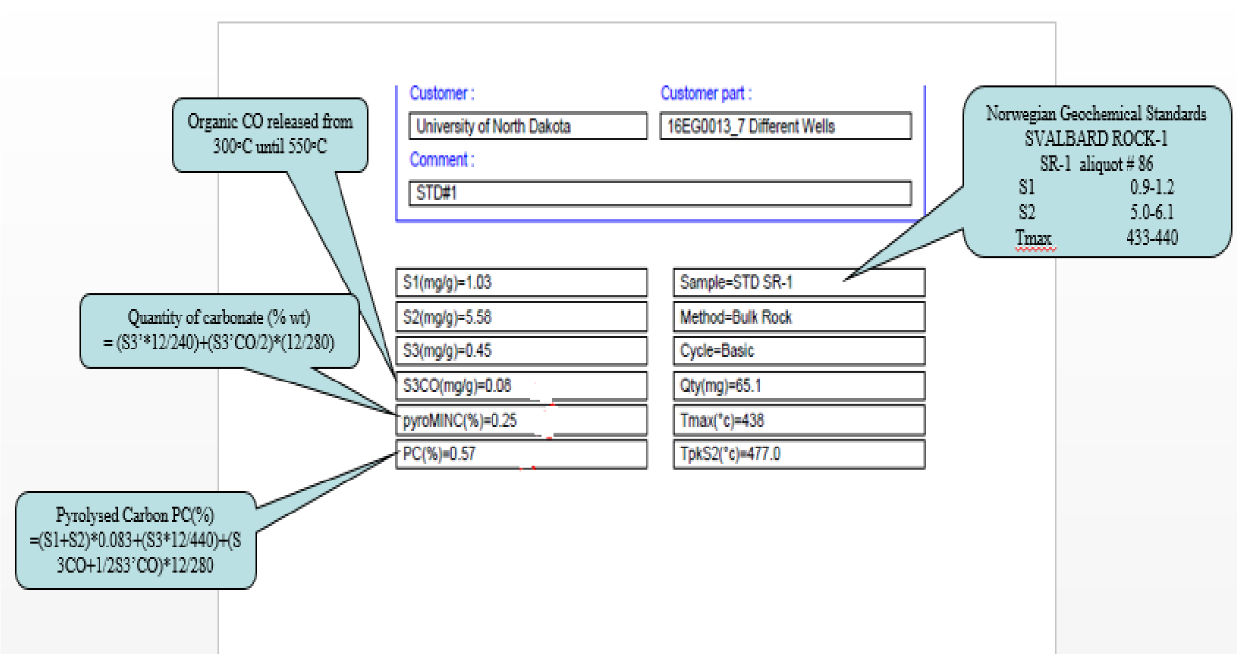

S1(mg/g)=2.65	Sample=UDEG000001
S2(mg/g)=0.93	Method=Bulk Rock
S3(mg/g)=0.36	Cycle=Basic
S3CO(mg/g)=0.04	Qty(mg)=62.6
pyroMINC(%)=0.23	Tmax(°c)=405
PC(%)=0.32	TpkS2(°c)=444.0

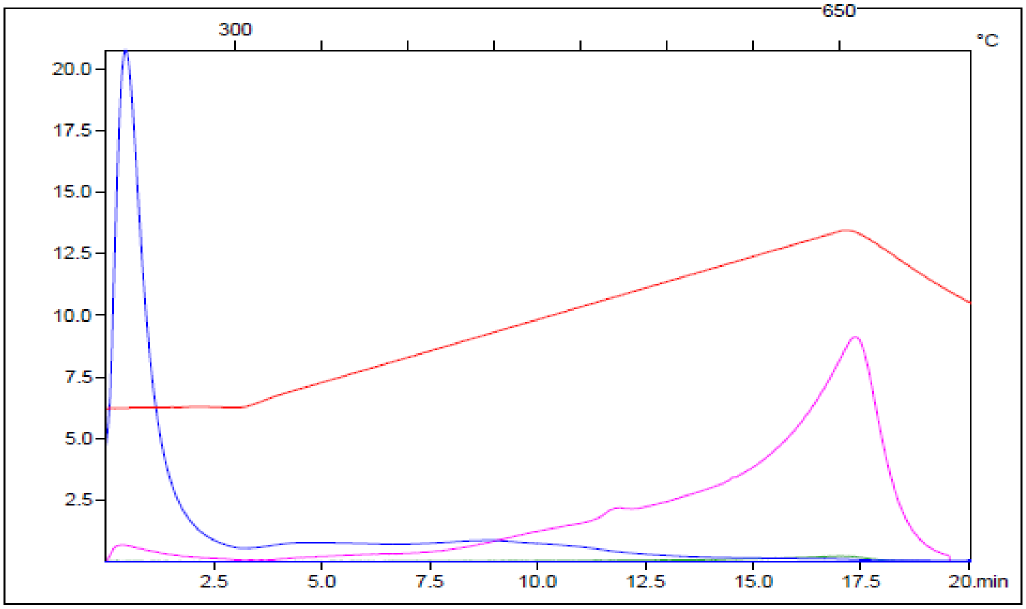

S1(mg/g)=1.36	Sample=UDEG000002
S2(mg/g)=0.55	Method=Bulk Rock
S3(mg/g)=0.41	Cycle=Basic
S3CO(mg/g)=0.09	Qty(mg)=67.2
pyroMINC(%)=0.23	Tmax(°c)=398
PC(%)=0.18	TpkS2(°c)=437.0

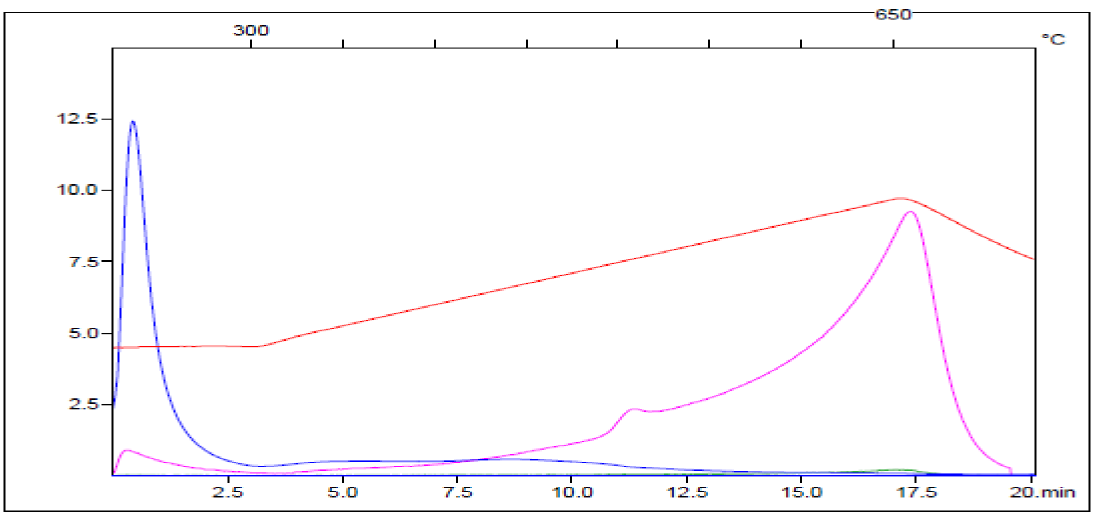

S1(mg/g)=0.08	Sample=UDEG000003
S2(mg/g)=0.07	Method=Bulk Rock
S3(mg/g)=0.48	Cycle=Basic
S3CO(mg/g)=0.05	Qty(mg)=62.9
pyroMINC(%)=0.41	Tmax(°c)=436
PC(%)=0.03	TpkS2(°c)=475.0

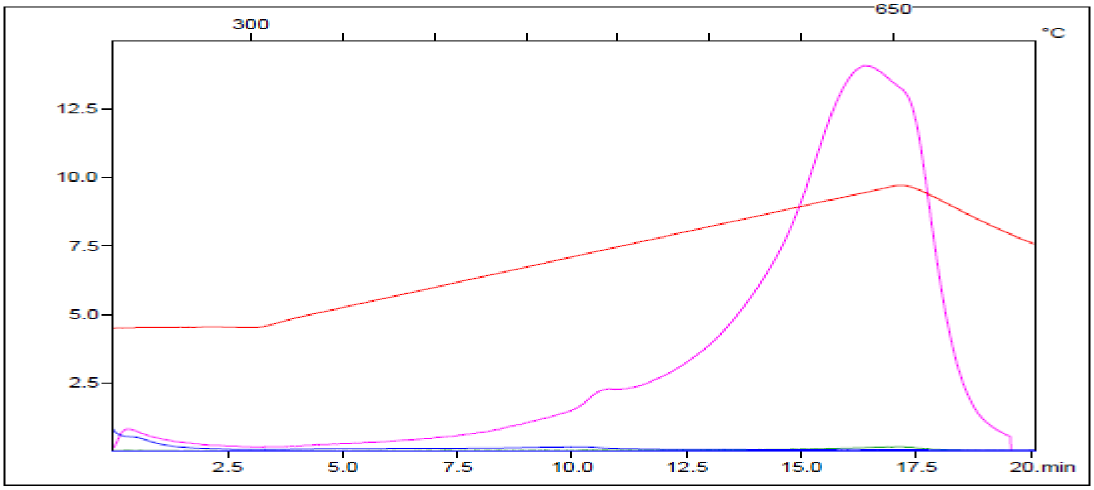

S1(mg/g)=0.12	Sample=UDEG000004
S2(mg/g)=0.12	Method=Bulk Rock
S3(mg/g)=0.25	Cycle=Basic
S3CO(mg/g)=0.01	Qty(mg)=63.5
pyroMINC(%)=0.23	Tmax(°c)=444
PC(%)=0.03	TpkS2(°c)=483.0

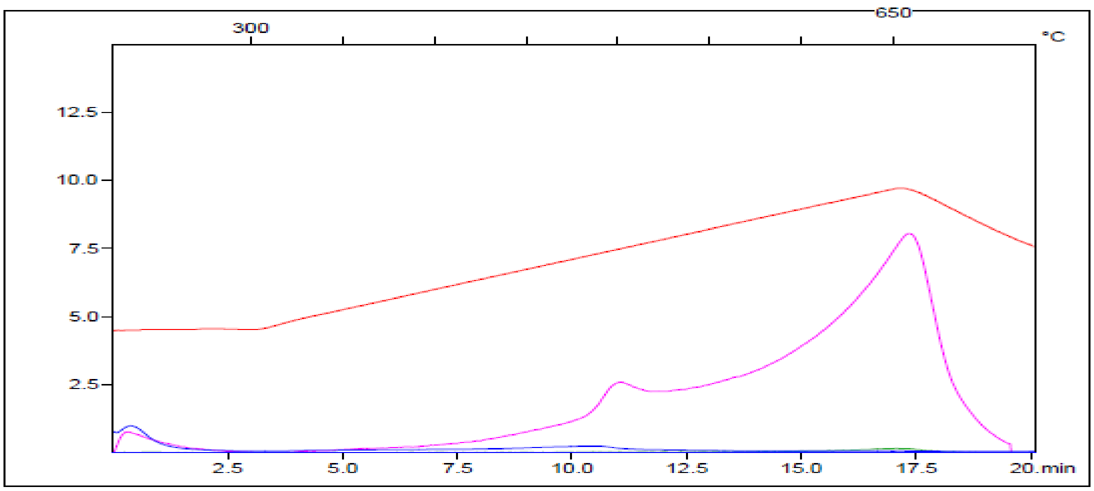

S1(mg/g)=0.15	Sample=UDEG000005
S2(mg/g)=0.18	Method=Bulk Rock
S3(mg/g)=0.55	Cycle=Basic
S3CO(mg/g)=0.05	Qty(mg)=66.7
pyroMINC(%)=1.95	Tmax(°c)=426
PC(%)=0.06	TpkS2(°c)=465.0

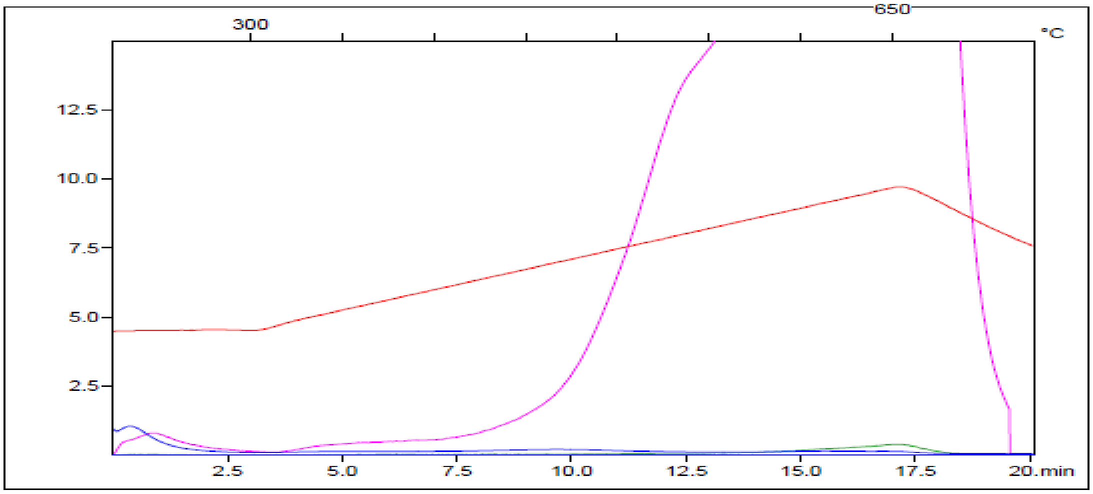

S1(mg/g)=0.07	Sample=UDEG000006
S2(mg/g)=0.06	Method=Bulk Rock
S3(mg/g)=0.28	Cycle=Basic
S3CO(mg/g)=0.05	Qty(mg)=66.0
pyroMINC(%)=0.07	Tmax(°c)=431
PC(%)=0.03	TpkS2(°c)=470.0

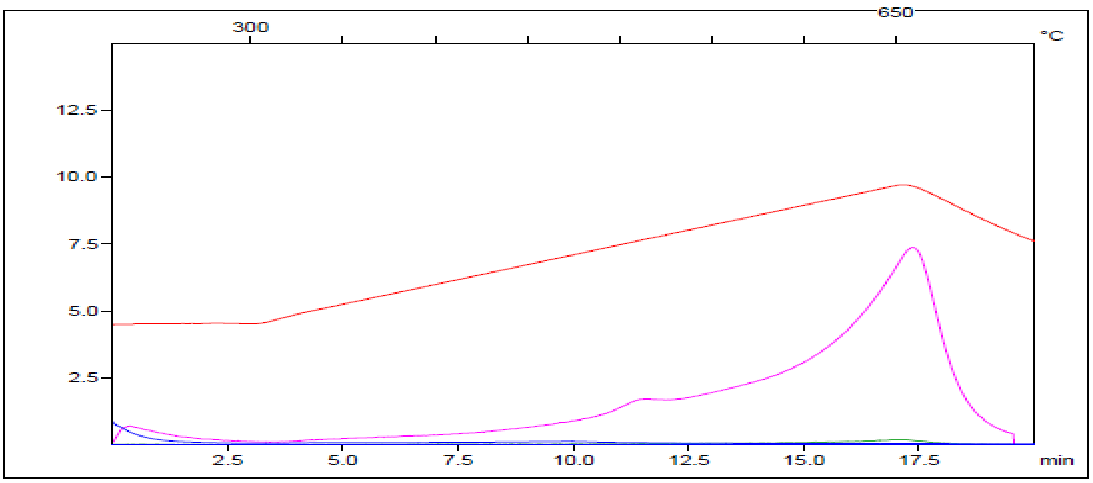

S1(mg/g)=0.09	Sample=UDEG000007
S2(mg/g)=0.11	Method=Bulk Rock
S3(mg/g)=0.42	Cycle=Basic
S3CO(mg/g)=0.08	Qty(mg)=63.3
pyroMINC(%)=0.39	Tmax(°c)=429
PC(%)=0.04	TpkS2(°c)=468.0

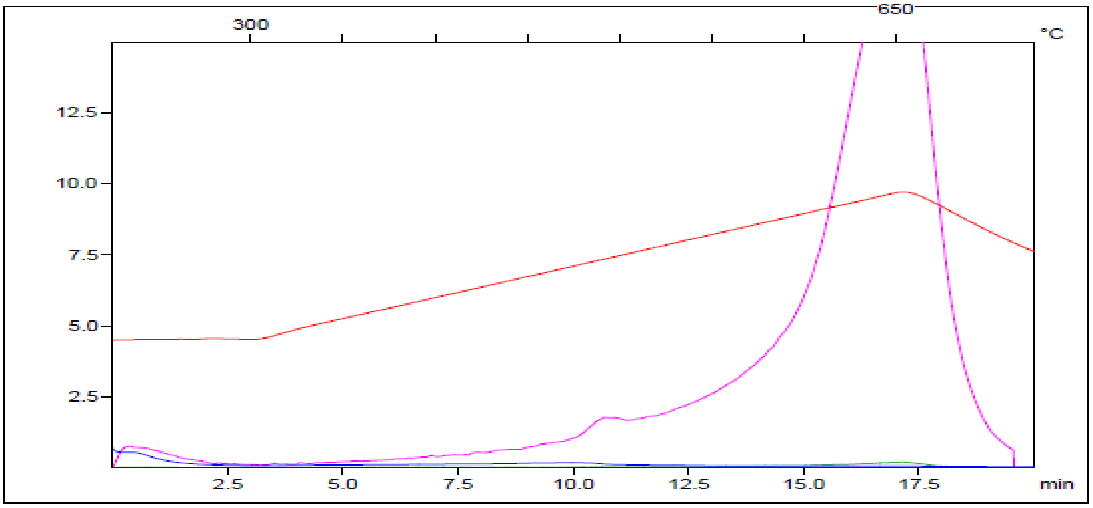

S1(mg/g)=0.04	Sample=UDEG000008
S2(mg/g)=0.03	Method=Bulk Rock
S3(mg/g)=0.81	Cycle=Basic
S3CO(mg/g)=0.02	Qty(mg)=65.7
pyroMINC(%)=0.22	Tmax(°c)=428
PC(%)=0.03	TpkS2(°c)=467.0

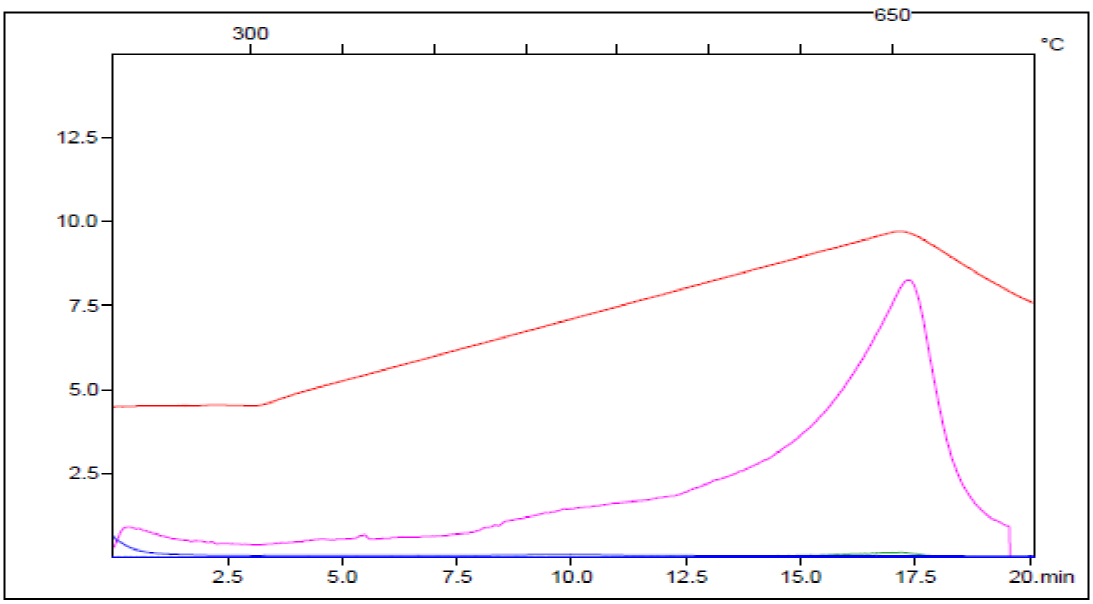

S1(mg/g)=0.15	Sample=UDEG000009
S2(mg/g)=0.88	Method=Bulk Rock
S3(mg/g)=0.46	Cycle=Basic
S3CO(mg/g)=0.06	Qty(mg)=67.4
pyroMINC(%)=0.13	Tmax(°c)=447
PC(%)=0.11	TpkS2(°c)=486.0

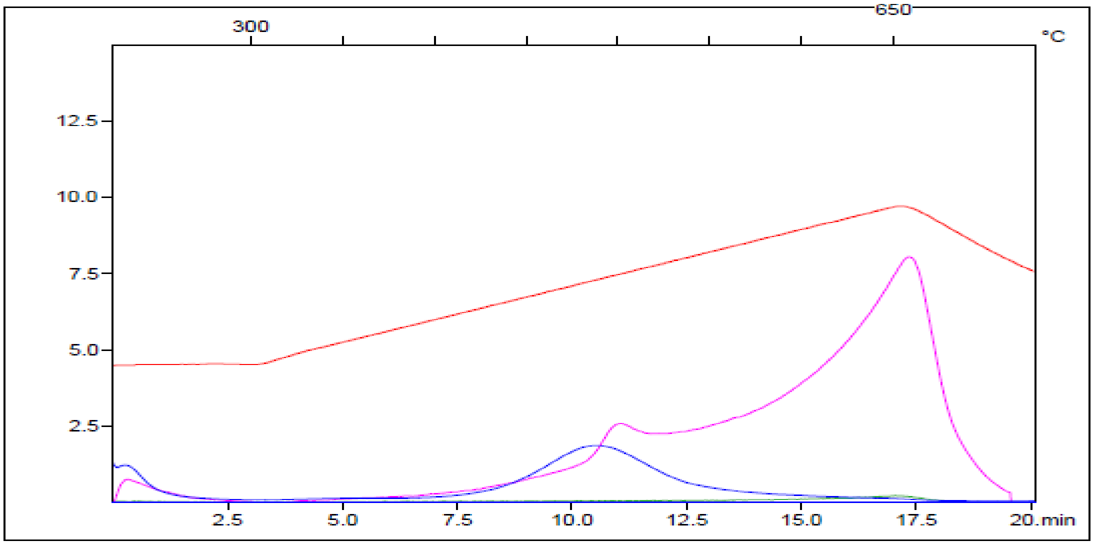

S1(mg/g)=1.04	Sample=STD SR-1
S2(mg/g)=5.64	Method=Bulk Rock
S3(mg/g)=0.41	Cycle=Basic
S3CO(mg/g)=0.19	Qty(mg)=64.7
pyroMINC(%)=0.25	Tmax(°c)=438
PC(%)=0.57	TpkS2(°c)=477.0

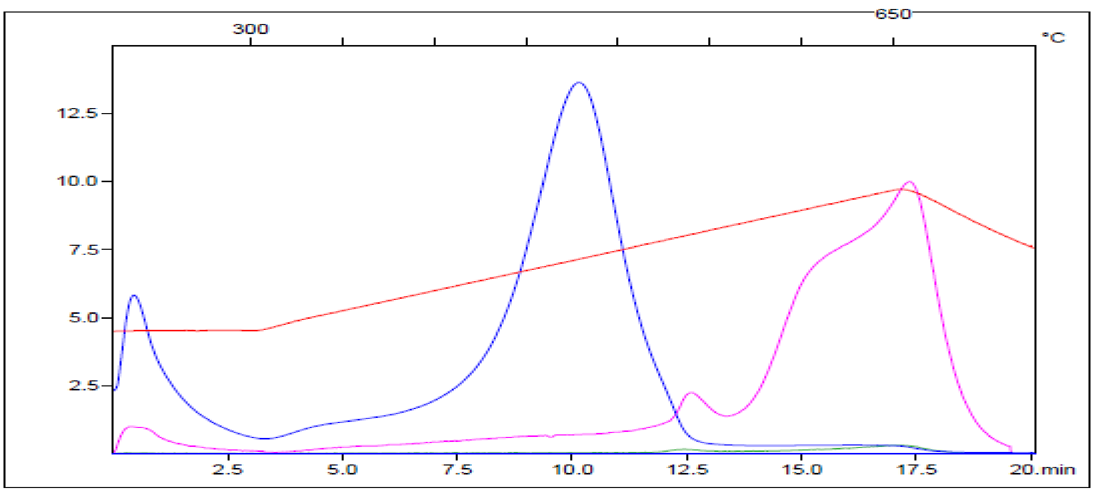

S1(mg/g)=0.12	Sample=UDEG000010
S2(mg/g)=0.19	Method=Bulk Rock
S3(mg/g)=0.39	Cycle=Basic
S3CO(mg/g)=0.06	Qty(mg)=67.4
pyroMINC(%)=1.34	Tmax(°c)=439
PC(%)=0.05	TpkS2(°c)=478.0

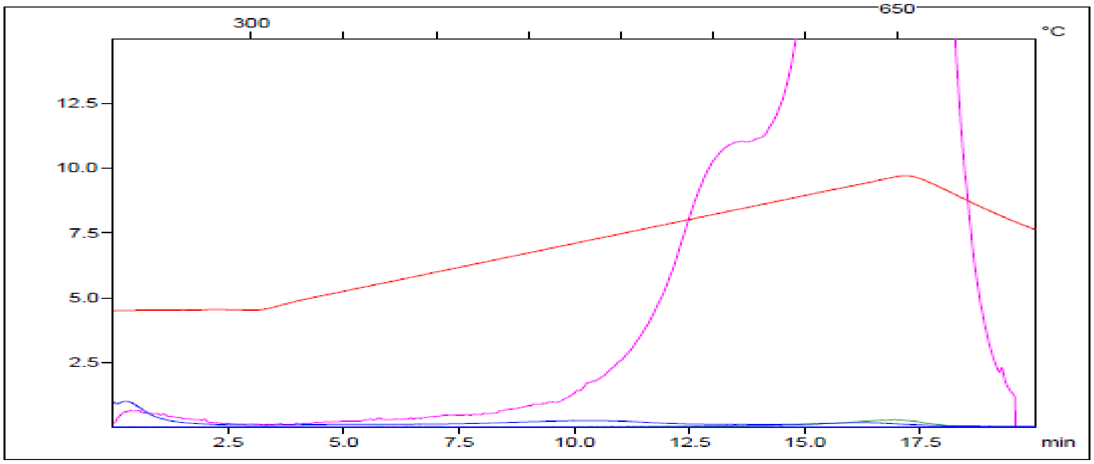

S1(mg/g)=0.1	Sample=UDEG000011
S2(mg/g)=0.18	Method=Bulk Rock
S3(mg/g)=0.5	Cycle=Basic
S3CO(mg/g)=0.04	Qty(mg)=64.3
pyroMINC(%)=3.48	Tmax(°c)=595
PC(%)=0.05	TpkS2(°c)=634.0

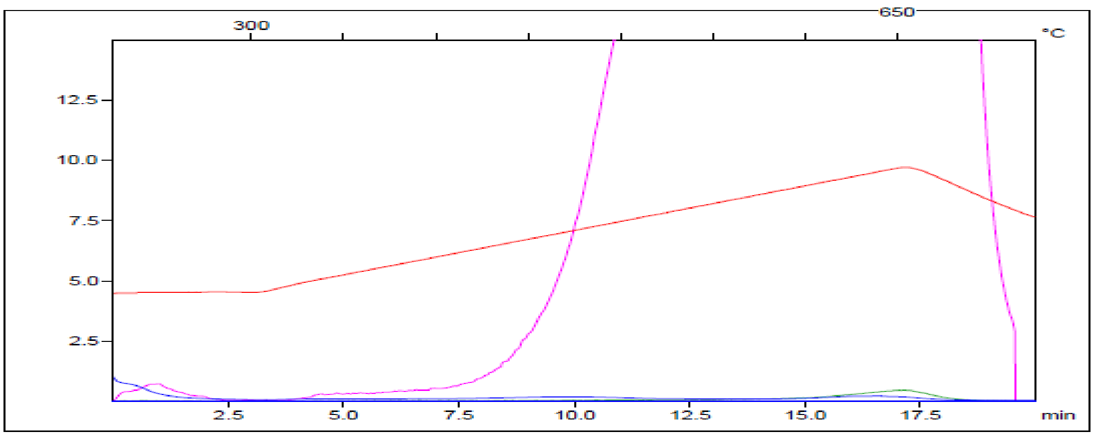

S1(mg/g)=0.39	Sample=UDEG000012
S2(mg/g)=0.43	Method=Bulk Rock
S3(mg/g)=0.37	Cycle=Basic
S3CO(mg/g)=0.02	Qty(mg)=68.4
pyroMINC(%)=0.18	Tmax(°c)=437
PC(%)=0.09	TpkS2(°c)=476.0

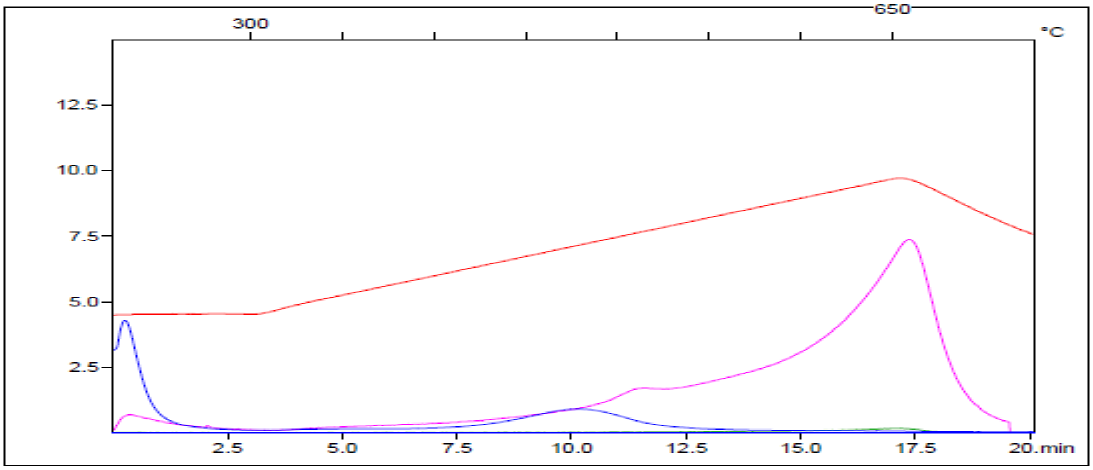

S1(mg/g)=0.31	Sample=UDEG000013
S2(mg/g)=0.39	Method=Bulk Rock
S3(mg/g)=0.38	Cycle=Basic
S3CO(mg/g)=0.06	Qty(mg)=67.9
pyroMINC(%)=0.02	Tmax(°c)=437
PC(%)=0.08	TpkS2(°c)=476.0

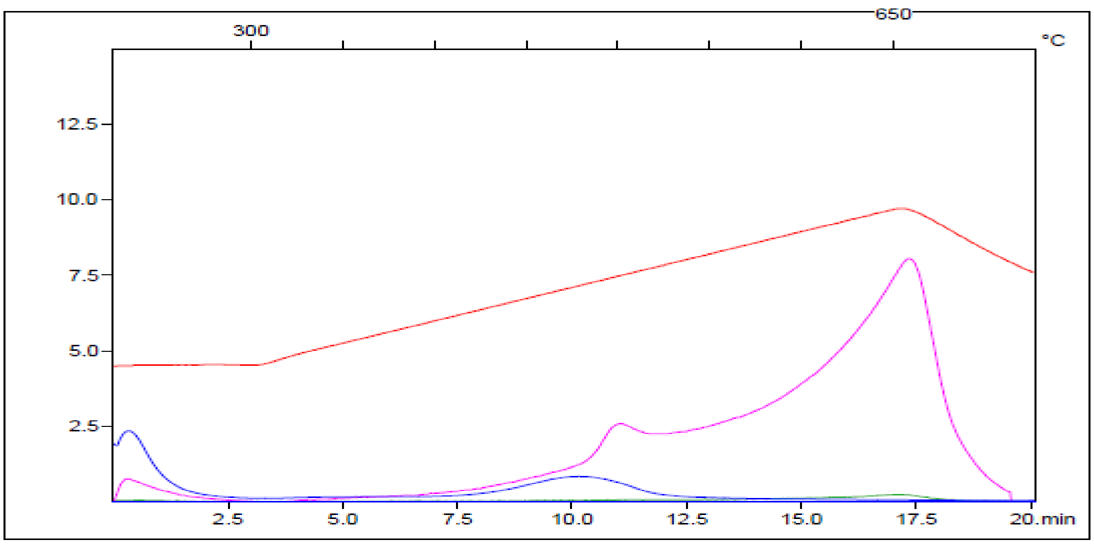

S1(mg/g)=3.21	Sample=UDEG000014
S2(mg/g)=0.47	Method=Bulk Rock
S3(mg/g)=0.54	Cycle=Basic
S3CO(mg/g)=0.04	Qty(mg)=63.1
pyroMINC(%)=3.19	Tmax(°c)=435
PC(%)=0.34	TpkS2(°c)=474.0

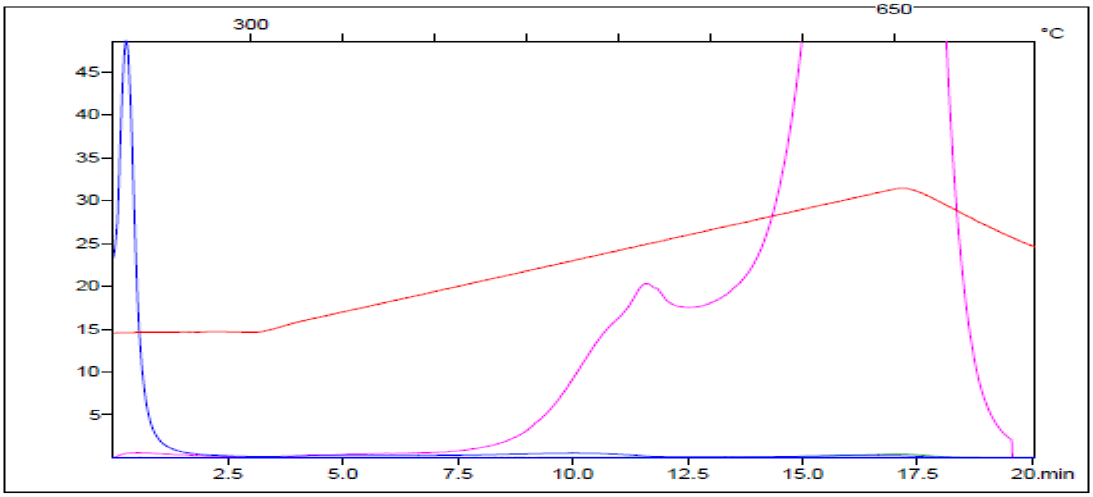

S1(mg/g)=0.95	Sample=UDEG000015
S2(mg/g)=0.18	Method=Bulk Rock
S3(mg/g)=0.6	Cycle=Basic
S3CO(mg/g)=0.03	Qty(mg)=68.9
pyroMINC(%)=1.25	Tmax(°c)=413
PC(%)=0.12	TpkS2(°c)=452.0

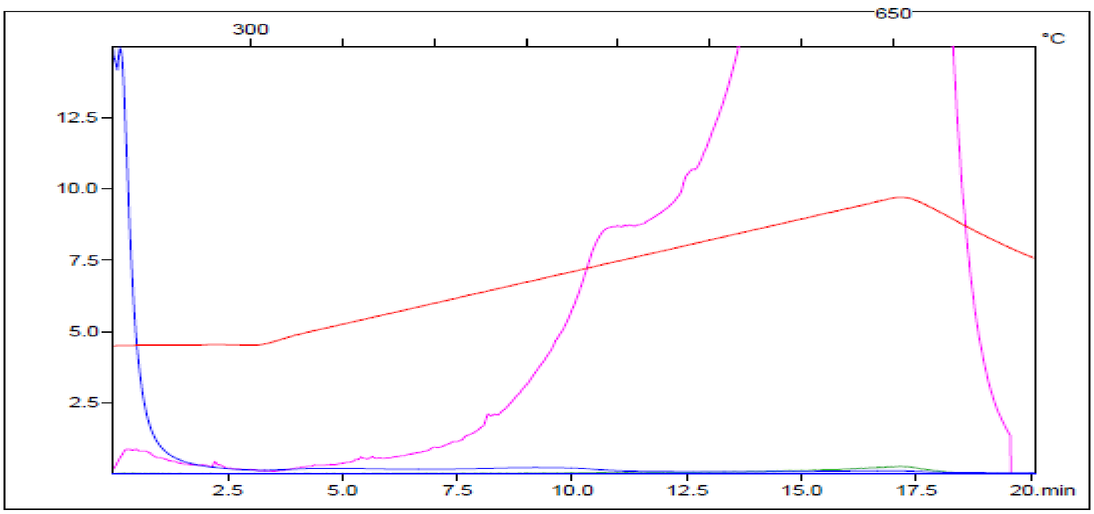

S1(mg/g)=0.07	Sample=UDEG000016
S2(mg/g)=0.05	Method=Bulk Rock
S3(mg/g)=0.37	Cycle=Basic
S3CO(mg/g)=0.02	Qty(mg)=68.5
pyroMINC(%)=0.38	Tmax(°c)=412
PC(%)=0.03	TpkS2(°c)=451.0

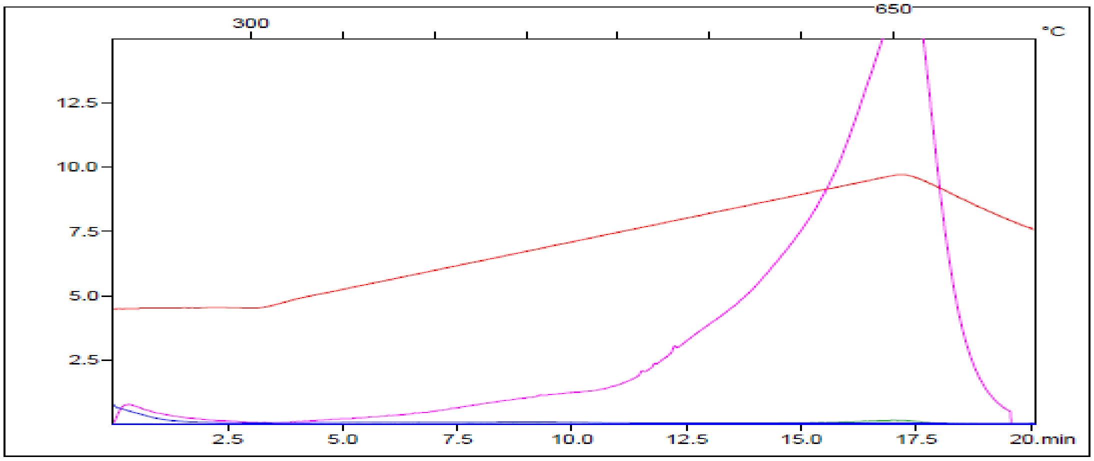

S1(mg/g)=0.05	Sample=UDEG000017
S2(mg/g)=0.04	Method=Bulk Rock
S3(mg/g)=0.41	Cycle=Basic
S3CO(mg/g)=0.04	Qty(mg)=62.8
pyroMINC(%)=0.21	Tmax(°c)=318
PC(%)=0.03	TpkS2(°c)=357.0

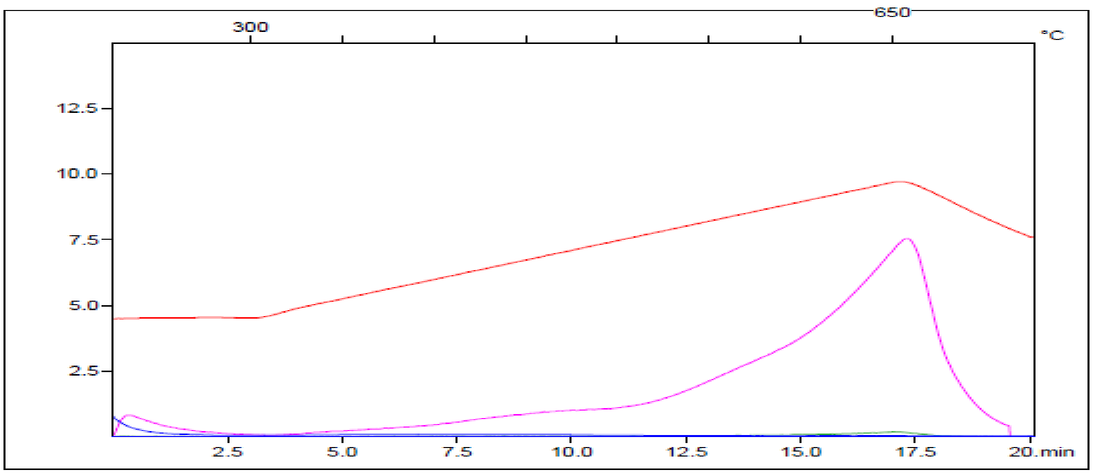

S1(mg/g)=0.5	Sample=UDEG000018
S2(mg/g)=0.9	Method=Bulk Rock
S3(mg/g)=0.63	Cycle=Basic
S3CO(mg/g)=0.12	Qty(mg)=67.6
pyroMINC(%)=0.76	Tmax(°c)=437
PC(%)=0.15	TpkS2(°c)=476.0

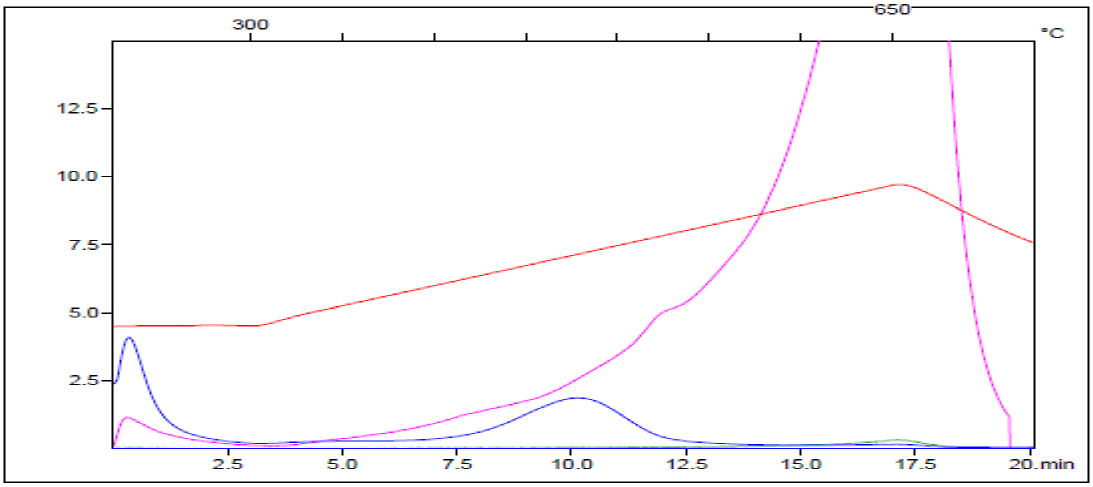

S1(mg/g)=1.03	Sample=STD SR-1
S2(mg/g)=5.69	Method=Bulk Rock
S3(mg/g)=0.46	Cycle=Basic
S3CO(mg/g)=0.08	Qty(mg)=64.5
pyroMINC(%)=0.25	Tmax(°c)=438
PC(%)=0.59	TpkS2(°c)=477.0

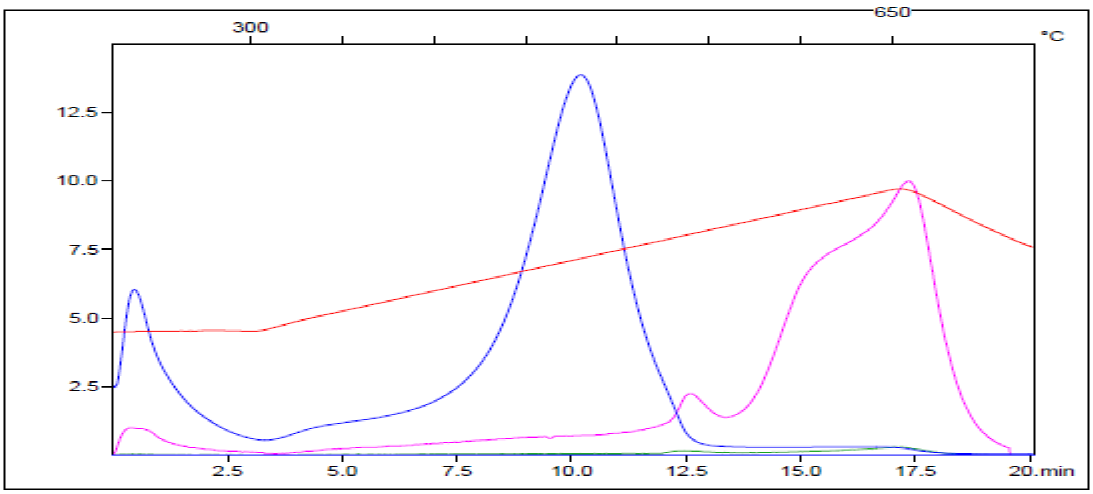

S1(mg/g)=2.94	Sample=UDEG000019
S2(mg/g)=0.53	Method=Bulk Rock
S3(mg/g)=1.59	Cycle=Basic
S3CO(mg/g)=0.08	Qty(mg)=66.7
pyroMINC(%)=0.29	Tmax(°c)=296
PC(%)=0.34	TpkS2(°c)=335.0

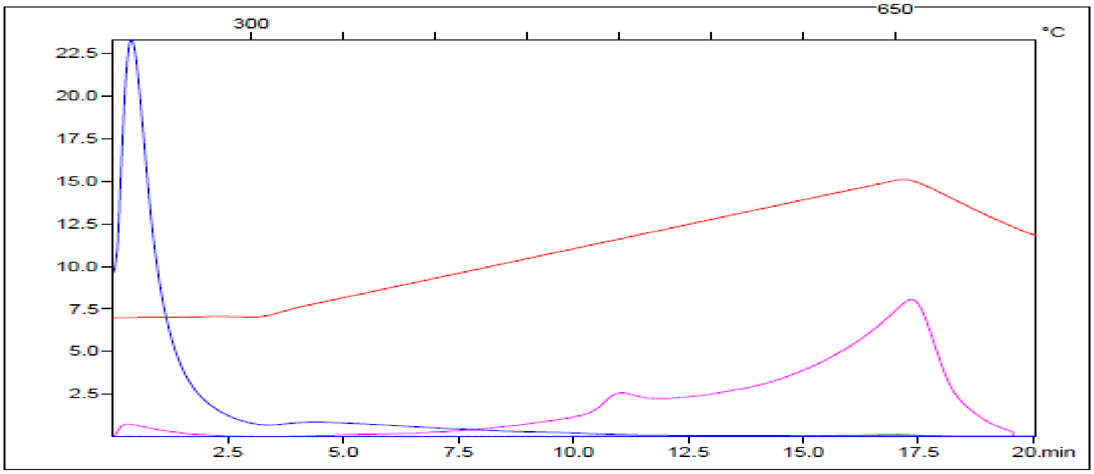

S1(mg/g)=0.26	Sample=UDEG000020
S2(mg/g)=0.21	Method=Bulk Rock
S3(mg/g)=0.4	Cycle=Basic
S3CO(mg/g)=0.03	Qty(mg)=67.9
pyroMINC(%)=0.14	Tmax(°c)=430
PC(%)=0.06	TpkS2(°c)=469.0

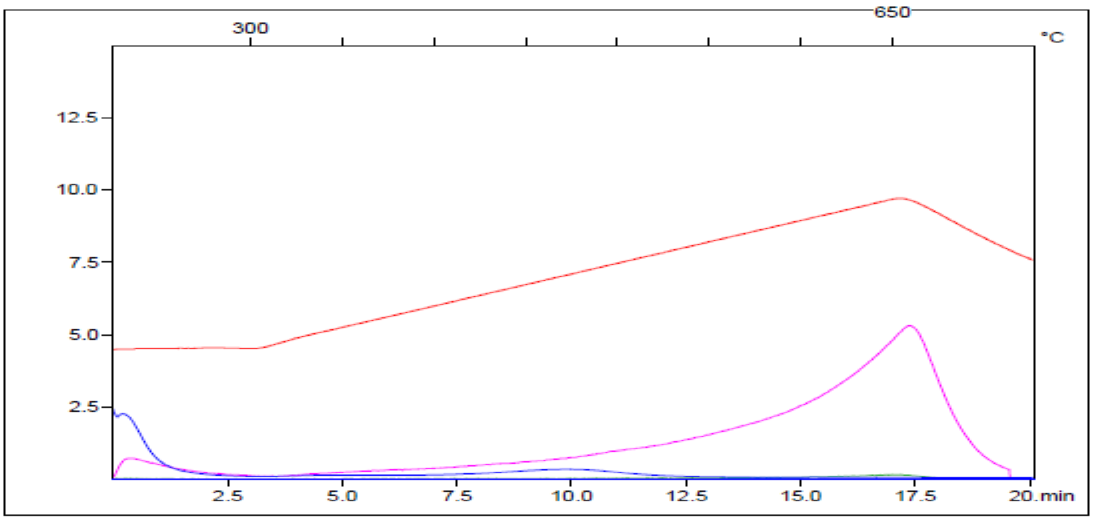

S1(mg/g)=1.34	Sample=UDEG000021
S2(mg/g)=0.34	Method=Bulk Rock
S3(mg/g)=0.62	Cycle=Basic
S3CO(mg/g)=0.11	Qty(mg)=64.7
pyroMINC(%)=1.96	Tmax(°c)=421
PC(%)=0.17	TpkS2(°c)=460.0

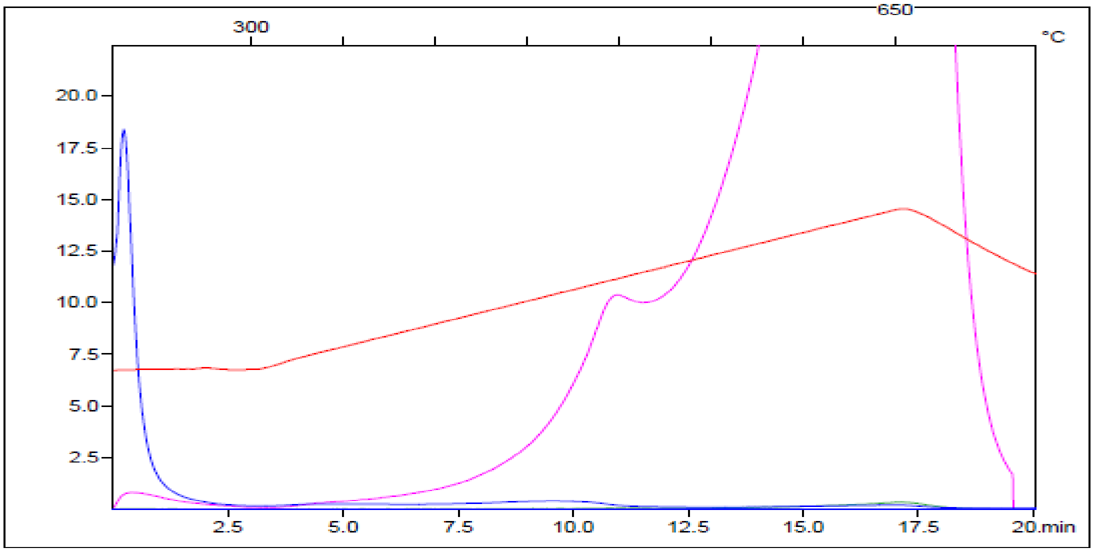

S1(mg/g)=1.67	Sample=UDEG000022
S2(mg/g)=0.44	Method=Bulk Rock
S3(mg/g)=0.54	Cycle=Basic
S3CO(mg/g)=0.12	Qty(mg)=67.1
pyroMINC(%)=2.14	Tmax(°c)=407
PC(%)=0.2	TpkS2(°c)=446.0

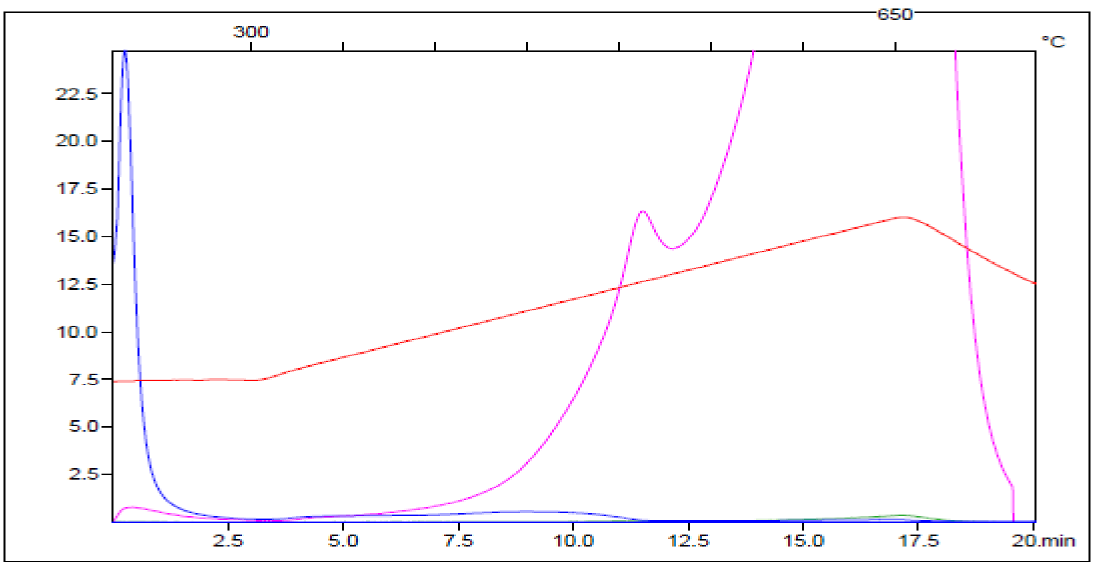

S1(mg/g)=0.05	Sample=UDEG000023
S2(mg/g)=0.15	Method=Bulk Rock
S3(mg/g)=0.19	Cycle=Basic
S3CO(mg/g)=0.09	Qty(mg)=68.8
pyroMINC(%)=0.09	Tmax(°c)=440
PC(%)=0.03	TpkS2(°c)=479.0

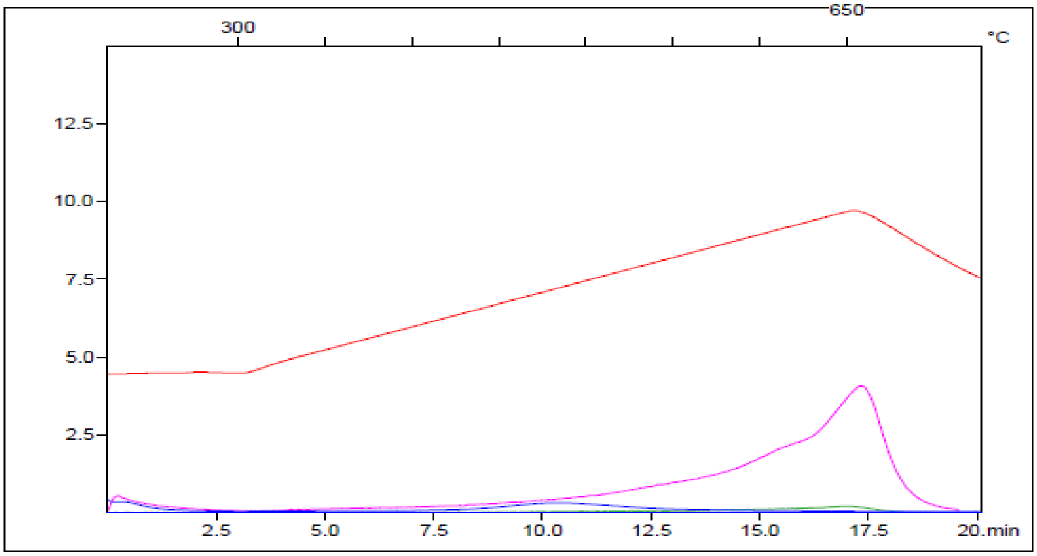

S1(mg/g)=0.07	Sample=UDEG000024
S2(mg/g)=0.1	Method=Bulk Rock
S3(mg/g)=0.34	Cycle=Basic
S3CO(mg/g)=0.04	Qty(mg)=63.8
pyroMINC(%)=0.09	Tmax(°c)=432
PC(%)=0.03	TpkS2(°c)=471.0

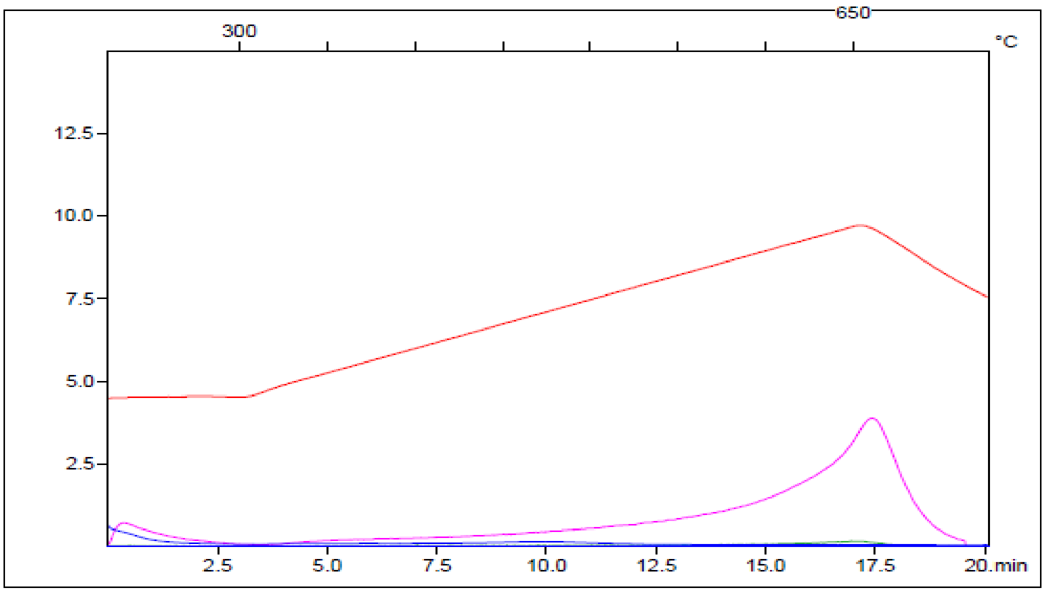

S1(mg/g)=0.06	Sample=UDEG000025
S2(mg/g)=0.11	Method=Bulk Rock
S3(mg/g)=0.82	Cycle=Basic
S3CO(mg/g)=0.05	Qty(mg)=62.4
pyroMINC(%)=2.62	Tmax(°c)=606
PC(%)=0.05	TpkS2(°c)=645.0

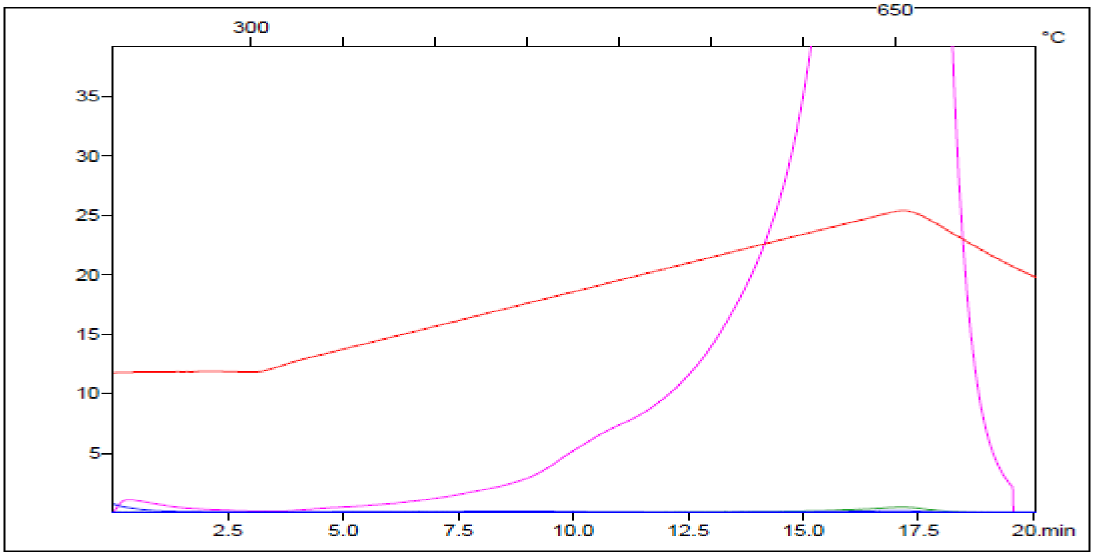

APPENDIX V

PRODUCTION CURVES OF SOME WELLS IN THE STUDY AREA FROM THE NORTH DAKOTA INDUSTRIAL COMMISSION

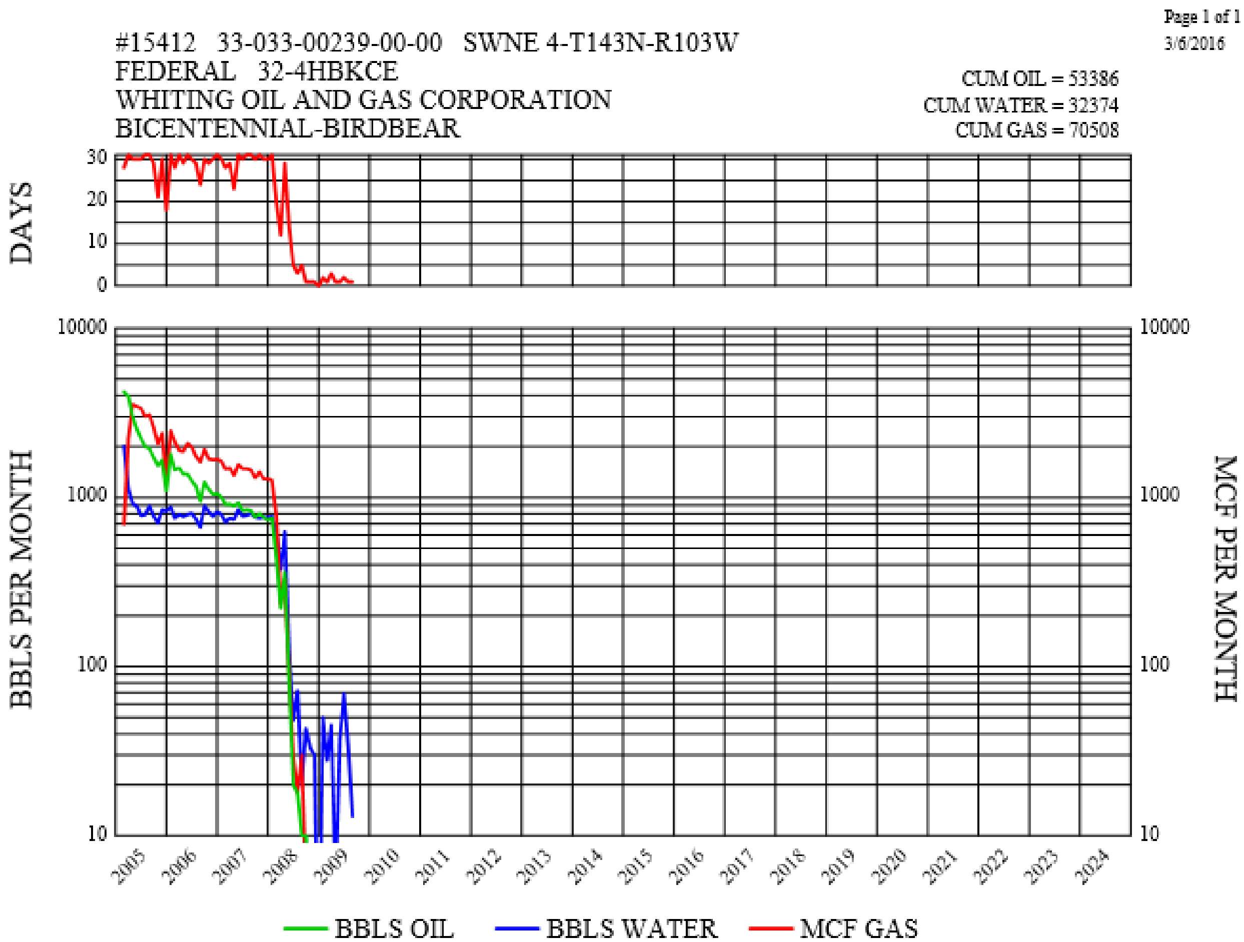

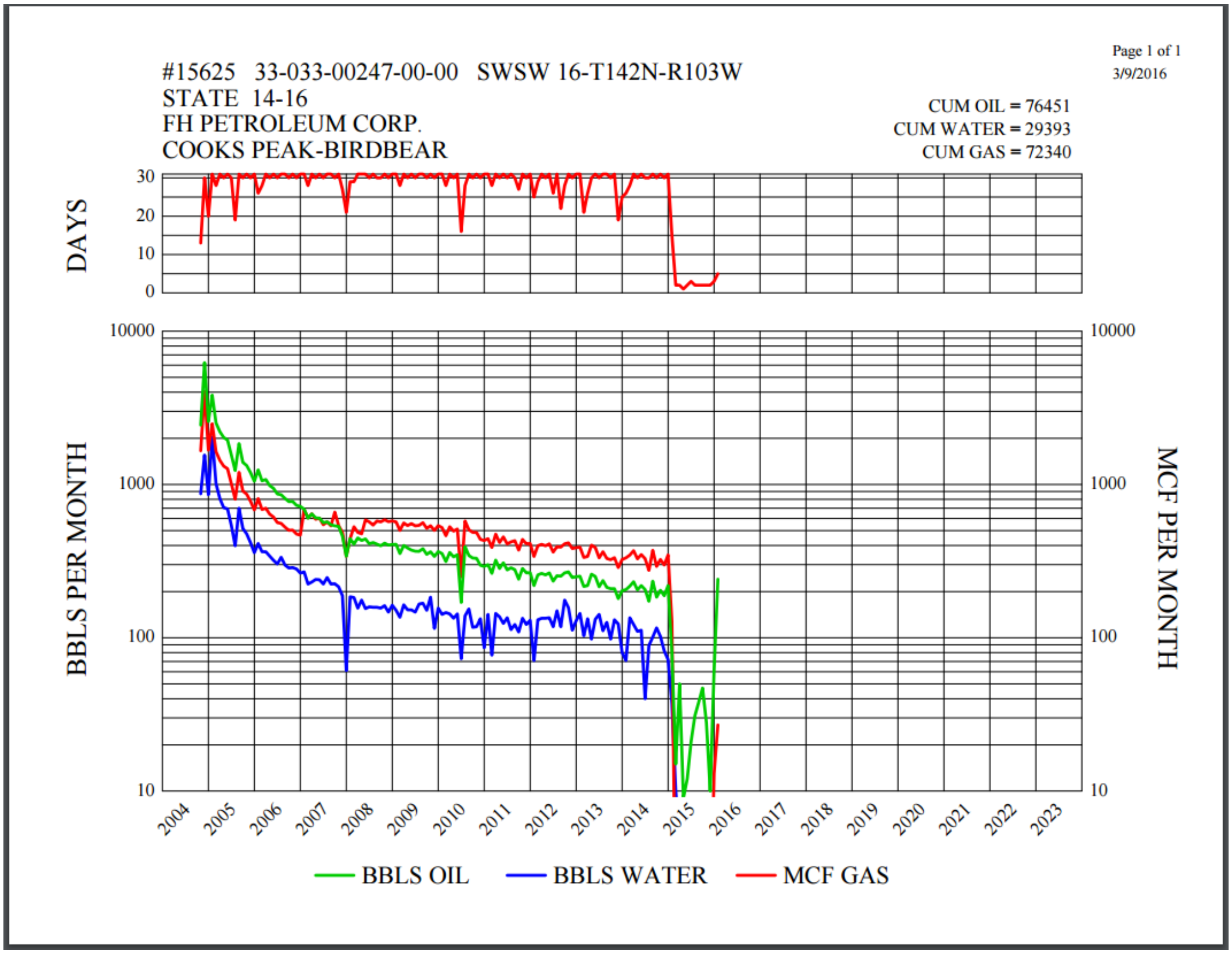

Page 1 of 1
3/9/2016
#15625 33-033-00247-00-00 SWSW 16-T142N-R103W
STATE 14-16
FH PETROLEUM CORP.
COOKS PEAK-BIRDBEAR
CUM OIL = 76451
CUM WATER = 29393
CUM GAS = 72340
DAYS
0
10
20
30
BBLS PER MONTH
MCF PER MONTH
10
100
1000
10000
2004
2005
2006
2007
2008
2009
2010
2011
2012
2013
2014
2015
2016
2017
2018
2019
2020
2021
2022
2023
BBLS OIL
BBLS WATER
MCF GAS

APPENDIX VI

TABLES OF DATA

Showing the Wells, Locations, Density Porosity, Gamma Ray, Neutron Porosity and Sonic Log Values in the Study Area.

UWI	SURFLAT	SURFLON	Dens.Por.	G. Ray	Neut.Por.	SONIC
3300700024	46.877613	-103.39697		106.00		90.91
3300700045	47.237551	-103.50283		3.39		51.43
3300700054	46.866484	-103.41286				51.54
3300700071	46.776453	-103.29136		27.59		94.64
3300700124	46.653633	-103.30782		48.25		
3300700138	46.992469	-103.34168		30.74		
3300700149	46.711905	-103.25569	-0.47	32.32	0.36	
3300700203	47.304209	-103.08239	-1.99	20.64	3.94	
3300700206	47.072812	-103.05095	-5.19	29.96	2.12	
3300700209	47.179275	-103.43078	-0.31	19.25	7.73	
3300700221	47.318737	-103.09307	-1.33	19.12	2.52	
3300700223	47.209431	-103.50097	-1.32	18.68	3.74	
3300700230	47.173124	-103.38463	-2.38	25.04	4.26	
3300700231	47.321631	-103.5323	-2.29	21.84	3.98	
3300700233	47.166299	-103.36814	0.39	20.24		
3300700236	47.175963	-103.39417		19.69		
3300700238	47.177083	-103.3879	-3.87	17.90	2.91	
3300700245	47.112525	-103.09327	-1.99	23.34	1.71	
3300700250	47.213916	-103.08797	-1.39	16.36	6.40	
3300700259	47.170302	-103.39298	-0.01	23.02	0.07	
3300700261	47.021703	-103.4463	6.39	21.89	9.97	
3300700268	47.164	-103.38814	-0.74	21.58	4.25	
3300700275	47.170489	-103.0989	-1.40	21.02	1.39	
3300700279	47.024834	-103.45753	-2.03	366.15	1.76	
3300700282	47.167091	-103.04637	-0.04	17.56	0.02	
3300700285	47.020201	-103.44001		18.71	0.02	51.25
3300700288	46.805458	-103.28545	-0.05	-51.51	0.03	
3300700292	47.109109	-103.21504	-3.29	30.60	5.15	

UWI	SURFLAT	SURFLON	Dens.Por.	G. Ray	Neut.Por.	SONIC
3300700296	47.107762	-103.38826	-4.36	-50.79		
3300700306	47.040659	-103.43904	-0.70	-10.36	2.98	
3300700314	47.06524	-103.41815	-2.30	25.47	1.27	
3300700321	47.01031	-103.40028	-0.02	22.94	0.03	
3300700322	47.227867	-103.49592	-0.74	27.83		
3300700323	47.221586	-103.23683	-0.01	26.37	0.03	
3300700325	47.036309	-103.44735	-3.06	25.28	1.76	
3300700326	47.046971	-103.43827	-0.03		0.03	
3300700344	47.113193	-103.38775	-0.02	-44.57	0.03	
3300700349	47.071999	-103.42119		24.62		-0.78
3300700354	47.006835	-103.40573	-0.02		0.03	
3300700359	47.039347	-103.43131				54.40
3300700360	47.029373	-103.32651	-0.01	-55.08	0.04	
3300700369	46.990111	-103.39997	-0.02		0.02	
3300700375	47.060276	-103.40974	-0.03		0.01	
3300700380	47.082638	-103.57478	-0.01	20.88	0.05	
3300700383	47.141065	-103.34172	-0.02	27.45	0.02	
3300700386	47.159525	-103.38403		20.61	3.99	
3300700392	47.078215	-103.41906	-0.03		0.02	
3300700398	47.036402	-103.33171	-0.02		0.04	
3300700401	47.113357	-103.39571		24.28	3.09	
3300700402	47.220224	-103.48376	-0.02		0.04	
3300700424	47.072246	-103.34685	-0.01		0.03	
3300700429	47.285687	-103.46422	-0.03	22.34	0.04	
3300700439	47.22418	-103.37952	-0.01		0.06	
3300700440	47.090681	-103.38924				52.22
3300700441	47.228107	-103.1977				51.34
3300700454	47.049872	-103.42975	-0.03		0.01	
3300700456	47.239273	-103.09856				51.10
3300700467	47.309885	-103.0984				51.81
3300700472	47.079101	-103.34621	-0.02		0.02	
3300700474	47.007605	-103.35186	-1.27		1.90	
3300700481	47.163549	-103.66031	-0.03		0.06	53.08
3300700488	46.990148	-103.09305	-0.02		0.01	51.64
3300700509	47.042273	-103.61741	-0.03		0.02	51.91
3300700521	47.282077	-103.58664	-1.57		4.07	52.19
3300700522	46.714458	-103.26282	-0.02		0.03	
3300700529	47.151727	-103.20835	-0.02		0.03	
3300700538	47.259589	-103.41921	-0.02		0.04	

UWI	SURFLAT	SURFLON	Dens.Por.	G. Ray	Neut.Por.	SONIC
3300700552	47.259589	-103.41921	-0.05	30.12	0.02	51.64
3300700563	47.06483	-103.34279			3.48711	
3300700571	47.078998	-103.32529	-0.01		0.04	
3300700616	47.270687	-103.64867	-0.01		0.06	
3300700618	47.130051	-103.50089	-0.01		0.03	
3300700622	46.961076	-103.32868				51.06
3300700631	47.325866	-103.53544	-0.03		0.03	
3300700634	46.991238	-103.35222	-0.02		0.06	
3300700641	47.004474	-103.33672	-0.02		0.02	
3300700666	47.194467	-103.5683	-2.20		3.70	
3300700676	47.120911	-103.49077	-0.02		0.02	
3300700692	46.674857	-103.2654	-0.03		0.03	
3300700703	47.260421	-103.25128	-0.03		0.01	
3300700708	46.751093	-103.23428	-0.02		0.03	
3300700725	47.223538	-103.53241	-0.02	16.37	0.03	52.06
3300700740	47.198683	-103.35171	-0.01		0.05	
3300700764	47.065794	-103.14139	-0.01		0.02	
3300700766	47.322705	-103.5432	0.00		0.05	
3300700767	47.142311	-103.61859	0.54		7.04	
3300700769	46.9849	-103.2762	-1.45		3.97	
3300700771	47.270795	-103.63795	-0.71			
3300700773	47.000188	-103.23605	-0.26		6.56	
3300700778	47.012855	-103.64282	-0.03		0.02	
3300700782	47.322099	-103.35854	-0.81		2.83	
3300700783	47.322923	-103.56984	-0.02		0.06	
3300700784	47.267577	-103.046	-0.01		0.02	
3300700785	47.061294	-103.32573	-0.01		0.03	
3300700820	47.317903	-103.52621		25.86	0.04	51.91
3300700829	47.310399	-103.57601	-0.01		0.05	
3300700840	47.094673	-103.13573	-1.35		3.56	
3300700841	47.285306	-103.29986	0.00		0.02	
3300700843	47.27097	-103.5322		16.72		
3300700845	47.263445	-103.63276	-0.01		0.07	
3300700846	47.322454	-103.41496	-0.02		0.07	
3300700852	47.085909	-103.63197	-0.01		0.05	
3300700874	46.998557	-103.34282	-0.02		0.04	
3300700897	47.294089	-103.37773	-0.02	18.40	0.05	51.44
3300700898	47.316592	-103.4048	-0.03		0.02	
3300700921	47.035524	-103.48509	-2.26		2.16	

UWI	SURFLAT	SURFLON	Dens.Por.	G. Ray	Neut.Por.	SONIC
3300700952	46.972494	-103.36031	-0.01		0.05	
3300700954	46.966238	-103.35504	-0.02		0.03	
3300700960	47.29409	-103.42908	-0.03		0.04	
3300700961	47.214034	-103.6002	-0.01		0.03	
3300700962	47.165385	-103.59025	-0.01		0.05	
3300700965	46.975189	-103.33301	-0.03		0.01	
3300700967	46.981775	-103.37866	-0.04		0.03	
3300700968	46.960126	-103.36109	-0.03		0.03	
3300700978	46.967648	-103.36595	-0.03		0.04	
3300700980	47.264034	-103.3312	-0.02		0.02	
3300700982	47.033554	-103.17085	-0.47		3.64	
3300700994	47.101543	-103.17264	-1.80		2.67	
3300700995	46.978254	-103.36342	-0.01		0.05	
3300701002	46.971108	-103.35399	-0.03		0.01	
3300701015	47.27314	-103.14231	-0.02		0.02	
3300701022	47.200306	-103.65036	-0.02		0.04	
3300701039	47.134787	-103.63398	-0.01		0.06	
3300701042	46.870067	-103.51182	-0.77		6.44	
3300701043	46.899551	-103.47528	-2.08		2.58	
3300701070	46.891638	-103.42907	-0.02		0.02	
3300701080	47.150513	-103.65198	0.00		0.10	
3300701095	47.06461	-103.37363	-0.02		0.02	
3300701135	47.155446	-103.66133	-0.02		0.06	
3300701140	47.170103	-103.58494	-1.12	19.94	7.63	52.68
3300701147	47.042281	-103.50198	-0.08	22.49	0.02	51.81
3300701422	47.245172	-103.64297	0.00	27.37	0.08	
3300701430	47.210272	-103.10903		21.68		
3300701431	47.322214	-103.09682	-0.03	21.61	0.04	
3300701446	47.214988	-103.61036	-0.02	16.86	0.03	
3300701448	47.169606	-103.65473	-0.01	21.37	0.07	52.56
3300701469	47.322194	-103.40724	-0.03	16.34	0.05	51.63
3300701472	47.195787	-103.10381		24.82		
3300701501	47.118274	-103.59017	-0.02	20.64	0.07	
3300701502	47.107535	-103.38829	-0.03	0.07		
3300701507	47.083701	-103.04564	-0.02	16.34	0.05	50.911
3300701510	47.159893	-103.38228	-0.01	17.98	0.02	51.59
3300701513	47.173093	-103.38567	-0.02	17.62	0.04	52.13
3300701542	47.208932	-103.39633	-0.02	26.54	0.03	

UWI	SURFLAT	SURFLON	Dens.Por.	G. Ray	Neut.Por.	SONIC
3300701554	47.086099	-103.38976	-0.01	25.81	0.01	
3303300037	**47.00648**	**-103.97531**	**0.86**		**14.92**	
3303300045	46.580882	-103.85462	3.63		16.05	
3303300049	47.317277	-103.80997	-3.69		8.43	
3303300050	46.992393	-103.90142	-3.22		10.06	
3303300052	47.28104	-103.95316	-0.03		0.10	
3303300053	46.888821	-103.93167	-1.43		15.47	
3303300054	46.804765	-103.85671	1.00		16.56	
3303300055	47.176346	-103.69013	-2.86		5.26	
3303300056	47.170867	-103.68242	-0.02		0.03	
3303300057	47.323962	-103.81019	-0.05		0.09	
3303300058	46.874032	-104.03095	2.56		17.26	
3303300060	46.995659	-103.79644	0.00		0.10	
3303300062	47.290217	-103.78721	-0.04		0.07	
3303300063	47.324143	-103.8406	-2.41		9.95	
3303300069	47.140177	-103.71695	-0.03		0.05	
3303300077	47.289826	-103.77843	-0.04		0.06	
3303300078	47.001588	-103.79531	-0.02		0.10	
3303300080	47.046671	-103.90135	-4.27		7.26	
3303300081	47.184155	-103.70398	-0.02		0.02	
3303300084	46.646041	-103.6878	-0.93		11.95	
3303300085	47.072046	-104.01165	0.02		0.15	
3303300086	46.790855	-103.70035	-0.01		0.10	
3303300088	46.618493	-103.90798	0.01		0.13	
3303300092	47.041231	-103.8934	-0.03		0.09	
3303300096	47.050256	-103.95402	0.00		0.12	
3303300097	47.122684	-103.90657	-0.02		0.09	
3303300100	46.990919	-103.7786	-0.02		0.10	
3303300102	47.264795	-103.74396	-2.16		9.21	
3303300105	46.974901	-103.84734	-0.03		0.09	
3303300106	47.016547	-103.81709	-0.02		0.08	
3303300109	47.274183	-103.958	-0.02		0.09	
3303300110	47.075773	-104.0174	0.02		0.14	
3303300111	47.154923	-103.84738	-2.45		9.64	
3303300113	47.043063	-103.95139	0.00	15.50	0.10	52.68
3303300114	46.975726	-103.96807	0.02	26.07	0.14	
3303300118	47.144092	-104.0071	-0.09	24.74	0.08	
3303300119	47.190763	-103.71656	-1.35		4.93	

UWI	SURFLAT	SURFLON	Dens.Por.	G. Ray	Neut.Por.	SONIC
3303300120	46.859294	-103.926	1.80		15.02	
3303300123	47.075883	-103.98619	0.00		0.13	
3303300126	47.017635	-103.92225	5.46		13.73	
3303300127	47.266955	-103.96336	-0.03		0.09	
3303300129	46.894931	-103.82145	-1.49		7.99	
3303300133	47.31743	-103.71179	-1.78		7.22	
3303300135	47.263754	-103.75514	-0.02		0.09	
3303300136	47.279522	-103.67483	-0.02		0.09	
3303300141	46.81251	-104.01452	-0.01		0.15	
3303300142	47.266884	-103.76444	-0.03		0.09	
3303300151	47.298679	-103.78655	-1.72		8.22	
3303300152	47.316665	-103.80853	-0.02		0.09	
3303300154	47.210276	-103.73324	0.00		0.07	
3303300158	46.607617	-103.87112	1.95		17.69	
3303300163	47.216251	-103.73617	0.00		0.06	52.68
3303300182	46.66767	-104.03672	2.61		13.56	
3303300188	47.176154	-103.69055	-2.80		3.15	
3303300213	47.171224	-103.68272	-1.47		6.55	
3303300217	46.901883	-103.9696	0.03		0.16	
3303300219	47.199849	-103.72263	3.53		4.18	
3303300223	47.185028	-103.71379	-0.65		5.34	
3303300224	47.193083	-103.73291	-0.01		0.07	
3303300225	47.169235	-103.92807	-0.02	55.79	0.13	
3303300226	47.259617	-103.73977	-0.02		0.08	
3303300227	47.162281	-103.66902	-0.03		0.05	
3303300228	47.264443	-103.74308	-0.02		0.08	
3303300230	47.187426	-103.71195	-0.03	20.75	0.03	
3303300233	47.201206	-103.69594	-0.03		0.03	
3303300234	47.274032	-103.75913	-0.04	21.97	0.08	
3303300241	47.145076	-103.67127	-0.03	22.77	0.06	
3303300282	47.173846	-103.69301	-0.03	22.36	0.04	52.14
3303300291	46.899397	-103.98867	1.78	33.31	0.13	
3303300297	47.301565	-103.79601	-0.03	20.65	0.09	
3303300298	47.013434	-103.85093	-0.02	26.89	0.11	51.68
3303300299	47.034242	-103.95784		28.15		53.76
3303300309	47.006852	-103.91182	-0.04	29.61		
3303300310	47.058035	-103.97533		28.45		53.85
3303300312	47.0581	-103.95931	0.01	30.16	0.12	54.69

UWI	SURFLAT	SURFLON	Dens.Por.	G. Ray	Neut.Por.	SONIC
3303300313	47.031987	-103.97642	0.02	19.58	0.13	55.51
3303300315	47.072418	-104.0178	0.05	24.17	0.15	56.60
3303300316	47.012876	-103.82378	0.00	21.38	0.10	53.35
3303300317	47.003566	-103.96976	0.00	24.58	0.10	
3303300318	47.046714	-103.99035	0.03	27.11	0.14	56.66
3303300323	47.014843	-103.91695	0.00	30.03	0.10	51.89
3303300324	47.009332	-103.80567		23.90	0.10	53.25
3303300325	47.108582	-103.90464	-1.53	23.36	0.09	53.44
3303300326	46.9966	-103.89148	-0.03	22.27	0.08	50.31
3303300329	47.019282	-103.88977	-0.01	25.90	0.08	52.33
3303300331	47.021085	-103.86893	-0.02	22.07	0.09	50.01
3303300335	47.068415	-104.02794	0.04	24.52	0.12	55.53
3303300336	47.022241	-103.80558	-0.03	23.46	0.07	51.59
3303300337	47.090075	-103.91104	-0.01	26.69	0.08	52.97
3303300338	47.128355	-103.94598	-0.03	29.28	0.07	
3303300342	46.990505	-103.94539				51.38
3303300343	47.025404	-103.83999	-0.01	17.90	0.10	52.19

List of wells, Birdbear Fm, Duperow Fm and the anhydrite tops with the calculated thicknesses of the Birdbear Formation and the anhydrites.

UWI/API	BIRDBEAR	DUPEROW	ANHYDRITE	Birdbear Thick	Anhydrite Thick
3300700001	10640	10717	10656	77	16
3300700006	11184	11271		87	
3300700016	10877	10973		97	
3300700024	10470	10545		75	
3300700045	10899	10979		80	
3300700054	10367	10439		72	
3300700071	10514	10585	10537	71	22
3300700085	10300	10435		136	
3300700124	10271	10344	10293	74	22
3300700138	10653	10733	10679	80	26
3300700149	10284	10362	10309	78	25
3300700203	11265	11354	11291	90	26
3300700206	11001	11093	11035	92	34
3300700209	10882	10970	10913	88	31
3300700221	11201	11294	11231	93	30

UWI/API	BIRDBEAR	DUPEROW	ANHYDRITE	Birdbear Thick	Anhydrite Thick
3300700223	10743	10821	10767	79	24
3300700230	10911	10998	10942	86	30
3300700231	10669	10746	10696	77	27
3300700233	10984	11066		82	
3300700234	10888	10975	10918	87	30
3300700236	10883	10971		88	
3300700238	10936	11016	10961	80	25
3300700244	11206	11291	11229	85	23
3300700245	11145	11227	11170	82	24
3300700246	11233	11332	11269	99	36
3300700250	11193	11284	11221	91	28
3300700256	10940	11026	10974	86	34
3300700258	11305	11403		98	
3300700259	10957	11048	10988	91	30
3300700261	10580	10658	10602	78	22
3300700262	11059	11144		85	
3300700268	10972	11056	11000	84	28
3300700275	11283	11367	11305	83	22
3300700279	10543	10621	10565	78	22
3300700282	11228	11312	11251	84	23
3300700285	10590	10666	10621	76	31
3300700286	11371	11456		85	
3300700288	10453	10527	10476	73	23
3300700292	11231	11317	11257	86	26
3300700296	10712	10793	10736	81	24
3300700297	10961	11042	10993	81	32
3300700306	10589	10664		75	
3300700314	10585	10663	10609	78	24
3300700316	10967	11048	10994	81	27
3300700318	10784	10864	10815	80	31
3300700321	10607	10683	10630	77	24
3300700322	10676	10758	10708	82	31
3300700323	11386	11472	11412	87	27
3300700325	10706	10781	10729	76	23
3300700326	10640	10718	10664	77	23
3300700327	10998	11075		77	
3300700331	10969	11054	11006	85	37
3300700334	10725	10806	10764	81	39

UWI/API	BIRDBEAR	DUPEROW	ANHYDRITE	Birdbear Thick	Anhydrite Thick
3300700341	10988	11069		81	
3300700344	10716	10800	10743	84	27
3300700345	10644	10725	10669	81	25
3300700349	10644	10717		73	
3300700350	10811	10889	10843	78	31
3300700351	10961	11044	10973	83	11
3300700353	11069	11148	11082	79	13
3300700354	10589	10663	10612	74	23
3300700356	10623	10702		79	
3300700359	10599	10693		94	
3300700360	10853	10933	10877	80	24
3300700361	10640	10717	10669	77	29
3300700363	11028	11107	11054	79	26
3300700368	10709	10783		74	
3300700369	10575	10650	10596	75	21
3300700372	10649	10726		77	
3300700375	10651	10732	10675	81	24
3300700379	11005	11088	11018	84	14
3300700380	10404	10479	10427	75	23
3300700381	10737	10814	10758	77	21
3300700383	11093	11174	11118	81	25
3300700385	10756	10836	10790	80	34
3300700386	11004	11067		63	
3300700388	10498	10581	10527	83	29
3300700389	10643	10719	10667	76	24
3300700392	10679	10757	10704	78	24
3300700398	10919	10997	10943	78	24
3300700401	10675	10754		79	
3300700402	10719	10797	10748	78	29
3300700405	11001	11084	11018	83	17
3300700416	11039	11122	11070	83	31
3300700424	10757	10836	10779	79	22
3300700426	11035	11117		82	
3300700429	10796	10882	10826	86	29
3300700430	10566	10647	10598	81	33
3300700433	11401	11488	11425	87	24
3300700434	10940	11027	10972	87	32
3300700435	10630	10706	10660	76	30

UWI/API	BIRDBEAR	DUPEROW	ANHYDRITE	Birdbear Thick	Anhydrite Thick
3300700436	10509	10587	10536	78	27
3300700439	10844	10925	10869	82	26
3300700440	10950	11031		81	
3300700441	11405	11493		88	
3300700442	10940	11020		80	
3300700443	11021	11107	11031	86	10
3300700444	10991	11074		83	
3300700447	11025	11105	11057	80	32
3300700448	10918	10997		79	
3300700454	10619	10697	10640	78	21
3300700455	11098	11178		80	
3300700456	11123	11209		86	
3300700467	11233	11323	11258	91	26
3300700470	10719	10796	10743	76	24
3300700472	10779	10861	10801	82	22
3300700474	10788	10865	10810	77	22
3300700481	10718	10792	10744	74	26
3300700488	10807	10884	10824	77	18
3300700498	10983	11084	11008	101	25
3300700501	11109	11188	11134	79	25
3300700504	10838	10919		81	
3300700505	11359	11444	11384	85	25
3300700509	10458	10530	10480	72	22
3300700516	10963	11041	10994	78	31
3300700518	10760	10838		78	
3300700521	10569	10647	10595	77	26
3300700522	10336	10405	10356	69	20
3300700524	11123	11206	11147	83	24
3300700526	10696	10768		72	
3300700527	10802	10887	10830	85	28
3300700529	11296	11382	11322	86	26
3300700538	11073	11156	11102	83	29
3300700543	10707	10783	10733	76	26
3300700552	10635	10709		74	
3300700563	10740	10820		81	
3300700564	10804	10882		78	
3300700567	10543	10616		73	
3300700571	11010	11091	11032	81	22

UWI/API	BIRDBEAR	DUPEROW	ANHYDRITE	Birdbear Thick	Anhydrite Thick
3300700576	10642	10718	10668	76	26
3300700588	10711	10788		77	
3300700589	11278	11361	11316	83	38
3300700590	10977	11061	11003	84	26
3300700594	10959	11039	10989	80	30
3300700599	10811	10885		74	
3300700605	11087	11173		86	
3300700607	10617	10694		77	
3300700608	10802	10879		77	
3300700611	10717	10793		76	
3300700616	10635	10712	10664	77	29
3300700617	10646	10725	10669	79	24
3300700618	10629	10704	10654	75	25
3300700620	11325	11414		89	
3300700622	10699	10774	10723	75	24
3300700624	10975	11056	11006	81	31
3300700631	10701	10777	10731	76	30
3300700634	10615	10691	10638	75	22
3300700638	10908	10988	10923	81	16
3300700641	10788	10865	10810	77	22
3300700642	11040	11124	11052	84	12
3300700643	10590	10670	10620	80	30
3300700644	11042	11128	11053	86	11
3300700645	10585	10659	10604	74	19
3300700650	10639	10717	10662	78	23
3300700657	10754	10834	10776	80	22
3300700659	10613	10688	10623	75	10
3300700661	10408	10486		78	
3300700663	10820	10899	10845	79	26
3300700664	10715	10794	10729	78	14
3300700665	10484	10556	10512	72	29
3300700666	10543	10619	10570	76	27
3300700672	10749	10827	10776	77	26
3300700676	10604	10677	10630	74	27
3300700678	10781	10868	10798	87	17
3300700682	10700	10776	10720	76	20
3300700686	10730	10807	10750	76	20
3300700687	11080	11155		75	

UWI/API	BIRDBEAR	DUPEROW	ANHYDRITE	Birdbear Thick	Anhydrite Thick
3300700692	10302	10386	10329	84	28
3300700693	10623	10700	10654	77	31
3300700700	10969	11048	11008	79	39
3300700702	10864	10943		79	
3300700703	11350	11440	11378	90	28
3300700704	10726	10802		76	
3300700707	10878	10958		80	
3300700708	10399	10468	10420	69	21
3300700711	10507	10582	10531	75	24
3300700714	11244	11333		89	
3300700715	10988	11065	11008	77	20
3300700716	10670	10749	10700	79	30
3300700717	10831	10910	10863	79	32
3300700725	10748	10826		78	
3300700726	10772	10854	10792	82	20
3300700735	10750	10826		76	
3300700740	11099	11186	11126	87	27
3300700741	10986	11064	11012	78	26
3300700744	10794	10878		84	
3300700747	11081	11157	11102	75	
3300700749	10776	10853	10814	77	38
3300700752	11227	11312		85	
3300700753	10577	10654	10599	77	22
3300700761	11046	11130	11071	84	25
3300700764	10975	11054	10993	79	19
3300700766	10707	10784	10736	77	29
3300700767	10618	10692	10640	74	22
3300700769	10944	11019	10965	75	21
3300700771	10795	10876	10822	81	27
3300700773	10996	11074	11017	77	21
3300700778	10487	10560	10510	73	22
3300700779				0	0
3300700782	11211	11296	11241	85	30
3300700783	10881	10960	10908	79	27
3300700784	11136	11221	11161	85	25
3300700785	10965	11046	10990	80	24
3300700792	10987	11064	11001	77	14
3300700796	10632	10708	10651	76	19

UWI/API	BIRDBEAR	DUPEROW	ANHYDRITE	Birdbear Thick	Anhydrite Thick
3300700799	11047	11130	11075	83	28
3300700801	11119	11208	11142	89	23
3300700806	10709	10790		81	
3300700811	11070	11154	11082	84	12
3300700818	10560	10639	10594	79	34
3300700820	10697	10778	10709	81	12
3300700825	11054	11148		94	
3300700829	10990	11069	11020	79	30
3300700832	10723	10803	10753	80	31
3300700840	11118	11202	11141	84	23
3300700841	11312	11404	11338	92	26
3300700843	10652	10734	10663	82	11
3300700845	10787	10867	10815	80	28
3300700846	11122	11208	11150	86	28
3300700849	11281	11362		81	
3300700852	10738	10809	10760	71	22
3300700858	10760	10839	10792	79	32
3300700869	10918	10996		78	
3300700874	10781	10857	10804	76	23
3300700892	10976	11061	10984	85	9
3300700894	11360	11449	11372	89	12
3300700896	10950	11036	10962	86	12
3300700897	11153	11239		86	
3300700898	11254	11332	11283	79	30
3300700904	11035	11120	11048	85	13
3300700921	10503	10577	10526	74	23
3300700922	11198	11285	11231	87	33
3300700927	11291	11376	11307	86	17
3300700938	10482	10556		75	
3300700952	10535	10612	10558	77	23
3300700954	10565	10642	10585	77	21
3300700960	10846	10932	10876	86	30
3300700961	10749	10826	10775	77	26
3300700962	10408	10488	10432	80	25
3300700965	10654	10727	10676	73	22
3300700967	10550	10626	10574	76	24
3300700968	10541	10617	10564	76	23
3300700970	11034	11118	11045	84	12

UWI/API	BIRDBEAR	DUPEROW	ANHYDRITE	Birdbear Thick	Anhydrite Thick
3300700973	10594	10673	10629	79	35
3300700978	10553	10630	10576	77	22
3300700980	11004	11088	11032	84	28
3300700981	10719	10801	10755	82	36
3300700982	10962	11043	10982	81	20
3300700994	11176	11260	11200	84	24
3300700995	10554	10636	10579	82	25
3300700996	10455	10527		72	
3300700997	10709	10792	10731	83	22
3300701002	10562	10642	10586	80	24
3300701003	10516	10595	10547	79	31
3300701006	10728	10808	10762	80	34
3300701007	11009	11094		85	
3300701008	10678	10760		82	
3300701009	10466	10539		73	
3300701015	11288	11377	11315	89	27
3300701019	10731	10810	10753	79	22
3300701022	10592	10671	10619	79	27
3300701025	11187	11273		86	
3300701037	10574	10647		73	
3300701039	10583	10658	10607	75	24
3300701040	10968	11053	10982	85	14
3300701042	10233	10307	10256	74	24
3300701043	10317	10390	10334	73	17
3300701045	11225	11307		82	
3300701048	10340	10412		71	
3300701052	11173	11260	11207	87	34
3300701055	10309	10385		76	
3300701057	10548	10619	10571	71	23
3300701065	10719	10753		35	
3300701066	10471	10543		72	
3300701070	10443	10516	10464	73	21
3300701078	11066	11147	11096	81	30
3300701079	11039	11130		91	
3300701080	10567	10642	10594	75	27
3300701085	11260	11339	11292	79	32
3300701094	10829	10911	10865	82	36
3300701095	10654	10734	10678	80	24

UWI/API	BIRDBEAR	DUPEROW	ANHYDRITE	Birdbear Thick	Anhydrite Thick
3300701099	10804	10880	10830	76	26
3300701102	10512	10584	10530	72	18
3300701113	10892	10973	10915	81	23
3300701125	10526	10602		76	
3300701126	11201	11292		91	
3300701132	11107	11189		82	
3300701135	10629	10701	10655	72	26
3300701140	10402	10481	10429	80	28
3300701145	10551	10630		79	
3300701147	10541	10621	10565	79	24
3300701154	10691	10771		80	
3300701156	10489	10567		78	
3300701175	10632	10710	10658	78	26
3300701229	10361	10440		79	
3300701287	10699	10771	10720	72	21
3300701304	11173	11256	11185	84	13
3300701325	10979	11064		85	
3300701360	11116	11196	11127	80	11
3300701369	12128	12164		36	
3300701388	10515	10585		70	
3300701391	10820	10897	10847	78	27
3300701405	11030	11106	11047	76	17
3300701416	10654	10728	10678	74	24
3300701417	10672	10753	10702	81	30
3300701422	10911	10991	10936	80	25
3300701430	11291	11377	11316	86	25
3300701431	11240	11332	11260	92	20
3300701446	10733	10811		78	
3300701448	10589	10666	10611	77	22
3300701459	11171	11255	11203	84	32
3300701469	11159	11242		83	
3300701472	11287	11369		82	
3300701501	10574	10650		76	
3300701502	10715	10794	10740	79	25
3300701507	11002	11078		76	
3300701510	10986	11068		82	
3300701513	10916	11003		87	
3300701542	11051	11136		85	

UWI/API	BIRDBEAR	DUPEROW	ANHYDRITE	Birdbear Thick	Anhydrite Thick
3300701554	10727	10805	10747	78	20
3300701563	10750	10830	10774	80	24
3300701580	10610	10687	10638	77	27
3300701638	10698	10843	10745	145	47
3300701640	10919	10995	10939	76	20
3300701641	10739	10816	10762	77	23
3302500106	10877	10960		83	
3302500158	11281	11372		91	
3302500186	11158	11243		85	
3302500189	11187	11280	11211	93	24
3302500286	10691	10771		80	
3302500329	11007	11085	11019	78	12
3302500360	10989	11074		85	
3302500415	10902	10983		81	
3303300008	9904	9944		40	
3303300037	10248	10297		49	
3303300045	9350	9401		51	
3303300049	10722	10810	10758	88	36
3303300050	10457	10514	10472	57	15
3303300051	10796	10867		71	
3303300052	10673	10745	10702	72	29
3303300053	10211	10253	10215	42	4
3303300054	9955	10007	9964	52	8
3303300055	10740	10817	10768	77	28
3303300056	10715	10790	10739	75	24
3303300057	10772	10846	10802	74	30
3303300058	9975	10009		34	
3303300060	10456	10521	10474	65	17
3303300061	10691	10770	10723	79	32
3303300062	10896	10969	10924	73	28
3303300063	10830	10904	10857	74	27
3303300064	10788	10861		73	
3303300065	10650	10725	10684	75	35
3303300068	10695	10769	10723	74	28
3303300069	10705	10778	10732	73	27
3303300076	10612	10685	10642	73	30
3303300077	10701	10779	10730	78	29
3303300078	10438	10499	10456	61	19

UWI/API	BIRDBEAR	DUPEROW	ANHYDRITE	Birdbear Thick	Anhydrite Thick
3303300080	10457	10509	10466	52	9
3303300081	10758	10827	10783	69	25
3303300084	9856	9917	9870	60	13
3303300085	10263	10303		40	
3303300086	9985	10053	10004	68	19
3303300088	9571	9614		43	
3303300092	10487	10534	10496	48	9
3303300096	10460	10515	10473	56	14
3303300097	10627	10688	10647	61	19
3303300100	10501	10568	10517	67	16
3303300102	10489	10563	10516	74	27
3303300103	10600	10676	10627	76	27
3303300105	10613	10672	10629	58	15
3303300106	10630	10692	10644	62	14
3303300107	10598	10653		55	
3303300109	10687	10760	10715	73	28
3303300110	10240	10284	10246	44	6
3303300111	10638	10709	10665	71	27
3303300112	10866	10941	10894	76	29
3303300113	10468	10522	10478	54	10
3303300114	10241	10284		43	
3303300118	10347	10405		58	
3303300119	10610	10691	10647	81	37
3303300120	10137	10181		44	
3303300121	10475	10542	10494	68	20
3303300123	10422	10471	10429	50	7
3303300126	10505	10555	10512	50	7
3303300127	10526	10597	10555	71	29
3303300129	10397	10461	10417	64	20
3303300133	10676	10756	10707	81	32
3303300135	10604	10683	10628	79	24
3303300136	10721	10801	10749	80	28
3303300141	9906	9940		34	
3303300142	10720	10796	10750	76	30
3303300151	10762	10834	10791	72	29
3303300152	10732	10807	10759	75	27
3303300154	10504	10578	10528	74	24
3303300156	10114	10156		42	

UWI/API	BIRDBEAR	DUPEROW	ANHYDRITE	Birdbear Thick	Anhydrite Thick
3303300158	9581	9624		43	
3303300163	10547	10621	10571	74	24
3303300180	10469	10531	10485	62	16
3303300182	9524	9571		47	
3303300188	10750	10823	10778	73	28
3303300199	10331	10371		39	
3303300212	10674	10749	10700	75	26
3303300213	10714	10790	10739	76	25
3303300217	10143	10182		39	
3303300219	10553	10627	10574	74	21
3303300223	10660	10734	10687	73	27
3303300224	10669	10748	10699	79	31
3303300225	10390	10452	10406	62	16
3303300226	10434	10510	10463	76	29
3303300227	10610	10684	10634	74	24
3303300228	10484	10560		76	
3303300229	10595	10669	10618	74	23
3303300230	10663	10738	10692	74	29
3303300231	10436	10511	10462	75	26
3303300232	10541	10613	10561	73	21
3303300233	10756	10831	10781	75	25
3303300234	10721	10797		76	
3303300239	10691	10767	10715	76	24
3303300241	10679	10755		76	
3303300248	10514	10590	10539	76	25
3303300251	10713	10787	10738	74	25
3303300282	10782	10854		72	
3303300291	10119	10157		37	
3303300297	10788	10866		78	
3303300298	10650	10709		60	
3303300299	10437	10494		57	
3303300309	10488	10539		51	
3303300310	10379	10428		49	
3303300312	10480	10534	10492	54	12
3303300313	10370	10423		53	
3303300315	10255	10294		39	
3303300316	10600	10658		59	
3303300317	10289	10336		47	

UWI/API	BIRDBEAR	DUPEROW	ANHYDRITE	Birdbear Thick	Anhydrite Thick
3303300318	10370	10420		51	
3303300323	10469	10522		53	
3303300324	10600	10662		62	
3303300325	10549	10615	10571	66	22
3303300326	10537	10590		53	
3303300329	10586	10641		55	
3303300331	10550	10608		59	
3303300335	10309	10348		39	
3303300336	10645	10713		68	
3303300337	10548	10612		64	
3303300338	10505	10570		65	
3303300342	10339	10390		51	
3303300343	10621	10682		61	
3308700007	9968	10040		72	
3308700008	9934	10007		73	
3308700009	9979	10053		75	
3308700010	10001	10010		9	
3308700105	9975	10047	9988	72	13
3308700108	9964	10032	9974	69	10
3308700112	9731	9794	9744	63	13
3308900006	10324	10402		78	
3308900210	10400	10473		73	
3308900228	10277	10348	10287	71	10
3308900243	10629	10708		79	
3308900244	10457	10530		73	
3308900272	10675	10749	10694	74	18
3308900278	10707	10781		74	
3308900286	10693	10770		77	
3308900314	10736	10804		68	
3308900452	10702	10771		70	
3308900509	10618	10691	10629	73	11
303300308	10490		10509		19

REFERENCES

Anna, L.O., Pollastro, Richard, and Gaswirth, S.B., 2013, Williston Basin Province—Stratigraphic and structural framework to a geologic assessment of undiscovered oil and gas resources, chap. 2 *of* U.S. Geological Survey Williston Basin Province Assessment Team, Assessment of undiscovered oil and gas resources of the Williston Basin Province of North Dakota, Montana, and South Dakota, 2010 (ver. 1.1, November 2013): U.S. Geological Survey Digital Data Series 69–W, 17 p.

Archie, G. E., 1942, The electrical resistivity log as an aid in determining some reservoir characteristics: *Petroleum Transactions of the AIME, v. 146, p. 54-62.*

Baillie, A.D., 1953, Devonian names and correlations in Williston Basin area: *American Association of Petroleum Geologist Bulletin, v. 37, p. 444-452.*

Burke, R. B., & Sperr, T. J. (2006). Birdbear Formation lithofacies in west-central North Dakota; some characteristics and insight. *Geo News*, *33*(1), 17-21.

Dembicki, H., Jr. (2009). Three common source rock evaluation errors made by geologists during prospect or play appraisals. *Bulletin of the American Association of Petroleum Geologists, 93*(3).

Dunham, R.J., 1962, Classification of carbonate rocks according to depositional texture, *in* Ham, W.E., ed., Classification of carbonate rocks: *American Association of Petroleum Geologists Memoir, p. 108-121.*

Folk, R.L., 1959, Practical petrographical classification of limestones: *American Association of Petroleum Geologist Bulletin, v. 43, p. 1-38.*

Gerhard, L. C., Anderson, S. B., LeFever, J. A., & Carlson, C. G. (1982). Geological development, origin, and energy mineral resources of Williston Basin, North Dakota. *Bulletin of the American Association of Petroleum Geologists, 66*(8)*, 989-1020. 341-356.*

Golden Software Inc. (2013). Surfer Version 11.4.958, Golden, CO.

Gregg, J.M., and Sibley, D. F., 1987, Classification of dolomite rock textures: *Journal of Sedimentary Petrology, v. 57, p. 967–975.*

Halabura, S., (1982). Depositional environments of the Upper Devonian Birdbear formation, Saskatchewan; *in* Proceedings of a Symposium - International Williston Basin Symposium*, Special Publication - Saskatchewan Geological Society 4*, 113-124.

Ham, E.W., and Pray, L.C. 1961. Modern Concepts and Classification of Carbonate Rocks. In *Classification of Carbonate Rocks: A Symposium*. American Association of Petroleum Geologists Memoir 1, ed. W.E. Ham, 2-19.Tulsa, Oklahoma: AAPG.

Hans G. M., and James H. A., 1989. Pervasive Surface Dolomitization of the Dolomitization of the Nisku Formation in Central Alberta. *Journal of Sedimentary petrology, vol. 59, No. 6, P. 891-911*

IHS Inc. (2013). PETRA Version 3.8.3, Tulsa, Ok.

James, N. P., and P. W. Choquette, 1984. Diagenesis 9: Limestones-the meteoric diagenetic environment: *Geoscience Canada, v. 11, p. 161-194.*

Kent, D. M. (1968). The geology of the Upper Devonian Saskatchewan group and equivalent rocks in western Saskatchewan and adjacent areas. *Report - Department of Mineral Resources (Regina),* 221.

Kent, D. M., & Kreis, L. K. (1998). Diagenetically altered stromatoporoid banks; seals for dolomicrite reservoirs in Birdbear and Duperow rocks of southern Saskatchewan*; in* Proceedings of a Symposium - International Williston Basin Symposium; Core Workshop*, Special Publication - Saskatchewan Geological Society, 8*, 105-142.

Kissling, D. L., & Ehrets, J. R. (1984). Depositional models for the Duperow and Birdbear formations; implications for correlation and exploration: *in* Lorsong, J. A. and Wilson, M. A. (eds.), Proceedings of a Symposium - International Williston Basin Symposium, *Special Publication - Saskatchewan Geological Society, 7*, unpaginated.

Langford, F.F. and Blanc-Valleron, M.M., 1990, Interpreting Rock-Eval pyrolysis data using graphs of pyrolizable hydrocarbons vs. total organic carbon: *American Association of Petroleum Geologist Bulletin, vol. 70, no. 6, p. 799-804.*

LeFever, J. A., Martiniuk, C. D., Dancsok, E. F. R., & Mahnic, P. A. (1991). Petroleum potential of the middle member, Bakken Formation, Williston Basin*; in* 6th Internation Williston Basin Symposium, *Special Publication - Saskatchewan Geological Society 6*, 74-94.

Loeffler, P. T. Depositional environment and diagenesis, Birdbear Formation (Upper Devonian), Williston Basin, North Dakota *Thesis – University of North Dakota, 1-181.*

Leighton, M. W., & Pendexter, C., (1962). Classification of Carbonate Rocks. *American Association of*

Petroleum Geologist, mem., 1: 33-61.

Longman, M. W., 1982. Carbonate Diagenesis as a Control on Stratigraphic Traps (with Examples from the Williston Basin). *Am. Assoc. Petrol. Geol. Education Course Note Series No.* 21. Tulsa. 159 pp.

Lucia, F.J. 1983. Petrophysical Parameters Estimated from Visual Descriptionof Carbonate Rocks: A Field Classification of Carbonate Pore Space. *J. PetTech* **35** (3): 626-637. http://dx.doi.org/10.2118/10073-PA.

Lucia, F.J. 1995. Rock-Fabric/Petrophysical Classification of Carbonate PoreSpace for Reservoir Characterization. *Am. Assoc. Pet. Geol. Bull.* ***79*** (9): 1275-1300.

Lucia, F.J. 2007. Carbonate Reservoir Characterization: An Integrated Approach. *New York, New York: Springer-Verlag.*

Martiniuk, C. D., Young, H. R., & LeFever, J. A. (1995). Lithofacies and petroleum potential of the Birdbear Formation (Upper Devonian), southwestern Manitoba and north-central North Dakota; *in* Hunter, L. D. and Shalla, R. A. (eds.), 7th Internation Williston Basin Symposium, *Special Publication - Saskatchewan Geological Society*, *12*, 89-102.

Murray, R., 1964, Origin and diagenesis of gypsum and anhydrite: Journal of Sedimentary Petrology, v. 34, p. 512-523.

Nahnybida, C., Hutcheon, I., & Kirker, J. (1982). Diagenesis of the Nisku formation and the origin of late-stage cements. *The Canadian Mineralogist*, *20*(*May), 129–140.*

Nordeng, S.H., 2012, Basic geochemical evaluation of unconventional resource plays: Geows, https://www.dmr.nd.gov/ndgs/newsletter/2012%20January/Basic%20 Geochemical%20Evaluation%20of%20Unconventional%20Resource%20Plays.pdf

Obermajer, M., Osadetz, K. G., Fowler, M. G., & Snowdon, L. R. (1999). Geochemistry and familial association of crude oils from the Birdbear Formation in southeastern Saskatchewan, Williston Basin. *Bulletin of Canadian Petroleum Geology*, *47*(3), 255-269.

Osadetz, K., Brooks, P. W., & Snowdon, L. R. (1992). Oil families and their sources in Canadian Williston Basin, (southeastern Saskatchewan and southwestern Manitoba). *Bulletin of Canadian Petroleum Geology, 40*, 254-273.

Peters, K.E., and Cassa, M.R., 1994, Applied source rock geochemistry, in Magoon, L.B., and Dow, W.G., eds., The petroleum system—From source to trap: Tulsa, Okla., *American Association of Petroleum Geologist Memoir 60, p. 93-117.*

Plumley, W.J., Risley, G.A., Graves, R.W. et al. 1962. Energy Index for Limestone Interpretation and Classification. In Classification of Carbonate Rocks*: A Symposium. American Association of Petroleum Geologists Memoir 1,ed. W.E. Ham, 58-107. Tulsa, Oklahoma.*

Sandberg, C. A., & Hammond, C. R. (1958). Devonian System in Williston basin and central Montana. *Bulletin of the American Association of Petroleum Geologists, 42*, 2293-2333.

Williston Basin [Online image]. (2014). Retrieved January, 2015 from https://www.dmr.nd.gov/ndgs/resources/

Scholle, P. A. 1979. A Color Illustrated Guide to Constituents, Textures, Cements, and Porosities of Sandstones and Associated Rocks. *Am. Asso. Petrol. Geol. Memoir 28. 201 pp., 360 color photos. Tulsa.*

Slatt, R.M., Singh, P., Borges, G., 2009, Reservoir characterization of unconventional gas shale reservoirs: example from the Barnett Shale, Texas, U.S.A, *Oklahoma City Geological Society Shale Shaker, vol. 60, no. 1, p. 15–31.*

Snowdon, L.R., Fowler, M.G., Riediger, and C.L., 1998, Interpretation of organic geochemical data: Short Course Notes, *CSPG, November 5-6, 1998, Calgary, Alberta.*

Stasiuk, L.D., Addison, G., and Steedman, R., 1998, An evaluation of hyrdrocarbon migration in the Birdbear Formation of southeastern Saskatchewan, *Eighth International Williston Basin Symposium, p. 50-57.*

Swenson, R. E., 1967, Trap mechanics in Nisku Formation of northeast Montana: AAPG Bulletin, v. 51, p. 1948–1958.

Tissot, B., B. Durand, J. Espitalie, and A. Combaz, 1974, Influence of nature and diagenesis of organic matter in formation of petroleum: *AAPG Bulletin, v. 58, p. 499-506.*

van Krevelen, D. W., 1961, Coal: Amsterdam, *Elsevier, 514 p.*

Wardlaw, N. C., 1979. Pore systems in carbonate rocks and their influence on the hydrocarbon recovery efficiency. Geology of Carbonate Porosity . *American Association of Petroleum Geologist, Cont. Edu. Course Note Series, 11: E-1 –E-24.*